Taking into account radiation dose distributions to the heart in predicting radiation-induced valvulopathy : application on data from childhood cancer survivors

Stefania Chounta

▶ **To cite this version:**

Stefania Chounta. Taking into account radiation dose distributions to the heart in predicting radiation-induced valvulopathy : application on data from childhood cancer survivors. Statistics [math.ST]. Université Paris-Saclay, 2023. English. NNT : 2023UPASR013 . tel-04190535

HAL Id: tel-04190535
https://theses.hal.science/tel-04190535v1

Submitted on 29 Aug 2023

HAL is a multi-disciplinary open access archive for the deposit and dissemination of scientific research documents, whether they are published or not. The documents may come from teaching and research institutions in France or abroad, or from public or private research centers.

L'archive ouverte pluridisciplinaire **HAL**, est destinée au dépôt et à la diffusion de documents scientifiques de niveau recherche, publiés ou non, émanant des établissements d'enseignement et de recherche français ou étrangers, des laboratoires publics ou privés.

université PARIS-SACLAY

Taking into account radiation dose distributions to the heart in predicting radiation-induced valvulopathy: application on data from childhood cancer survivors.

Prise en compte de la distribution de la dose d'irradiation au cœur à la prédiction d'une valvulopathie radio-induite: application aux données des survivants des cancers pédiatriques

Thèse de doctorat de l'université Paris-Saclay

École doctorale n° 570, Santé Publique (EDSP)
Spécialité de doctorat: biostatistiques et data science
Graduate School : Santé publique, Référent : Faculté de médecine

Thèse préparée dans les unités de recherche CESP (Université Paris-Saclay, UVSQ, Inserm, CESP) et Mathématiques et Informatique pour la Complexité et les Systèmes (Université Paris-Saclay, CentraleSupélec), sous la direction de Rodrigue Allodji, CRCN (PhD-HDR), la co-direction de Sarah Lemler, PhD-maîtresse de conférence et de Véronique Letort-le Chevalier, PhD-maîtresse de conférences

Thèse à soutenir à Paris-Saclay, le 30 juin 2023, par

Stefania CHOUNTA

Composition du jury

Pierre Blanchard Professeur des Universités - PH (MD-PhD, HDR), Université Paris Saclay	Président
Maria Blettner Professeuse- Prof. Dr., Johannes Gutenberg University Mainz, Mainz, Germany	Rapporteur & Examinatrice
Jean-Emmanuel Bibault Professeur (PU-PH, HDR), Université de Paris	Rapporteur & Examinateur
Karen Leffondré Professeure (PU, HDR), ISPED - Université de Bordeaux	Examinatrice
Olivier Keunen Group Leader, Translational Radiomics (PhD), Luxembourg Institute of Health	Examinateur

THESE DE DOCTORAT
NNT : 2023UPASR013

université PARIS-SACLAY | ÉCOLE DOCTORALE Santé Publique (EDSP)

Titre: Prise en compte de la distribution de la dose d'irradiation au cœur à la prédiction d'une valvulopathie radio-induite: application aux données des survivants des cancers pédiatriques.
Mots clés: modèle de Cox, dosiomics, forêts aléatoires, histogramme dose-volume, sélection de variables

Résumé: Le taux moyen de guérison des cancers de l'enfant atteint aujourd'hui 70 à 80 %. La radiothérapie est l'un des traitements les plus préconisés, mais elle peut provoquer, à long terme, des effets iatrogènes importants, notamment des valvulopathies radio-induites. Des modèles identifiant les patients les plus à risques pourraient permettre de personnaliser les protocoles de suivi et d'identifier précocement ces effets indésirables. Actuellement, les modèles de prédiction de ces effets sont encore peu fiables et utilisent principalement la dose moyenne de radiations reçues au niveau des organes, omettant ainsi les effets potentiels de la forte hétérogénéité spatiale des doses reçues. Nos travaux explorent l'intégration de nouvelles variables et de nouveaux types de modèles pour une caractérisation plus fine des patients à risque. A l'aide des données de la corhorte French Childhood Cancer Survivors Study (FCCSS), nous avons montré que le risque de valvulopathie, estimé via un modèle à risques proportionnels de Cox, dépendait de l'histogramme dose-volume : il augmente pour des doses élevées mais également, bien que de manière moins significative, pour des doses de 5 à 20 Gy reçues sur plus de 90 % du volume du cœur. Dans un second temps, nous avons exploité les récents développements des dosiomics pour extraire des informations agrégées des matrices de doses. Nous avons ainsi montré que lorsque les variables cliniques sont disponibles, la dose moyenne au cœur pourrait être un prédicteur suffisant mais que la sélection d'indicateurs dosiomics était une bonne alternative pour des populations ayant reçu une dose au cœur non-homogène. Enfin, nous avons évalué nos approches sur une deuxième cohorte, la cohorte européenne PanCare. Les résultats fournis contribueront à améliorer les recommandations internationales pour la surveillance des survivants du cancer chez l'enfant pour le risque de valvulopathie.

Title: Taking into account radiation dose distributions to the heart in predicting radiation-induced valvulopathy: application on data from childhood cancer survivors.
Keywords: Cox proportional hazard model, dosiomics, random forests, dose-volume histogram, variable selection

Abstract: The average recovery rate for childhood cancers is now 70 to 80%. Radiotherapy is one of the most recommended treatments, but it can cause critical iatrogenic effects in the long term, notably radiation-induced valvulopathy. Models identifying the patients most at risk could make it possible to personalize follow-up protocols and identify these adverse effects early on. Currently, predictive models of these effects still need to be determined and mainly use the average radiation dose received at the organ level, thus omitting the potential effects of the high spatial heterogeneity of the received doses. Our work explores the integration of new variables and new types of models for a more refined characterization of patients at risk. Using data from the French Childhood Cancer Survivors Study (FCCSS), we have shown that the risk of valvulopathy, estimated via a Cox proportional hazards model, depended on the dose-volume histogram: it increases for high doses but also, although less significantly, for doses of 5 to 20 Gy, received over more than 90% of the heart volume. Secondly, we have exploited recent developments in dosiomics to extract aggregated information from dose matrices. We have shown that when clinical variables are available, the average dose to the heart could be a sufficient predictor. However, selecting dosiomics indicators is a good alternative for populations receiving a non-homogeneous dose to the heart. Finally, we evaluated our approaches in a second European PanCare cohort. The provided results will improve international surveillance guidelines for childhood cancer survivors for risk of valvulopathy.

"You miss 100% of the shots you don't take. -Wayne Gretzky"
-Michael Scott

Acknowledgements

More than seven long years in Paris, a few university degrees, one global pandemic, and a lot of writing and erasing later, here it is; my thesis is camera ready! It took much effort not to give up whenever things became dark, several meetings with the best supervisors in the world, Sarah, Rodrigue, and Véronique, much courage to unwrap both the context for this thesis and myself, and much patience to finally wrap all of the hard work up.

I would like to thank my supervisors, Rodrigue Allodji, Sarah Lemler, and Véronique Letort- le Chevalier, first for trusting me with this subject and also for shedding light on every aspect of this thesis. This Ph.D. thesis consists of three imaginary babies, the three main chapters-contributions; however, while preparing it, three very real babies arrived and brightened our weekly meetings. An eternal thank you to Véronique and S., Rodrigue and N., and Sarah and E. for being present for three years and a half (at least three of you!) despite the uncommon pandemic times we all experienced, for our discussions that pushed me to think beyond my ordinary boundaries and find solutions, the ideas you shared with me, the constructive criticism, and the suggestions that formed and improved this dissertation. I cannot thank you enough for investing all of your precious time to discuss and read time and again manuscript after manuscript, revision after revision. Sarah, thank you for that phone call when I was so disappointed and angry; I will always keep your kind and soothing words in my heart; Rodrigue, thank you for being an active listener during complicated times; Véronique thank you for watching my back, especially whenever my rebel self took over. Sarah, Rodrigue, and Véronique, I will be eternally grateful for the time and effort we spent together to write this thesis.

Thank you as well to the PrediTools project, especially to Mahmoud Bentriou and Duyen Do, for their endless generosity, patience, and kindness.

I would also like to thank Dr. Mrs. Maria Blettner and Dr. M. Jean-Emmanuel Bibault, who did me the honor of accepting to be rapporteurs of this thesis. Also, a big thank you to Dr. Mrs. Karine Leffondré and Dr. M. Olivier Keunen for accepting to be examiners and to Dr. M. Pierre Blanchard for completing the jury of my defense as its president.

A special enormous thank you to Françoise Terrier and Fabienne Brosse for their services and patience.

A big thank you to the staff of the Epidemiology of Radiations team and especially to: Brice Fresneau, Charlotte Demoor-Goldschmidt, Ibrahima Diallo, and Florent de Vathaire, for their profound scientific guidance, remarks, and priceless additions; Neige Journy, Nadia Haddy, and Imène Mansouri for sharing their ideas and code that launched my doctoral research; Giao, Vincent S., Martine, Isao, Amel la petite, and Amel la grande, for every aspect of technical, as well as moral support; Monia, and Claire and Thibaud, my "colloques du bureau," for always allowing to let some steam off; Naïla, who patiently edited my street french; Arnaud, Aude, David, Marina, May, Daniel, and Vincent Z. for all the lunch breaks, the coffee breaks, the corridor chats, the farewell parties, and the afterworks.

Another big thank you to the members of the MICS lab and the βiomathematics team, and especially to: Paul-Henry Cournède and Céline Hudelot for discretely standing by and providing help at critical moments; Elvire, my Ph.D. classmate, just so you know "t'es coincé avec moi" too; Brice

H. and Sylvain for their tasteful music and beer suggestions; Mathilde for that bit of code and the excellent afterworks; Yoann for keeping the score and for being a constant reminder of how not to get type 2 diabetes; Romain for the moral support and the lame sense of humor; Joe, Mihir, and Stergios for being a fantastic MICSture of experts.

Especially thank you to Stergios Christodoulidis (x2) and Maria Vakalopoulou, for answering every scientific, technical, or existential question with similar rigorousness and patience, whether it was Friday morning at the lab or Saturday afternoon at the park, for all your suggestions and the motivation talks, thank you time and again.

From the greater European area, I would like to thank with all my heart: Alexandra Elbakyan, the Robin Hood of science; Panagiotis Alexandros, for being the most considerate and warm-hearted barrista of the city; Booze, my birthday buddy; Nikolas, my unfinished-scrapping-tools comrade; Phaedon, who always knows how to put words in the proper order; Lili, Dafni (the world's best stress relief), and Stergios (x3): the warmest foster family, as well as Athina for that "conclusive" rosé; my ISUP squad and especially Lilith, Ruby, Baptiste, and Adel, for generously brightening the darkest of my days; Eliza, Penny, and Konstantinos: parmi nous, since 2015; Sofia, Diamantis, and Aggerou, my chosen family; my Samos squad, and especially, Mimis, Chris, and Korina, who have always been available to share a coffee or an existential crisis; Giorgos, Kostas, and Elli for all the fishy wine and the mischiefs; Akis, Ilias, Edo, and Dimitra: la brigade du manuscrit; Maria S., my other half in "les demoiselles de Blomet"; Erifyli, my other half in omg-look-how-tired-I-am-let's-go-fall-asleep-at-the-movies; Vaggos, Simsis and Sotos for all our Kithira; Nicki and Maria Ch. thank you for the memories and for lending me my vagabond shoes; Fenia, my eternal $\delta\iota\alpha\kappa\sigma\pi\sigma\tau\alpha\acute{\iota}\rho\iota$; Alexandra, my favorite seal and otter observer; my Flawless squad and especially Olga, for the fabulous cover; Myrto, mi Bruja, and Katerina, mio Tsitso, an eternal thank you for that part of myself, the least rational and most magical, that belongs to you, that I promise to always cherish and take good care of; E. M., pour toutes les heures (du régard) à l'écoute; Yannis, for all the hours you put into waiting, for your excellent, elegant advice, always to the point, for carefully listening, and for sincerely caring.

And the warmest thank you to my sweet parents, Nana and Nasos, my older brother Spyros, my aunts Amalia and Miranda, uncle Giannis and Ghislaine, my cousins Elena and Joy, my foster mother Maria, my adopted sisters Elena and Thania, and my late grandma Zoe, thank you for your immense support, the assets you provided me with, the resources, curiosity, willpower, independence, and eagerness to learn and evolve, for being loving and caring, and for always creating safety nets; infinitely thank you, from the bottom of my heart.

Let's wander.[1]

[1] I hope I am not forgetting anyone!

Communications and supervisions

Articles

- **Published Paper - The Green Journal | Radiotherapy and Oncology**
  Chounta S, Lemler S, Haddy N, Fresneau B, Mansouri I, Bentriou M, Demoor-Goldschmidt C, Diallo I, Souchard V, Do TD, Veres C, Surun A, Doz F, Llanas D, Vu-Bezin G, Rubino C, de Vathaire F, Letort V, Allodji RS.

  The risk of valvular heart disease in the French Childhood Cancer Survivors' Study: contribution of dose-volume histogram parameters

  DOI: 10.1016/j.radonc.2023.109479

  PMID: 36657724

- **Conference Paper, ACML- 2022**
  Bentriou M, Chounta S, Allodji RS, Lemler S, Thi Do D, De Vathaire F, Diallo I, Christodoulidis S, Vakalopoulou M, Letort Le Chevalier V.

  Deep learning-based representations for cardiac voxelized dosimetric data from childhood cancer therapy

- **Published Paper - Cancers (Basel)**
  Chounta S, Allodji RS, Vakalopoulou M, Bentriou M, Thi Do D, De Vathaire F, Diallo I, Fresneau B, Charrier T, Zossou V, Christodoulidis S, Lemler S, Letort Le Chevalier V.

  Dosiomics-based prediction algorithms of radiation-induced valvulopathy (application on data from childhood cancer survivors in France)

  DOI: 10.3390/cancers15123107

  PMID: 37370717

- **Paper In Progress**
  Bentriou M, Chounta S, Balde MH, Allodji RS, Thi Do D, Letort Le Chevalier V, Lemler S.

  Using clustering methods to explore the heart radiation dose distribution to predict late valvulopathy after childhood cancer

- **Paper In Progress**
  Chounta S, Allodji RS, Bentriou M, Thi Do D, Letort Le Chevalier V, Lemler S.

  External validation of the dosiomics signature of radiation-induced valvulopathy with data of childhood cancer survivors.

Oral and Poster Presentations

- **Posters, 2021 ISCB42**- virtual, July 2021 and **SIOP 2021**- virtual, September 2021
  Chounta S., Allodji RS, Letort Le Chevalier V, Lemler S.
  The risk of valvular heart disease after childhood cancer: contribution of dose-volume histogram parameters
- **Oral presentation, September 2022- Mardis Scientifiques du CESP**
  Chounta S, Aba N.
  Les pathologies cardiaques dans la FCCSS : études de dosimétrie et de transcriptome
- **Poster, 2022 RadReS** 68th Annual Meeting, Hawaii October 2022 and **ISORED 2023** - Spain, May 2023
  Chounta S., Allodji RS, Letort Le Chevalier V, Lemler S.
  Dosiomics-based prediction algorithms of radiation-induced valvulopathy
- **Oral presentation, May 2023- ISORED**
  Chounta S., Allodji RS, Letort Le Chevalier V, Lemler S.
  The risk of valvular heart disease in the French Childhood Cancer Survivors' Study: contribution of dose-volume histogram parameters

Other Publications

- **Paper under revision - JACC: CardioOncology**
  Charrier Th., Haddy N., Schwartz B., Journy N., Fresneau B., Demoor-Goldschmidt C., Diallo I., Surun A., Aerts I., Doz F., Souchard V., Vu-Bezin G., Laprie A., Letort V., Rubino C., Chounta S., de Vathaire F., Latouche A., Allodji RS
  Increased Cardiac Risk After a Second Malignant Neoplasm Among Childhood Cancer Survivors, an FCCSS Study

Research Supervisions

- **Assistant to the professor, 2019-2021** Tutoring and Practical labs (winter semester)- Modeling for life sciences (Prof. V. Letort-Le Chevalier)
- **Co-supervisor, 2020** end-of-year project - *Impact of the BMI variation in oncology survival* (Prof. V. Letort-Le Chevalier)
- **Co-supervisor, 2022** end-of-studies internship and master thesis of Mamadou Hady Balde (Modélisation et Analyse Mathématique Université de Rouen Normandie)
  Supervisors: Allodji RS, Bentriou M, Chounta S, Lemler S, Letort Le Chevalier V.
  Using clustering methods to explore the heart radiation dose distribution to predict late valvulopathy after childhood cancer

Contents

List of Tables

List of Figures

Abbreviations

BRF	-	*Balanced Random Forest*
CC	-	*Childhood Cancer*
DVH	-	*Dose-Volume Histogram*
ERR	-	*Excess of Relative Risk*
FCCSS	-	*French Childhood Cancer Survivors' Study*
GLCM	-	*Gray Level Co-occurrence Matrix*
GLDM	-	*Gray Level Dependence Matrix*
HR	-	*Hazard Ratio*
ICCC	-	*International Classification of Childhood Cancer*
MHD	-	*Mean Heart Dose*
RF	-	*Random Forest*
TPS	-	*Treatment Planning Software*
VHD	-	*Valvular Heart Disease*
wtRF	-	*weighted Random Forest*

Résumé long en français

Contexte : Vers des modèles prédictifs personnalisés des risques de valvulopathie liés aux effets iatrogènes des radiations

Le cancer est la première cause de mortalité prématurée en France et dans le monde, à ce titre, la prise en charge des cancers est un enjeu prioritaire de santé publique ("Institut National Du Cancer", 2023). Les progrès thérapeutiques sur les cancers pédiatriques de ces dernières années ont permis dans les pays développés d'obtenir un taux de survie à 5 ans (après leur diagnostic) de plus de 80% ("Cancer Atlas", 2023). On estime qu'il y a actuellement en Europe entre 300 000 et 500 000 personnes guéries d'un cancer de l'enfant, et qu'une personne sur 1000 est une personne guérie d'un cancer de l'enfant.

Parmi les patients atteints de cancer, plus de 50% ont reçu un traitement de radiothérapie. La radiothérapie est une méthode de traitement local des cancers, utilisant les rayonnements ionisants pour détruire les cellules cancéreuses tout en épargnant les tissus sains périphériques. Elle peut être utilisée seule ou en association avec la chirurgie et la chimiothérapie. Son efficacité est unanimement reconnue. Malheureusement, son principal inconvénient est qu'en irradiant une tumeur, on ne peut éviter complètement d'irradier les tissus sains environnants. Du fait de leur faible corpulence, les enfants peuvent être davantage affectés. Les effets des rayonnements ionisants sur la santé humaine, en particulier chez les enfants, suscitent de nombreux débats et sont un sujet de préoccupation majeur en santé publique. Cela d'autant plus que les études effectuées suite aux bombardements d'Hiroshima et Nagasaki, ont montré que les enfants sont plus sensibles que les adultes à l'irradiation. Du fait qu'en irradiant une tumeur, même de manière ciblée, les tissus qui entourent la tumeur sont irradiés sur plusieurs centimètres car le corps rediffuse les doses reçues, ce qui peut entraîner des effets iatrogènes à plus ou moins long terme (Armanious et al., 2018; Erdmann et al., 2021; Landier et al., 2018).

Contrairement aux cancers de l'adulte, qui surviennent le plus souvent à un âge avancé, les cancers de l'enfant touchent des personnes qui ont toute la vie devant elles. Les personnes guéries d'un cancer de l'enfance peuvent être confrontées à un large spectre d'événements iatrogènes, notamment des cancers secondaires, des pathologies cardiovasculaires, des complications neurosensorielles et un éventuel vieillissement précoce par rapport à l'âge biologique réel. Si les publications sont très nombreuses sur ce thème, il persiste encore beaucoup d'incertitudes sur le rôle précis de la radiothérapie dans la survenue de ces évènements iatrogènes. De plus, l'étude des risques associés aux rayonnements ionisants dans la population des personnes traitées par radiothérapie permet d'évaluer l'impact des différents niveaux doses (élevées, modérées et faibles) ce qui n'est strictement pas possible dans d'autres populations d'étude. Parmi les évènements iatrogènes tardifs, les maladies cardiaques et les seconds cancers sont les plus graves et les plus menaçants pour la vie des patients des anciens patients de cancer pédiatrique. La valvulopathie est l'un des troubles cardiaques les plus fréquents chez les enfants ayant survécu à un cancer (Haddy et al., 2016; Mulrooney et al., 2020; Nathan et al., 2016).

Une détection tardive des les évènements iatrogènes limite les possibilités de traitement et un

dépistage fréquent pour tous peut ne pas être rentable dans le contexte d'optimisation des ressources. Par conséquent, la l'identification des patients à haut risque d'événements iatrogènes secondaires permettrait de mieux les prévenir, dépister et traiter rapidement et d'accroitre ainsi leurs chances de guérison.

Les lignes directrices du Children's Oncology Group Long-Term Follow-Up Guidelines for Survivors of Childhood, Adolescent, and Young Adult Cancers (Hudson et al., 2021) fournissent des recommandations de surveillance pour les anciens patients de cancers pédiatriques qui se présentent pour un suivi médical de routine basé sur l'exposition. Étant donné la grande variabilité interindividuelle de la réponse des enfants aux traitements, en particulier à long terme, de tels protocoles standardisés de suivi des patients après des traitements de radiothérapie peuvent conduire à une détection erronée ou tardive d'événements iatrogènes. En outre, l'adoption de programmes de dépistage à haute fréquence ne serait pas viable à long terme et pourrait être très anxiogène pour les patients, voire préjudiciable à leur santé. Les avantages d'un dépistage aussi équitable que possible apparaissent ainsi de manière évidente.

L'augmentation des taux de survie et la nécessité croissante d'un dépistage rigoureux des complications tardives ont conduit à la création de grandes cohortes avec des suivis longitudinaux de longue durée. La Childhood Cancer Survivor Study (États-Unis et Canada), la British Childhood Cancer Survivor Study, la French Childhood Cancer Survivor Study et le consortium PanCareSurFup créé pour rassembler de nombreuses cohortes européennes sont quelques exemples de cohortes de survivants à 5 ans. Cependant, parmi celles-ci, l'étude French Childhood Cancer Survivors Study (FCCSS) est la seule à disposer d'une dosimétrie individuelle voxélisée pour presque tous les membres de la cohorte traités par radiothérapie.

Notre cas d'étude : les valvulopathies

Contrairement à l'insuffisance cardiaque et à la maladie coronarienne (Bates et al., 2019; Mansouri et al., 2019; Shrestha et al., 2021), les facteurs de risque potentiels d'une valvulopathie tardive (VHD) après traitement pour un cancer pédiatrique n'ont pas encore été étudiés et compris de manière approfondie.

La VHD est l'une des complications les plus graves de la radiothérapie en raison de son association avec d'autres complications cardiaques. Plus précisément, selon le CDC, 2023, s'ils ne sont pas diagnostiqués et traités correctement, les problèmes de valves cardiaques peuvent entraîner une arythmie, une pression sanguine dans les poumons, une insuffisance cardiaque, ou même, un arrêt cardiaque. Une étude a également établi un lien statistique entre les VHD et la maladie coronarienne (Matta & Moussallem, 2019).

En ce qui concerne le risque radio-induit d'avoir une VHD, de nombreuses questions restent peu clair.

Approches traditionnelles sur la modélisation du risque radio-induite

Alors que les avancements médicales rendre de plus en plus rare une dose moyenne au cœur élevée, les nouvelles techniques d'administration de la radiothérapie, telles que l'IMRT ou la VMAT, peuvent augmenter le volume recevant des doses de rayonnement faibles et intermédiaires. La survenue d'une

VHD radio-induite doit donc être étudiée en relation avec le niveau de la dose d'irradiation délivrée au cœur ainsi qu'avec le volume du cœur absorbant des doses d'un certain niveau. Il existe un risque établi pour les fortes doses (> 30 Gy) (Cella et al., 2011; Gujral et al., 2016). Des hypothéses (Patil et al., 2022) sur le rôle des doses plus faibles ont aussi été faites : une étude récente a démontré que les grands volumes cardiaques irradiés avec de faibles doses pourraient augmenter le taux de toute maladie cardiaque (Bates et al., 2019). Mais il n'y a toujours pas de consensus sur la VHD particuliérement, et il est donc crucial d'étudier les détails du risque de VHD induit par l'irradiation et le rôle du volume cardiaque irradié.

On peut distinguer deux grandes tendances pour les modèles de risque radio-induit : les approches traditionnelles reposant principalement sur une variable agrégée (généralement la dose moyenne ou médiane à l'organe concerné) et les tendances récentes avec des représentations spatialement explicites de la distribution de la dose.

Les variables indépendantes les plus couramment utilisées pour modéliser le risque de VHD radio-induite sont la dose moyenne et la dose médiane au cœur (Cutter et al., 2015; van der Pal et al., 2015a). Cependant, on ne sait pas si la relation entre la dose moyenne au cœur (MHD) et la survenue d'une VHD est linéaire (Cutter et al., 2015). En outre, la dose moyenne et la dose médiane au cœur ne permettent pas de comprendre le rôle de l'hétérogénéité spatiale des doses absorbées ; cette question reste peu étudiée dans la littérature, principalement en raison du manque de données adéquates à l'échelle du voxel pour le cœur entier ou ses sous-structures.

La disponibilité de la reconstruction de la dose à l'échelle du voxel ouvre la possibilité d'aller au-delà de la utilisation simplement de la MHD pour décrire les effets des rayonnements dans les modèles de risque. Certains auteurs (Cella et al., 2015) ont proposé de calculer l'histogramme dose-volume (DVH) pour résumer les distributions de dose 3D dans un graphique informatif 2D. Les histogrammes cumulatifs sont tracés avec les doses par binôme le long de l'axe des x, et le k^{th} percentile est noté D_{100-k} (par exemple, D_{50} est la médiane). La première colonne représente le volume du cœur ayant absorbé une dose supérieure ou égale à la dose du bac. Par exemple, $V_{40:Gy}$ est le volume du cœur qui a absorbé une dose de ≥ 40 Gy. Certaines études ont déjà utilisé les indicateurs DVH avec des résultats prometteurs, comme (Cella et al., 2015; Shrestha et al., 2021) chez les adultes et Mansouri et al., 2019 et Bates et al., 2019 en oncologie pédiatrique. Cette définition des variables V_k ne permet pas d'étudier l'effet des faibles doses indépendamment du risque induit par les fortes doses. Pour résoudre ce problème, nous avons étudié chaque indicateur V_d dans des intervalles de doses, avec une coupure sur les fortes doses qui se traduit par une troncature de la population.

Pour étudier plus en profondeur le rôle de la distribution spatiale des doses, certaines études récentes ont introduit le calcul et l'incorporation dans les modèles de classification des caractéristiques *dosiomics* (Liang et al., 2019; Wu et al., 2020; Yang et al., 2022). Inspirée par l'approche *radiomics*, traditionnellement mise en œuvre pour l'analyse de l'imagerie médicale via un algorithme de caractérisation des données, l'extraction de ces caractéristiques a le potentiel de révéler des associations spatiales de la distribution de la dose au cœur avec l'occurrence de la VHD radio-induite après le traitement d'un cancer chez l'enfant. Les caractéristiques dosiomiques se sont révélées prometteuses et, dans certains cas, plus efficaces que les paramètres DVH (Murakami et al., 2022; Ren et al., 2021).

Les cohortes et les données

Pour répondre à ces objectifs, nous nous sommes appuyés sur les données de deux cohortes, la FCCSS et PanCare-Sur-Fup-ProCardio : En nous basant sur le design de ces deux cohortes, nous avons adapté le choix des modèles utilisés tout au long des analyses. Les prérequis statistiques de nos analyses sont brièvement rappelés dans le chapitre 2.

- La FCCSS est une cohorte de 7670 survivants à 5 ans traités entre 1946 et 2000 pour les cancers solides de l'enfant les plus fréquents en France. Les analyses effectuées dans le cadre de cette thèse ont porté sur 7492 survivants disposant de données complètes (97.7% de la cohorte FCCSS), dont 3906 avaient été traités par radiothérapie. Quatre-vingt-un individus (1 %) ont développé une VHD tardive grave après traitement pour un cancer chez l'enfant ; parmi eux, 63 avaient été traités par radiothérapie. Par conséquent, certaines des méthodes employées tiennent compte de la nature déséquilibrée de la cohorte en ce qui concerne la prévalence de la VHD.

- L'étude cas-témoins imbriquée dans PanCareSurFup-ProCardio, une vaste cohorte paneuropéenne de plus de 42 000 survivants à 5 ans, a été conçue pour évaluer en détail les facteurs de risque de VHD liés au traitement. Au total, 274 survivants ont été inclus dans une étude cas-témoins appariée, et 224 d'entre eux, dont les données dosimétriques étaient complètes, ont été inclus dans nos analyses. Chaque cas de VHD a été apparié à un témoin sur la base du sexe, de l'âge au premier diagnostic de cancer primaire (1 an), de l'année du premier diagnostic de cancer primaire (3 ans), de la durée du suivi (le suivi de chaque patient témoin a été au moins aussi long que le suivi du cas apparié) et du centre de traitement.

Notre première contribution consiste en quelques analyses descriptives de la cohorte FCCSS et, dans une moindre mesure, de la cohorte PanCareSurFup-ProCardio, en ce qui concerne les caractéristiques liées à la VHD (voir Chapitre 3).

Les principales contributions

L'objectif principal de cette thèse a été d'explorer la distribution de la dose de radiation au cœur à l'aide de matrices de dose à l'échelle du voxel et de proposer des approches alternatives dans la modélisation du risque radio-induit de la VHD après le traitement pour un cancer chez l'enfant.

De nouveaux indicateurs dose-volume, mettant en lumière le rôle de faibles doses

Tout d'abord, nous avons confirmé certains résultats antérieurs selon lesquels il y a une augmentation du risque d'occurrence de VHD parmi les survivants de la FCCSS qui ont été traités par radiothérapie. De plus, l'analyse des données dosimétriques nous a permis d'observer que la dose moyenne au cœur (MHD) est positivement associée au risque d'occurence de VHD. Nous avons également pu exprimer le risque radio-induit aussi en termes de volume cardiaque irradié au lieu du niveau de dose absorbé par le cœur (*indicateurs de dose-volume bornés*) et nous avons constaté que des doses faibles à modérées absorbées par un grand volume cardiaque sont également un facteur de risque. Plus précisément, l'analyse des indicateurs dose-volume bornés ($V_{d_1}|_{V_{d_2}=0\%}$) a

permis d'obtenir les résultats suivants : les doses élevées (≥ 40 Gy) sont statistiquement associées à une VHD tardive, même lorsqu'elles sont absorbées par $< 10\%$ du volume cardiaque ; les doses 20-40 Gy induisent un risque statistiquement significatif lorsque plus de 90% du volume cardiaque est impliqué ; et enfin les doses 5-20 Gy induisent un risque statistiquement significatif de subir une VHD lorsque de grands volumes du cœur (90%) sont impliqués dans le champ d'irradiation. L'hypothèse selon laquelle des doses modérées et faibles (<15 ou 20 Gy) à un volume cardiaque étendu pourraient être un facteur de risque n'avait été émise qu'avant notre étude (Cutter et al., 2015), et à notre connaissance, il s'agit de la première étude à fournir des preuves à l'appui de cette hypothèse. Ces résultats justifient que l'utilisation d'indicateurs dose-volume définis par des intervalles de dose bornés $(d_1 - d_2)$ pourrait être informative et devrait être généralisée dans les travaux épidémiologiques. Ce détail méthodologique semble simple (déjà proposé par Bates et al., 2019), cependant, l'inclusion d'indicateurs dose-volume bornés n'est pas encore standardisée dans la littérature, alors qu'elle permet d'étudier et d'exprimer l'effet de doses plus faibles indépendamment de l'effet déjà établi de doses plus élevées.

Les résultats de ces travaux ont été publiés dans le Green Journal (Radiotherapy and Oncology) (Chounta et al., 2023).

L'approche dosiomique

Des caractéristiques dosiomiques ont été extraites et évaluées à l'aide d'algorithmes d'apprentissage supervisé. Un riche ensemble de variables a été pris en compte pour les modèles d'apprentissage supervisé, afin de tenir compte des caractéristiques spatiales complexes de la dose délivrée au cœur. L'extraction des caractéristiques était basée sur des biomarqueurs d'image standardisés (Zwanenburg et al., 2020), et leur pouvoir prédictif a été comparé à celui du modèle de base basé sur la dose moyenne au cœur. À notre connaissance, il s'agit de la première étude explorant la performance des caractéristiques dosiomiques dans la prédiction d'une VHD tardive.

Nos résultats indiquent que cette hypothèse pourrait se vérifier, car les modèles de classification basés sur de multiples caractéristiques descriptives ont un pouvoir prédictif supérieur à celui du modèle de base basé sur la dose cardiaque moyenne. Nous avons donc proposé une signature *dosiomique* pour la FCCSS et avons complété l'étude en testant cette signature sur une cohorte européenne indépendante.

Nos résultats montrent qu'une combinaison de caractéristiques descriptives de la dose pourrait être plus efficace que les modèles basés uniquement sur la dose moyenne au cœur dans la prédiction d'une VHD tardive lorsqu'ils sont entraînés sur une population dont les doses au cœur ne sont pas homogènes (uniformité de la dose < 1 Gy). Cette approche repose sur l'hypothèse que l'hétérogénéité spatiale des doses reçues par le cœur peut être associée à la survenue d'une VHD, au-delà du risque déjà établi induit par les fortes doses. Si cette hypothèse se vérifie, cela pourrait signifier que les statistiques sommaires telles que la dose moyenne ou médiane au cœur sous-estiment le risque induit et que les caractéristiques spatiales de la dose devraient être prises en considération. Avec l'aide de l'algorithme Random Forest, qui permet de prendre en compte des relations autres que linéaires, et de certaines caractéristiques spatiales détaillées, nous avons pu améliorer les prédictions par rapport à la modélisation linéaire classique basée sur la dose moyenne au cœur.

Les améliorations apportées par les caractéristiques dosiomiques par rapport à la dose moyenne ne sont peut-être pas encore totalement convaincantes, probablement en grande partie à cause de

la nature déséquilibrée des données (environ 1 % dans la FCCSS et environ 3 % chez les survivants dont les doses cardiaques ne sont pas homogènes). D'autres études sont absolument nécessaires.

Les résultats de l'approche dosiomiques, ont été soumis au journal *Cancers* et revus, et sont en cours de révisions.

Confrontation des résultats à la cohorte PanCare

La confrontation avec l'étude cas-témoins de la cohorte PanCare a permis d'obtenir des résultats optimistes. La signature dosiomique proposée par les analyses de la FCCSS a été incluse dans les algorithmes de classification visant à prédire les cas de l'étude PanCare. Cela nous a permis de comparer l'importance des caractéristiques en commun entre les deux cohortes, et d'observer des caractéristiques au délà des statistiques classiques, telles que la Grande dépendance d'Accentuation du Niveau de gris élevé (Large Dependence High Gray Level Emphasis- GLDM), la Racine de la Moyenne Quadratique (Root Mean Squared- Statistiques de Premier Ordre), la Somme Moyenne (Sum Average- GLCM), ainsi que la Dose Cardiaque Moyenne (MHD- Statistiques de Premier Ordre), qui figurent parmi les caractéristiques les plus importantes dans les deux cohortes.

Discussion et perspectives

Les analyses approfondies de la FCCSS ont permis d'obtenir d'autres résultats sur le risque de subir une VHD tardive après un cancer de l'enfant. Une observation importante est que l'excès de risque relatif (ERR) dans la FCCSS est très faible avant l'âge de 30 ans (4 %), et augmente chaque décennie suivante (94 %, 228 % et 312 % pour les survivants âgés de plus de 50 ans). Nous n'avons pas observé de changement dans les estimations du risque lorsque les modèles ont été ajustés sur l'âge au moment du diagnostic de cancer et aucune association n'a été observée avec l'année au moment du diagnostic.

Comme Cutter et al., 2015, nous n'avons pas mis en évidence des preuves sur l'association des anthracyclines ou d'autres agents avec la survenue d'une VHD. Une explication possible est que, bien que l'utilisation d'anthracyclines ait déjà été associée à la cardiotoxicité (Haddy et al., 2016), et à la VHD, en particulier, (Mulrooney et al., 2009), dans cette étude, les survivants ayant subi un autre événement cardiaque avant leur diagnostic de VHD n'ont pas été considérés comme ayant subi l'événement. Dans les études futures, il pourrait être nécessaire de prendre en compte les risques concurrents de complications cardiaques et de mortalité avant la survenue d'une VHD.

Le fait que la dose cardiaque moyenne ou médiane se distingue est également un résultat important. Le fait que la dose moyenne ou médiane au cœur puisse être une caractéristique explicative suffisante pour la prédiction du risque est une conclusion très précieuse et rassurante pour les praticiens, en particulier pour les cohortes où les données dosimétriques voxélisées ne sont pas disponibles. Cependant, il est plus difficile de tirer une conclusion "négative" comme celle-ci, car il faut s'assurer que les modèles eux-mêmes ne peuvent pas être améliorés. Ce travail constitue la première étape de cette vaste question de recherche.

Les résultats fournis par cette thèse contribueront à améliorer les recommandations internationales pour la surveillance des survivants du cancer chez l'enfant pour le risque de valvulopathie.

Synthèse du manuscrit

Ce mémoire est organisé en sept chapitres. Dans le Chapitre 1 nous avons présenté le contexte médicale et le raisonnement derriere nos analyses. Le Chapitre 2 présente les généralités sur les approches méthodologiques statistiques. Le Chapitre 3 contient les descriptifs de la cohorte FCCSS ainsi que de l'étude cas-témoins niche dans la cohorte PanCareSurFup-Procardio. Dans le Chapitre 4 sont présentés les résultats de l'analyse de survie et les modèles de risque sur les données de la FCCSS. Le chapitre 5 est composé par le résultats des modèles de classification basés sur les features dosiomiques, et d'une analyse de sensibilité basée sur l'heterogeneité de la dose au cœur, toujours sur les données de la FCCSS. Dans le Chapitre 6 nous avons présenté la confrontation des modèles precedents avec l'étude cas-témoins de la cohorte PanCareSurFup-Procardio. Finalement, dans le dernier Chapitre 7 nous faisons la discussion générale, et nous présentons nos contributions, les limitations et les perspectives de nos travaux.

1 - Introduction

Survival rates of childhood cancer have significantly risen during the last few decades; however, so has the occurrence of late effects of childhood cancer treatments. Traditionally, radiation-induced risk of cardiovascular disease is estimated from the total or the mean dose absorbed by the heart or its components. In this thesis, we explore approaches that allow taking into account the spatial heterogeneity of radiation doses absorbed by the heart while modeling the risk of experiencing a late valvular heart disease after treatment for childhood cancer.

1.1 . Incidence and survival rates of Childhood Cancer

Incidence Rates

Childhood cancer has an average annual worldwide incidence of 140 new cases per million children under 15 years old ("Cancer Atlas", 2023). Cancer incidence in children and adolescents has increased by 0.5 to 1 percent per year in high-income countries with established cancer registries over the past few decades. It is estimated that between 300,000 and 500,000 people are cured of childhood cancer in Europe, which translates to one in every 1,000 individuals.

In France, a standardized incidence rate of 156 cases per million children per year is estimated, representing about 1,700 new cases diagnosed each year in children under 15 years and 800 in teenagers from 15 to 18 years old ("Institut curie", 2023; "Institut National Du Cancer", 2023; "RNCE", n.d.). The most frequent pediatric cancers are leukemias (29%), followed by central nervous system tumors (23%), and lymphomas (10%).

Incidence rates vary when we take into consideration the age of diagnosis ("RNCE", n.d.). For example, among one-year-olds, the most frequent type of childhood cancer is neuroblastomas, followed by CNS neoplasms and leukemias, while the prevalence of lymphomas is very low. In contrast, leukemia and CNS neoplasms are among the two most common types diagnosed among children older than one-year-old. Lymphomas are children's third most frequent type of childhood cancer despite their low prevalence among one-year-olds, followed by soft-tissue sarcomas, renal tumors, and bone tumors (Table 1.1).

Survival Rates

Thanks to pediatric oncology advances, survival rates have also increased over the last several decades in high-income countries (Botta et al., 2022; "SEER Cancer Statistics Review", n.d.). More

than 80% of childhood cancer patients in high-income countries survive five years after their diagnosis ("Cancer Atlas", 2023). Trends in survival rates from the UK registry are figured in 1.1.

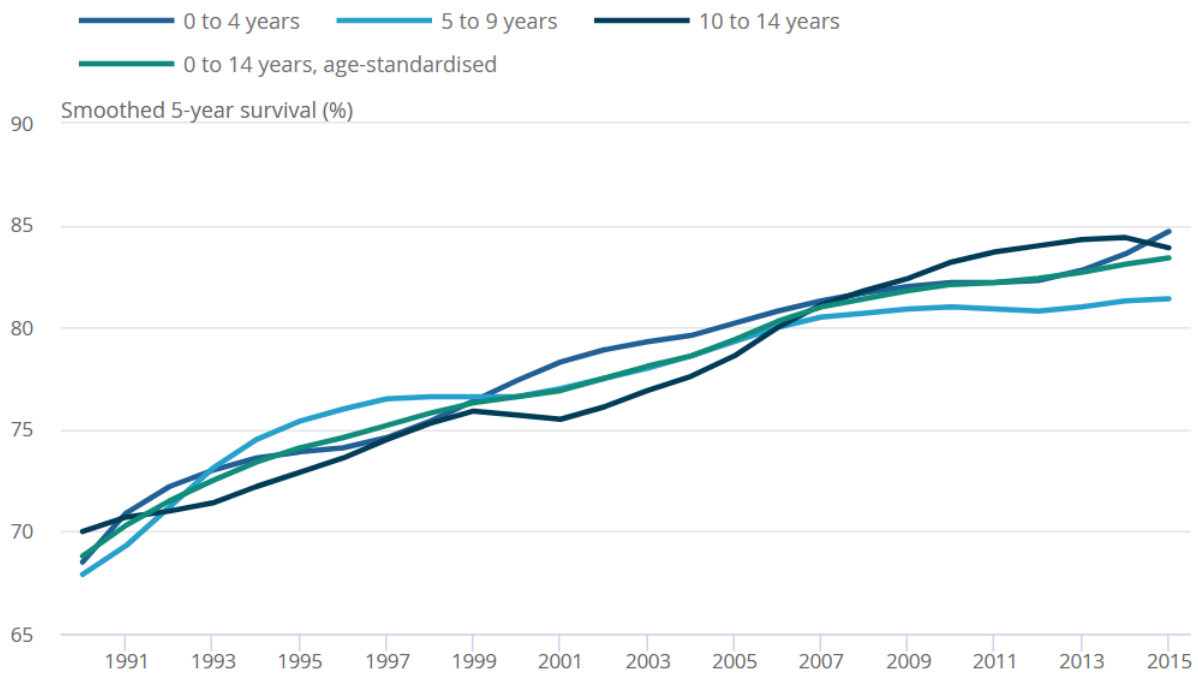

Figure 1.1: Smoothed trends in 5-year survival (%) of childhood cancers between 1990 and 2015 in the UK ((UK), 2023).

In France, between 2010-2016, the survival rate for leukemias was 87.6%, for CNS neoplasms 76.5% and lymphomas 95.8%, and up to 100% for retinoblastoma. The lowest survival rate of 73.1% was observed for bone tumors (Table 1.1).

The increase in survival rates is a very important achievement of modern medicine. It has led, however, to a growing population of childhood cancer survivors, who are susceptible to experiencing complications later in life, partially due to treatments they received at a young age. Late iatrogenic effects are, unfortunately, an existing public health issue, and guidelines are constantly emerging for effective follow-up of childhood cancer survivors.

1.2 . Treatment and late effects

The majority of children nowadays are treated according to standardized protocols.

Table 1.1: Incidence rate of childhood cancers between 2010 and 2014 in France (mainland) and 5-year survival rates of patients treated between 2010 and 2016 (% [95% interval]) according to the National Registry of Childhood Cancer of France ("RNCE", n.d.).

Type of Childhood Cancer diagnosis	Incidence rate (per million)	Survival Rate	
Leukemias, myeloproliferative diseases, and myelodysplastic diseases	514	87.6	[86.4-88.7]
Lymphomas and reticuloendothelial neoplasms	184	95.8	[94.6-96.8]
CNS and miscellaneous intracranial and intraspinal neoplasms	442	76.5	[75.0-78.0]
Neuroblastomas and other peripheral nervous cell tumors	142	80.3	[77.5-82.9]
Retinoblastomas	48	100	-
Renal tumors	98	93.3	[91.0-95.0]
Hepatic tumors	20	87	[79.8-91.7]
Malignant bone tumors	82	73.1	[68.9-76.8]
Soft tissue and other extraosseous sarcomas	112	74.8	[71.4-77.8]
Germ-cell tumors, trophoblastic tumors, and neoplasms of gonads	60	96.5	[94.3-97.9]
Other malignant epithelial neoplasms and malignant melanomas	64	93.3	[90.5-95.4]
Other and unspecified malignant neoplasms	4	81.8	[63.9-91.4]
All cancers (excluding Langherhans cell histiocytosis)	1770	84.6	[83.9-85.2]

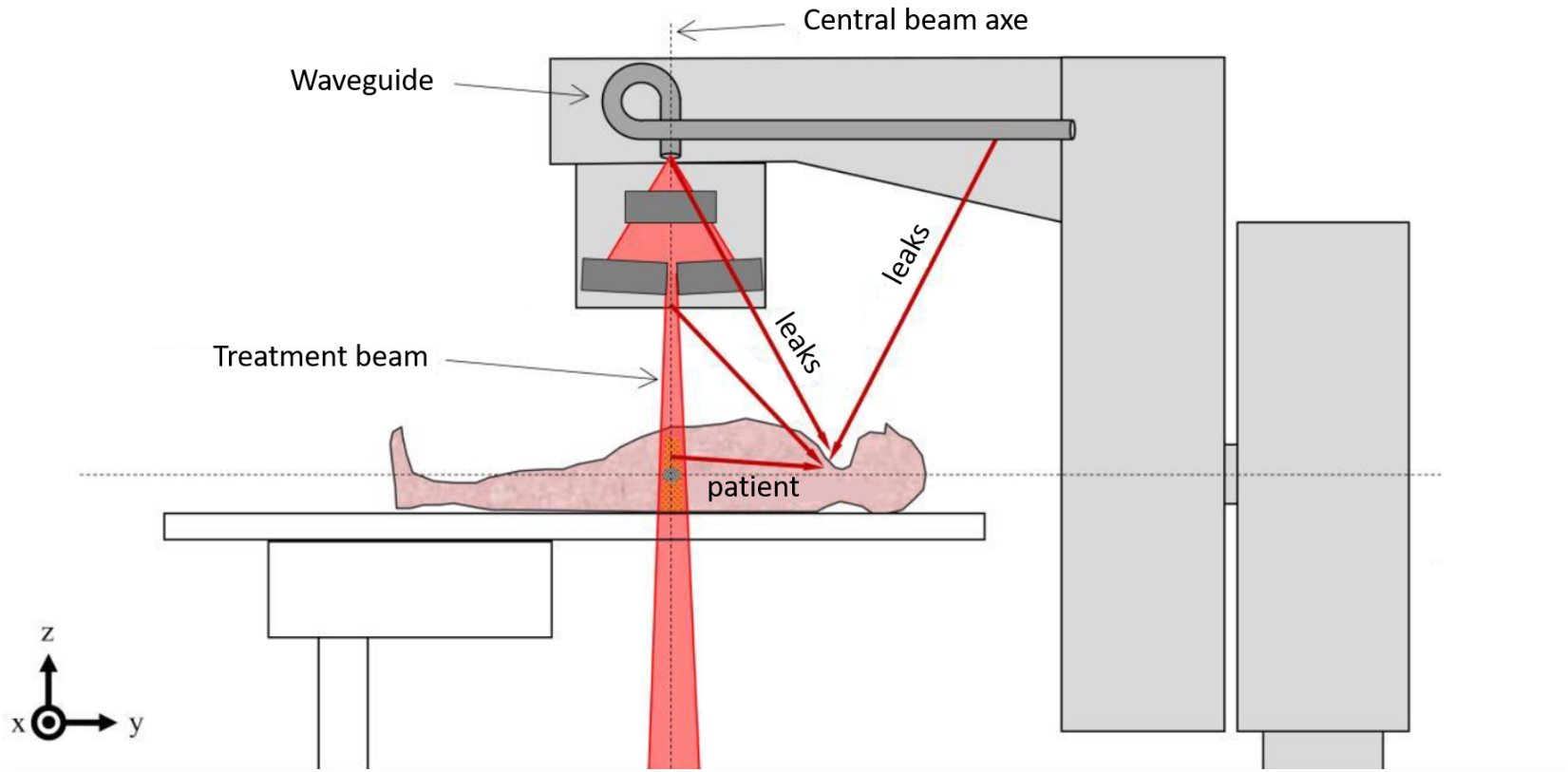

Figure 1.2: Figure illustrating the main sources contributing to the out-of-field dose on the patient's body at a given point. The red arrows illustrate the direction of photons starting from each source. Figure by Jérémy V$\tilde{u}$ Bezin.

Radiotherapy

Since Marie Skłodowska-Curie described radioactivity more than 100 years ago, radiotherapy has become one of the main assets of oncology, along with surgery and chemotherapy. Protocols are defined according to the type of cancer and the patient's age. Treatments are constantly evolving to become more effective against cancer and safer regarding their secondary effects. However, despite recent technologic advancements (Hoppe et al., 2012), the irradiation of surrounding healthy tissues is still difficult to avoid and often leads to late iatrogenic effects.

Two main types of radiotherapy can be distinguished: internal and external beam radiation therapy. In internal radiation therapy (brachytherapy), radioactive material is injected directly or close to a tumor in order to shrink it. External beam radiation therapy is a treatment where cancer cells are targeted with high doses of radiation from outside the body, aiming for tumor shrinkage. It is usually combined with chemotherapy and/or surgery. It is used on many cancer patients to treat several types of tumors, including head and neck, breast, lung, colon, and prostate cancers. Specialized computer software adjusts the beam's size and shape. Different radiation types for external beam therapy include orthovoltage x-ray machines, Cobalt-60 machines, linear accelerators, proton beam machines, and neutron beam machines. In this thesis, we study the late effects of external beam radiation therapy.

Radiotherapy treatment planning requires specifying two elements: radiation level and radiation field. The radiation level in external beam radiation depends on the tumor location: cancers located deeper in the body are treated with high-energy radiation. Low-energy radiation does not penetrate very deeply into the body and is used mainly to treat surface tumors such as skin cancer. Stereotactic radiation therapy, a practical and effective approach in treating small tumors such as those in the head and brain, involves focusing the radiation beam on a small area and delivering very high doses. With this approach, a tumor is targeted from many different directions so the radiation beams converge on it. This way, the ideal amount of radiation needed to destroy tumor cells is delivered directly to the growing tumor while the exposure to the area surrounding the tumor is minimized. Radiation fields are determined so that the maximum radiation dose is provided to the tumor while it is minimized for surrounding organs. Recent advancements like stereotactic radiation help target cancerous tissues while avoiding vital organs more accurately. However, due to localization uncertainties when targeting a tumor and leakage radiations (Figure 1.2), healthy tissues may not be entirely excluded from the radiation field. This is typically the case for mediastinal radiation for Hodgkin lymphoma: the tumor can be close to the heart, and, therefore, irradiation of normal vital structures is sometimes unavoidable and may lead to chronic complications ("SEER Cancer Statistics Review", n.d.).

The optimization of dose delivery is called *medical dosimetry*. There exist a few different SI units of radiation dose. Data analyzed in this thesis are provided in gray (Gy), that is, the energy absorbed per unit of mass (J/kg) ("ICRPaedia", 2023). Delivery parameters of a prescribed dose are determined during treatment planning using specialized treatment planning software (TPS). The planner will design a plan that delivers a uniform dose to the tumor from several angles or sources to sum to the total necessary dose while minimizing doses to surrounding healthy tissues.

Dose reconstruction

Radiation doses an organ absorbs during a radiotherapy session cannot be directly measured. Estimations are, however, required for reasons that concern radiation protection. Consequently, retrospective estimation has been developed for survivors with available long-term follow-up and monitoring data. It is nowadays possible to retrieve the three-dimensional distribution of the administered radiation dose according to the patient's anatomy during radiation. Voxel-scaled dose distributions can be provided as a dose matrix (Alziar et al., 2009; Veres et al., 2014).

A model of the human anatomy is required for this task. Numerous models, representing adult males and females, children and pregnant women, have been developed from carefully segmented and labeled whole-body images (Xu, 2008; Zaidi, 2007). It is possible nowadays to produce realistic individual patient-adjusted whole-body virtual phantoms (Diallo et al., 1996; Francois et al., 1988), far from the earlier mathematical phantoms characterized by a somewhat schematic anatomic appearance (anatomy being represented by geometric bodies: spheres, cones, and cylinders). Such phantoms, along with the increasing computational capacities and the availability of high-resolution computed tomography (CT) scan and magnetic resonance imaging (MRI) of patients, make it possible to produce an individual voxel-scaled retrospective estimation of radiation doses to organs of interest. Dosimetry data for large populations are becoming available for investigation, and descriptive statistics derived from such data have the potential to shed light on the role of radiation dose distribution.

Numerous experimental and epidemiological studies have reported the existence of radiation-induced effects. Inference of such effects can be deduced by the collection and analysis of dosimetry data; they are helpful both for accurate and safe follow-up of childhood cancer survivors and for the radio-protection of individuals (figure 1.3). Such results are regularly synthesized (e.g., *Health Risks from Exposure to Low Levels of Ionizing Radiation*, 2006) by international scientific committees such as the United Nations Scientific Committee on the Effects of Atomic Radiation and elaborated into norms of radioprotection of the public, workers, and patients by the International Commission on Radiological Protection (ICRP).

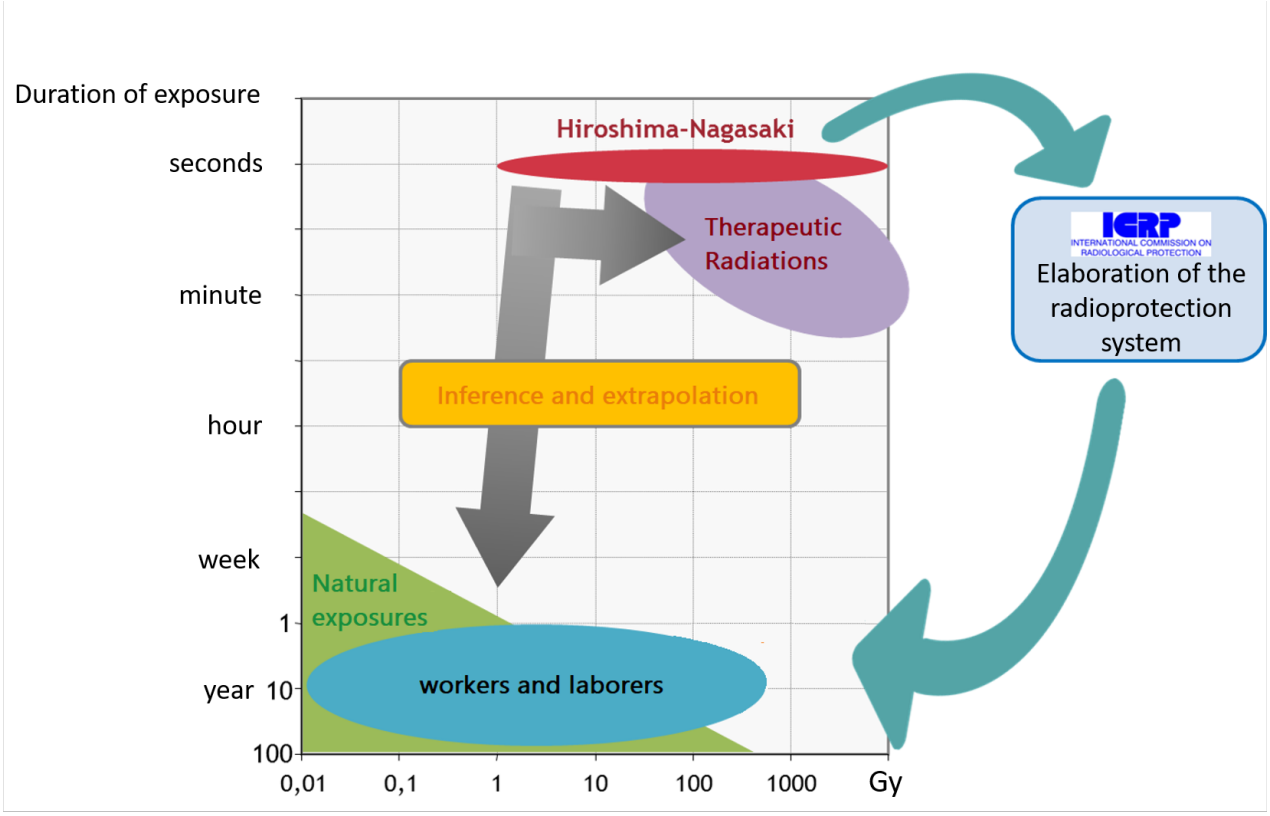

Figure 1.3: Elaboration of the International Commission on Radiological Protection (ICRP) radioprotection system. Figure by Rodrigue Allodji.

Finally, radiation dose estimates result from combining information on patient anatomy, the TPS, and the characterization of the irradiation source. They are, therefore, subject to three different sources of uncertainty, subject to varying types of error (Vũ Bezin et al., 2017). Uncertainties associated with the dose reconstruction process are assessed according to the accuracy of the patient's radiotherapy record. For instance, if an anthropomorphic phantom is used for old records before the era of CT scans, the uncertainties are mainly due to discrepancies between the phantom anatomy and the patient's actual anatomy. In this thesis, we will focus on uncertainties associated with estimation procedures and not consider reconstruction uncertainties.

Late iatrogenic effects

With overall childhood cancer survival being more than 80%, and while irradiation of healthy tissues cannot be avoided entirely, long-term toxicity after radiotherapy for childhood cancer is a significant public health concern. Long-term toxicity or *late iatrogenic effects* or *complications* are defined as health problems that can occur years after treatment for childhood cancer has ended. The three main factors that affect the risk of late effects are the location of cancer (e.g., if a tumor affects the functioning of vital organs), clinical factors concerning the patient's characteristics (age at treatment, previous health problems, epigenetics, socioeconomic status), and treatment-related factors (type of chemotherapy, combination of treatments).

Specifically, studies from the Childhood Cancer Survivor Study (CCSS) cohort ("St Jude Children's research hospital", 2023) report that two out of three survivors treated during the end of the last century developed at least one treatment-associated life-threatening disease in adulthood (Armanious et al., 2018; Erdmann et al., 2021; Landier et al., 2018). Cancer treatments are an established risk factor for cardiac diseases (Hau et al., 2019; Leerink et al., 2020; Olsen et al., 2014). Heart failure, coronary artery disease, as well as valvular heart disease are frequent cardiac disorders among childhood cancer survivors (Mulrooney et al., 2020; Nathan et al., 2016) and in the French Childhood Cancer Survivor Study (FCCSS) in particular (Haddy et al., 2016).

Advancements in treatments for childhood cancer, as well as diagnostic tools, have, of course, helped decrease mortality. While most late effects are not directly life-threatening, they may cause serious problems that affect the health and quality of life of survivors ("Cancer.gov", 2023). According to the Centers for Disease Control and Prevention (CDC, 2023), the three most common causes of death in childhood cancer survivors are a cancer recurrence, a second primary neoplasm of different types later in life, and heart and lung damage. Therefore, while treatment with irradiation has proven life-saving and highly efficient, it comes along, unfortunately, with significant drawbacks that necessitate some long-term follow-up.

The need for personalized follow-up protocols

Currently, a great effort is taking place for follow-up protocols to be standardized. The *Children's Oncology Group Long-Term Follow-Up Guidelines for Survivors of Childhood, Adolescent, and Young Adult Cancers* (COG LTFU Guidelines) provide screening recommendations for asymptomatic survivors of pediatric malignancies for routine exposure-based medical follow-up. Given the high inter-individual variability of children's response to treatments, especially in the long term, such standardized protocols of patients' follow-up after radiotherapy treatments can lead to mis- or late detection of iatrogenic events. Moreover, adopting high-frequency screening schemes would not be sustainable in the long term and could be very anxiety-triggering for the patients and even detrimental to their health. The benefits of an as fair as possible evaluation of each patient's risk are therefore obvious. It is essential to implement personalized medical monitoring tools to identify people at high risk of an iatrogenic event, support clinical decisions, and facilitate communication between clinicians and patients.

Taking into account comorbidities, demographic characteristics, as well as treatment-related risks to propose accurate personalised follow-up to survivors has proven very challenging. To date, two clinical prediction tools are available by American teams for childhood cancer survivors (Chow et al., 2015; Kovalchik et al., 2013). These tools focus on the risk of experiencing late cardiovascular disease and second primary thyroid cancer. However, these tools have shortcomings both in the data used (absence of detailed dosimetric data) and in the methodology (very traditional analysis models) and are, therefore, susceptible to leading to biased estimates and uncertainties in risk predictions.

The increase in survival rates and the increasing need for rigorous screening of late complications has led to the creation of large cohorts with longitudinal follow-ups of long duration. The Childhood Cancer Survivor Study (the United States and Canada), the British Childhood Cancer Survivor Study, the French Childhood Cancer Survivor Study, and the PanCareSurFup consortium created to put together many European cohorts are some examples of 5-year survivor cohorts. However, among those, the French Childhood Cancer Survivor Study is the only one with individual voxelized dosimetry for almost every cohort member treated with radiotherapy.

Radiation-induced valvular heart disease

Mainly, radiation-induced heart disease is very diverse: it ranges from early manifestations, such as acute coronary syndromes, where screening should start < 5 years after radiotherapy, to late effects, like valvular heart disease (VHD), where screening is routinely performed ≈ 10 years after radiotherapy (Desai et al., 2019). However, to our knowledge, unlike heart failure and coronary

artery disease (Bates et al., 2019; Mansouri et al., 2019; Shrestha et al., 2021), the potential risk factors for experiencing a VHD after treatment for childhood cancer are not thoroughly investigated and understood yet. In this thesis, we are interested in the risk of a childhood cancer survivor experiencing a radiation-induced VHD.

VHD is among the most critical complications of radiotherapy because of its association with other cardiac complications (Figure 1.4). Specifically, according to the CDC, 2023, if not diagnosed and treated correctly, heart valve problems can lead to arrhythmia, blood pressure in the lungs, heart failure, or cardiac arrest. A study has also statistically associated VHD with coronary artery disease (Matta & Moussallem, 2019).

The precise pathophysiological mechanisms of radiation-induced valvulopathy are not altogether understood (Nadlonek et al., 2012; Veinot & Edwards, 1996; Yarnold & Brotons, 2010). However, irradiation is thought by radiation biologists to directly affect the calcification of the valvular apparatus in patients with breast cancer. In addition, pathologic fibrosis has been observed in lymphoma patients who have been treated with radiotherapy. According to the authors, this difference is likely due to the young age of radiation exposure in lymphoma patients (Patil et al., 2022). Nowadays, a high MHD is becoming increasingly exceptional during treatment for childhood cancer, except for a primary mediastinal tumor where these children get a boost up to 30 Gy. However, many patients that did not benefit from modern protocols are still being followed. Especially for old cases of primary mediastinal tumor, where it was impossible to spare parts of the heart or modern methods like breath gating or deep inspiration breath hold was not standardized yet, establishing care with a cardio-oncologist for close cardiac monitoring would facilitate early detection and allow for timely preventative and therapeutic interventions.

In order to provide personalized follow-up guidelines, accurate risk estimation is required, which would take into account the specific treatments, clinical history, and any other relevant available characteristics for each survivor. Specifically for the radiation-induced risk of experiencing a VHD, many open questions still exist.

1.3 . Modelling the radiation-induced risk of valvular heart disease

While recent advancements have made increasingly rare a high mean heart dose nowadays, novel radiotherapy delivery techniques such as IMRT or VMAT may increase the volume that receives low-to-intermediate radiation doses. The occurrence of radiation-induced VHD must, therefore, be studied in relation to the level of the dose delivered to the heart as well as the volume of the heart absorbing doses of a certain level. There is an established risk of high doses (> 30 Gy) (Cella et al.,

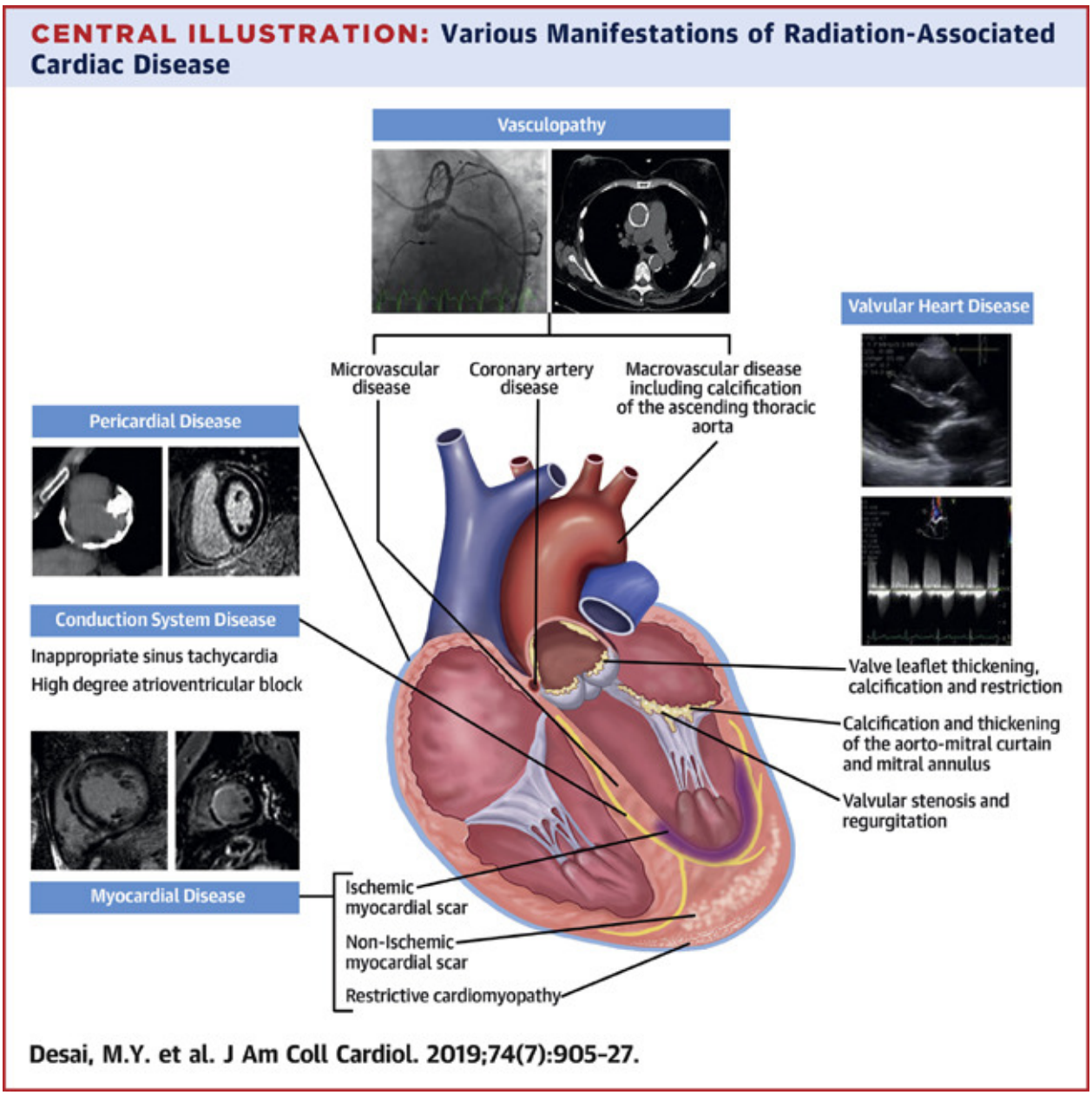

Figure 1.4: Radiation-associated cardiac disease covers a spectrum of deleterious effects, ranging from pre-clinical findings to symptomatic disease. Source:Desai et al., 2019

2011; Gujral et al., 2016). Some evidence exists in the literature (Patil et al., 2022) about the role of the lower doses: a recent study has demonstrated that large heart volumes irradiated with low doses could increase the rate of any cardiac disease (Bates et al., 2019). But there is still no consensus, so investigating the details of the radiation-induced risk of experiencing a VHD and the role of irradiated heart volume remains crucial.

Two main trends can be distinguished for radiation-induced risk models: traditional approaches relying mainly on one aggregated variable (generally the mean of median dose to the organ of interest) and recent tendencies with spatially explicit representations of the dose distribution.

Traditional approach: mean dose to the heart

The most commonly used independent variables to model the risk of radiation-induced VHD are the mean and median dose to the heart (Cutter et al., 2015; van der Pal et al., 2015a). However, it is not known whether the relationship between the Mean Heart Dose (MHD) and the occurrence of a VHD is linear (Cutter et al., 2015). Moreover, the mean and median dose to the heart do not provide insight into the role of spatial heterogeneity of absorbed doses; this issue remains understudied in the literature, mainly due to a lack of adequate voxel-scale data for the whole heart or its substructures.

Recent approaches: dose-volume histograms and dosiomics

The availability of dose reconstruction at the voxel scale opens the possibility of going beyond the mere use of MHD to describe the radiation effects in risk models. Some authors (Cella et al., 2015) proposed to define the dose-volume histogram (DVH) to summarize 3D dose distributions in a 2D informative graph. Cumulative histograms are plotted with bin doses along the x-axis, and the k^{th} percentile is denoted D_{100-k} (e.g. D_{50} is the median). The first column represents the volume of the heart that absorbed a dose greater than or equal to the dose of the bin. For example, $V_{40\,Gy}$ is the volume of the heart that absorbed a dose of ≥ 40 Gy. Some studies have already made use of DVH indicators with promising results, like (Cella et al., 2015; Shrestha et al., 2021) in adults and Mansouri et al., 2019 and Bates et al., 2019 in pediatric oncology.

However, this definition of V_k variables cannot allow studying the effect of low doses. There was a need to find a way to express the radiation-induced risk of low doses independently of the already established risk induced by strong doses. To solve this issue, we studied each V_d indicator in dose intervals, with a cutoff on high doses that translated into population truncation.

To further investigate the role of the spatial distribution of doses, some recent studies have introduced the calculation and incorporation in classification models of *dosiomics* features (Liang et al., 2019; Wu et al., 2020; Yang et al., 2022). Inspired by the *radiomics* approach, traditionally

implemented for the analysis of medical imaging via data-characterization algorithm, the extraction of such features has the potential to reveal spatial associations of the dose distribution to the heart with the occurrence of radiation-induced VHD after treatment for childhood cancer. Dosiomics features have proven promising and, in some cases, more effective than the DVH parameters (Murakami et al., 2022; Ren et al., 2021).

1.4 . Objectives and contributions

Objectives

The main objectives of this study were to quantify the risk of a radiation-induced VHD in the FCCSS, to evaluate the impact of low-to-moderate doses, and explore the potential existence of lower dose-volume threshold levels. A specific objective was to explore the role of heterogeneity and the spatial traits of the heart dose in radiation-induced risk. Finally, an important goal of this thesis was to provide evidence that an efficient predictive algorithm of a late VHD can be implemented when a retrospective dose reconstruction is available.

Contributions

To deal with these objectives, we relied on data coming from two cohorts, the FCCSS and PanCare-SurFup-ProCardio:

- The FCCSS is a cohort of 7670 5-year survivors treated between 1946 and 2000 for France's most common childhood solid cancers. Analyses in the context of this thesis included 7492 survivors with complete data (97.7% of the FCCSS cohort), 3906 of whom had been treated with radiotherapy. Eighty-one individuals (1%) developed a severe VHD after childhood cancer treatment; of those, 63 had been treated with radiotherapy. Therefore, some of the methods that were employed consider the imbalanced nature of the cohort regarding the prevalence of VHD.

- The nested case-control study within PanCareSurFup-ProCardio, a wide pan-European of more than 42K 5-year survivors, was designed to assess treatment-related risk factors for valvulopathy in detail. A total of 274 survivors were nested in an individual paired case-control study, and 224 with complete dosimetric data were available and included in our analyses. Each valvulopathy case was matched to one control based on gender, age at first primary cancer diagnosis ($\pm$ one year), year of first primary cancer diagnosis ($\pm$ three years),

follow-up duration (the follow-up of each control patient was at least as long as the follow-up of their matched case) and treatment center.

Our first contribution consists of some descriptive analyses of the FCCSS cohort and, to a lesser extent, of the Pancare cohort, regarding the VHD-related characteristics (see Chapter 3).

The next part of this thesis concerns the survival analyses conducted in the FCCSS. We confirmed the literature's results on the radiation-induced risk of experiencing a VHD and observed a statistical association of the Mean Heart Dose with that risk. We compared some Excess Relative Risk models to evaluate the risk's form (exponential, linear, quadratic, and linear-quadratic).

Moreover, thanks to the voxelized dosimetry data, we could express the radiation-induced risk in terms of affected heart volume instead of dose level. This implementation seen in Bates et al., 2019 has been seen in some studies. Still, to our knowledge, it is the first work where the risk of experiencing a late VHD is expressed in terms of cardiac volume instead of dose level, allowing an in-depth exploration of moderate and low doses independently of the already established risk of high doses. The results of this work were published in the Green Journal (Radiotherapy and Oncology), Chounta et al., 2023.

One additional contribution of this thesis was the exploration of modeling the radiation-induced risk of experiencing a VHD by combining multiple dose-volume histogram (DVH) indicators. A few approaches for combining codependent variables in risk models were tested, notably Principal Components Regression and Penalized Cox Regression. Risk models are not more informative than models based on the mean heart dose and were not considered for publication; however, they are discussed in the context of this thesis.

Next, we chose to tackle the subject as a classification problem of VHD prediction. Therefore, follow-up duration was no longer considered so that the implemented models could be used from the moment of treatment. In order to account for the spatial characteristics of the dose distribution, we extracted 93 dosiomics features and implemented them into random forests adapted for imbalanced classification. To evaluate the predictive performance of the models, we compared them to forests based on the mean heart dose. We also conducted sensitivity analyses on sub-populations of the FCCSS selected according to the level of heart-dose *uniformity*, based on the assumption that dose heterogeneity (lack of uniformity) is an important factor in the occurrence of VHD. We found that, among patients with non-heterogeneous heart doses, dosiomics-based models behaved significantly better than models based on the mean heart dose in terms of predictive performance. To our knowledge, this study was the first to use dosiomics features for heart doses to train prediction models. A *dosiomics signature* for late VHD after radiotherapy for childhood cancer was proposed. Results were submitted as a paper under the title *Dosiomics-based prediction algorithms of radiation-*

induced valvulopathy, and are under review in *Cancers* journal.

Finally, some preliminary results are presented on the confrontation of the contributions above with an independent cohort. For that, we employed the independent case-control study that was nested in the PanCareSurFup-ProCardio cohort. Some interesting results are observed on the dosiomics signature proposed in the previous chapter.

1.5 . Outline of the manuscript

This thesis consists of five parts. In Chapter 2, we describe the thesis's statistical framework and the models used to analyze the dosimetric data (for survival analysis, classification modeling, and machine learning implementations). Chapter 3 provides a detailed description of the FCCSS cohort, which we then use for further statistical analyses in the following two chapters. In Chapter 4, we investigate the long-term risk of experiencing a radiation-induced VHD in the FCCSS through survival modeling. Next, in Chapter 5, the question is confronted as a classification problem, and the dosiomics approach is implemented into adapted Random Forests for imbalanced classification. Finally, in Chapter 6, we attempted an external validation of the previous works with the help of the independent case-control study that was nested in the PanCareSurFup cohort.

2 - Methodological Background

In this section are detailed the models that were required during the analyses. More precisely, in Chapter 4, we study the radiation-induced risk of experiencing a VHD after treatment for childhood cancer. The Cox and the Poisson models were employed for the different types of risk models; Principal Components analysis and Penalized Cox Regression was used for multivariable modeling of radiation-induced risk; and cumulative incidence function was illustrated to estimate the risk of experiencing a VHD at every age after treatment for childhood cancer int he FCCSS. Elastic Net regression was then employed inle selection method before applying the classification algorithms. Random Forest and its adaptations for imbalanced data were used in Chapter 5 for classification with the potential of building a prediction algorithm. The analyses of these two chapters concern the right-censored study described in Chapter 3.1. Finally in Chapter 6, a conditional regression and a matched Forest, suitable for paired data (the Pancare cohort also described in Chapter 3.2) were used for the validation of the previously proposed model.

2.1 . Survival Analyses

Risk models in this thesis concern right-censored time-to-event data. Survivors are followed from the date of childhood cancer (CC) diagnosis until a certain moment in life: the date of diagnosis of valvular heart disease (VHD) for those who experienced one, the date of death, or the date of most recent medical news. The fact that measurements are no longer observed after that moment is called *right censoring*. Survival analysis is a branch of statistics that can deal with censored data. In survival analysis, we are interested in survival and hazard functions.

The Cumulative Incidence Function

Cumulative incidence is defined as the probability that a particular event, a VHD in the context of this thesis, has occurred before a given time. In order to plot the cumulative incidence function, we first needed to calculate the Kaplan-Meier estimator (Kaplan & Meier, 1958) for the survival function, where the probability that a VHD does not occur before t amount of time has elapsed, i.e., the survival function S, is estimated by:

$$\hat{S}(t) = \prod_{i:t_i \leq t} \left(1 - \frac{d_i}{n_i}\right),$$

a step function where t_i is the elapsed time until at least one event has occurred, d_i the number of events (in this case VHD) that happened in time t_i and n_i the number of individuals at risk (have not had the event or been censored) up to time t_i.
Then, the cumulative incidence is given by $1 - \hat{S}(t)$.

The Cox Proportional Hazards Model for risk estimation

Traditional regression models are unsuitable for handling censored data because the time-to-event is underestimated in the presence of censoring. Let us introduce an estimator of the survival function and the Cox proportional hazards model, one of the most classical models in survival analysis.
The hazard function, one of the key concepts of survival analysis, is given by

$$\lambda(t) = \lim_{\Delta t \to 0} \frac{\mathbb{P}(t \leq T < t + \Delta t | T \geq t)}{\Delta t}. \tag{2.1}$$

To model the hazard function, we used the Cox proportional hazards model (Cox, 1972). The survival risk model consists of two parts: the underlying baseline hazard function, denoted $\lambda_0(t)$, describing how the risk of event per time unit changes over time at baseline levels of covariates, and the effect parameters, describing how the hazard varies in response to explanatory covariates.
If $X_i = (X_{i1}, X_{i2}, ..., X_{ip})$ are the observed values of the covariates of subject i and $\beta = (\beta_1, \ldots, \beta_p)$ is the effect parameters, then the hazard function is denoted :

$$\begin{aligned} \lambda(t|X_i) &= \lambda_0(t) \exp(\beta_1 X_{i1} + \beta_2 X_{i2} + ... + \beta_p X_{ip}) \\ &= \lambda_0(t) \exp(X_i \cdot \beta) \end{aligned} \tag{2.2}$$

Expression (2.2) gives the hazard function at time t for subject i with covariate vector (explanatory variables) X_i. Between subjects, the baseline hazard $\lambda_0(t)$ is identical. According to the Cox model, if the assumption of hazards' proportionality holds (covariates are multiplicatively related to the hazard), it is possible to estimate the effect parameters β_i without knowing the baseline hazard function $\lambda_0(t)$.
The likelihood of the event to be observed occurring for subject i and time Y_i is given by the expression

$$L_i(\beta) = \frac{\lambda(Y_i \mid X_i)}{\sum_{j:Y_j \geq Y_i} \lambda(Y_i \mid X_j)} = \frac{\lambda_0(Y_i)\theta_i}{\sum_{j:Y_j \geq Y_i} \lambda_0(Y_i)\theta_j} = \frac{\theta_i}{\sum_{j:Y_j \geq Y_i} \theta_j} \tag{2.3}$$

where $\theta_j = \exp(X_j \cdot \beta)$ and the effect parameters β_i are then calculated by maximizing over β the log partial likelihood

$$\ell(\beta) = \sum_{i:status_i=1} \left(X_i \cdot \beta - \log \sum_{j:Y_j \geq Y_i} \theta_j \right). \tag{2.4}$$

where $status_i = 1$ indicates the occurrence of the event for survivor i.
The model is based on two assumptions: the hazard curves for the strata of patients defined by variable categories are proportional over time; the relationship between the log hazard and each covariate is linear.

The Poisson Model for the excess of relative risk

To go one step further, we also estimated the Excess Relative Risk (ERR) according to the Poisson model ("The EPICURE Regression Programs", n.d.; McCullagh & Nelder, 1983), which is defined as the rate of disease in an exposed population divided by the rate of disease in an unexposed population, minus 1 and is expressed as the excess relative risk per Gy. We fitted the exponential (multiplicative) model, the linear (additive) model, the quadratic model, and the linear-quadratic model.
Particularly, for $z(t)$ and β the vector of covariates and coefficients, respectively, the risk function is modeled as

$$f(z(t), \beta) = \exp(\beta \times z(t)) \tag{2.5}$$

in the exponential model,

$$f(z(t), \beta) = 1 + \beta \times z(t) \tag{2.6}$$

in the linear (additive) model, with the excess of relative risks as a linear function of the covariates, and finally

$$f(z(t), \beta) = 1 + \beta \times z^2(t) \tag{2.7}$$

in the quadratic. The number of cases follows a Poisson distribution with $\lambda_{Poisson}$ defined as the product of the number of person-years and the $f(z(t), \hat{\beta})$.

Multivariable modeling of radiation exposure

In Chapter 4, we attempted alternative modeling of the radiation-induced risk by combining multiple dose-volume histogram indicators, detailed in the Methods section of Chapter 4.

Principal Component Analysis

Principal Components Analysis (PCA) is usually employed for dimension reduction while maintaining as much information as possible. This is achieved by a linear transformation of the data into a new coordinate system with a trade-off between the number of coordinates/components and the explained variance of the initial data (Jolliffe, 2013; Le et al., 2008).

It is usually applied to correlated sets of variables in order to reduce their number into a new set of independent variables.

The first component of a set of p variables (with a normal joint distribution) is the derived variable formed as a linear combination of the original variables and explains most of the data variance. The second principal component explains most of the variance left once the first component's effect is no longer considered. There can be as many as p components until the variance is entirely explained.

If we consider the $n \times p$ matrix X derived from the data frame containing the variables (centered). The transformation will result in one per component p-dimensional vector of weights $w_{(l)} = (w_1, w_2, \ldots, w_p)$ that maps each variable (i.e., each vector x_i of the matrix X) to a new vector of principal component scores $t_{l(i)} = x_i \times w_l$.

The weights of the first component w_1 are defined as the unit vector that satisfies

$$w_1 = \arg\max_{\|w\|=1} \left\{ \sum_i (t_1)^2_{(i)} \right\} = \arg\max_{\|w\|=1} \left\{ \|Xw\|^2 \right\} = \arg\max \left\{ \frac{w^T X^T X w}{w^T w} \right\}$$

where the maximum possible value is the largest eigenvalue of the (positive semidefinite matrix) matrix $X^T X$, which occurs when w is the corresponding eigenvector.

Then the k^{th} component is found by subtracting the first $k-1$ principal components from X

$$\hat{X_k} = X - \sum_{j=1}^{k-1} X w_{(j)} w_{(j)}^T$$

and then calculating the weight vector like previously, with the new matrix in the place of X

$$w_{(k)} = \arg\max_{\|w\|=1} \left\{ \|Xw\|^2 \right\}$$

The number l of components is chosen by visual inspection of the scree plot (at the point of inflection of the line that connects the bin tops). Once the components are calculated, models are fitted as they would on variables.

Penalized Cox Regression

The Cox proportional hazards model is not adapted for estimating many coefficients at once when features are correlated. The problem can be avoided by adding a penalty term on the coefficients (Friedman et al., 2010; Simon et al., 2011; Zou & Hastie, 2005). Then the regularized coefficient $\bar{\beta}$ has the general form

$$\bar{\beta} = \arg\max_{\beta} \Big\{ \log l(\beta) - \lambda \sum_{j=1}^{p} \big(\alpha \beta_j^2 + (1-\alpha)|\beta_j| \big) \Big\} \tag{2.8}$$

, where $l(\beta)$ is the partial likelihood of the Cox model, and p is the total number of features.
For $\lambda = 1$ and alpha=0 in equation 2.8, the penalty is called LASSO. For $\lambda = 1$ and alpha=1, the penalty is called Ridge.
Finally, the Elastic Net penalty is a combination of the two, and then, λ and α can be tuned via cross-validation.

Comparison of Risk Models

Two measures of comparison of the risk models were employed: Harrel's C-index (Harrell et al., 1982) and the AIC criterion.

C-index

Harrell's C-index (i.e., concordance index) measures the goodness of fit of risk models that account for censored data. For every pair of patients i and j (with $i \neq j$), we look at their risk scores η_i and η_j and times-to-event T_i and T_j. If both T_i and T_j are not censored, we can observe when both patients got the disease. We say that the pair (i, j) is a concordant pair if $\eta_i > \eta_j$ and $T_i < T_j$, and it is a discordant pair if $\eta_i > \eta_j$ and $T_i > T_j$.
Harrell's C-index is simply given by the expression $\dfrac{\#\text{ concordant pairs}}{\#\text{ concordant pairs} + \#\text{ discordant pairs}}$. The closer the C-index to 1, the better the model.

AIC

The Akaike information criterion (AIC) is a metric for evaluating how well a model fits the data it was generated from. It provides a means for model selection. Suppose that we have a statistical model of some data. If k is the number of estimated parameters in the model and $\hat{L}$ is the maximized value of the likelihood function for the model, then the AIC value of the model is given by

$$AIC = 2k - 2\ln(\hat{L}) \tag{2.9}$$

A small AIC is interpreted as less information loss from the model.

2.2 . Classification Models

To train prediction algorithms that can be employed early on during survivors' follow-up and be considered for follow-up guidelines, we cannot take into account the time-to-event. We decided, therefore, to use classification approaches for the second part of the analysis.

Since this part explores a multivariable approach detailed in Chapter 5, the algorithm pipeline starts with a variable selection that a Random Forest follows.

Elastic Net penalty

Regularisation was already described for linear regression problems before the application to the Cox model (Tibshirani, 1996). In general, the purpose of regularization is to prevent overfitting, making use of a criterion similar to the following:

$$\bar{\beta} = \arg\min_{\beta} \Big\{ \sum_{i=1}^{N} \big(y_i - \beta_0 - \sum_{j=1}^{p} x_{ij}\beta_j\big)^2 + penalty\ parameter \Big\} \tag{2.10}$$

where N is the total number of observations. For the penalty parameter, we chose the Elastic Net (Zou & Hastie, 2005) given by the formula:

$$\lambda \sum_{j=1}^{p} \Big(\alpha\beta_j^2 + (1-\alpha)|\beta_j| \Big) \tag{2.11}$$

where p is the total number of features. Elastic Net penalty is a combination of LASSO (when alpha=0 in 2.11) and Ridge penalty (when alpha=1 in 2.11). LASSO uses shrinkage, meaning that certain variable coefficients were shrunk to zero, making the classification model more sparse and more straightforward to interpret.

Random Forest for classification

As a classification algorithm, we chose the Random Forest (RF), where accuracy is achieved with minimal hyperparameter tuning (Breiman, 2001). Random Forests is a modification of *bagging* (bootstrap aggregation), an ensemble technique that grows a collection of de-correlated trees (high variance- low bias) and then averages them. The advantage of bagging is that it reduces the variance of an estimated prediction function and helps avoid overfitting.

Algorithm 15.1 *Random Forest for Regression or Classification.*

1. For $b = 1$ to B:
   (a) Draw a bootstrap sample $\mathbf{Z}^*$ of size N from the training data.
   (b) Grow a random-forest tree T_b to the bootstrapped data, by recursively repeating the following steps for each terminal node of the tree, until the minimum node size n_{min} is reached.
      i. Select m variables at random from the p variables.
      ii. Pick the best variable/split-point among the m.
      iii. Split the node into two daughter nodes.
2. Output the ensemble of trees $\{T_b\}_1^B$.

To make a prediction at a new point x:

Regression: $\hat{f}_{\text{rf}}^B(x) = \frac{1}{B}\sum_{b=1}^{B} T_b(x)$.

Classification: Let $\hat{C}_b(x)$ be the class prediction of the bth random-forest tree. Then $\hat{C}_{\text{rf}}^B(x) = \textit{majority vote}\ \{\hat{C}_b(x)\}_1^B$.

Figure 2.1: The Random Forest algorithm, from *The elements of statistical learning: Data mining, inference, and prediction, second edition*, 2009

The RF algorithm is described in figure 2.1. For step 1.(b) of the algorithm, the CART (Classification and Regression Tree) algorithm is deployed, and therefore for step 1.(b).ii. (both for which feature should be placed at the root node and which will be the chosen variable's threshold that will define the rule for the first split) the *Gini index* (or Gini impurity) needs to be calculated. The Gini index is given by the formula:

$$Gini(v) = 1 - \sum_{i=1}^{c}(P_i)^2,$$

where v is the node, c is the total number of outcome classes, and P_i denotes the probability of an element being classified for a distinct class, ranging from 0 to 0.5 (the smaller, the better). Then the simplified Gini Information Gain of a feature z for splitting at node v, noted $IG(z, v)$, is computed by

$$IG(z, v) = Gini(v) - p_{v_{left}} Gini(v_{left}) - p_{v_{right}} Gini(v_{right})$$

where v_{left} the left node of the split of parent node v and $p_{v_{left}}$ the expected value of v_{left} (respectively $p_{v_{right}}$ and v_{right} for the right node).

Feature importance can be derived from the RF by counting how much the tree nodes that use that feature reduce impurity across all trees in the forest. At each split in each tree, the improvement in the split criterion is the importance measure attributed to the splitting feature z. It is accumulated over all the trees in the forest separately for each feature. It is given by the formula:

$$FI(z) = \frac{1}{n_{tree}} \sum_{v \in \{v|s(v)=z\}} N_v IG(z, v) \tag{2.12}$$

where n_{tree} is the number of trees in the RF, $s(v)$ is the feature selected at node v and N_v is the number of instances reaching node v.

Finally, a result of the bagging process is the *out-of-bag error* (OOB error): for each observation X_i, the RF prediction is calculated by only averaging the trees that grow out of bootstrap samples where X_i was not selected. Once the OOB error stabilizes, the training can be terminated.

Chen et al. (Chen et al., 2004) proposed two possible adaptations of the classic Random Forest algorithm to tackle the problem of imbalanced data: Weighted Random Forest (wtRF) and Balanced Random Forest (BRF).

Weighted Random Forest

The wtRF is based on the idea of cost-sensitive learning to penalize misclassification of the minority class. A weight is assigned to each class and incorporated into two steps of the random forest algorithm: (i) in the tree induction procedure, class weights are used to weight the Gini criterion for finding splits, and (ii) in the terminal nodes of each tree where class weights are again taken into consideration to determine the prediction according to a weighted majority vote.

Balanced Random Forest

The BRF incorporates the idea of down-sampling the majority class during each bootstrap step by selecting a bootstrap sample from the minority class and then randomly drawing the same number of cases from the majority class.

Metrics of evaluation

In Chapter 5, there is a reference to a few metrics of evaluation of machine learning models trained for prediction purposes:

- Specificity
- Sensitivity (Recall)

Table 2.1: Confusion Matrix and Metrics of Evaluation of machine learning models.

Actual condition		Predicted condition N	Predicted condition P	
	N	TN	FP	$Specificity = \frac{TN}{N} = \frac{TN}{TN+FN}$
	P	FN	TP	$Sensitivity = \frac{TP}{P} = \frac{TP}{TP+FP}$
	N+P			$BalancedAccuracy = \frac{Sensitivity+Specificity}{2}$

- Balanced Accuracy

- AUC ROC

To clarify the definitions of those metrics, we should break down the confusion matrix inside 2.1. With N for *negative* and P for *positive*, we note the condition of the binary outcome, with positive being the number of survivors that experienced the event. Then with TN, we note the *True Negative*, a survivor that did not experience the event and whose prediction was correct, and with FN, the *False Negative*, a survivor who did experience the event was falsely predicted as not being at risk of experiencing it, respectively for the positive condition.

That being defined, *Specificity* is the so-called *True Negative Rate*, and is equal to the correct negative predictions divided by the number of negatives in the population, and *Sensitivity* is the *True Positive Rate*, calculated as the correct positive predictions divided by the number of positives in the population.

To evaluate the Sensitivity and Specificity of an algorithm simultaneously, we calculated the *Balanced Accuracy*, which is the arithmetic mean of Sensitivity and Specificity. Finally, the ROC (Receiver Operating Characteristic) is the plot of *Sensitivity versus 1- Specificity*, or True Positive Rate versus False Positive Rate, that reflects relative trade-offs between true positive (benefits) and false positive (costs). Then the AUC ROC (Area under the ROC Curve) measures the entire two-dimensional area underneath the ROC curve from (0,0) to (1,1). Figure 2.2 illustrates potential curves by classifier performance.

All of the described metrics take values between zero and 1, with 1 expressing the most favorable model.

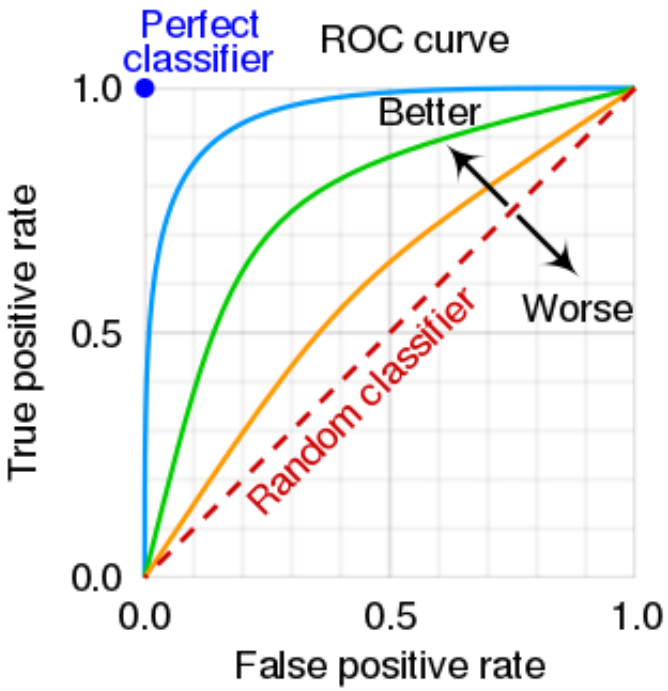

Figure 2.2: The ROC space for a "better" and "worse" classifier. Figure from Wikipedia, 2023.

2.3 . Conditional Classification

Data used in the last part of the thesis, Chapter 6, come from a paired case-control cohort (described in Chapter 3.2). Therefore, models had to be adapted.

Conditional Logistic Regression

For univariate and adjusted analyses, we fitted conditional logistic regression models. Logistic regression can account for stratification by including a different constant term for each stratum (defined as the pairs of matched cases and controls). If $Y_{ik} \in \{0, 1\}$ is the outcome of the k^{th} observation of the i^{th} stratum and $X_{ik} \in \mathbb{R}^p$ the vector of values of the corresponding predictors, then the likelihood of the observation is

$$\mathbb{P}(Y_{ik} = 1|X_{ik}) = \frac{\exp(\alpha_i + \beta^T X_{ik})}{1 + \exp(\alpha_i + \beta^T X_{ik})},$$

where α_i is a the constant term for the i^{th} stratum.

Matched Forest

Finally, in order to apply the RF algorithm to the paired data, we used the Matched Forest (Shomal Zadeh et al., 2020), an algorithm designed for variable selection in pair case-control data. Matched Forest consists of two simple steps:

1. a transformation to convert the variable selection problem into a supervised setting based on the potential outcome framework for causal inference,
2. a supervised learner, which can inherently detect the complex interactions involving both exposure and matching variables in a high-dimensional setting using the transformed dataset.

3 - The Cohorts

3.1 . The French Childhood Cancer Survivors' Study

The FCCSS is a retrospective observational cohort designed to improve the life of childhood cancer survivors by gaining knowledge on the long-term effects of cancer and its treatments. The main objectives of the study are to assess the risk of adverse health and social outcomes that can be observed after treatment for childhood cancer and, to help health care professionals provide early diagnosis and treatment by proposing adapted follow-up guidelines.

The cohort consists of 7670 5-year survivors treated between 1946 and 2000 before the age of 21 for the most common types of solid childhood cancers, including lymphomas, in five different cancer centers in France. It combines data from the Euro2K cohort, i.e. patients treated between 1942 and 1985 for any type of malignant neoplasm except leukemia in 5 cancer centers in France:

- Gustave Roussy Institute
- Curie Institute
- Cancer Institute Jean Godinot
- Antoine Lacassagne Cancer Center
- Claudius Régaud Center

and its extension, i.e. patients treated between 1986 and 2000 in Gustave Roussy and Curie Institut.

A regional committee and the French national agency regulating data protection have approved the FCCSS on ethics (*Commission Nationale Informatique et Liberté, agreements no. 902287 and no. 12038829*). Informed consent was obtained for patients who could be contacted by postal mail or during clinic long-term follow-up ($n = 3312$).

Additionally, a specific act in law was obtained from the French Council of State (*Conseil d'Etat*), the highest court in France (*Order 2014-96, 3 February 2014*), that approved the cession of the SNIIRAM data for all patients included in the FCCSS with or without informed consent. All methods were performed following the relevant guidelines and regulations.

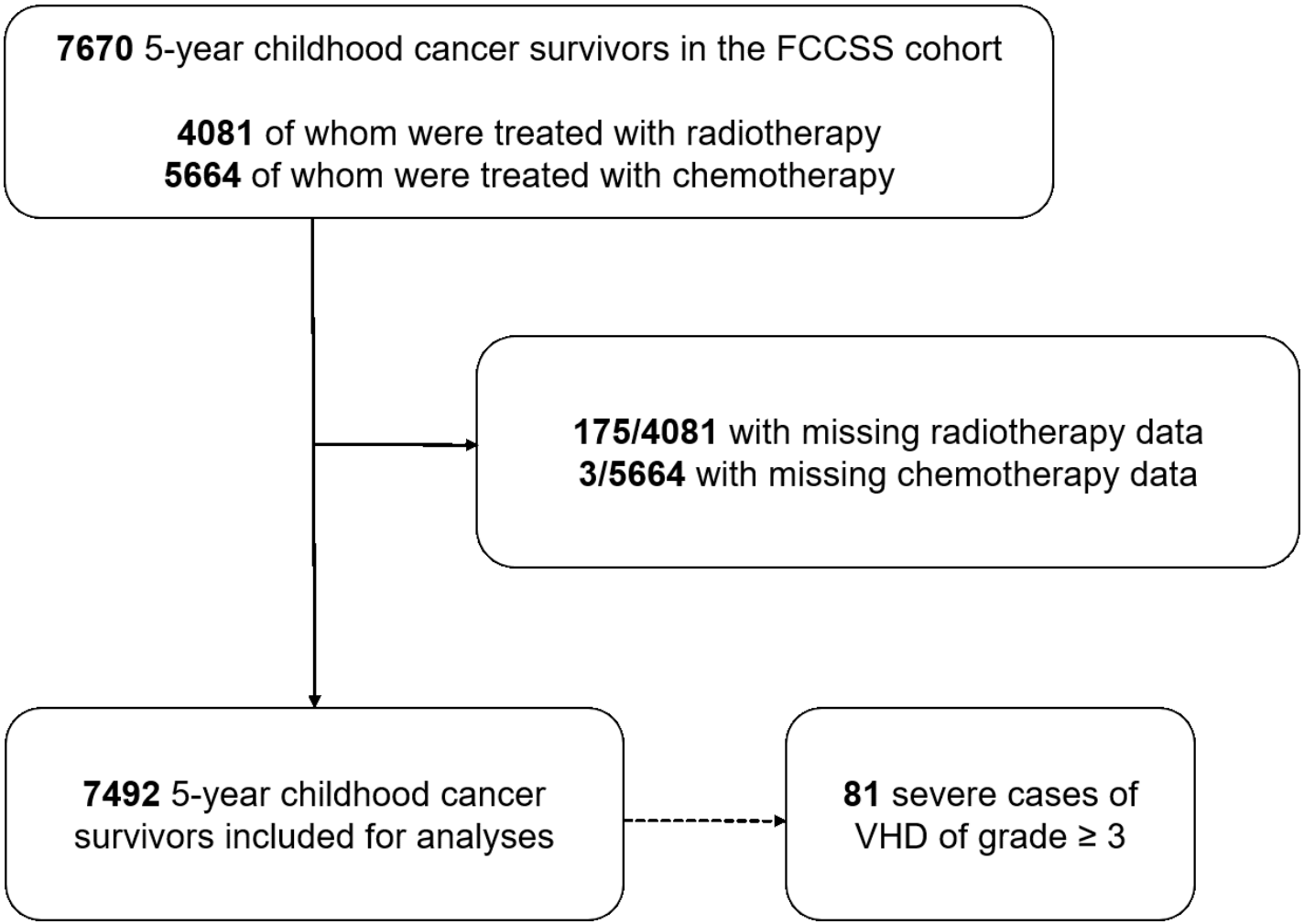

Figure 3.1: Flow diagram of the childhood cancer survivors' data used in the analyses

The particularity of the FCCSS is that it is the only study with a whole-body voxelized dosimetry reconstruction available for almost every participant that was treated with radiotherapy. That, in combination with the information on other treatments and interventions in the context of childhood cancer treatment, the long follow-up duration with available medical records, the access to the French Health Insurance Information System, as well as the adapted self-questionnaires, lead to reliable analyses that can be incorporated into international guidelines for rigorous and effective personalized follow-up of childhood cancer survivors.

Analyses in the context of this thesis included 7492 5-year survivors (97.7% of the FCCSS cohort) with complete treatment data (Flowchart 3.1).

Demographic and Treatment caracteristics

In the FCCSS, indications for radiotherapy, chemotherapy, or surgery were known from cohort survivors' medical records. The vital status was obtained and updated regularly for all patients by the *Center of epidemiology on medical causes of death* ("CépiDC", n.d.). Causes of death for deceased patients, coded according to the 9th and 10th versions of the *International Classification of Diseases* were also obtained and confirmed by the "CépiDC", n.d. Clinical and epidemiological follow-up was performed to identify the occurrence of iatrogenic effects from self-administered questionnaires and cohort linkage with the *French Hospital Database and Health Insurance Information System* SNIIRAM ("Système national d'information inter-régimes de l'Assurance maladie", 2022), as well as clinical long-term follow-up for the patients that had been treated in Gustave Roussy.

Valvular heart disease (VHD) events were identified, validated, and graded according to the *Common Terminology Criteria for Adverse Events* (CTCAE version 4.03 ("Common Terminology Criteria for Adverse Events (CTCAE)", n.d.)). For most survivors that experienced the event ($61/81$), the identification of a VHD was obtained or validated by the SNIIRAM: we looked into hospitalization archives for episodes of valvular dysfunctions and valve replacements, as well as prescribed treatments for valvular dysfunctions. Additionally, for one part of the cohort, long-term clinical follow-up allowed us to consider examinations that have been registered (e.g., heart echography). Identification was also obtained through long-term epidemiological follow-up via self-administered questionnaires confirmed by medical files. However, incidents that were only self-declared, and that we were not able to validate in any other way, were not taken into account.

Information on demographic and clinical characteristics received for the initial childhood cancer occurrence is reported in Table 3.1. The type of childhood cancer is defined according to the third edition of the *International Classification of Childhood Cancer* ("ICCC, Third Edition (ICD-O-3), Main Classification Table - SEER Recodes", n.d.). In the context of survival analyses, we needed

to take into account the time to event. For that purpose, the time of exit was defined as the date of: VHD diagnosis for VHD patients, death for the deceased survivors, or date of last medical news for the rest of the cohort (patient record, medical questionnaires, cohort linkage with the French National Health Data System- SNDS, phone call validation and long-term clinical follow-up for patients treated in Gustave Roussy institute). Follow-up was defined as the time that had lapsed between the date of childhood cancer diagnosis and the time of exit and attained age as the time between birth and the time of exit.

Among the 7492 5-year childhood cancer survivors of the FCCSS cohort with complete data, eighty-one (81) individuals ($\approx 1\%$) experienced a severe VHD after treatment for childhood cancer. Table 3.1 gathers demographic and treatment information for the members of the cohort with complete data, and in a separate column for the members that experienced a subsequent VHD. No particular imbalances are observed in the biological sex and age at the diagnosis of survivors. The median year of diagnosis in the cohort was 1986, while a decade earlier when calculated among survivors that experienced a VHD. We can also observe an over-representation of Hodgkin survivors among the sub-population of the cohort that developed a VHD (40.7%), while the same is not true throughout the cohort (6.3%). Moreover, 86.4% of the patients who developed a VHD were treated with chemotherapy, 77.8% with radiotherapy, and 40.5% with both. Most people who experienced a VHD had been treated with both chemotherapy and radiotherapy (66.7%). The median age for experiencing a VHD was 31.8 years old. The median follow-up of the cohort was 30.6 years.

In this study, only severe VHD cases were taken into account (grade ≥ 3), a decision based on the fact that non-severe cardiovascular disease is often self-declared and could cause a reporting bias in the results (Taylor et al., 2010). Therefore, we didn't take into account incidents that we were unable to confirm, while for patients with VHD among their causes of death, VHD was directly considered of grade 5.

Chemotherapy

Chemotherapy data is available for most patients. Drug names and administration dates are available for initial and subsequent therapy for CC, as well as the total dose per unit of body surface area as milligrams per square meter (mg or g/m2) of every antineoplastic drug. Antineoplastic drugs are categorized into pharmacological groups according to their known mechanisms of action in the cell: anthracycline, alkylating agents, vinca alkaloids, antimetabolites, other antibiotics/antineoplastic agents, and other cytotoxic drugs. Details concerning the mean administered dose by sub-group and the concerned population size are provided in Table 3.2.

Table 3.1: Demographic and treatment features of five-year survivors of the FCCSS and of survivors who experienced valvular heart disease (VHD) after treatment for childhood cancer(CC) with complete data.

Factors	7492 CCS No. (%) or median [Range]	81 VHD No. (%) or median [Range]
Biological sex		
Male	3386 (45.2)	37 (45.7)
Female	4106 (54.8)	44 (54.3)
Age at childhood cancer diagnosis		
Median (in years)	*5.3 [0-20.6]*	*7.5 [0.2-18.8]*
$\leq$ 5 years	3615 (48.3)	26 (32.1)
5-10 years	1646 (22)	26 (32.1)
10-15 years	1606 (21.4)	19 (23.5)
15 years	625 (8.3)	10 (12.3)
Year of childhood cancer diagnosis		
Median (in years)	*1986 [1946-2000]*	*1976 [1961-2000]*
$\leq$ 1980	2422 (32.3)	55 (67.9)
1981-1989	2422 (32.3)	18 (22.2)
$\geq$ 1990	2648 (35.3)	8 (9.9)
Type of childhood cancer		
Hodgkin Lymphoma	471 (6.3)	33 (40.7)
Other lymphomas and reticuloendothelial neoplasms	788 (10.5)	9 (11.1)
CNS and miscellaneous intracranial and intraspinal neoplasms	1124 (15)	4 (4.9)
Neuroblastoma and other peripheral nervous cell tumors	1029 (13.7)	8 (9.9)
Soft tissue and other extraosseous sarcomas	846 (11.3)	7 (8.6)
Retinoblastoma	519 (6.9)	1 (1.2)
Renal tumors	1137 (15.2)	7 (8.6)
Hepatic tumors	79 (1.1)	1 (1.2)
Malignant bone tumors	680 (9.1)	5 (6.2)
Germ cell tumors, trophoblastic tumors, and neoplasms of gonads	469 (6.3)	6 (7.4)
Others	350 (4.7)	0
Chemotherapy		
Yes	5664 (75.6)	70 (86.4)
No	1828 (24.4)	11 (13.6)
Radiotherapy (RT)		
Yes	3906 (52.1)	63 (77.8)
No	3586 (47.9)	18 (22.2)
Mean Dose to the Heart (MHD)		
Median (in Gy, on those treated with radiotherapy)	*1.37 [0-61.2]*	*28.26 [0.004-49.1]*
MHD (categorized) *(in Gy)*		
No RT	3586 (47.9)	18 (22.2)
$[0, 1]$	1799 (24)	5 (6.2)
(1, 5]	747 (10)	4 (4.9)
(5, 15]	584 (7.8)	6 (7.4)
15 Gy	776 (10.4)	48 (59.3)
Combination of treatments		
RT (alone)	871 (11.6)	9 (11.1)
Chemotherapy (alone)	2629 (35.1)	16 (19.8)
Both	3035 (40.5)	54 (66.7)
Neither/missing	957 (12.8)	2 (2.5)
Attained age		
Median (in years)	*37.9 [5.4-79.8]*	*39.9 [5.7-61.1]*
$\leq$ 20 years	431 (5.8)	6 (7.4)
20-30 years	1574 (21)	9 (11.1)
30-40 years	2272 (30.3)	26 (32.1)
40-50 years	2121 (28.3)	29 (35.8)
50 years	1094 (14.6)	11 (13.6)
Follow up $^{\neq}$		
Median (in years)	*30.6 [3-73.9]*	*31.8 [3-49.5]*
$\leq$ 10 years	365 (4.9)	4 (4.9)
10-20 years	578 (7.7)	8 (9.9)
20-30 years	2664 (35.6)	25 (30.9)
30-40 years	2268 (30.3)	25 (30.9)
40 years	1617 (21.6)	19 (23.5)
Deceased	1459 (19.5)	40 (49.4)

$\neq$: Follow-up was defined as the difference between the date of childhood cancer diagnosis and VHD diagnosis for VHD patients, death or date of last medical news for the rest of the cohort

Table 3.2: Descriptive of chemotherapy exposure by pharmacological group in the FCCSS.

Pharmacological group of chemotherapy agents	All five-year survivors (7492)		VHD	
	No (%)	Mean dose (min ; max)	No (%)	Mean dose (min ; max)
Alkylating Agents (in g/m2) Dacarbazine, Streptozocin, Fotemustine, Carboplatine-Jm8, Cisplatin, Lomustine-Ccnu, Carmustine-Bcnu, Mechlorethamine, Chlorambucil, Cyclophosphamide, Nitrogen Mustard, Altretamine-Hexamethylmelanine, Ifosfamide, Melphalan, Procarbazine, Thiotepa, Temozolomide, Busulfan, Peptichimio	4233 (56.5)	14.29 [0-100]	47 (58)	10.68 [0-83]
Anthracyclines (in g/m2) Adriamycine, Doxorubicine, Daunorubicine, Epi-adriamycin, Zorubici	2741 (36.6)	0.25 [0.02-0.8]	27 (33.3)	0.26 [0.08-0.47]
Vinca Alcaloids (in g/m2) Vincristine, Vinblastine VLB, Vindesine, Navelbine	4390 (58.6)	0.03 [0-1]	52 (64.2)	0.06 [0-0.51]
Antimetabolites (in mg/m2) Methotrexate-MTX, Cytarabine, Arabinosyl Cytosine, Hydroxycarbamide, Hydroxy-urea, 6-Mercaptopurine (6-MP), Thioguanine-6 TG, Fludarabine Phosphate, 5-Fluorouracil (5-FU) + olinic acid, Methylguanine, MGG	1380 (18.4)	46.63 [0.01-1598.44]	13 (16)	48.31 [0.29-220.68]
Other Antibiotics and Antineoplastic Agents (in mg/m2) Mitoxantrone, Actinomycin D, Rufomycin, Mitomycin, Bleomycin	2506 (33.4)	31.73 [0.3-4302]	23 (28.4)	48.95 [1.63-193.02]
Other cytotoxics (in mg/m2) Asparaginase, Elliptinium Acetate, Amsacrine, Irinotecan, Interferon alpha-IFN-a, Interleukin 2 (IL2)	369 (4.9)	1683.54 [0.1-391684]	3 (3.7)	144.83 [100.13-234.22]

Radiation dosimetry and heart dose-volume histogram

Whole-body voxelized dosimetry matrices are available for 3906/4081 survivors who had received radiotherapy. The methodology of the radiation dose reconstruction that has been described in published works (Veres et al., 2014; Vũ Bezin et al., 2017). Of the patients with missing data, only one had experienced a severe VHD. Dose-volume metrics can be calculated for any organ or anatomical region of interest selected within the three-dimensional voxel phantom. In the context of this thesis, we considered the doses absorbed by the heart (Figure 3.2) and calculated the cumulative DVH to the heart for each patient. In Figure 3.3 are represented the average cumulative DVHs by type of CC. We also calculated the Mean Heart Dose (MHD), as well as the median, minimum, and maximum dose to the heart. In addition, we extracted for each patient the DVH parameters indicating the heart volume that received at least d Gy ($V_{d\,Gy}$), with thresholds set to 0.1 Gy, 5 Gy, 20 Gy, and 40 Gy. To thoroughly evaluate the association of low to moderate radiation doses to the heart with a subsequent VHD, we also analyzed heart DVH parameters with an upper bound of $5\ Gy$ ($V_{0.1\ Gy|V5\ Gy=0\%}$), $20\ Gy$ ($V_{5\ Gy|V20\ Gy=0\%}$), and $40\ Gy$ ($V_{20\ Gy|V40\ Gy=0\%}$), respectively, by truncating the population of the study. These are hereafter referred to as bounded DVH parameters (Bates et al., 2019). Some descriptives, particularly about the number of survivors that they are concerned about, are included in the table and figure of results in Chapter 4.

The median of the MHD among irradiated people who developed a VHD was 28.26 Gy compared to the median of the cohort, which was 1.37 Gy (Wilcoxon's test (Taylor et al., 2010) P-value < 0.0001). Additional comparisons with respect to the type of childhood cancer are detailed in table 3.3. A significantly different MHD is observed between survivors of Hodgkin lymphoma who experienced a VHD in comparison to those who did not. A similar conclusion can be reached for survivors of Neuroblastoma, Soft tissue sarcoma, and germ cell tumors. The same is not observed for survivors of renal tumors, despite the big difference (1.12 Gy among survivors without VHD versus 17.41 Gy among survivors with VHD), or survivors of central nervous system neoplasms (0.81 Gy versus 15.29 Gy).

In Table 3.4, we provide some additional information on the levels of heart radiation dose by type of radiotherapy technique and by field of irradiation. The two columns represent survivors who were treated with radiotherapy. Just like for Table 3.1, in the first column, descriptives concern all of the survivors of the FCCSS that were treated with radiotherapy, and in the second, only those who experienced a VHD. Most of the survivors were treated with Cobalt and next with Photon LINAC.

Among survivors that experienced a VHD, the median MHD is higher when they were treated with Cobalt and next with Photon LINAC. We can observe an elevated median MHD when the irradiation field was the Thorax or the Abdomen, particularly among survivors that experienced a VHD.

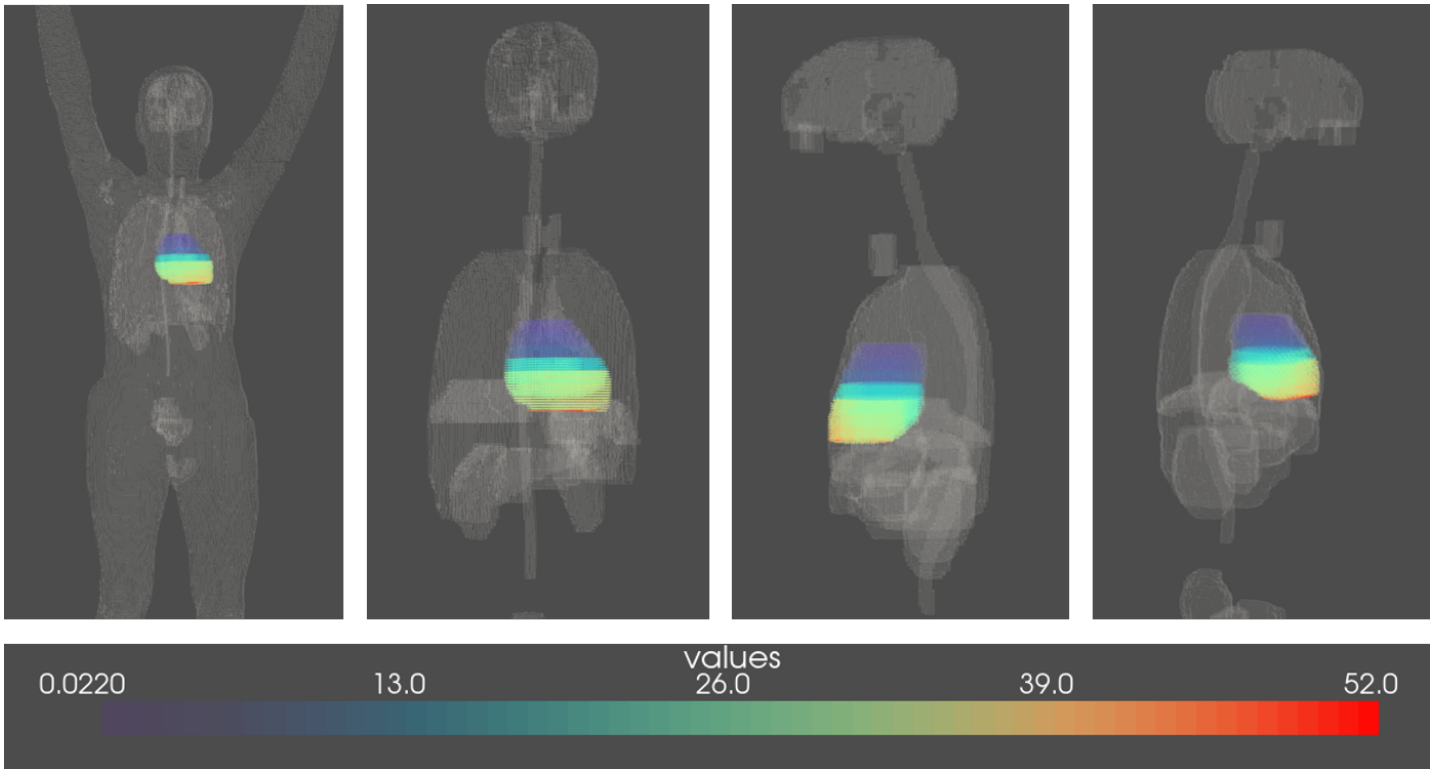

Figure 3.2: Representation of the voxelized heart-dose reconstruction; four views (front, back, left, and right) of one childhood cancer survivor; voxels are of size $2mm^3$, and the color shades represent the level of the radiation dose (in Gy). This survivor was treated at 3.5 years old, in 1961 for Hodgkin lymphoma and received a mean heart dose of 19.6 Gy. Figure: Duyen DO

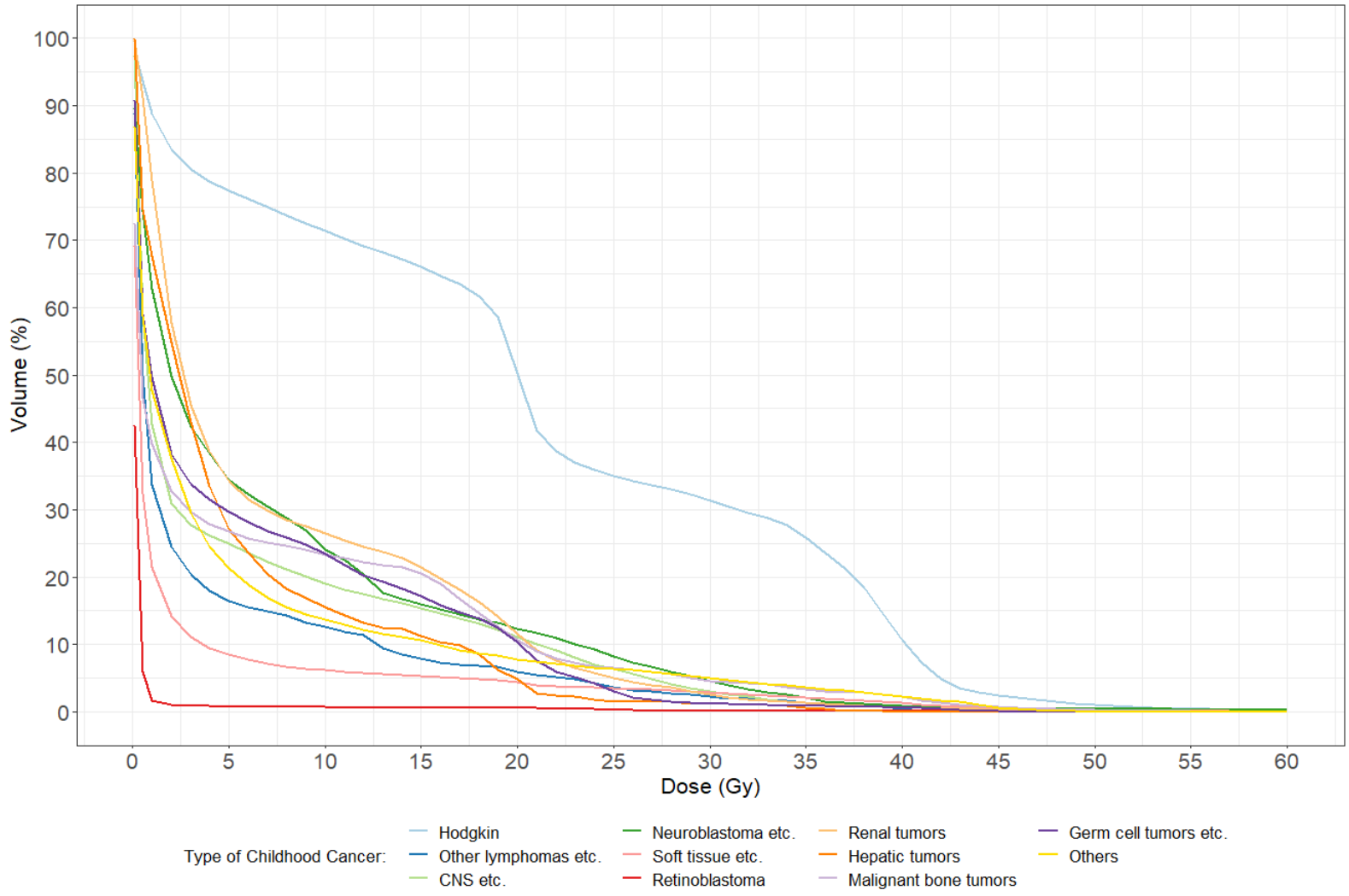

Figure 3.3: Cumulative dose-volume histograms (DVH) according to the type of childhood cancer; the average DVH as calculated by type of childhood cancer.

Finally, we calculated the cumulative incidence in the FCCSS while stratifying on radiotherapy (categorized Mean Heart Dose, $V_{5\,Gy|V20\,Gy=0\%}$, $V_{20\,Gy|V40\,Gy=0\%}$, $V_{40\,Gy}$), based on the attained age as time-scale. Cumulative incidence at 40 years old was 0.6% in the non-irradiated subpopulation and 4% among those who received radiotherapy with MHD $> 15Gy$ (Figure 3.4). For patients who received 5-20, 20-40, and ≥ 40 Gy to the heart, cumulative incidences increase as the dose increases (0.2%, 1.5%, and 5.2% at 40 years old). Cumulative incidence at 65 years old was 1.7% in the non-irradiated subpopulation and 25.8% in the irradiated population when MHD $> 15\ Gy$.

Additional plots with the cumulative incidences according to the DVH parameters (Figures A.2, A.3 and A.4) and detailed cumulative incidence estimates at age 40 and age 65 (Table A.1) can be found in the Appendix A. Indicatively, cumulative incidences were: 0.2% at 40 years old and 3.9% at 65 years old among patients treated with residual doses of $5 - 20$ Gy to the heart, 1.5% at 40 years old, and 8.3% at 65 years old among patients treated with residual doses of $20 - 40$ Gy to the heart and 5.2% at 40 years old and 24.2% at 65 years old among patients treated with residual doses of ≥ 40 Gy to the heart.

Table 3.3: Median MHD, by type of childhood cancer, calculated in the sub-population of the FCCSS that had been treated with radiotherapy (3906), and Wilcoxon's test p-value.

Type of Childhood Cancer	**No VHD**		**VHD**		p-value (MHD)
	No	MHD (Median)	No	MHD (Median)	
Hodgkin Lymphoma	411	18.67	33	33.9	$<$0.0001
Other lymphomas and reticuloendothelial neoplasms	244	0.5	4	12.26	0.217
CNS and miscellaneous intracranial and intraspinal neoplasms	962	0.81	2	15.29	0.078
Neuroblastoma and other peripheral nervous cell tumors	376	3.05	6	17.08	0.011
Soft tissue and other extraosseous sarcomas	454	0.22	5	31.15	0.001
Retinoblastoma	208	0.01	1	0.18	0.343
Renal tumors	627	3.42	6	12.16	0.136
Hepatic tumors	17	5.45	0	0	-
Malignant bone tumors	284	0.37	3	3.42	0.708
Germ cell tumors, trophoblastic tumors, and neoplasms of gonads	134	1.12	3	17.41	0.032
Other	122	1.27	0	0	-
All survivors treated with radiation therapy	3839	1.37	63	28.26	< 0.0001

Table 3.4: No. of survivors, the median, minimum, and maximum dose to the heart, by type of radiotherapy technique and field of irradiation, calculated for the cohort and the subpopulation that experienced a Valvular Heart Disease (VHD).

Type of Radiotherapy	FCCSS (3906)		VHD (63)	
	No*	Median MHD [min-max]	No*	Median MHD [min-max]
Type of radiotherapy technique				
Kilovoltage X-rays	276	2.2 [0-34]	3	22.53 [0-49.12]
Cobalt	1751	1.94 [0-61.2]	41	35.6 [20.73-41.36]
Photon LINAC	1544	1.22 [0-60.66]	16	28.26 [12-44.66]
Electron LINAC	255	0 [0-44.66]	3	22.53 [0-49.12]
Field of irradiation				
Abdomen	1254	5.53 [0-50.44]	21	20.73 [1.36-44.66]
Arm and Hand	21	0.25 [0.06-37.71]	1	37.71
Head and Neck	1614	0.51 [0-61.2]	9	18.74 [0.18-39.16]
Leg and Foot	191	0.12 [0-41.63]	2	4.74 [0-9.47]
Pelvis	315	0.81 [0-50.44]	6	9.62 [0.14-30.46]
Thorax	1406	15.34 [0-61.2]	50	30.59 [9.47-49.12]

*The sum does not always correspond to the total mentioned above, because of multiple sites and sessions of irradiation.

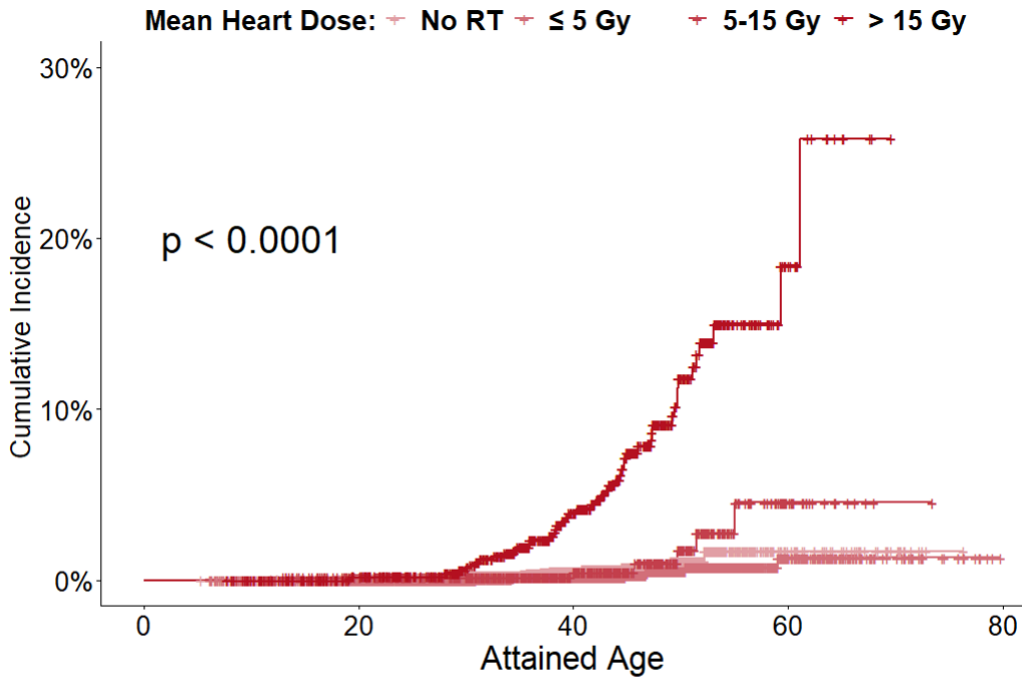

	Attained Age:	20 years old	40 years old	65 years old
No RT	Events	3	14	18
	Survivors at risk	3468	1207	28
MHD ≤ 5Gy	Events	0	4	9
	Survivors at risk	2355	1318	57
5Gy < MHD ≤ 15Gy	Events	1	2	6
	Survivors at risk	532	293	5
MHD > 15 Gy	Events	2	21	48
	Survivors at risk	706	398	5

Figure 3.4: Cumulative incidence of VHD in the FCCSS cohort (7492 survivors with complete data, 81 of whom developed a VHD) by attained age, stratified on the MHD. A P-value is given for the log-rank test. Abbreviations: RT: Radiotherapy; VHD: Valvular Heart Disease; MHD: Mean Heart Dose

3.2 . PanCareSurFup and ProCardio nested case-control study - European cohort

Collaborative efforts initiated that aim to pool data from two EU-funded consortia to create a large cohort of survivors (42.361 survivors): the PanCareSurFup cardiac study and the project ProCardio.

PanCareSurFup is a network of professionals, survivors, and their families, from 16 European institutions. It includes more than 80,000 5-year childhood and adolescent cancer survivors, and its aim is to carry out a series of epidemiologic studies of the most severe complications of long-term survival (Grabow et al., 2018; Hjorth et al., 2015; "PanCareSurFup", 2023).

We used the nested case-control study within this merge of cohorts designed to assess treatment-related risk factors for valvulopathy, to attempt external validation of our predictive models of risk for valvulopathy after childhood cancer.

A total of 274 survivors were individually paired in a case-control study, and 224 of them with complete dosimetric data were available to us and included in our analyses. Each case with valvulopathy was matched to one control based on biological sex, age at first primary cancer diagnosis ($\pm$ one year), year of first primary cancer diagnosis ($\pm$ three years), follow-up duration (the follow-up of each control patient was at least as long as the follow-up of their matched case) and treatment center.

Radiation exposure

Similarly to the methodology followed for the FCCSS, the radiation dosimetry for the whole body, including the heart, was reconstructed for all cases and controls who received radiotherapy. From the voxelized dosimetry matrices, we were able to calculate the Mean Heart Dose, the median, min, and max dose to the heart, as well as some DVH parameters indicatively, likewise to Section3.1.

Finally, we plotted the average cumulative DVH of heart doses by type of childhood cancer, illustrated in Figure 3.5. Similarly to the FCCSS, among survivors treated for lymphomas, the affected heart volume is on average higher for doses 15 to $<$40 Gy.

Demographic and treatment caracteristics

In Table 3.5, the demographic and treatment characteristics of a nested case-control study are detailed. Some characteristics are, by definition, statistically similar between cases and controls, as the populations were matched. The matching variables were the biological sex, age, and year at CC diagnosis, follow-up, and treatment center. A column of p-values of univariate conditional logistic regression estimates is provided for the variables that were not considered during the pairing.

We can observe differences in the prevalence of the different types of childhood cancer: for example, lymphomas are the most common type of childhood cancer both among controls and among cases; however, its prevalence is 64.3% in cases and 25.9% among controls. Also, Neuroblastoma is among the most common types among cases (8%), but it is less frequent among controls. On the contrary, renal tumors, which are frequent among controls (11.6%), are less common among cases (2.7%). The type of cancer, being highly correlated to the type of treatment, was not chosen as a matching variable.

Concerning treatment characteristics, we can observe a similar proportion of survivors treated with chemotherapy in both controls and cases and no statistically significant association (p-value= 0.684). The same cannot be said about radiotherapy exposure, where we observe an $\approx 20\%$ difference in the exposure, between controls and cases (67.9% versus 89.3%). Radiotherapy exposure as well as the mean heart dose sort is significantly associated with the outcome (p-value= $<$ 0.001 for both variables). Finally, a statistical association is also observed when survivors were treated with a combination of chemotherapy and radiation therapy (p-value= 0.001).

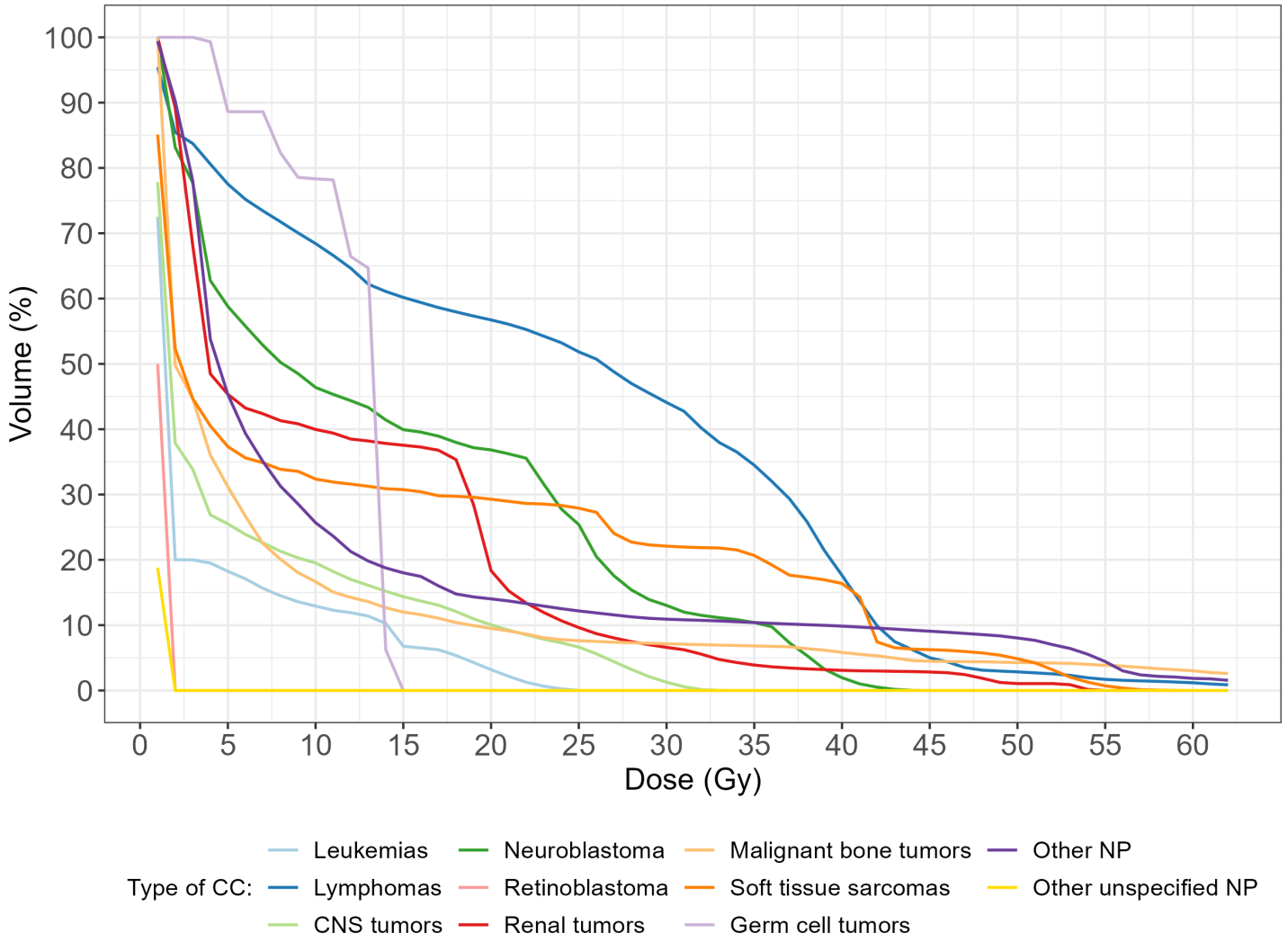

Figure 3.5: Cumulative dose-volume histograms (DVH) in the population of PanCare-ProCardio according to the type of childhood cancer; the average DVH as calculated by the type of childhood cancer.

Table 3.5: Demographic and treatment features of five-year survivors with complete data of the nested case-control study of the PanCare cohort, paired on the biological sex, age, and year of childhood cancer diagnosis and follow-up duration.

Factors	Control No. (%) or median [Range]	Case No. (%) or median [Range]	p-value
Biological sex			*
Male	66 (58.9%)	66 (58.9%)	
Female	46 (41.1%)	46 (41.1%)	
Age at childhood cancer diagnosis			*
Median (in years)	9.1 [0.3-16.7]	8.8 [0.3-17]	
$\leq$ 5 years	32 (28.6%)	29 (25.9%)	
5-10 years	33 (29.5%)	33 (29.5%)	
10-15 years	43 (38.4%)	46 (41.1%)	
15 years	4 (3.6%)	4 (3.6%)	
Year of childhood cancer diagnosis			*
Median (in years)	1976 [1955-2003]	1975 [1954-2001]	
$\leq$ 1980	87 (77.7%)	83 (74.1%)	
1981-1989	19 (17%)	23 (20.5%)	
$\geq$ 1990	6 (5.4%)	6 (5.4%)	
Type of childhood cancer			$<$0.0001
Leukemias, myeloproliferative diseases, and myelodysplastic diseases	10 (8.9%)	6 (5.4%)	0.279
Lymphomas and reticuloendothelial neoplasms	29 (25.9%)	72 (64.3%)	0.006
CNS and miscellaneous intracranial and intraspinal neoplasms	20 (17.9%)	4 (3.6%)	0.958
Neuroblastoma and other peripheral nervous cell tumors	4 (3.6%)	9 (8%)	0.017
Retinoblastoma	2 (1.8%)	2 (1.8%)	0.390
Renal tumors	13 (11.6%)	3 (2.7%)	0.768
Hepatic tumors	(0%)	(0%)	-
Malignant bone tumors	10 (8.9%)	2 (1.8%)	0.895
Soft tissue and other extraosseous sarcomas	15 (13.4%)	10 (8.9%)	0.334
Germ cell tumors, trophoblastic tumors, and neoplasms of gonads	2 (1.8%)	3 (2.7%)	0.455
Other malignant epithelial neoplasms and malignant melanomas	6 (5.4%)	1 (0.9%)	(ref.)
Other and unspecified malignant neoplasms	1 (0.9%)	0 (0%)	0.999
Chemotherapy			0.684
No	43 (38.4%)	40 (35.7%)	
Yes	69 (61.6%)	72 (64.3%)	
Radiotherapy (RT)			$<$0.0001
No	36 (32.1%)	12 (10.7%)	
Yes	76 (67.9%)	100 (89.3%)	
Mean Dose to the Heart (MHD)			
Median (in Gy, on those treated with radiotherapy)	0 [0-29.2]	0.8 [0-48.2]	$<$0.0001
MHD (categorized) *(in Gy)*			$<$0.0001
No RT	36 (32.1%)	12 (10.7%)	(ref.)
$[0, 1]$	49 (43.8%)	44 (39.3%)	0.036
(1, 5]	11 (9.8%)	1 (0.9%)	0.285
(5, 15]	5 (4.5%)	6 (5.4%)	0.093
$>$15 Gy	11 (9.8%)	49 (43.8%)	$<$0.0001
Combination of treatments			0.004
RT (alone)	27 (24.1%)	38 (33.9%)	0.002
Chemotherapy (alone)	20 (17.9%)	10 (8.9%)	0.094
Both	49 (43.8%)	62 (55.4%)	0.001
Neither/missing	16 (14.3%)	2 (1.8%)	(ref.)
Attained age			
Median (in years)	41 [11-65]	41 [6-66]	
$\leq$ 20 years	7 (6.2%)	8 (7.1%)	
20-30 years	13 (11.6%)	13 (11.6%)	
30-40 years	33 (29.5%)	33 (29.5%)	
40-50 years	43 (38.4%)	40 (35.7%)	
50 years	16 (14.3%)	18 (16.1%)	
Follow up $^{\neq}$			*
Median (in years)	31 [6-55]	31 [5-55]	
$\leq$ 10 years	8 (7.1%)	8 (7.1%)	
10-20 years	8 (7.1%)	8 (7.1%)	
20-30 years	36 (32.1%)	36 (32.1%)	
30-40 years	36 (32.1%)	36 (32.1%)	
40 years	24 (21.4%)	24 (21.4%)	
Deceased	10 (8.9%)	31 (27.7%)	

$\neq$: Follow-up was defined as the difference between the date of the first childhood cancer diagnosis and VHD diagnosis for VHD patients, death or date of last medical news for the rest of the cohort

4 - Survival risk models based on dose-volume indicators

4.1 . Context

In this chapter, we present the results of the first study conducted in the FCCSS cohort on the risk of experiencing severe VHD (grade ≥ 3) after treatment for childhood cancer. The choice of risk models was based on what is classically used in radiation epidemiology studies (Cox and ERR based on the mean dose to the heart). Similarly, the variables we chose for the estimation of the radiation-induced risk are also traditionally utilized in studies based on voxelized dosimetric data. An additional result of this study was the incorporation of volume indicators into risk models, which allowed us to describe the radiation-induced risk of experiencing a VHD in terms of irradiated heart volume, instead of the level of radiation dose.

4.2 . Methods

Association and descriptive analyses were carried out on 7492 survivors of the FCCSS with complete data (see Figure 3.1). For each patient, we only considered the first incidence of VHD. If a cardiac event had taken place before the VHD occurrence (Cutter et al., 2015) it was not considered as an event. The deemed time scale throughout the analyses was the attained age (Chalise et al., 2016), which was calculated as the time between the date of birth and:

- the date of diagnosis of the event for survivors that presented a severe VHD, or the date of death for survivors with VHD among their causes of death
- the date of death for survivors that passed without presenting a known VHD
- the date of last medical news for the rest of the cohort.

The Cox model

Hazard ratios (HR) and 95% confidence intervals ($CI_{95\%}$) (Borgan, 2001; Therneau et al., 2021) were estimated according to the Cox proportional hazards model (see Section 2.1 for more details). Ties were calculated with the Breslow method, and the proportional hazards assumption was verified in every model (Grambsch & Therneau, 1994). We initially conducted univariate analyses with demographic or treatment covariates. We then estimated the radiation-induced risk first in relation to radiotherapy exposure, next the MHD as well as its categorized version, using the MHD distribution (rounded) quantiles of the cohort as cut-offs:

- 1 Gy
- 5 Gy
- 15 Gy

Finally, we estimated the radiation-induced risk of experiencing a late VHD in relation to the Dose Volume Histogram (DVH) parameters, with and without truncating the population for a predefined cut-off:

- $V_{0.1\,Gy}$ and $V_{0.1\,Gy|V5\,Gy=0\%}$
- $V_{5\,Gy}$ and $V_{5\,Gy|V20\,Gy=0\%}$
- $V_{20\,Gy}$ and $V_{20\,Gy|V40\,Gy=0\%}$
- $V_{40\,Gy}$

We categorized each of the $V_{d\,Gy}$ parameters mentioned above into the following classes of survivors:

- were not treated with radiotherapy
- received less than d Gy to the heart
- received d Gy to $\leq 50\%$ of the heart
- received d Gy to $> 50\%$ of the heart.

The reference category contained survivors not treated with radiotherapy.

Looking for a potential risk induced by chemotherapy treatment on the occurrence of a VHD, we tested some alternatives exposures:

- chemotherapy (binary)
- exposure to agents belonging to a particular pharmacological group among the following: alkylating agents, anthracyclines, and vinca alkaloids.

However, the final multivariable models were adjusted on chemotherapy exposure, a decision justified by the results.

The Excess Relative Risk

Additionally, we modeled the dose-effect relationship of the MHD with Poisson regression (see section 2.1) to investigate the linearity of the dose-response relationship by estimating the Excess of Relative Risk (ERR) (Suissa, 1999) per Gy (linear term) and Gy^2 (quadratic term). We compared the linear model to:

- the exponential
- the quadratic
- and the linear-quadratic

to assess a possibly nonlinear behavior of the dose-effect relationship (see Section 2.1 for more details).

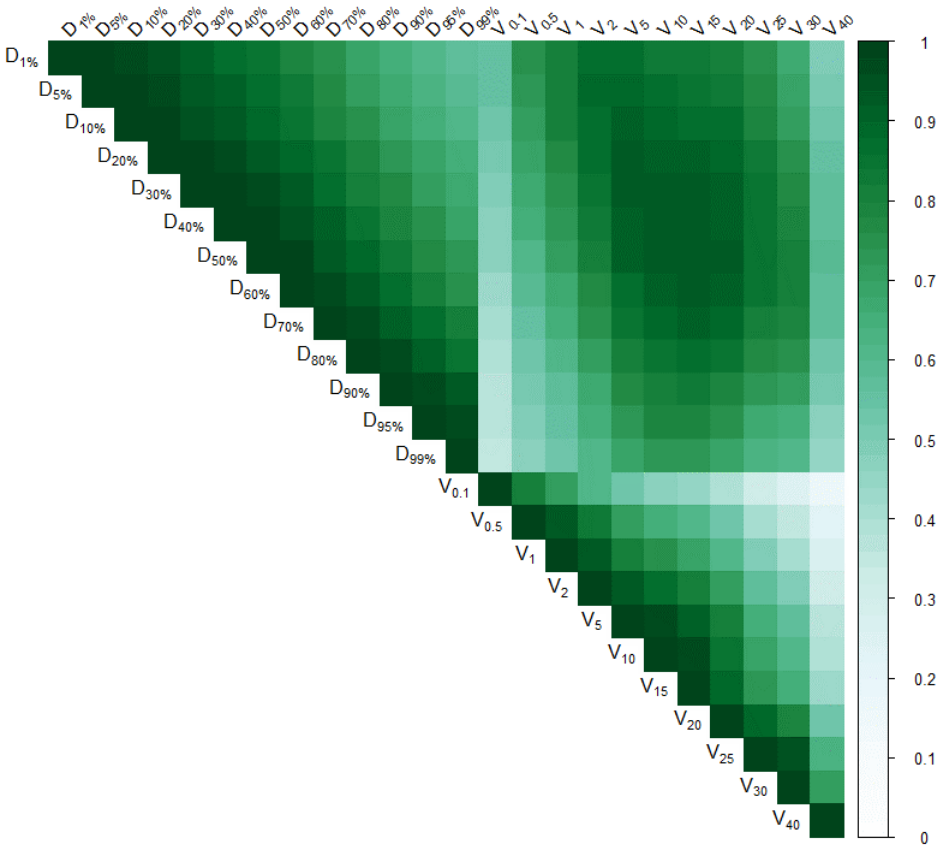

Figure 4.1: Correlation matrix of dose and volume indicators.

Multivariable modeling of the radiation-induced risk of experiencing a VHD

In order to go one step further in studying the role of heart radiation dose in the risk of VHD, we explored the possibility of combining multiple DVH parameters into one adjustment. DVH parameters have two advantages: first, they are known to physicians, and second, they are implemented to the TPS and can be automatically extracted.

In that context the following percentiles of the heart dose distribution ($D_{v\%}$ represents the minimum dose received by a percentage of the heart volume) were computed: $D_{1\%}$, $D_{5\%}$, $D_{10\%}$, $D_{20\%}$, $D_{30\%}$, $D_{40\%}$, $D_{50\%}$ (median heart dose), $D_{60\%}$, $D_{70\%}$, $D_{80\%}$, $D_{90\%}$, $D_{95\%}$ and $D_{99\%}$; the following volume indices ($V_{d\,Gy}$ represents the percentage of the heart volume receiving at least a level of dose) were computed: $V_{0.1\,Gy}$, $V_{0.5\,Gy}$, $V_{1\,Gy}$, $V_{2\,Gy}$, $V_{5\,Gy}$, $V_{10\,Gy}$, $V_{15\,Gy}$, $V_{20\,Gy}$, $V_{25\,Gy}$, $V_{30\,Gy}$ and $V_{40\,Gy}$.

Particular attention was paid to the problem of multicollinearity between variables, significant for combinations of DVH parameters (Figure 4.1). Dose and volume parameters were combined in three groups: dose parameters alone, volume parameters alone, and finally, dose and volume parameters together (complete model). For each group, four different approaches were applied, resulting in 12 different scenarios for modeling the radiation-induced risk of experiencing a VHD after treatment for childhood cancer according to a combination of dosimetry indicators. We first considered Principal Components Analysis (PCA) (Jolliffe, 2013; Le et al., 2008), where the number of components to calculate was decided by scree plots. Then, three types of penalized Cox regression (Friedman et al., 2010; Simon et al., 2011; Zou & Hastie, 2005) were employed: Least Absolute Shrinkage and Selection Operator (LASSO), Ridge, and Elastic Net. The penalty parameter λ of penalized Cox regression was chosen via 10-fold cross-validation in each case by comparing the models' deviance. The number of retained components for the PCA was defined according to the Kaiser criterion. AIC (Akaike Information Criterion) and Harrell's C-index are included for model comparison.

All of the survival analyses and graphs of this section were conducted using R version 4.0.3 (2020-10-10) – "Bunny-Wunnies Freak Out" Copyright (C) 2020 – *The R Foundation for Statistical Computing* (Therneau, 2023; Wickham, 2016; Wickham et al., 2019; Wickham et al., 2023). Additional multivariate analyses provided in the supplementary material were performed with R packages FactoMineR, Coxnet, pec, and glmnet (Gerds, 2023; Lê et al., 2008; Simon et al., 2011; Tay et al., 2023). The Poisson regression was conducted in EPICURE ("The EPICURE Regression Programs", n.d.). All P-values were two-sided, and we fixed the significance threshold at 0.05 throughout the analyses.

4.3 . Results

Hazard Ratios

VHD risk was significantly associated with the type of childhood cancer (p-value for heterogeneity<0.001), however only when treated for Hodgkin lymphoma was the risk statistically associated with experiencing a VHD (HR=6.18, $CI_{95\%}$: 2.96-12.92)- Table 4.1).

Chemotherapy (HR = 2.83, $CI_{95\%}$: 1.49-5.39, as well as vinca alkaloids exposure (HR = 1.71, $CI_{95\%}$: 1.07-2.72) were also associated with experiencing a VHD- Table 4.1). However, no antineoplastic agents group seems to induce a statistically significant risk of experiencing a VHD after adjustment for MHD and age at childhood cancer diagnosis - Table 4.4).

Survivors treated with radiotherapy were twice more likely to experience a subsequent VHD (HR = 2, $CI_{95\%}$: 1.18-3.41, see Table 4.2). The radiation-induced risk estimates hardly changed when we adjusted for chemotherapy or/and age at childhood cancer diagnosis.

We also tested for interactions; none was observed (see Table 4.1).

Additional results can be found in Table 4.3 where hazard ratios are calculated by technique and field of irradiation, adjusted on chemotherapy and the MHD. While the risk of VHD is significant for patients treated with Cobalt or Photon LINAC (HR = 4.58, $CI_{95\%}$: 1.39-15.1 and HR = 4.01, $CI_{95\%}$: 1.13-14.2 respectively), the risk is no longer significant when the MHD is included in the model. The same applies when accounting for patients treated with thoracic radiotherapy. We propose this alternative model (adjusted on chemotherapy) in the case where the MHD is unavailable but information on the type and field of irradiation is.

Sensitivity analysis

Hodgkin lymphoma sorts as a risk factor for experiencing a VHD. However, the type of childhood cancer is strongly correlated to the type of treatment, and it cannot be included in a Cox model next to the treatment-related variables. Therefore, a sensitivity analysis was conducted to express radiation-induced risk among survivors treated for Hodgkin lymphoma.

Survivors that received heart radiation following Hodgkin lymphoma diagnosis have a high risk of experiencing a late VHD, which increases when models are adjusted on chemotherapy and age at diagnosis (see Table 4.5). Among survivors treated with radiotherapy for Hodgkin lymphoma, the estimated risk of experiencing a subsequent VHD increased more than nine times as the MHD increased by 1 Gy (HR/Gy = 9.29, $CI_{95\%}$: 5.21-16.54) and was similarly high when adjusted on chemotherapy ex-

Table 4.1: Univariate Analysis for the risk of a subsequent VHD in the FCCSS.

Population and therapy characteristics	**HR [CI 95%]**	**P-value/ P-trend△**
Sex (ref. : F)	1.02 [0.66-1.58]	0.93
Age at diagnosis of CC	1 [0.96-1.04]	0.95
Year of Diagnosis of CC	1 [0.97-1.02]	0.79
Type of CC diagnosis		<0.001
CNS and miscellaneous intracranial and intraspinal neoplasms	0.48	0.22
Neuroblastoma and other peripheral nervous cell tumors	1.14 [0.44-2.95]	0.79
Soft tissue and other extraosseous sarcomas	0.77 [0.29-2.07]	0.61
Retinoblastoma	0.5 [0.06-3.94]	0.51
Renal tumors	0.56 [0.21-1.51]	0.26
Hepatic tumors	2.54 [0.32-20.15]	0.38
Malignant bone tumors	0.65 [0.22-1.93]	0.44
Germ cell tumors, trophoblastic tumors, and neoplasms of gonads	1.16	0.78
Other (no VHD events)	-	-
Hodgkin Lymphoma	6.18 [2.96-12.92]	<0.001
Other lymphomas and reticuloendothelial neoplasms	(ref.)	
Hodgkin lymphoma (ref.: Any other types of First cancer diagnosis)	8.41 [5.40-13.10]	<0.0001
Chemotherapy (ref.: No)	2.83 [1.49-5.39]	0.002
Anthracyclines (ref.: No)	1.09 [0.68-1.74]	0.72
Alkylating Agents (ref.: No)	1.48 [0.94, 2.32]	0.09
Vinca Alcaloids (ref.: No)	1.71 [1.07-2.72]	0.03
Antibiotics and Antineoplastic Agents	0.76 [0.47-1.23]	0.26
Cytotoxics	0.65 [0.21-2.08]	0.47
Radiotherapy (ref.: No)	2.00 [1.18 - 3.41]	0.01
Interactions:		
Chemotherapy*Age at FNP diagnosis	0.93 [0.82-1.05]	0.23
Radiotherapy*Age at FNP diagnosis	1.07 [0.97-1.18]	0.17
Radiotherapy*Chemotherapy	0.76 [0.15-3.86]	0.73

Hazard Ratio (HR); 95% confidence intervals (95% CI); Proportional Hazard's assumption was verified for every independent risk factor;
△: P-value for continuous variables, P-trend for heterogeneity for binary variables, P-trend for trend for ordinal variables.

Table 4.2: Risk of radiation-induced VHD in the FCCSS adjusted on chemotherapy exposure and age at childhood cancer diagnosis.

Factors	**HR [95%CI]** (univariate)	**HR [95%CI]** (Adjusted on chemotherapy)	**HR [95%CI]** (Adjusted on chemotherapy and age at childhood cancer diagnosis)
Radiotherapy (RT)			
No	(ref.)	(ref.)	(ref.)
Yes	2.00 [1.18 - 3.41]	1.96 [1.15 - 3.3]	1.97 [1.16 - 3.36]
MHD - *increase of 1 Gy*	1.10 [1.08 - 1.11]	1.09 [1.08 - 1.11]	1.10 [1.08 - 1.11]
MHD – in Gy (categorized)			
No RT	(ref.)	(ref.)	(ref.)
[0, 1]	0.35 [0.13 - 0.95]	0.36 [0.14 - 0.99]	0.36 [0.13 - 0.99]
(1, 5]	0.57 [0.19 - 1.7]	0.54 [0.18 - 1.61]	0.50 [0.17 - 1.50]
(5, 15]	1.28 [0.51 - 3.24]	1.22 [0.48 - 3.09]	1.14 [0.45 - 2.90]
>15 Gy	7.94 [4.59 - 13.72]	7.36 [4.25 - 12.76]	7.63 [4.39 - 13.29]

French Childhood Cancer Survivors Study (FCCSS); Valvular Heart Disease (VHD); reference (ref.); Mean Heart Dose (MHD); Hazard Ratio (HR); 95% confidence intervals (95% CI); Proportional Hazard's assumption was verified for all models.

Table 4.3: Risk of radiation-induced risk of VHD in the FCCSS according to radiotherapy (RT) techniques and fields of irradiation.

RT characteristics	N/n	HR [CI 95%]	Adjusted* HR [CI 95%]	Adjusted** HR [CI 95%]
Radiotherapy technique				
kV X-rays (ref.)	273/3	-		-
Cobalt	1713/42	4.58 [1.39-15.1]	3.85 [1.16-12.8]	1.82 [0.54-6.09]
Photon LINAC	1561/16	4.01 [1.13-14.2]	3.3 [0.92-11.84]	1.05 [0.29-3.86]
Electron LINAC	252/3	2.91 [0.58-14.68]	2.52 [0.5-12.78]	2.41 [0.48-12.18]
P-value		0.021	<0.001	<0.001
Irradiation fields* **				
Other fields (ref.)	1369/5	-	-	-
Thorax	1356/50	9.19 [3.66-23.04]	8.26 [3.28-20.82]	1.06 [0.34-3.3]
Abdomen	674/4	1.22 [0.33-4.56]	1.06 [0.28-3.96]	0.77 [0.21-2.91]
P-value		<0.001	<0.001	<0.001

N=Survivors; n= VHD event; *Adjustment for chemotherapy; **Adjustment for chemotherapy and mean heart dose; other fields = Arm and Hand, Head and Neck, Leg and Foot, Pelvis; *** One field was emphasized per patient. In the case of conflict because of multiple sites of irradiation, thorax was favored over abdomen and abdomen over other fields.

posure and age at childhood cancer diagnosis(HR/Gy =8.23, $CI_{95\%}$:[4.59-14.76] and HR=10.39, $CI_{95\%}$: [5.57-19.38 respectively).

Excess Relative Risk

Finally, we observe in Figure 4.2 that the ERR increase is described more appropriately by the quadratic model than the linear or the linear quadratic. These comparisons are also summarized in Table 4.6, where, however, the best model according to the deviance seems to be the linear quadratic.

In addition, as illustrated in Figure 4.3, the ERR/GY increased remarkably with attained age. It was 0.04 ($CI_{95\%}$: 0-0.17) up to 30 years old, 0.94 ($CI_{95\%}$: 0.47-1.83) up to 40 years old, 2.28 ($CI_{95\%}$: 1.23-4.23) up to 50 years old and finally 3.12 ($CI_{95\%}$: 1.31-6.71) after the age of 50 years old.

Dose-Volume Histogram parameters

Concerning the heart DVH parameters, we found a 2.19 times higher risk of experiencing the event ($CI_{95\%}$: 1.29-3.73) when survivors had received a dose ≥ 0.1 Gy to more than 50% of the heart volume ($V_{0.1\,Gy} > 50\%$) in comparison to survivors who had not been treated with radiotherapy (Table 4.7). However, this risk was no longer present once we eliminated survivors that received > 5 Gy to the heart from the estimates ($V_{0.1\,Gy|V5\,Gy=0\%}$).

We also observed a risk increase with $V5$ Gy (HR = 5.4, $CI_{95\%}$: 3.14-9.29, 4.7) that became non-significant once we eliminated patients that received > 20 Gy to the heart ($V_{5\,Gy|V20\,Gy=0\%}$-HR = 2.75, $CI_{95\%}$: [0.92-8.24], see Table 4.7), from the estimates. However, the estimated risk was significant for a different heart-volume threshold (90% receiving doses between 5 and 20 Gy) (HR = 3.94, CI95%: 1.15-13.49, see Table 4.4).

Doses over 20 Gy ($V_{20\,Gy}$ and $V_{20\,Gy|V40\,Gy=0\%}$) were associated with an increased VHD risk (HR = 9.74, $CI_{95\%}$: 5.57-17.04, and HR = 5.03, $CI_{95\%}$: 2.35-10.76, see Table 4.7) when $> 50\%$ of the heart-volume had been irradiated. High doses ($V_{40\,Gy}$) even to small heart volumes ($< 50\%$) were also associated with an increased VHD risk (HR = 7.96, $CI_{95\%}$: 4.26-14.88, see Table 4.7).

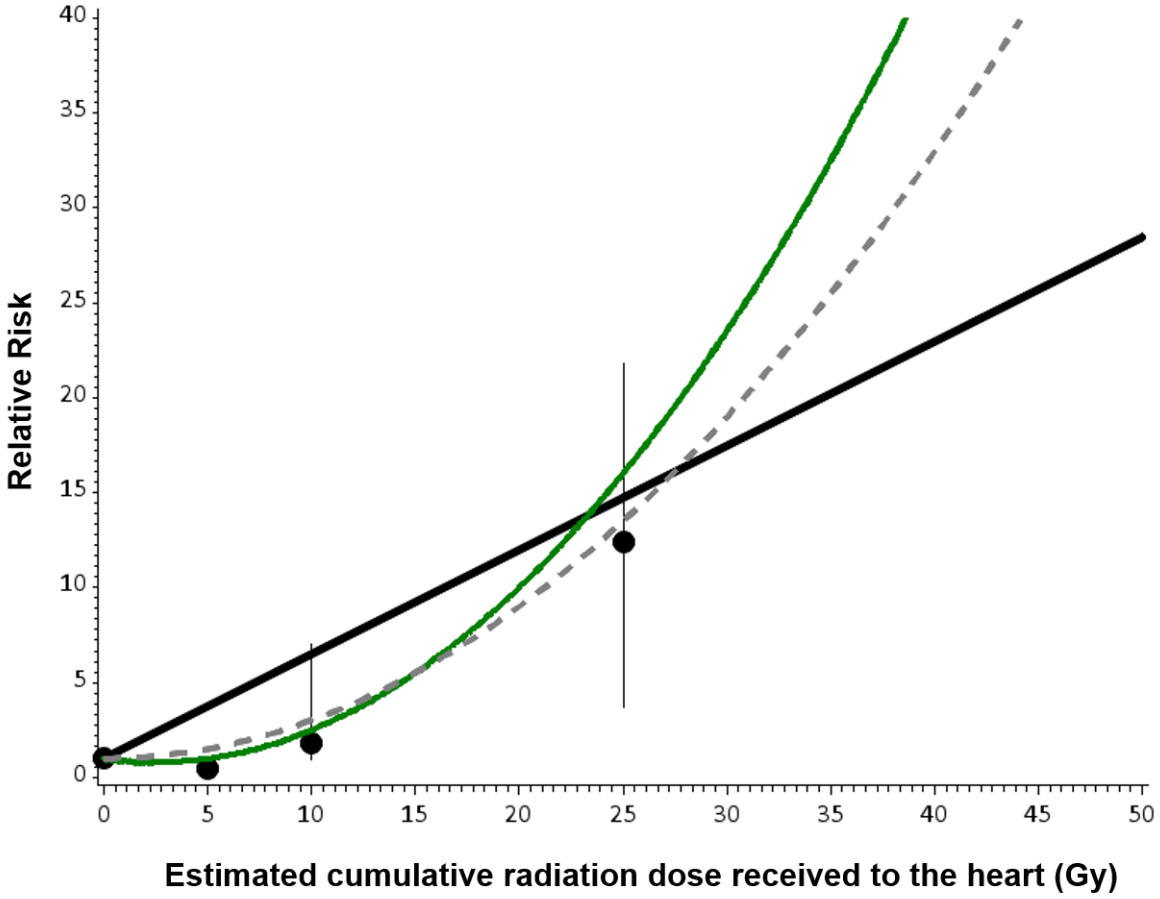

Figure 4.2: Radiation dose–response relationship for risks of VHD in the FCCSS. Relative risk (circles) with the corresponding 95% confidence intervals and fitted linear excess relative risk model (solid black line), linear-quadratic excess relative risk model (green line) and quadratic excess relative risk model (dashed grey line)

Multivariable Approaches

Information criteria and performance indices are presented in Table 4.8, according to each of the four approaches applied to address multicollinearity: PCA, LASSO, Ridge, and Elastic Net, as ordered in the first row. Those methods were applied to three groups of variables, detailed in the first column; dose variables, volume variables, and the complete model (the combination of dose and volume variables). The PCA coefficients (number of retained components was defined according to the Kaiser criterion) and the estimated coefficients of the penalized regressions can be found in the Appendix (Tables A.6 and A.7).

We chose the model where the radiation-induced risk is estimated with the Mean Heart Dose with AIC=1143.72 as the reference model. The model that seemed to be the closest to the reference model according to the AIC was the PCA on the complete model (1145.96), followed by PCA on the dose parameters (1146.42), but none of them seemed closer to the real model than the model based on the MHD. The best C-index was also estimated for the PCA on the complete model (0.744) and was slightly greater than the C-index of the reference model (0.74).

Overall, none of the multivariable models seems to outperform the MHD-based model entirely.

Table 4.4: Hazard ratios of the risk of a subsequent VHD with respect to anthracycline, alkylating agents, and vinca alkaloid exposure instead of chemotherapy exposure (alternative adjustments for Table 2 for the FCCSS).

Alternative chemotherapy exposure	**Hazard Ratio [95% CI]** Adjusted on MHD	**Hazard Ratio [95% CI]** Adjusted on MHD and age at the first cancer diagnosis
Chemotherapy	2.05 [1.08-3.89]	2 [1.05-3.81]
ANTHRA	1.3 [0.81-2.09]	1.38 [0.86-2.23]
ALKYL	1.2 [0.76-1.88]	1.26 [0.79-1.99]
VINCA	1.13 [0.71-1.80]	1.11 [0.69-1.77]

Table 4.5: Risk of radiation-induced VHD in the FCCSS adjusted on chemotherapy exposure according to Hodgkin lymphoma as type of childhood cancer (471 survivors among whom 33 experienced a VHD).

Factors	**N (VHD events)**	**HR [95%CI]** (univariate)	**HR [95%CI]** (Adjusted on chemotherapy)	**HR [95%CI]** (Adjusted on chemotherapy and age at first cancer diagnosis)
Hodgkin and radiotherapy (RT)				
No Hodgkin and no RT	3559 (18)	(ref.)	(ref.)	(ref.)
No Hodgkin and RT	3462 (33)	1.03 [0.57-1.86]	1.02 [0.57-1.85]	0.95 [0.52-1.73]
Hodgkin and no RT*	27 (0)	0 [0-Inf]	0 [0-Inf]	0 [0-Inf]
Hodgkin and RT	444 (33)	9.29 [5.21-16.54]	8.23 [4.59-14.76]	10.39 [5.57-19.38]

Valvular Heart Disease (VHD); Hazard Ratio (HR); 95% confidence intervals (95% CI); Proportional Hazard's assumption was verified for all models. *: no events of VHD in this class

Table 4.6: Radiation dose–response relationship for the risk of VHD in the FCCSS - Excess relative risk per Gy of radiation dose received to the heart.

Model	Loglinear term RR/Gy* [95% CI]	Linear Term ERR/Gy* [95%CI]	Quadratic Term ERR/Gy* [95%CI]	Deviance	P-value
Null model** $\mu = t \times e^{(\alpha \times chemotherapy)}$	—	—	—	758.225	(ref.)
Exponential model** $\mu = t \times e^{(\alpha \times chemotherapy + \beta_0 Dose)}$	1.11 [1.09-1.12]	—	—	621.379	$<$0.0001[a]
Linear ERR model** $\mu = t \times e^{(\alpha \times chemotherapy)}(1 + \beta_1 Dose)$	—	0.54 [0.31-0.96]	—	639.230	$<$0.0001[a]
Linear- quadratic ERR model** $\mu = t \times e^{(\alpha \times chemotherapy)}(1 + \beta_1 Dose + \beta_2 Dose^2)$	—	-0.15 [-0.32-0.13]	0.03 [0.01-0.04]	620.312	$<$0.0001[b]
Quadratic ERR model** $\mu = t \times e^{(\alpha \times chemotherapy)}(1 + \beta_2 Dose^2)$	—	—	0.02 [0.01- 0.04]	621.721	$<$0.0001[b]

Abbreviations: Valvular Heart Disease (VHD); French Childhood Cancer Survivors Study (FCCSS); Excess of Relative Risk (ERR) *RR/Gy: relative risk per Gy of radiation dose received to the heart; ERR/Gy: Excess relative risk per Gy of radiation dose received to the heart; **μ = E(Y) = model the expected value of Y where y_i = number of valvular heart disease events; t is referred to as an "offset"; a: P-values relative to the null model with chemotherapy $[\mu = t \times e^{(\alpha \times chemotherapy)}]$; b: P-values relative to the Linear ERR model $[\mu = t \times e^{(\alpha \times chemotherapy)}(1 + \beta_1 Dose)]$

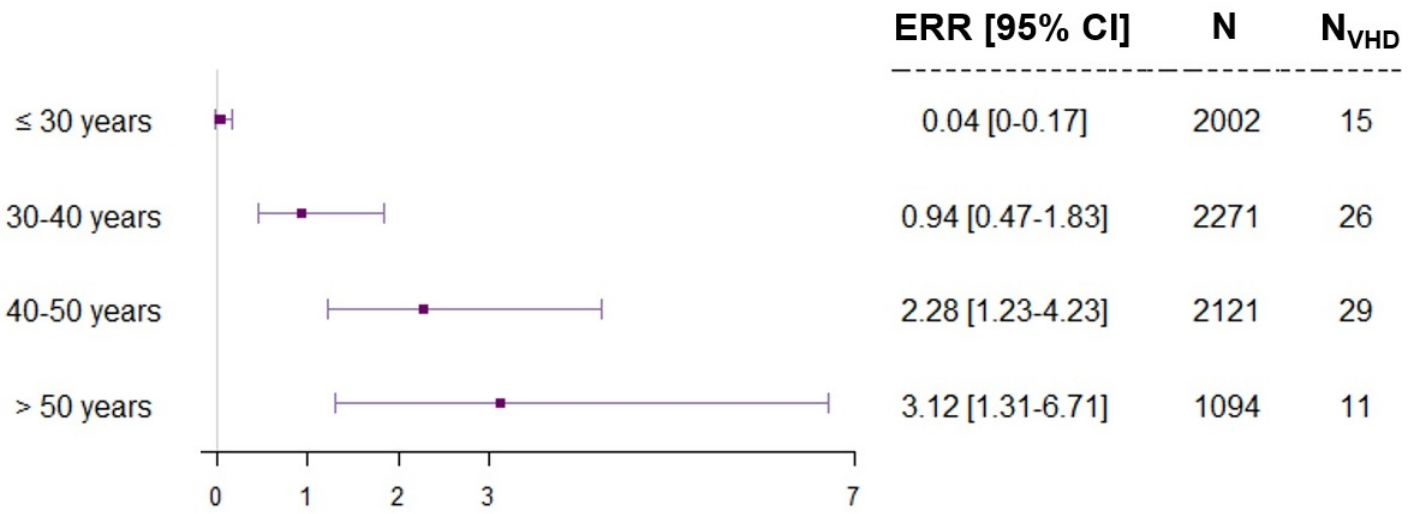

Figure 4.3: Excess relative risk of Valvular Heart Disease per Gray (ERR/Gy) in the FCCSS cohort (7492 survivors with complete data, 81 of whom developed a VHD) of radiation to the heart and chemotherapy exposure according to attained age.

Table 4.7: Risk of radiation-induced valvular heart disease (VHD) in the French Childhood Cancer Survivors'Study (FCCSS) calculated by the percentage of irradiated heart volume (in four classes), adjusted on chemotherapy; first according to a minimum dose, then by dose interval and by truncating the population affected by a maximum dose.

Whole FCCSS cohort (7492))			**Truncated Population**		
Heart dose-volume indicators (%)	N_{VHD}	**HR (95% CI)**	**Bounded heart dose-volume indicators (%)**	N_{VHD}	**HR (95% CI)**
$V_{0.1Gy}$			$V_{0.1Gy\|V5Gy=0}$		
No RT	18		No RT	18	(ref.)
<0.1 Gy	1	0.42 [0.06-3.18]	<0.1 Gy	1	0.45 [0.06-3.38]
]0, 50] % of ≥ 0.1Gy	0	-	]0, 50] % of $\geq$ 0.1 to 5 Gy	0	0 [0-inf]
>50% of $\geq$ 0.1 Gy	62	2.19 [1.29-3.73]	>50% of $\geq$ 0.1 to 5 Gy	6	0.53 [0.21-1.36]
V_{5Gy}			$V_{5Gy\|V20Gy=0}$		
No RT	18	(ref.)	No RT	18	(ref.)
<5 Gy	7	0.44 [0.18-1.06]	<5 Gy	7	0.44 [0.18-1.08]
]0, 50] % of ≤ 5 Gy	3	0.45 [0.13-1.55]	]0, 50] % of $\geq$ 5 to 20 Gy	2	0.48 [0.11-2.12]
>50% of $\geq$ 5 Gy	53	5.40 [3.14-9.29]	>50% of $\geq$ 5 to 20 Gy	4	2.75 [0.92-8.24]*
V_{20Gy}			$V_{20Gy\|V40Gy=0}$		
No RT	18	(ref.)	No RT	18	(ref.)
<20 Gy	13	0.61 [0.29-1.24]	<20 Gy	13	0.6 [0.29-1.24]
]0, 50] % of $\geq$ 20 Gy	7	1.09 [0.45-2.62]	]0, 50] % of $\geq$ 20 to 40 Gy	7	1.28 [0.53-3.08]
>50% of $\geq$ 20 Gy	43	9.74 [5.57-17.04]	>50% of $\geq$ 20 to 40 Gy	11	5.03 [2.35-10.76]
V_{40Gy}					
No RT	18	(ref.)			
<40 Gy	31	1.08 [0.6-1.95]			
]0, 50] % of $\geq$ 40 Gy	23	7.96 [4.26-14.88]			
>50% of $\geq$ 40 Gy	9	19.92 [8.91-44.53]			

Abbreviations: Hazard Ratio (HR); 95% confidence intervals (95% CI); Radiotherapy (RT); N_VHD is the number of events in the class. Proportional Hazard's assumption was verified for all models; Hazards that were not calculated due to lack of events in the respective class, are noted with a dash. *becomes significant when the percentage of irradiated heart volume exceeds 90% (HR= 3.94, CI95%: 1.15-13.49)

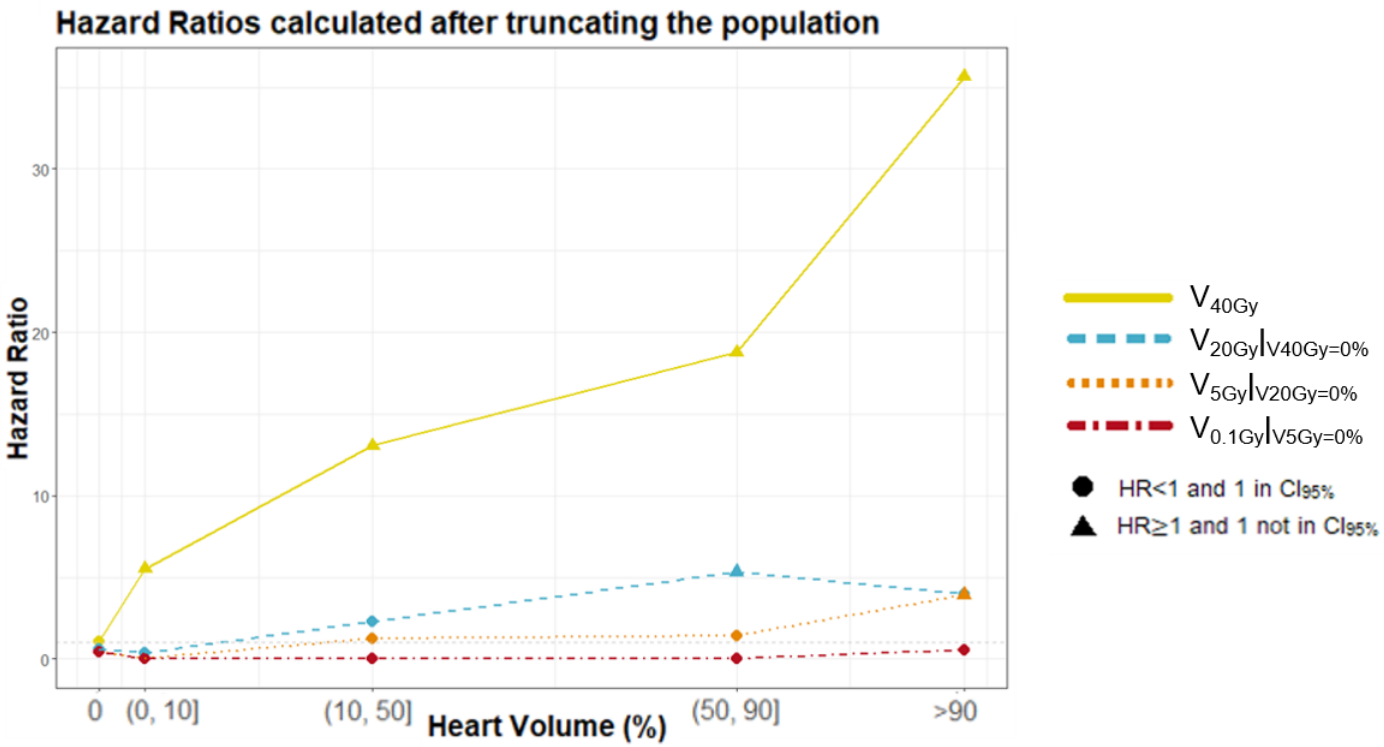

Survivors that experienced a VHD by each sub-category:

V_{40Gy}	49	11	12	8	1
$V_{20Gy}\|_{V40Gy=0}$	31	1	6	11	0
$V_{5Gy}\|_{V20Gy=0}$	25	0	2	1	3
$V_{0.1Gy}\|_{V5Gy=0}$	19	0	0	0	6

Figure 4.4: Hazard Ratio evolution along five subparts of irradiated heart volume (with reference group the patients that were not treated with radiotherapy), for four dose-intensity intervals, adjusted on chemotherapy; calculated by truncating the part of the population that received a dose to the heart superior to the respected upper bound)

Table 4.8: Models' comparison based on different types of variables that take into account radiation exposure in the FCCSS.

Set of variables (adjusted on chemotherapy)		**PCA**$^{\triangle}$	**LASSO**	**Ridge**	**Elastic Net** (alpha=0.05)*	**Reference model**
Dose indicators ($D_{1\%}$, $D_{5\%}$, $D_{10\%}$, $D_{20\%}$, $D_{30\%}$, $D_{40\%}$, $D_{50\%}$, $D_{60\%}$, $D_{70\%}$, $D_{80\%}$, $D_{90\%}$, $D_{95\%}$, $D_{99\%}$)	*Retained variables*	All	$D60\%$, $D70\%$	All	$D40\%$, $D50\%$, $D60\%$, $D70\%$	**MHD** AIC=1143.72 C-index=0.74
	AIC	1146.42	1167.01	1199.91	1176.43	
	C-index	0.739	0.697	0.721	0.697	
Volume indicators ($V_{\geq 0.1Gy}$, $V_{\geq 0.5Gy}$, $V_{\geq 1Gy}$, $V_{\geq 2Gy}$, $V_{\geq 5Gy}$, $V_{\geq 10Gy}$, $V_{\geq 15Gy}$, $V_{\geq 20Gy}$, $V_{\geq 25Gy}$, $V_{\geq 30Gy}$, $V_{\geq 40Gy}$)	*Retained variables*	All§	$V_{\geq 25Gy}$, $V_{\geq 30Gy}$	All	$V_{\geq 20Gy}$, $V_{\geq 25Gy}$, $V_{\geq 30Gy}$, $V_{\geq 40Gy}$	
	AIC	1187.82	1173.39	1194.65	1177.71	
	C-index	0.724	0.725	0.725	0.721	
Combination of dose and volume indicators (complete model)	*Retained variables*	All	$D60\%$, $D70\%$, $V_{\geq 25Gy}$, $V_{\geq 40Gy}$	All	$D40\%$, $D50\%$, $D60\%$, $D70\%$, $V_{\geq 25Gy}$, $V_{\geq 30Gy}$	
	AIC	1145.96	1169.08	1217.39	1175.46	
	C-index	0.744	0.698	0.717	0.698	

Abbreviations: Valvular Heart Disease (VHD); French Childhood Cancer Survivors Study (FCCSS); Principal Components Analysis (PCA); Akaike Information Criterion (AIC); Bayesian Information Criterion (BIC); Concordance index (C-index); Brier Score (BS) ; Mean Heart Dose (MHD) $\triangle$: Linear combination of the dose indicators according to the two first components (95.4% of the total inertia explained), of the volume indicators according to the two first components (84.1% of the total inertia explained), and of both dose and volume indicators according to the three first components (90.4% of the total inertia explained). Parameters are provided in the supplementary material. *: alpha is the mixing parameter of the penalty §: Hazard's proportionality is not respected for the variable corresponding to the linear combination according to the first component after PCA, according to the Schoenfeld Individual test (P-value= 0.03).

Confirmation of the influence of high doses

We conducted this study on a large, well-defined population of childhood cancer survivors over a long period of treatment time (1946-2000), with longitudinal follow-up and data collected from self-reported questionnaires, hospital-based databases/registries, as well as some clinically assessed data for survivors evaluated in the long-term follow-up clinic at Gustave Roussy. We confirm prior study results, reporting that the risk of experiencing late VHD increases with the MHD (Cella et al., 2015; Cutter et al., 2015) as well as with high doses to the heart (Bates et al., 2019; Schellong et al., 2010). Finally, we found that the ERR increases with attained age (Henson, 2016; Monte et al., 2020).

The role of low and moderate doses

In addition, our data allow us to calculate DVH parameters and specify the VHD risk induced by low (< 5 Gy) and low-to-moderate ($5 - 20$ Gy) radiation doses. The latter was possible using bounded heart DVH parameters that restrained the heart volume affected by high doses to the heart. We report novel findings with practical clinical implications to help identify survivors at higher risk for VHD after radiation therapy. Our results suggest that doses < 5 Gy might introduce no additional risk of experiencing a VHD; however, we found a substantially elevated risk of VHD associated with either low-to-moderate radiation dose ($V_{5\,Gy|V20\,Gy=0\%}$) to a large volume of the heart ($> 90\%$). This fruitful conclusion is in line with Bates et al. (Bates et al., 2019), who also observed an increased relative risk for any cardiac event when half of the heart volume or more received $5 - 20$ Gy (see Figure 4.4). However, it remains to be confirmed with larger cohorts. Eventually, the composite nature of the heart could also be considered to deepen the analyses by investigating if the dose effect would be modified depending on which specific substructures are irradiated.

A non-linear risk increase with dose

Cutter et al., 2015 has examined the relationship between VHD and radiation therapy for Hodgkin lymphoma in a case-control study with 66 severe cases of VHD and 200

control survivors. This study showed a non-linear relationship, with little or no increase following doses below 30 Gy. For doses over 30 Gy, the hazard ratio estimates increase progressively as the dose to the valves increases. In our study, we observe an elevated risk for an $MHD > 15$ Gy (Table 4.2) and an ERR that increases with the MHD. From the metrics in Table 4.6, the linear-quadratic model seems to outperform the other models slightly. A visual inspection of Figure 4.2 would favor the quadratic model. Our findings are consistent with those in the study of Cutter et al., 2015.

Association with other variables: year of diagnosis, chemotherapy

Additionally, no association was observed between the year of diagnosis and the occurrence of a VHD (Univariate analysis, Table 4.1), which agrees with Henson, 2016, who did not find a significant variation of AER within a decade of diagnosis. In the present analysis, VHD risk was independently associated with chemotherapy but not with anthracyclines or any other particular agent (Table 4.4). These results are consistent with those of Cutter et al., 2015. In contrast, Mulrooney et al., 2009 reported an increased risk of developing VHD following treatment with anthracyclines after childhood cancer. A possible explanation for this apparent inconsistency could be a lack of power due to a small number of patients that experienced a late VHD receiving anthracyclines, as we only considered severe cases of VHD. Furthermore, to our knowledge, the underlying pathophysiologic mechanism of this association remains poorly understood. Future studies are needed to clarify the sound effect of anthracyclines in valvular dysfunction.

Methodological aspects

Finally, one of the aims of this study was to explore the potential of combining multiple DVH indicators that are classically estimated through the TPS into one unique model. Such a combination provides a picture of the dose distribution more representative than the Mean Heart Dose, allowing for deductions on the radiation-induced VHD risk for the entire spectrum of doses. However, the interpretation of PCA or variable selection is not apparent. Therefore, it is not easy to conclude if a significant trade-off exists in claiming that the PCA regressions are slightly more informative than the MHD-based model. Consequently, more robust methods of taking into account dose characteristics are required.

Limitations

Some limitations of this study merit discussion, even though they do not call our main conclusions into question.

Due to the long period considered (1946 - 2000), most patients did not have computer tomography scans for planning to allow for individual anatomy-based DVH. Still, instead, a phantom-based reconstruction algorithm was used. This is an established approach but has its known limitation regarding inter-individual anatomic variability. However, this limitation is shared by all retrospective dosimetric studies with a follow-up long enough to address cardiac diseases after radiotherapy.

Moreover, the labeling of our data would allow for calculations of metrics to the following sub-structures: myocardium, left and right ventricle, left and right atrium, and the four valves. However, the potential role of the different sub-structures of the heart will be further investigated in future studies. Because of the potential anatomic uncertainties associated with the valves' location, we considered the whole heart in this study.

In addition, whole-body radiation dose reconstruction is not available for 175 out of the 4081 survivors of the FCCSS cohort treated with external irradiation. However, this missing data has little impact because the risk associated with radiation therapy (yes/no) remains unchanged with or without including these survivors. In addition, we could not specify the affected valve of each subsequent VHD (Cutter et al., 2015) and study each type of VHD separately because data were collected from multiple sources. For the same reason, we could not include lifestyle and medical adjustment factors like smoking, obesity, and other cardiovascular factors like hypertension and diabetes, which have been associated with VHD risk after treatment for cancer in previous studies (Bijl et al., 2016; van Nimwegen et al., 2015) conducted on survivors of adult cancer.

Finally, 1 % of our cohort experienced a severe VHD, i.e., of grade ≥ 3. A previous study identified a lower prevalence of grade 3-5 valvular disease (0.1 %) among siblings (that was considered the healthy/control population) compared to survivors (0.5 %) in the Childhood Cancer Survivor Study (Armstrong et al., 2013). Severe VHD increased from 54 to 70 (Bates et al., 2021) in this cohort, resulting in a VHD frequency close to our study's.

Conclusion

This study provides new insight concerning the association of low and moderate doses to an extended part of the heart with VHD. The results can potentially impact treatment planning and highlight the need for cardiologic follow-up (van Kalsbeek, van der Pal, et al., 2021) several decades after childhood cancer treatment for survivors with elevated risk for a VHD. Further research is needed to determine the costs and benefits of early cardiovascular screening for these survivors.

5 - Dosiomics approach for classification

5.1 . Context

In this chapter, we present the reasoning behind the dosiomics approach and the results of the classification models. We extracted 93 features for radiation doses to the heart. We then trained and tested Random Forests adapted for imbalanced classification. We evaluated them based on aggregated metrics. Additionally, we did a sensitivity analysis, by partitioning the cohort based on the Dose Uniformity, a measure of heart dose heterogeneity.

Dosiomics Features

It has been established that the risk of experiencing VHD increases along with the level of radiation absorbed by heart tissues during radiotherapy (Cella et al., 2015; Chounta et al., 2023; Cutter et al., 2015). In addition, an association of high (> 25 Gy) radiation doses to the heart with the occurrence of VHD has already been reported, both for adults' (Cella et al., 2011; Gujral et al., 2016) and pediatric (Cutter et al., 2015; Schellong et al., 2010; van der Pal et al., 2015b) cancer treatment. There is, however, an open question concerning the potential risk induced by extensive low and moderate radiation doses to the cardiac region. In (Bates et al., 2019), the relative risk of cardiac events was expressed with respect to the percentage of the heart volume absorbing a dose between 5 and 20 Gy and is found significant when more than 50% of the heart volume is affected.

Meanwhile, in (Cutter et al., 2015), it is suggested that a cut-off might exist below which there is no risk of subsequent valvular heart disease. In the previous chapter (Chounta et al., 2023), evidence is provided that such a threshold could be around 5 Gy and that doses between 5 and 20 Gy absorbed by more than 90% of the heart volume are statistically associated with the occurrence of a VHD. Consequently, we hypothesize that some distribution patterns could also be associated with the occurrence of a VHD.

The most common explanatory variables to model the radiation-induced risk of VHD are the mean or the median dose to the heart (Cella et al., 2011; Cella et

al., 2015; Galper et al., 2011). However, mean and median dose to the heart do not provide insight into the role of spatial heterogeneity of received doses; this issue remains understudied in the literature, mainly due to a lack of adequate whole-body voxel-scale data. In some studies with access to such data, the role of dose-volume histogram parameters in experiencing a cardiac disease has been investigated with fruitful results (Bates et al., 2019; Cella et al., 2011; Chounta et al., 2023; Shrestha et al., 2021). These first results encourage further investigation of the potential role of heart dose heterogeneity in experiencing a VHD with more systematic approaches.

In this chapter, we adopted the dosiomics approach, which involves extracting first-order statistics and 3D spatial features from radiation dose distribution to go one step further. Studies have been exploring the role of dosiomics in risk modeling to predict radiation-induced temporal lobe injury (Yang et al., 2022), radiation pneumonitis (Liang et al., 2019), locoregional recurrences after treatment for head and neck carcinoma (Wu et al., 2020), and radiation-induced hypothyroidism (Ren et al., 2021), to name a few applications. Dosiomics features have proven promising and, in some cases, more effective than the conventionally used dose-volume histogram parameters (Murakami et al., 2022; Ren et al., 2021).

To our knowledge, this is the first study where dosiomics are extracted from the heart dose to estimate the risk of a subsequent VHD. We chose to tackle the subject as a classification problem of VHD prediction several decades after treatment with radiotherapy for childhood cancers. We grew Random Forests based on the mean heart dose (MHD) (baseline model) and dosiomics features of survivors that experienced a VHD to deduce a signature of high-risk survivors. The main objectives of this study were to identify critical variables in risk estimation (*dosiomics signature*) and to grow efficient Random Forests that can accurately screen high-risk childhood cancers survivors prone to experiencing a VHD.

We extracted 93 dosiomics features from the dose to the heart using the pyradiomics package (3.0.1) (van Griethuysen et al., 2017). The features can be categorized into six classes as presented in Table 5.1.

The extracted features provide information on the dose intensities and have already been described (van Griethuysen et al., 2017). Shape features (2D and 3D) were not calculated as they concern the size and shape of the region of interest. In the context of this study, the region of interest is the heart. As the shape and size of the organs

have been approximated by phantoms for many survivors, and there is often uncertainty in relation to organ contouring, it would not be informative to include size features in the models. The binwidth of dose histograms was set to 0.1 Gy where applicable (set according to the Freedman-Diaconis rule (Freedman & Diaconis, 1981).

5.2 . Methods

Feature selection, Imbalanced classification

These analyses concern the FCCSS, a retrospective cohort where survivors experienced a VHD up to 50 years after treatment for childhood cancer. We attempted to identify high-risk survivors with a supervised classification problem. However, only 1% of the survivors have been diagnosed with severe VHD. Therefore, we are dealing with an imbalanced classification problem of identifying survivors diagnosed with a severe VHD, where the prediction that no survivor is at risk would result in a 99% Accuracy (Number of correct predictions/ Total number of predictions).

Chen et al. (Chen et al., 2004) proposed two possible adaptations of the classic Random Forest algorithm to tackle the problem of imbalanced data: Weighted Random Forest (wtRF) and Balanced Random Forest (BRF) detailed in Chapter 2.

To evaluate the models based on the extracted dosiomics features, we compared them to forests grown from the MHD. An adjusted version is also presented based on the following adjustment variables: biological sex, age (in years) and year at the first childhood cancer diagnosis, and chemotherapy exposure (binary: 1 if chemotherapy was administrated during childhood cancer, 0 otherwise).

Table 5.1: The full list of calculated features as defined in the pyradiomics package.

Feature class	First-order statistics	Gray Level Co-occurrence Matrix (GLCM)	Gray Level Run Length Matrix (GLRLM)	Gray Level Size Zone Matrix (GLSZM)	Gray Level Dependence Matrix (GLDM)	Neighbouring Gray Tone Difference Matrix (NGLDM)
Number of features	18	24	16	16	14	5
	mean heart dose (MHD)	autocorrelation	gray level non-uniformity	gray level non-uniformity	dependence entropy	busyness
	median	cluster prominence	non-uniformity normalized	gray level nonuniformity normalized	dependence non-uniformity	coarseness
	minimum	cluster shade	gray level variance	gray level variance	dependence non-uniformity normalized	complexity
	maximum	cluster tendency	high gray level run emphasis	high gray level zone emphasis	dependence variance	contrast
	variance	contrast	long run emphasis	large area emphasis	gray level non-uniformity	strength
	skewness	correlation	long run high gray level emphasis	large area high gray level emphasis	gray level variance	
	kurtosis	difference average	long run low gray level emphasis	large area low gray level emphasis	high gray level emphasis	
	entropy	difference entropy	low gray level run emphasis	low gray level zone emphasis	large dependence emphasis	
	uniformity	difference variance	run entropy	size zone non-uniformity	large dependence high gray level emphasis	
	10^{th} percentile	Inverse Difference (ID)	run length non-uniformity	size zone non-uniformity normalized	large dependence low gray level emphasis	
	90^{th} percentile	Inverse Difference Moment (IDM)	run length non-uniformity normalized	small area emphasis	low gray level emphasis	
	energy	Inverse Difference Moment Normalized (IDMN)	run percentage	small area high gray level emphasis	small dependence emphasis	
	total energy	Inverse Difference Normalized (IDN)	run variance	small area low gray level emphasis	small dependence high gray level emphasis	
	range	Informational Measure of Correlation 1 (IMC1)	short run emphasis	zone entropy	small dependence low gray level emphasis	
	interquartile range	Informational Measure of Correlation 2 (IMC2)	short run high gray level emphasis	zone 6 percentage		
	mean absolute deviation	inverse variance	short run low gray level emphasis	zone variance		
	robust mean absolute deviation	joint average				
	root mean squared	joint energy				
		joint entropy				
		Maximal Correlation Coefficient (MCC)				
		maximum probability				
		sum average				
		sum entropy				
		sum squares				

Modeling workflow

We split the data into 30 random, balanced (with respect to the proportion of VHD incidents) overlapping iterations of train and test sets. For the dosiomics-based models, as demonstrated in Figure 5.1, we started the pipeline with variable selection through an Elastic Net (Zou & Hastie, 2005), where the regularization hyper-parameters are tuned through a grid search with cross-validation. Then, we performed 5-fold cross-validation on the train set to calibrate the Random Forest parameters (number of trees to grow and maximum leaf nodes). We then calculated variable importances for each instance (computed as the mean and standard deviation of accumulation of the impurity decrease within each tree) and confusion matrices. From the confusion matrix, we calculated and presented in the Results section the following metrics, aggregated on the 30 instances: Sensitivity (Recall), Specificity, Balanced Accuracy (BA), and AUC ROC (defined below). Metrics results are presented in the corresponding section as $average \pm standard\ deviation$. All p-values computed for the performance comparisons are obtained from t-tests under the assumption of variance homogeneity. For the MHD-based models, the pipeline is similar, except for the feature selection step.

Dosiomics Signature

Each presented feature was selected from at least 25 of the 30 iterations of the Elastic Net. Feature importance was evaluated by the Random Forest algorithm and is impurity-based (the sum over the number of splits -across all trees- that include the feature, proportionally to the number of samples it splits). A feature was selected for inclusion in the dosiomics signature if it was, on average, among the 30 most important features according to the Random Forest while having been selected by the Elastic Net. Features are ordered by feature class and then alphabetically.

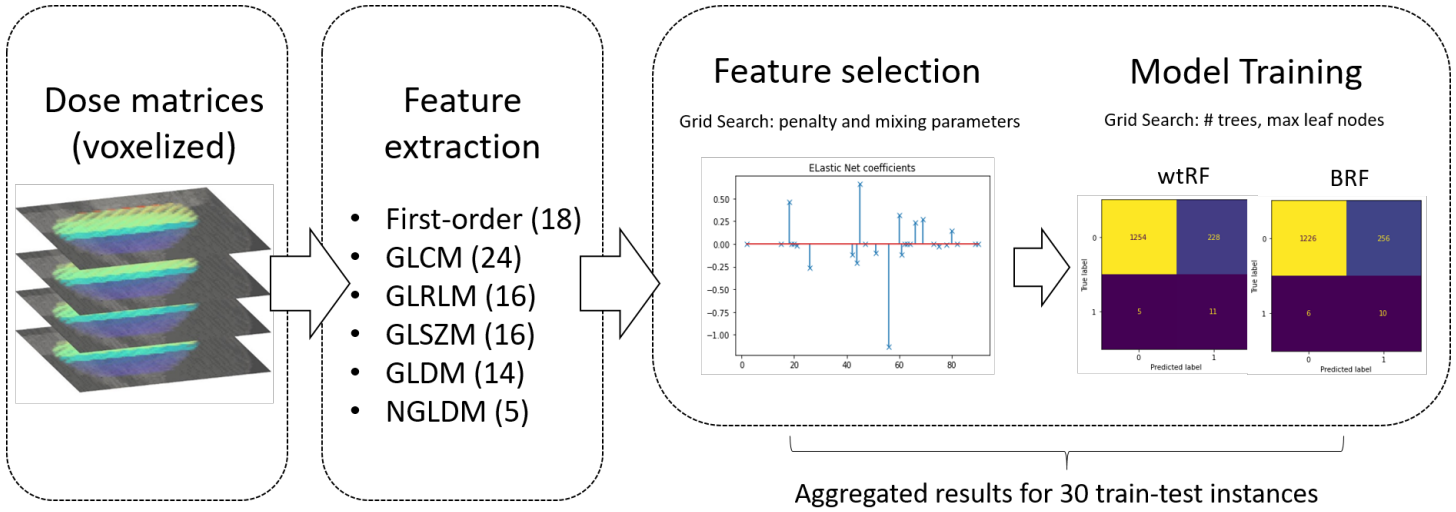

Figure 5.1: Workflow of the dosiomics-based models as described in the Methods part. We extracted 93 dosiomics features from the radiation dose to the heart matrices, split the cohort into train-test groups 30 times, used the Elastic Net to make a variable selection, and then trained the weighted (wtRF) and balanced random forests (BRF). Then we calculated the metrics of performance for each of the two types of Random Forest by aggregating the results of the 30 splits.

Model evaluation

The two types of wrong predictions have different implications: False Positives (i.e., falsely predicting that a survivor is at high risk of experiencing the event) would cost childhood cancers survivors and the health system resources and time, while a False Negative (i.e., falsely predicting that a survivor is not at risk) could put childhood cancers survivors' lives at risk. The statistical challenge is to accurately identify as many as possible high-risk individuals (True Positives) with the least possible 'cost' of wrong predictions (the so-called 'avalanche problem' -Dkengne Sielenou et al., 2021). Notably, Sensitivity (Recall) is the metric that evaluates the algorithm's ability to detect True Positives and not misclass them falsely as Negatives. On the other hand, Specificity is the probability of correctly identifying a survivor that will not experience the event; therefore, it evaluates the 'cost' of the algorithm in False Positives. Thus, in this specific medical application, a low Recall means that the algorithm is inappropriate, while a low Specificity is much more tolerable and secondary in priorities to improvement. Finally, Balanced Accuracy (BA) is the average of Sensitivity (Recall) and Specificity, and AUC is the area under the ROC curve (the integral of the curve of Sensitivity against 1-Specificity at various threshold settings). Therefore both BA and AUC simultaneously combine multiple quadrants of the confusion matrix (True Positives, False Positives, True Negatives, and False Negatives), providing an in-depth evaluation of models.

Cohort Partition based on heart dose heterogeneity

To explore and work out the imbalanced classification problem, we proposed a partition of the data based on the assumption that heart-dose heterogeneity might be an important factor for the occurrence of a VHD. Two potential features measure heterogeneity: Entropy and Uniformity, negatively correlated. We chose Uniformity, a normalized measure (taking values between 0 and 1). Uniformity is calculated as the sum of squares of each intensity value

$$\textit{Uniformity} = \sum_{i=1}^{N_g} p(i)^2 \tag{5.1}$$

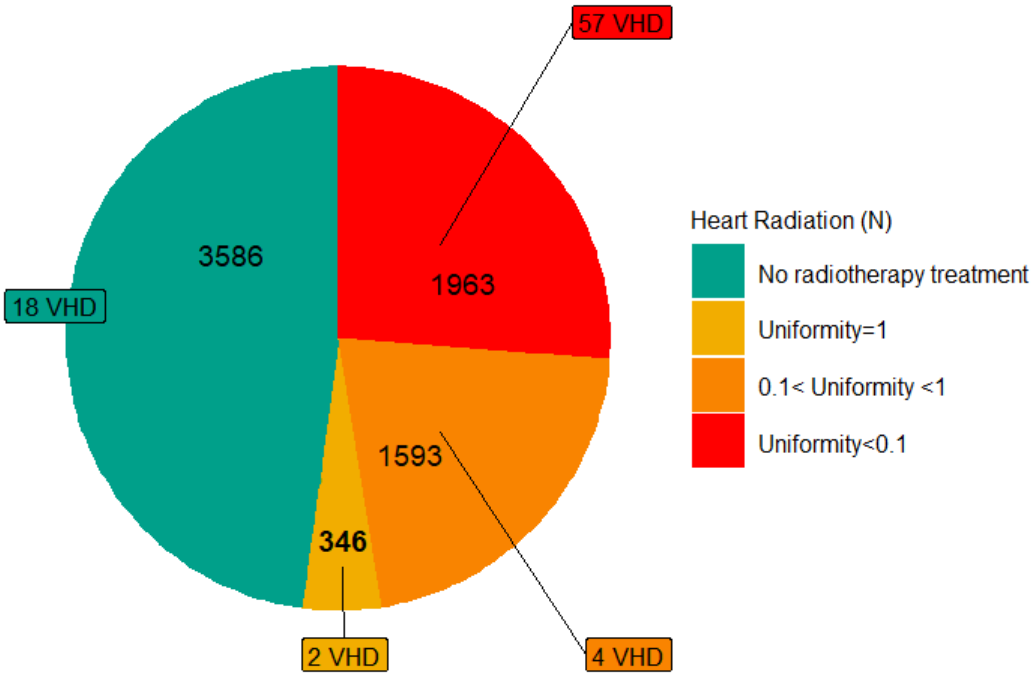

Figure 5.2: Uniformity in the cohort and the repartition of survivors that experienced a VHD (81 in total in the FCCSS).

where in Equation 5.1, N_g is the number of non-zero bins of intensity levels, equally spaced from 0 with a width defined in the binwidth parameter, and $p(i) = \frac{P(i)}{N_p}$ the normalized first order histogram $P(i)$, and N_p the total number of voxels. It measures the homogeneity of the radiation dose distribution. In this study, it is only computed for the doses absorbed from the heart. A high Uniformity (close to 1) is interpreted either as homogeneity in the dose distribution or a smaller range of discrete intensity values (van Griethuysen et al., 2017).

We trained the wtRF and the BRF on three cohorts: (i) the entire cohort (7488 survivors, 81 of whom experienced a VHD) using dummy feature values for the patients that had not been treated with radiotherapy, by setting to 0 the dose level absorbed by

the heart voxels, (ii) the sub-population that had been exposed to non-homogeneous heart radiation (3556 survivors with Uniformity < 1, 61 of whom experienced a VHD) and finally (iii) the sub-population with very heterogeneous heart doses (1963 survivors with Uniformity < 0.1, 57 of whom experienced a VHD) - Figure 5.2.

Analyses were performed with Python 3.8.13. Data analysis was done with the libraries pandas (pandas development team, 2020), numPy (Harris et al., 2020), seaborn (Waskom, 2021), and matplotlib (Hunter, 2007), dosiomics were extracted with the pyradiomics library (van Griethuysen et al., 2017), and the pipelines for the modeling were built with Scikit-learn (Pedregosa et al., 2011) and imbalanced-learn (Lemaître et al., 2017). The threshold of significance is set to 0.05.

5.3 . Results

Descriptive Analysis

In Table 5.2 and Table 5.3, we gathered information on the FCCSS and the sub-cohorts, defined according to the value of Uniformity: no treatment with radiotherapy, Uniformity$= 1$, Uniformity inside the range $[0.1, 1)$, and Uniformity < 0.1.

From the 7488 5-year survivors of the FCCSS with complete data, 81 experienced a VHD ($\approx 1\%$). Sixty-three of the survivors that experienced the event had been treated with radiotherapy, among whom two had a heart-dose Uniformity $= 1$, 4 had a Uniformity between 0.1 and 1, and 57 had a Uniformity < 0.1. The prevalence of VHD among survivors with Uniformity < 0.1 is, thus, 2.9%. In the sub-population with Uniformity $= 1$, the average mean, median, and maximum dose to the heart were all very low (0.2, 0.2, and 0.4 Gy, respectively), as well as each of their maximum values (0.25, 0.25, and 0.26 Gy respectively). On the contrary, among survivors with Uniformity < 0.1, the average mean, median, and maximum dose to the heart increased by three orders of magnitude. In Table 5.3, we gathered information on the repartition of childhood cancer types in each cohort part. It is noteworthy that 84% of the survivors of Hodgkin lymphoma (394) had Uniformity < 0.1. In addition, among survivors treated for renal tumors, 47% (531) had Uniformity below 0.1, 9% between 1 and 0.1, and the rest (44%) were not treated with radiotherapy. Finally, 35% of survivors treated for the central nervous system and miscellaneous intracranial and intraspinal neoplasms (395) were among the 1963 survivors with Uniformity < 0.1.

Uniformity descriptive boxplots are also provided in Figure 5.3.

Dosiomics versus Mean Heart Dose

We first trained the models on the FCCSS (Table 5.4, rows 1-4). According to the BA and the AUC, models based on either the MHD or the dosiomics features performed similarly when trained with the wtRF algorithm (within the margin of error for the BA and the AUC). The dosiomics-based model seemed to perform better when trained with the BRF algorithm (BA $0.74 > 0.73$ and AUC $0.77 > 0.76$), but the comparisons were not statistically significant (p-values=0.23 and 0.35, respectively). Similarly, considering Sensitivity, the dosiomics-based models outperformed the MHD-based model ($0.59 > 0.57$ with the wtRF and $0.62 > 0.61$ with the BRF), but the comparisons were not statistically significant (p-values=0.32 and 0.63 respectively). Specificity was higher with the MHD-based wtRF ($0.90 > 0.88$, p-value=0.32), but the comparison was not statistically significant. Specificity was higher, and the comparison was statistically significant with the dosiomics-based BRF ($0.86 > 0.84$, p-value=0.001).

We then trained the same forests on the sub-population with non-homogeneous doses to the heart (3556 out of the 3902 survivors that had been treated with radiotherapy, based on the heart-dose Uniformity being < 1 - Table 5.4, rows 5-8). All models seemed to improve (overall, metrics are higher for both types of Random Forests, wtRF or BRF, and both heart radiation measures, MHD or dosiomics features). The dosiomics-based BRF outperforms the MHD-based BRF, based on all four metrics (Table 5.4 row 8). The comparisons are statistically significant for all the metrics but the Sensitivity.

Finally, we attempted a stricter cut-off for the cohort partition and trained the models on the subpopulation with heart-dose Uniformity < 0.1 (Table 5.4, rows 9-12). Results were similar according to the BA. The BA with the BRF and the AUC with both types of forests were higher with the dosiomics-based model, but the comparisons were not statistically significant. Sensitivity was higher for the MHD-based model with the wtRF and higher for the dosiomics-based model with the BRF, but again, comparisons were not statistically significant. The dosiomics-based model outperforms the MHD-based model according to all four metrics (Table 5.4 line 12). However, comparisons were statistically significant only for Specificity (p-value=0.002).

Table 5.2: Descriptive table of the cohort (FCCSS) in the first column; then by radiotherapy status: survivors that had not been treated with radiotherapy (No RT), and survivors that had been treated with radiotherapy and had a Uniformity $= 1$, between 0.1 included and 1, and finally < 0.1.

	FCCSS[1]	No RT[2]	Uniformity$=1$	Uniformity in $[0.1, 1)$	Uniformity<0.1
Total	7488	3586	346	1593	1963
VHD[3]	81 (1.08%)	18 (0.5%)	2 (0.58%)	4 (0.25%)	57 (2.9%)
Age at CC[4] diagnosis	6.62 [0-20.61]	6.18 [0-20.41]	6.01 [0-18.41]	7.08 [0-20.28]	7.17 [0-20.61]
Year at CC diagnosis	1984 [1946-2000]	1988 [1949-2000]	1983 [1951-2000]	1982 [1946-2000]	1980 [1948-2000]
Attained age	37.76 [5.39-79.83]	35.79 [5.392-76.37]	39.37 [7.27-79.83]	38.94 [6.16-78.65]	40.12 [6.66-77.82]
Biological Sex					
Male	3384 (45.19%)	1622 (45.23%)	146 (42.2%)	701 (44.01%)	915 (46.61%)
Female	4104 (54.81%)	1964 (54.77%)	200 (57.8%)	892 (55.99%)	1048 (53.39%)
Chemotherapy					
No	1828 (24.41%)	957 (26.69%)	109 (31.5%)	480 (30.13%)	282 (14.37%)
Yes	5660 (75.59%)	2629 (73.31%)	237 (68.5%)	1113 (69.87%)	1681 (85.63%)
Mean dose to the heart	6.82 [0-61.20]	0 [0-0]	0.02 [0-0.25]	0.98 [0-37.65]	12.76 [0-61.20]
Median dose to the heart	6.75 [0-67.54]	0 [0-0]	0.02 [0-0.25]	0.88 [0-37.66]	12.69 [0-67.54]
Maximum dose to the heart	13.68 [0-109.43]	0 [0-0]	0.04 [0-0.26]	2.18 [0.1-60.28]	25.424 [1.326-109.43]
Heart dose uniformity	0.27 [0.003-1]	1 [1-1]	1 [1-1]	0.4 [0.1-1)	0.036 [0.003-0.1]

For continuous variables, the average is given as well as minimum and maximum (average [min - max]). For categorical variables, percentages are calculated over the total of the relevant sub-population. [1] French Childhood Survivors Study; [2] No Radiotherapy; [3] Valvular Heart Disease ; [4] Childhood Cancer

Table 5.3: The distribution of the type of first cancer in the cohort (FCCSS) in the first column; then by radiotherapy status: survivors that had been treated without radiotherapy (No RT), Uniformity of radiation dose to the heart $= 1$, between 0.1 included and 1, and < 0.1.

	FCCSS[1]	No RT[2]	Uniformity$=1$	Uniformity in $[0.1, 1)$	Uniformity<0.1
Total	7488	3586 (48%)	346 (5%)	1593 (21%)	1963 (26%)
VHD[3]	81	18 (22%)	2 (2%)	4 (5%)	57 (70%)
Type of CC[4]:					
Hodgkin lymphoma	471	27 (6%)	5 (1%)	45 (10%)	394 (84%)
Other lymphomas and reticuloendothelial neoplasms	788	540 (69%)	16 (2%)	158 (20%)	74 (9%)
CNS and miscellaneous intracranial and intraspinal neoplasms	1124	160 (14%)	17 (2%)	552 (49%)	395 (35%)
Neuroblastoma and other peripheral nervous cell tumors	1028	646 (63%)	12 (1%)	144 (14%)	226 (22%)
Retinoblastoma	519	310 (60%)	114 (22%)	91 (18%)	4 (1%)
Renal tumors	1136	503 (44%)	0 (0%)	102 (9%)	531 (47%)
Hepatic tumors	79	62 (78%)	0 (0%)	5 (6%)	12 (15%)
Malignant bone tumors	679	392 (58%)	64 (9%)	124 (18%)	99 (15%)
Soft tissue and other extraosseous sarcomas	846	387 (46%)	99 (12%)	261 (31%)	99(12%)
Germ cell tumors, trophoblastic tumors, and neoplasms of gonads	469	332 (71%)	6 (1%)	65 (14%)	66 (14%)
Other	349	227 (65%)	13 (4%)	46 (13%)	63 (18%)

Percentages are calculated over the cohort totals (column *FCCSS*).[1] French Childhood Survivors Study; [2] No Radiotherapy; [3] Valvular Heart Disease ; [4] Childhood Cancer

Models trained on the sub-population of the FCCSS with heart-dose Uniformity < 1 perform better than models trained on the sub-population with heart-dose Uniformity < 0.1.

Models adjusted on clinical variables

We also attempted to train the models adjusted on clinical variables. MHD-based models seemed to outperform the dosiomics-based models, but comparisons were non-statistically significant (except for Specificity in some cases). Aggregated performance metrics for models trained on the entire FCCSS (Table 5.5 - lines 1-4) and the sub-populations with heart-dose Uniformity < 1 (Table 5.5 - lines 5-8) and 0.1 (Table 5.5 - lines 9-12) are also presented.

Sensitivity analysis according to the type of first childhood cancer

In Table 5.6, are presented results from a sensitivity analysis. We trained the models on survivors that had been treated for Hodgkin lymphoma, central nervous system malignancies, and renal tumors. Aggregated metrics and p-values are presented on non-adjusted and adjusted models. Comparisons were not statistically significant and we cannot conclude that one model would outperform the others.

Dosiomics signature

In Table 5.7, we provide information on the most important features by population (FCCSS, Uniformity< 1, and Uniformity< 0.1) and on whether they were selected as one of the most important features by each type of Random Forest (weighted and balanced). We present the following 22 features that we propose as a dosiomics signature of a late VHD in the FCCSS:

- First Order Statistics: 10^{th} Percentile, 90^{th} percentile, Energy, Kurtosis, Mean Heart Dose, Median Heart Dose, Minimum Heart Dose, Root Mean Squared, Total Energy.

- GLCM: Autocorrelation, IDMN, IDN, Joint Average, Sum Average.

- GLDM: High Gray Level Emphasis, Large Dependence High Gray Level Emphasis, Small Dependence High Gray Level Emphasis.
- GLRLM: High Gray Level Run Emphasis, Long Run High Gray Level Emphasis, Short Run High Gray Level Emphasis.
- GLSZM: High Gray Level Zone Emphasis, Small Area High Gray Level Emphasis.

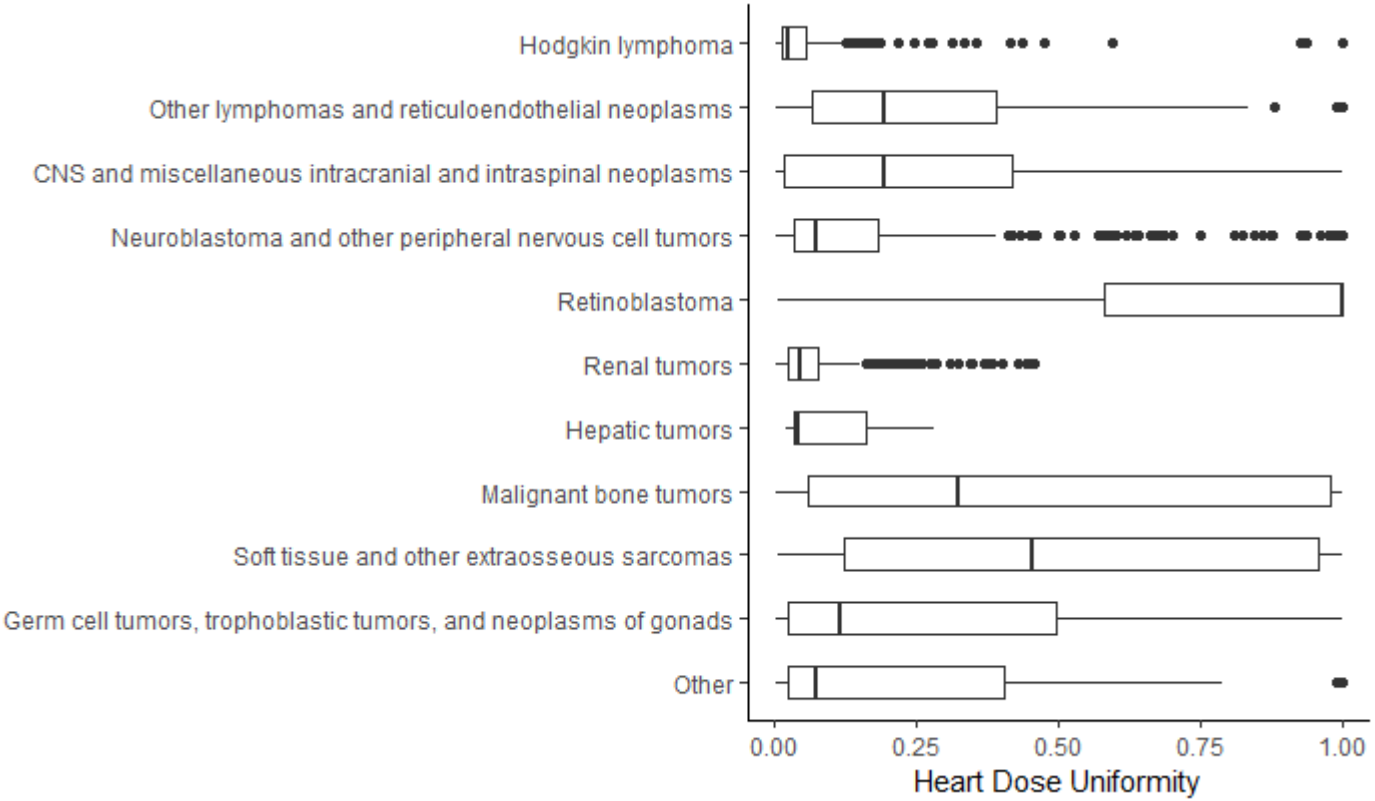

Figure 5.3: Uniformity boxplots by type of childhood cancer.

Table 5.4: Performance metrics, derived from training forests on the FCCSS and two subpopulations of the FCCSS (the part of the cohort with Uniformity < 1, and the part of the cohort with Uniformity < 0.1), according to two types of classification algorithms (weighted Random Forest - wt RF, and Balanced Random Forest- BRF), where the radiation-induced risk is explained by either the mean heart dose (MHD) or a selection of dosiomics features. Results are aggregated over the 30 instances of train-test spitting, and here we present the mean $\pm$ standard deviation of each metric.

		Heart radiation measure	Balanced Accuracy	AUC ROC	Sensitivity (Recall)	Specificity	
FCCSS	wt RF	**Mean heart dose**	0.74 ± 0.04	0.77 ± 0.051	0.57 ± 0.083	**0.90 ± 0.019**	
		Dosiomics features	0.74 ± 0.038	0.77 ± 0.047	0.59 ± 0.075	0.88 ± 0.015	
	p-values		*0.792*	*0.883*	*0.319*	*0.001*	
	BRF	**Mean heart dose**	0.73 ± 0.04	0.76 ± 0.046	0.61 ± 0.088	0.84 ± 0.034	
		Dosiomics features	0.74 ± 0.039	0.77 ± 0.051	0.62 ± 0.074	**0.86 ± 0.018**	*4*
	p-values		*0.234*	*0.358*	*0.627*	*0.044*	
$Uniformity < 1$	wt RF	**Mean heart dose**	0.78 ± 0.057	0.85 ± 0.059	0.72 ± 0.127	0.84 ± 0.029	
		Dosiomics features	0.78 ± 0.057	0.86 ± 0.059	0.73 ± 0.126	0.83 ± 0.031	
	p-values		*0.981*	*0.483*	*0.617*	*0.057*	
	BRF	**Mean heart dose**	0.74 ± 0.054	0.83 ± 0.057	0.73 ± 0.113	0.76 ± 0.043	
		Dosiomics features	**0.79 ± 0.056**	**0.86 ± 0.057**	0.78 ± 0.113	**0.79 ± 0.021**	*8*
	p-values		*0.004*	*0.046*	*0.08*	*<0.001*	
$Uniformity < 0.1$	wt RF	**Mean heart dose**	0.76 ± 0.068	0.81 ± 0.069	0.71 ± 0.146	0.79 ± 0.031	
		Dosiomics features	0.76 ± 0.062	0.82 ± 0.073	0.69 ± 0.13	**0.82 ± 0.026**	
	p-values		*0.909*	*0.773*	*0.4*	*0.001*	
	BRF	**Mean heart dose**	0.72 ± 0.076	0.79 ± 0.064	0.72 ± 0.151	0.73 ± 0.052	
		Dosiomics features	0.75 ± 0.056	0.8 ± 0.071	0.74 ± 0.126	**0.77 ± 0.028**	*12*
	p-values		*0.162*	*0.437*	*0.701*	*0.002*	

The last column corresponds to the enumeration of the table lines. P-values correspond to two-sided t-tests. The bolded metrics' values are the ones that, compared to the model of the same type of forest but with a different heart radiation measure, are significantly higher.

Table 5.5: Models trained and metrics calculated on the entire FCCSS (7488) cohort, and then on the sub-populations with heart-dose Uniformity < 1 and < 0.1, according to two types of classification algorithms (weighted Random Forest - wt RF, and Balanced Random Forest- BRF), where the radiation-induced risk is introduced by either the mean heart does - MHD or a selection of dosiomics features. Results are aggregated over the 30 instances of train-test spitting, and here we present the mean $\pm$ standard deviation of each metric. Models in this table are adjusted on clinical variables: year and age of childhood cancer diagnosis, biological sex, and chemotherapy (y/n).

		Heart radiation measure	Balanced Accuracy	AUC ROC	Sensitivity (Recall)	Specificity	
FCCSS	wt RF	**MHD**	0.75 ± 0.041	**0.8** ± 0.044	0.62 ± 0.091	0.89 ± 0.027	
		Dosiomics features	0.74 ± 0.039	0.77 ± 0.051	0.6 ± 0.077	0.88 ± 0.012	
	p-values		*0.208*	*0.028*	*0.403*	*0.141*	
	BRF	**MHD**	0.76 ± 0.045	0.8 ± 0.054	0.68 ± 0.097	0.84 ± 0.029	
		Dosiomics features	0.74 ± 0.04	0.78 ± 0.054	0.65 ± 0.073	0.82 ± 0.023	*4*
	p-values		*0.057*	*0.126*	*0.169*	*0.092*	
Uniformity < 1	wt RF	**MHD**	0.81 ± 0.054	0.87 ± 0.048	0.74 ± 0.108	**0.87 ± 0.028**	
		Dosiomics features	0.78 ± 0.063	0.86 ± 0.057	0.73 ± 0.134	0.83 ± 0.028	
	p-value		*0.117*	*0.594*	*0.666*	*<0.001*	
	BRF	**MHD**	0.82 ± 0.053	0.88 ± 0.046	0.82 ± 0.106	**0.82 ± 0.023**	
		Dosiomics features	0.8 ± 0.062	0.86 ± 0.057	0.8 ± 0.123	0.8 ± 0.019	*8*
	p-values		*0.171*	*0.219*	*0.526*	*<0.001*	
Uniformity < 0.1	wt RF	**MHD**	0.76 ± 0.077	0.85 ± 0.052	0.69 ± 0.155	0.83 ± 0.025	
		Dosiomics features	0.77 ± 0.061	0.85 ± 0.057	0.71 ± 0.145	0.83 ± 0.031	
	p-values		*0.718*	*0.086*	*0.811*	*0.482*	
	BRF	**MHD**	0.77 ± 0.059	0.84 ± 0.057	0.76 ± 0.123	0.78 ± 0.026	
		Dosiomics features	0.78 ± 0.049	0.86 ± 0.05	0.76 ± 0.113	0.8 ± 0.032	*12*
	p-values		*0.779*	*0.183*	*0.673*	*0.482*	

The last column corresponds to the enumeration of the table lines. P-values correspond to two-sided t-tests. The bolded metrics' values are the ones that, when compared to the model of the same type of forest but with a different heart radiation measure, are significantly higher.

Table 5.6: Comparison of the metrics of 4 models: MHD, dosiomics features and their adjusted versions in Hodgkin lymphoma, central nervous system malignancies and renal tumor survivors.

		Heart radiation measure	Balanced Accuracy	AUC ROC	Sensitivity (Recall)	Specificity	
Non Adjusted models	wt RF	**Mean heart dose**	0.78 ± 0.09	0.82 ± 0.071	0.7 ± 0.199	0.86 ± 0.033	
		Dosiomics features	0.75 ± 0.08	0.83 ± 0.053	0.66 ± 0.182	0.85 ± 0.028	
	p-values		*0.527*	*0.751*	*0.628*	*0.588*	
	BRF	**Mean heart dose**	0.78 ± 0.086	0.83 ± 0.062	0.73 ± 0.2	0.82 ± 0.035	
		Dosiomics features	0.76 ± 0.072	0.83 ± 0.065	0.71 ± 0.166	0.81 ± 0.029	*4*
	p-values		*0.712*	*0.870*	*0.801*	*0.705*	
Adjusted models	wt RF	**Mean heart dose**	0.79 ± 0.086	0.87 ± 0.059	0.71 ± 0.187	0.87 ± 0.033	
		Dosiomics features	0.76 ± 0.088	0.83 ± 0.059	0.67 ± 0.192	0.84 ± 0.028	
	p-values		*0.406*	*0.155*	*0.627*	*0.088*	
	BRF	**Mean heart dose**	0.8 ± 0.056	0.87 ± 0.059	0.76 ± 0.12	**0.84 ± 0.016**	
		Dosiomics features	0.78 ± 0.062	0.85 ± 0.064	0.73 ± 0.142	0.82 ± 0.027	*8*
	p-values		*0.394*	*0.544*	*0.723*	*0.022*	

The last column corresponds to the enumeration of the table lines. P-values correspond to two-sided t-tests. The bolded metrics' values are the ones that, compared to the model of the same type of forest but with a different heart radiation measure, are significantly higher.

Table 5.7: Dosiomics signature according to the sub-population (FCCSS, Uniformity < 1 and Uniformity < 0.1) and type of Random Forest (weighted or Balanced).

	FCCSS			Uniformity < 1			Uniformity < 0.1		
Features	wtRF	BRF	Average [min-max]	wtRF	BRF	Average [min-max]	wtRF	BRF	Average [min-max]
First Order Statistics:									
10^{th} percentile	✓	✓	1.78 [0-49.23]	✓	✓	3.75 [0-49.23]	✓	✓	6.18 [0-49.23]
90^{th} percentile	✓	✓	5.37 [0-89.78]			11.31 [0-89.78]			19.36 [1.01-89.78]
energy	✓	✓	3.7×10^6[0- 2.1×10^8]	✓	✓	7.9×10^6[2.49-2.1×10^8]	✓	✓	14×10^6[8.4×10^3-2.1×10^8]
kyrtosis		✓	3.49 [0-1753.9]			7.14 [1.1-1753.9]			6.03 [1.1-115.99]
mean heart dose	✓	✓	3.55 [0-61.09]	✓	✓	7.48 [0-61.09]	✓	✓	12.75 [0.64-61.09]
median heart dose	✓	✓	3.51 [0-67.91]	✓	✓	7.4 [0-67.91]	✓	✓	12.68 [0.44-67.91]
minimum heart dose	✓	✓	0.88 [0-38.24]	✓	✓	1.85 [0-38.24]			2.88 [0-38.24]
root mean squared	✓	✓	3.98 [0-64.33]	✓	✓	8.37 [0.01-64.33]	✓	✓	14.27 [0.7-64.33]
total energy	✓	✓	3×10^7[0-1.7×10^9]	✓	✓	6.3×10^7[19.89-1.7×10^9]	✓	✓	11×10^7[6.7×10^4-1.7×10^9]
GLCM:									
autocorrelation	✓	✓	0.58×10^4 [1-3.1×10^5]	✓	✓	1.2×10^4 [1-3.1×10^5]	✓	✓	2.1×10^4 [41-3.1×10^5]
IDMN		✓	1 [0.86-1]		✓	0.99 [0.86-1]			0.99 [0.86-1]
IDN		✓	0.99 [0.83-1]		✓	0.98 [0.83-1]	✓	✓	0.98 [0.83-1]
joint average	✓	✓	27.72 [1-512.79]	✓	✓	57.27 [1-512.79]	✓	✓	99.75 [5.38-512.79]
sum average	✓	✓	54.97 [1-10^4]	✓	✓	114.54 [2-10^4]	✓	✓	199.49 [10.76-10^4]
GLDM:									
high gray level emphasis	✓	✓	0.59x$10^4[1-3.1\times10^5$]	✓	✓	1.2×10^4 [1-3.1×10^5]	✓	✓	2.2×10^4 [42-3.1×10^5]
large dependence high gray level emphasis	✓	✓	0.89×10^6[1-7.9×10^7]			1.8×10^6[593-7.9×10^7]			3.3×10^6[4.2×10^3-7.9×10^7]
small dependence high gray level emphasis	✓	✓	325.95 [0-39643.4]	✓	✓	685.36 [0-39643.4]	✓	✓	1239.17 [0.18-39643.4]
GLRLM:									
high gray level run emphasis	✓	✓	6120.11 [1-321807.62]	✓	✓	12886.24 [1-321807.62]	✓	✓	23021.99 [45.97-321807.62]
long-run high gray level emphasis	✓	✓	55488.09 [1-9755180.03]	✓	✓	116805.48 [77.31-9755180.03]	✓	✓	205185.69 [514.48-9755180.03]
short run high gray level emphasis	✓	✓	4118.5 [0.05-247740.25]	✓	✓	8671.47 [0.07-247740.25]	✓	✓	15560.49 [14.08-247740.25]
GLSZM:									
high gray level zone emphasis	✓	✓	6717.88 [1-347651.5]			14144.98 [1.2-347651.5]			24962.32 [50.85-347651.5]
small area high gray level emphasis	✓	✓	1206.64 [0-99793.65]			2539.85 [0-99793.65]			4533 [0.09-99793.65]

A check mark indicates that the feature was among the 30 most important of the model (averaged on 30 iterations). All of the features were selected via Elastic Net at least 25 out of 30 times.

5.4 . Discussion

The main finding of this study is that a Random Forest performs better in predicting childhood cancer survivors at risk of a radiation-induced VHD under a selection of dosiomics features describing the heart dose compared to the mean heart dose. We also observe that the models perform best when trained on a population with some heterogeneity across the heart doses (Uniformity< 1). Finally, we found a dosiomics signature of cardiac doses for the prediction of a late VHD in the FCCSS. To the best of our knowledge, this is the first study that explores the role of dosiomics features in the occurrence of a late VHD after treatment for childhood cancer.

There is an established risk of VHD when strong doses ($> 25-30$ Gy) are absorbed by heart tissues during adult treatment (Gujral et al., 2016; Patil et al., 2022) or childhood cancer (Bates et al., 2019; Mulrooney et al., 2020; van der Pal et al., 2015b) and there exist hypotheses on the role of low and moderate doses (Bates et al., 2019; Chounta et al., 2023; Cutter et al., 2015). Meanwhile, studies claim that no level of radiation dose to the heart can be safe (Menezes et al., 2018). This study aimed to explore the effect of radiation doses absorbed by the heart by considering the heterogeneity of the dose. For that matter, we chose to extract dosiomics features from the dose matrices. This method is becoming popular (Placidi et al., 2021) and provides insight into radiation dose's spatial and statistical characteristics.

The role of heterogeneity of the heart dose in late valvular heart disease

We proposed a sensitivity analysis based on Uniformity. We observed that predictions improved when the models were trained on the sub-population of the FCCSS with Uniformity < 1, compared to models trained on the sub-population of the FCCSS with Uniformity < 0.1. It is noteworthy that the Uniformity is a measure of the homogeneity of the image array (dose distribution in this case) and that a higher Uniformity implies a greater homogeneity or a smaller range of discrete intensity values. It does not necessarily imply higher doses (Figure 5.4). However, as commented on Table 5.3, both the average Mean Heart Dose and the Maximum dose to the Heart increase when calculated among survivors with low Uniformity. We partitioned the cohort based on the assumption that Uniformity is, indeed, a meaningful factor in predicting the occurrence of a VHD. We observed that the model could not distinguish survivors most at risk of experiencing a VHD when trained among survivors with a small Uniformity range. This indicates that our assumption might hold, and it is one of the most fruitful results of this study.

We also included models trained on the entire FCCSS cohort that contains survivors treated and not treated with radiotherapy. The model underperforms compared to the models trained on the sub-population of the FCCSS with Uniformity < 1. Based on the assumption that cardiac radiation dose is not the only risk factor for a VHD, a

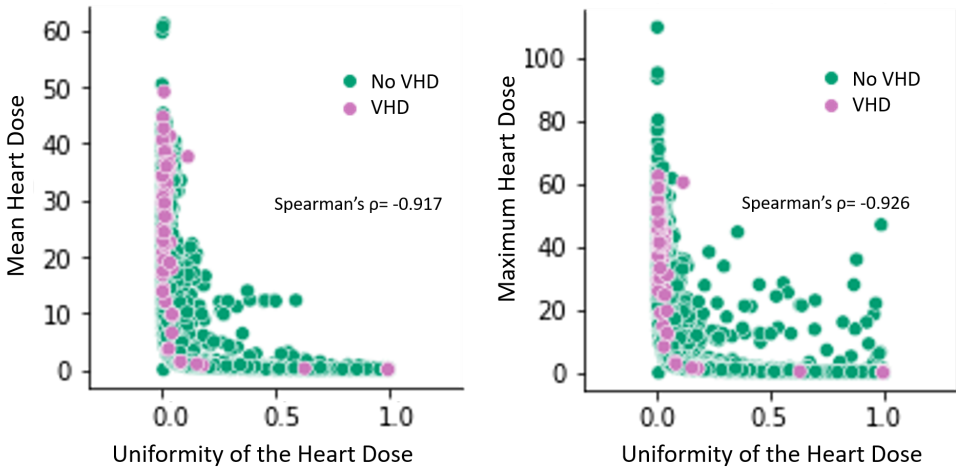

Figure 5.4: Pairplots of the Uniformity versus the Mean Heart Dose and the maximum dose to the heart.

dosiomics-based model is inappropriate for predicting the non-irradiated part of the cohort: the non-irradiated survivors that experience a VHD will always be incorrectly sorted in the model based on the radiation-induced risk.

Model Choice and Performance

In (Chen et al., 2004), weighted and balanced random forests both improve the prediction of the minority class in comparison to other algorithms. In our study, comparisons hold between models with different predictors; comparing different types of algorithms was not one of the objectives of this study. Among performance metrics, Sensitivity (or Recall or True Positive Rate) is the most important for this application. It gives away the existence of false negatives, whether all survivors who experienced the event were correctly sorted as high-risk. We also observe some models outperforming others based on Specificity. However, improving Specificity is a secondary objective of prediction models, as it evaluates the false positives. Therefore, between two models with contradictory results, we would choose the one with the highest true positive rate.

The two models with the highest Sensitivity are the MHD-based and the dosiomics-based BRF adjusted on clinical variables and trained on the sub-population with heart-dose Uniformity< 1 (0.8 and 0.82 respectively - Table 5.5). However, the comparison between them is not statistically significant, and we cannot conclude if one of them outperforms the other. Next is the dosiomics-based BRF, trained on the same pop-

ulation without adjustment on clinical variables (0.78 - Table 5.4). In this scenario, the difference from the Sensitivity of the MHD model (0.73) is close to being statistically significant. Considering that the other three metrics are significantly higher than the MHD-based model, we can derive that the dosiomics-based BRF trained on the subpopulation with Uniformity< 1 is the best-performing model in this study. Based on these observations, we conclude that the distribution of the radiation dose to the heart plays a complicated role in the occurrence of a VHD; the MHD cannot entirely capture that.

The dosiomics signature

The dosiomics signature can reflect the spatial complexity of the radiation dose and its association with the occurrence of a late VHD. It is noteworthy that, apart from very few exceptions, the two types of Random Forest evaluate the same variables as important in each sub-cohort. We observe that, in any case, MHD is among the most important features.

All of the features selected when models are trained among survivors with Uniformity < 0.1 are also selected in at least one more model, trained on a larger population that includes survivors with higher Uniformity (Uniformity < 1 and the entire FCCSS). All models select energy and total energy that depend on the magnitude of the voxel values in the region of interest and, according to the authors (van Griethuysen et al., 2017), are volume-confounded. The mean and median heart dose, as well as the root mean square, are selected by all models. GLCM features indicate how often pairs of voxels with specific values and in a specified spatial relationship occur. According to the authors, the sum average measures the relationship between pairs of voxels with lower intensity values and pairs of voxels with higher intensity values. We could therefore hypothesize that the sum average provides information on the effect of low doses in the occurrence of a late VHD. On the contrary, the high gray level emphasis and the Small Dependence High Gray Level Emphasis from the GLDM class of features, as well as the GLRLM and GLSZM classes, cover different aspects of the effect of high dose levels in the prediction of a late VHD.

Limitations

One inconvenience of the method of this paper is that the interpretability of the dosiomics features is not always apparent since most of the features are not widely used for statistical analyses. Also, dosiomics features are not directly extracted from the treatment-planning system. It is, therefore, not straightforward for the medical staff to incorporate them into prediction models.

Concerning the data content, a limitation also derives from the lack of information on comorbidities. Data related to comorbidities could improve prediction algorithms' performance and the reliability of the results. Also, there is still some uncertainty in estimating the absorbed doses in different types of studies (Vũ Bezin et al., 2017). We assume that the voxelized dataset we are treating is sufficiently reliable.

The most important limitation is the lack of a validation set, a common problem in this type of study (Appelt et al., 2022). The number of events in the cohort is too low. Therefore, further partitioning the population to put aside a validation set would lead to losing critical information necessary for the training. We decided the best strategy to eliminate some uncertainty from the results was to use the whole cohort in train-test partitioning and aggregate the results of 30 random stratified splits. External validation is, therefore, necessary. In this study, we aimed to propose a signal on the cardiac dosiomics signature for a late VHD and suggest incorporating information on dose heterogeneity into the design of prediction algorithms and TPS guidelines.

Perspectives

Radiotherapists do their best to protect vital organs from strong radiation exposure (Dumane et al., 2018). However, it is still unclear if and how harmful exposure to low and moderate doses to the heart (Gomarteli et al., 2017) could be. Meanwhile, while recent advancements make high MHD increasingly rare nowadays, novel radiotherapy delivery techniques such as IMRT or VMAT may increase the heart volume receiving low-to-moderate radiation doses (<15 Gy). Dosiomics features could provide helpful insight into spatially heterogeneous doses' effect on late effects like VHD. Extracting dosiomics features directly from the treatment-planning system could be an interesting and useful perspective in this case.

Conclusions

Dosiomics are proving to be a promising strategy for exploring the radiation dose distribution and exposing information on the underlying pathophysiology of radiation-induced pathologies. The dosiomics-based BRF outperforms the other models in this predictive attempt of a late VHD with data from the FCCSS and could prove beneficial in identifying high-risk individuals even in a context where detailed clinical data is unavailable. If these findings hold, the dosiomics signature may be incorporated into machine-learning classification algorithms for radiation-induced VHD risk assessment.

6 - Confrontation of the models to the PanCare-SurFup-ProCardio cohort

6.1 . Context

External Validation

The initial idea for the third contribution was to attempt testing the models proposed in Chapters 4 and 5. This would mean that having used the data from the FCCSS cohort to train and evaluate the performance of the classification models, we would, in this chapter, use the data from the independent PanCare cohort detailed in Section 3.2 to test the most powerful ones.

In order to validate a pre-trained model on an independent population, however, the data in the two populations need to be from the same distribution. Unfortunately, this is not the case in the available data for this scenario: the FCCSS is a cohort where $\approx 1\%$ of the survivors have experienced a VHD while PanCare is designed as a case-control population, with a 50-50 proportion of VHD cases.

However, it is still possible to adapt the models and discuss the results: instead of a risk model, we decided to fit a conditional logistic regression and discuss the odds ratios, and instead of a balanced and a weighted Random Forest, a classic Random Forest adjusted on the matching variables as well a Matched Random Forest and discuss the importance of each feature of the dosiomics signature proposed in Chapter 5.

6.2 . Methods

Likewise to our approach for the FCCSS cohort in Chapters 4 and 5, association and descriptive analyses were conducted for the nested case-control study of the PanCare cohort. Demographic and treatment characteristics are detailed in Table 3.5 of Chapter 3. For univariate analyses, we applied a conditional logistic regression and for the confrontation with the dosiomics signature proposed in Chapter 5 we applied both a Matched Forest, appropriate for paired case-control study designs, and a Random Forest adjusted on the pairing variables that are independent of follow-up.

Analyses were conducted with R version 4.0.3 (2020-10-10) – "Bunny-Wunnies Freak Out" Copyright (C) 2020 – The R Foundation for Statistical Computing and verified with Python 3.8.13. Conditional logistic regression was performed with the logit function of the R survival package (Therneau, 2023); Matched forest variable importance was assessed through the R implementation available from the authors of Shomal Zadeh et al., 2020; classic Random Forests were fitted and evaluated in R with Liaw and Wiener, 2002; Mogensen et al., 2012 and in python with Pedregosa et al., 2011. All P-values were two-sided, and we fixed the significance threshold at 0.05 throughout the analyses.

6.3 . Results

Baseline Models

We observe a 3.92-fold risk increase (Table 6.1) among survivors that had been treated with radiotherapy, which is twice the ratio presented in Table 4.2, when the hazard ratios are calculated in the FCCSS cohort. We also observe an 8 % risk increase among survivors treated with radiotherapy compared to 10% observed in the FCCSS. When categorized as well, the MHD is statistically associated with experiencing a VHD for doses up to 1 Gy (Odds Ratio= 2.68, CI95%= [1.24-5.78]), as well as doses $<$15Gy (Odds Ratio= 13.2, CI95%= [5.25 - 33.18]).

Likewise, when we calculated the hazard ratios in the FCCSS cohort in Chapter 4, adjusting the model on chemotherapy exposure does not seem to significantly affect the estimates, at least not in an interpretably meaningful way. We chose not to adjust on age at diagnosis (like we did in Table 4.2) as it was one of the matching variables during the case-control design of the cohort.

Random Forest

The results of some preliminary analyses are presented in Figure 6.1 in Figures 6.2a and 6.2b are presented the features of the FCCSS dosiomics signature to help with comparisons (as illustrated in Table 5.7), with decreasing order of average importance (we remind that variable importances and model metrics in Chapter 5 were averaged over 30 train-test instances).

Table 6.1: Odds ratios of conditional logistic regression, with and without adjustment on chemotherapy exposure.

Radiation exposure	**Odds Ratio [95% CI]** (Univariate)	**Odds Ratio [95% CI]** Adjusted on chemotherapy
Radiotherapy (RT)		
No	(ref.)	(ref.)
Yes	3.92 [1.92 - 8.03]	3.92 [1.92 - 8.04]
MHD - increase of 1 Gy	1.08 [1.05 - 1.11]	1.11 [1.07 - 1.14]
MHD - in Gy (categorized)		
No RT	(ref.)	(ref.)
[0,1]	2.68 [1.24 - 5.78]	2.25 [1.02 - 5]
(1,5]	0.27 [0.03 - 2.34]	0.35 [0.04 - 3.09]
(5, 15]	3.58 [0.93 - 13.81]	4.6 [1.14 - 18.51]
> 15 Gy	13.2 [5.25 - 33.18]	16.82 [6.31 - 44.8]
$\mathbf{V}_{15Gy}$ - 1 % increase of heart volume absorbing $\geq$ 15 Gy	32.25 [13.03 - 79.87]	33.37 [13.36 - 83.34]
$\mathbf{V}_{30Gy}$ - 1 % increase of heart volume absorbing $\geq$ 30 Gy	75.56 [18.07 - 315.97]	75.58 [18.06 - 316.26]

Reference class (ref.); Mean Heart Dose (MHD); 95% confidence intervals (95% CI);

Among the most influential features in both the Matched Forest and the Random Forest, we found:

- from the First Order Statistics: the Root Mean Squared and the Mean Dose to the Heart,
- from the GLCM: the Sum Average,
- and from the GLDM class of features: the Large Dependence High Gray-Level Emphasis.

When we compare the results from the case-control study to those derived by training the Random Forests on the FCCSS, we can observe that differences among feature importances vary less in the latter. However, the Mean Heart Dose remains an influential variable: it is among the most important features of the weighted Random Forest and around the median feature importance of the Balanced Random Forest. Finally, in results from both the weighted Random Forest and the Balanced Random Forest, the importance of the Large Dependence High Gray-Level Emphasis, the Root Mean Squared, and the Sum average are above the median importance.

Among the least influential features according to the Matched Forest are the IDMN and IDN of the GLCM class and the Kurthosis of the First order statistics; however, the latter is the 6^{th} most important feature of the Random Forest. Also, the Minimum dose to the heart that sorts as non-influential in the Matched Forest sorts above the median feature importance of the Random Forest and is among the most influential features of the Forests trained on the FCCSS. Similarly, among the least influential features according to the Random Forest are the Small dependence high gray level emphasis (GLDM) and High gray level run emphasis, which are the 5^{th} and 9^{th} most important features, respectively of the Matched Forest.

Moreover, we can observe that the Energy displays a relatively high feature importance with the Random Forest and is also very influential according to both the weighted and the Balanced Random Forest trained on the FCCSS but less important according to the Matched Forest.

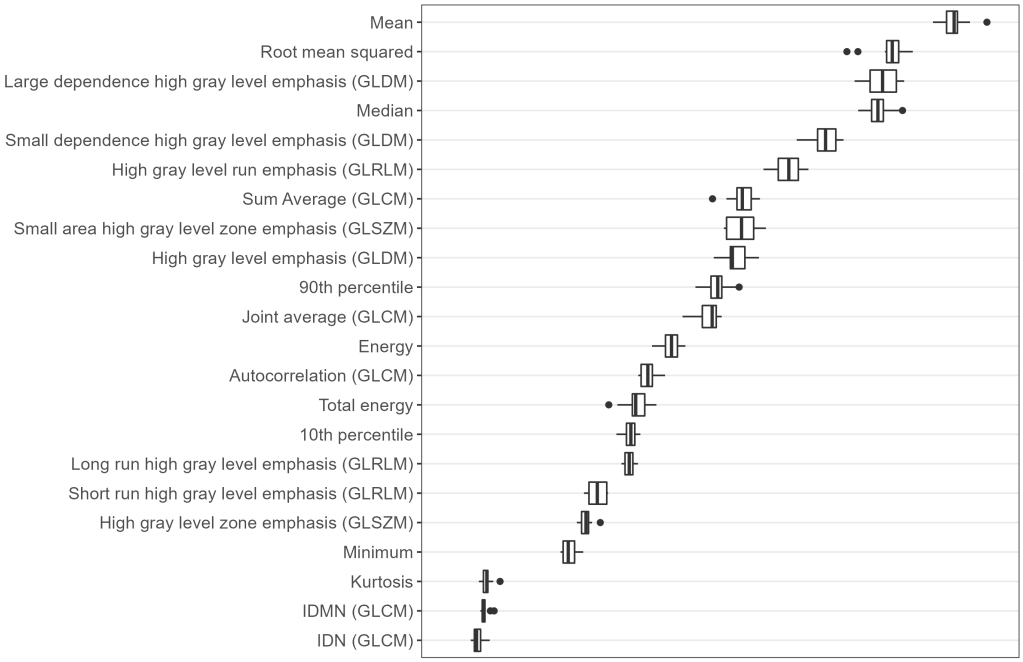

(a) Matched Forest

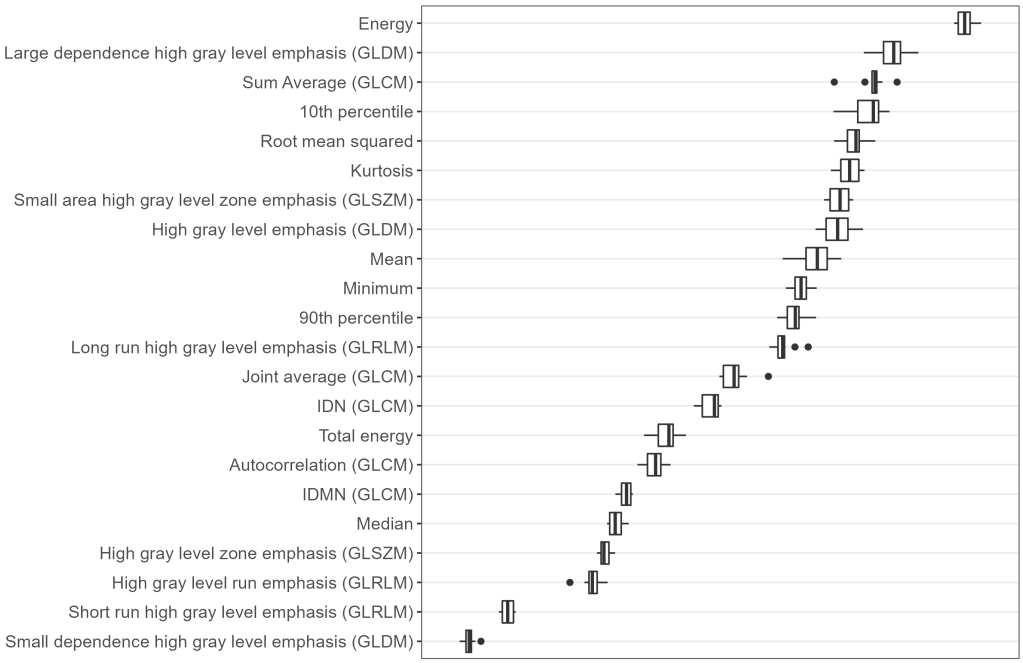

(b) Random Forest- adjusted on biological sex, and age and year at childhood cancer diagnosis

Figure 6.1: For adjustments on the paired case-control study of PanCare, with order of importance (from higher to lower average importance)

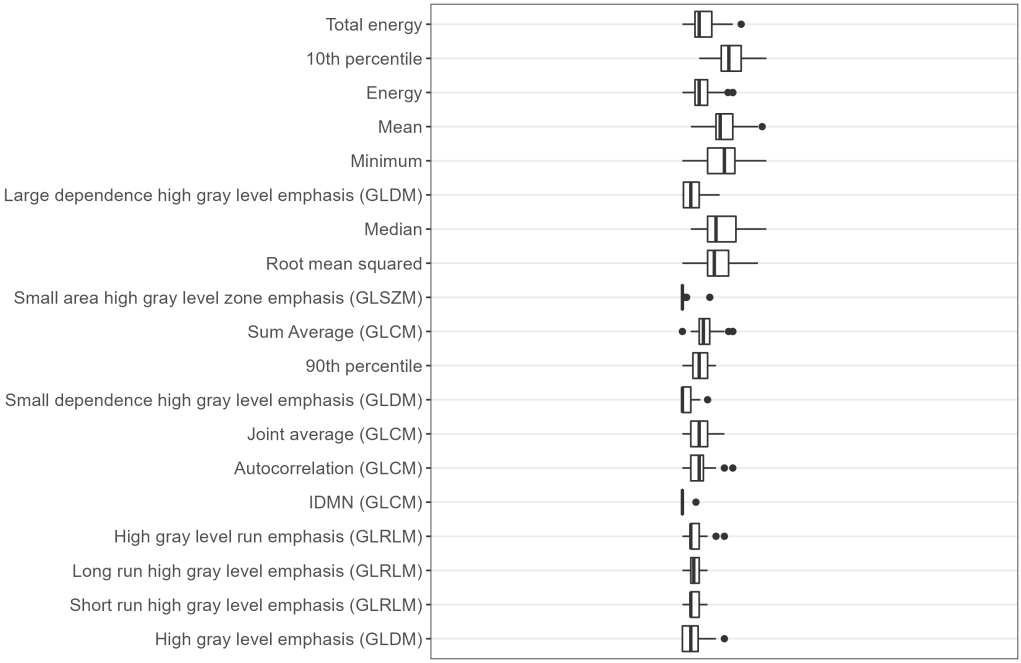

(a) Weighted Random Forest

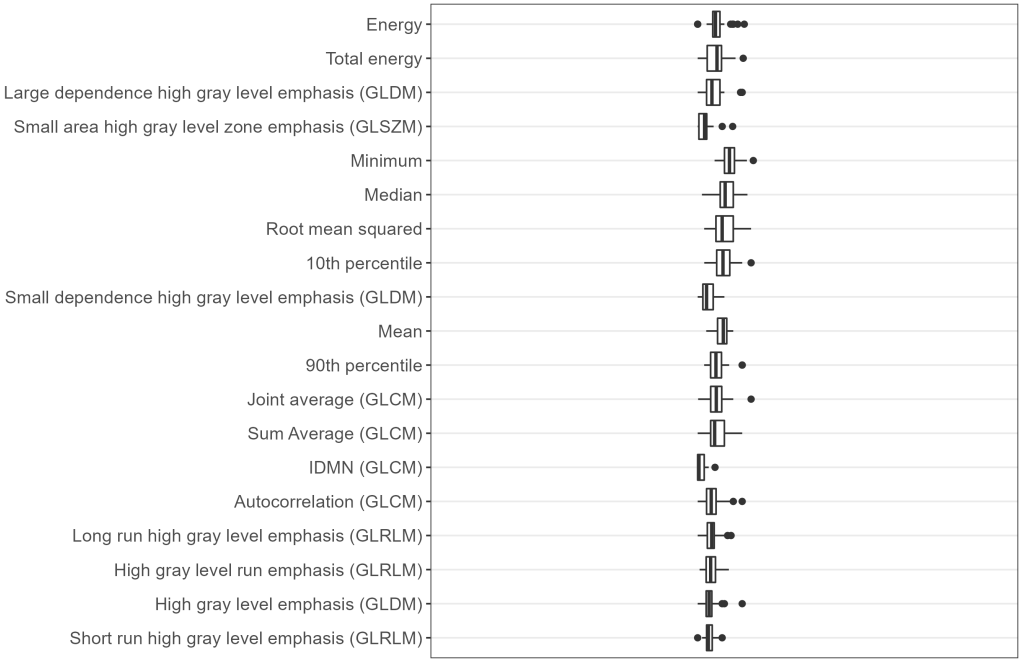

(b) Balanced Random Forest

Figure 6.2: For adjustments on the population of the FCCSS, with the order of importance (from highest to lowest average importance over 30 iterations of train and test)

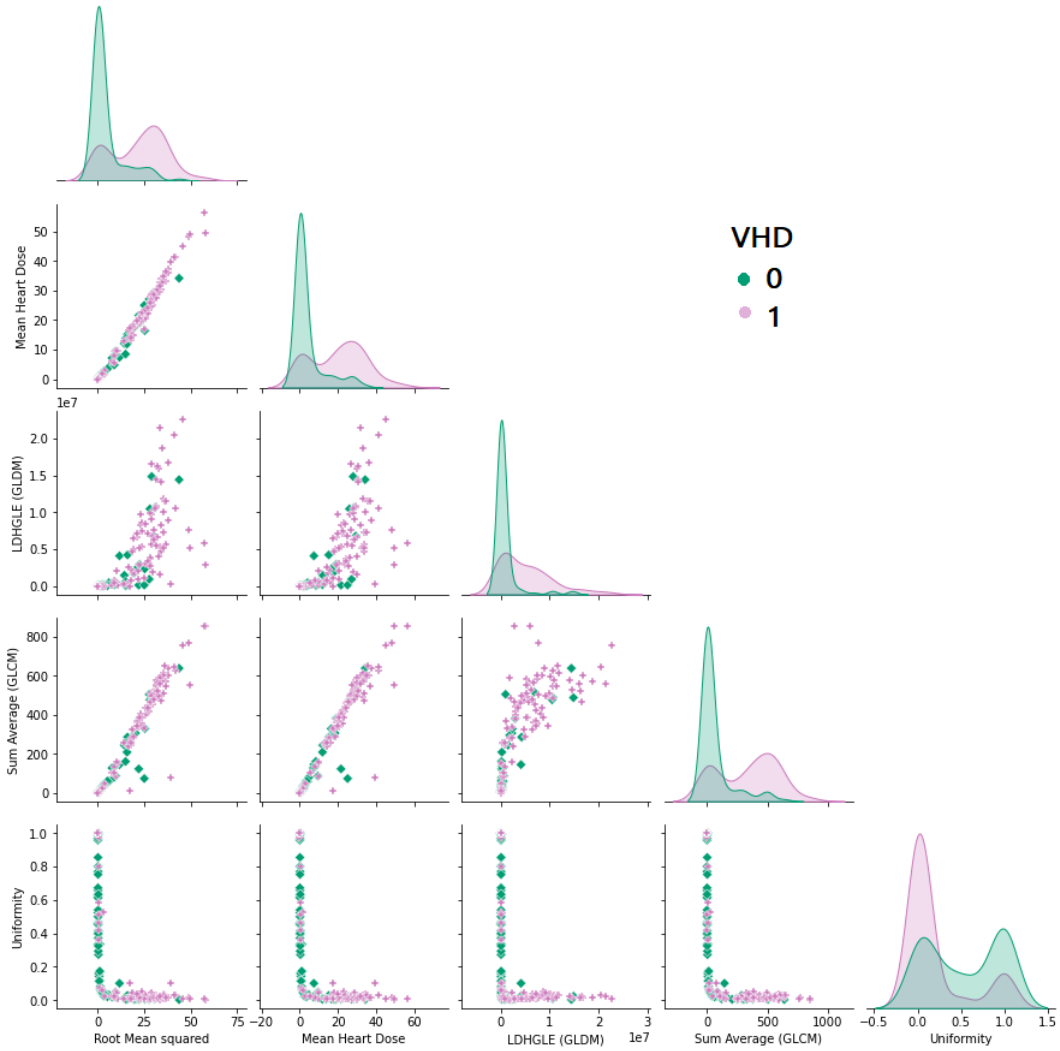

Figure 6.3: Pairplots illustrating the repartition of some features that stand out repetitively in the PanCare study, as well as the Uniformity, according to VHD status.

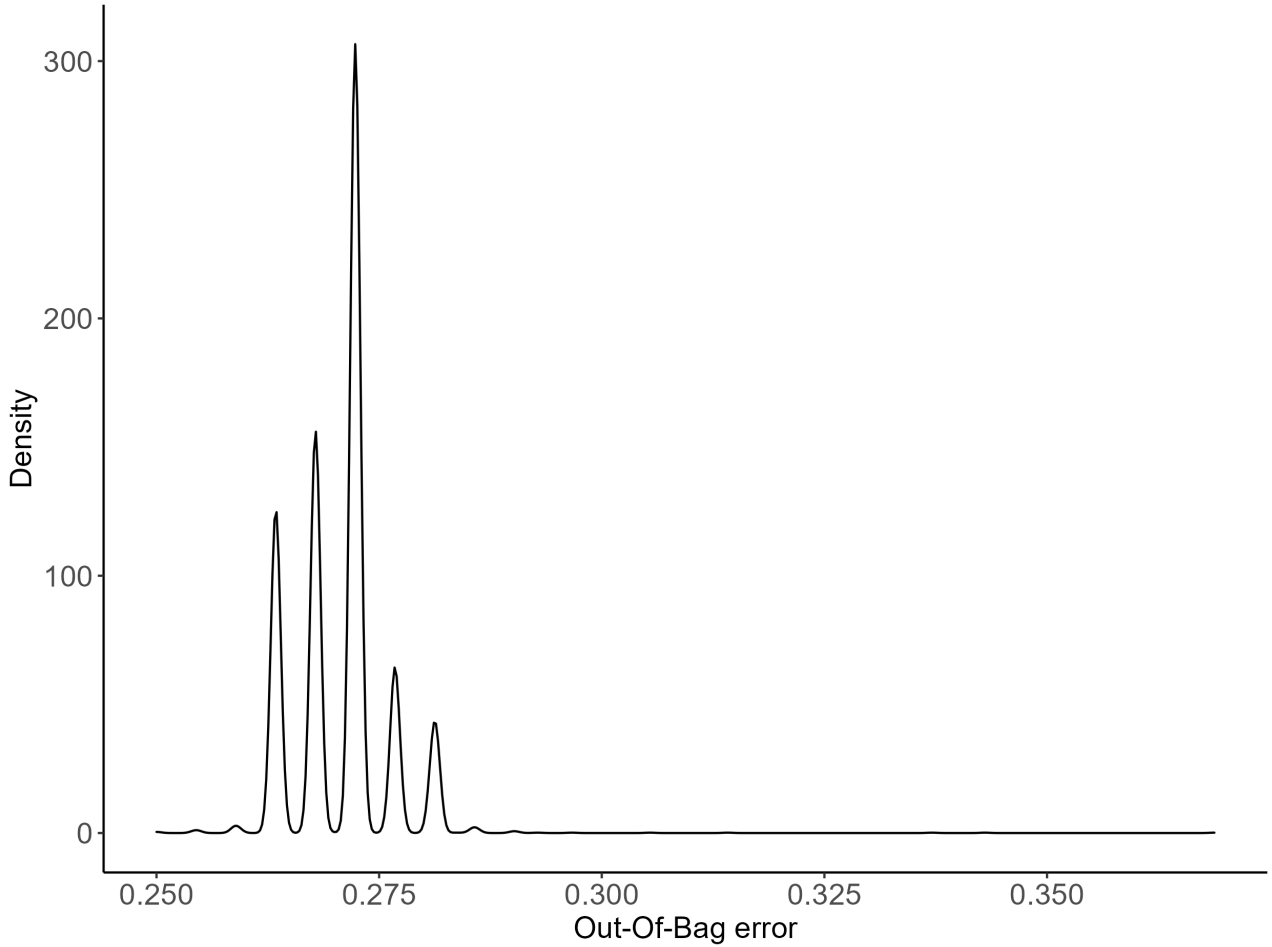

Figure 6.4: Density of the Out-Of-Bag error rate over 5000 trees for the PanCare population.

Table 6.2: Confusion Matrix for the Random Forest on the PanCare population.

	estimated negative	estimated positive	Class Error Rate
controls	89	23	0.21 FP
cases	38	74	0.34 FN

Finally, the median out-of-bag error rate of 10 runs of Random Forest (5000 trees per forest) was 27.4%, with 21% false positives and 34% false negatives. We may conclude that there is definitely room for improvement.

Descriptive Pairplots

An attempt to examine the repartition of influential features according to the VHD status and to compare them in pairs is presented in Figure 6.3. Uniformity, which determined the cohort partition criterion, was also included. The same features are represented in pairplots in the Appendix A for the FCCSS (Figure A.8).

We can observe that some pairs of features are linearly correlated (e.g., the Mean Dose to the Heart with the Root Mean Squared as well as with the sum average, with a few outliers). In the diagonal of the pairplots can be found the distribution of each feature in the population. We can observe that for most of the cases, Uniformity is close to zero. For the rest of the features, the opposite is observed: for most of the controls, the feature is close to zero.

6.4 . Discussion

Some stable results between the two cohorts, despite their different designs

Validating a model is never a simple task, especially in our case, where the study designs differ, and the prevalence of VHD is structurally different. However, we were able to establish some reassuring similarities between the two cohorts. Mainly, we were able to verify the importance of features belonging to the group of First order statistics, like the Mean Heart Dose, that are commonly employed in risk and prediction models.

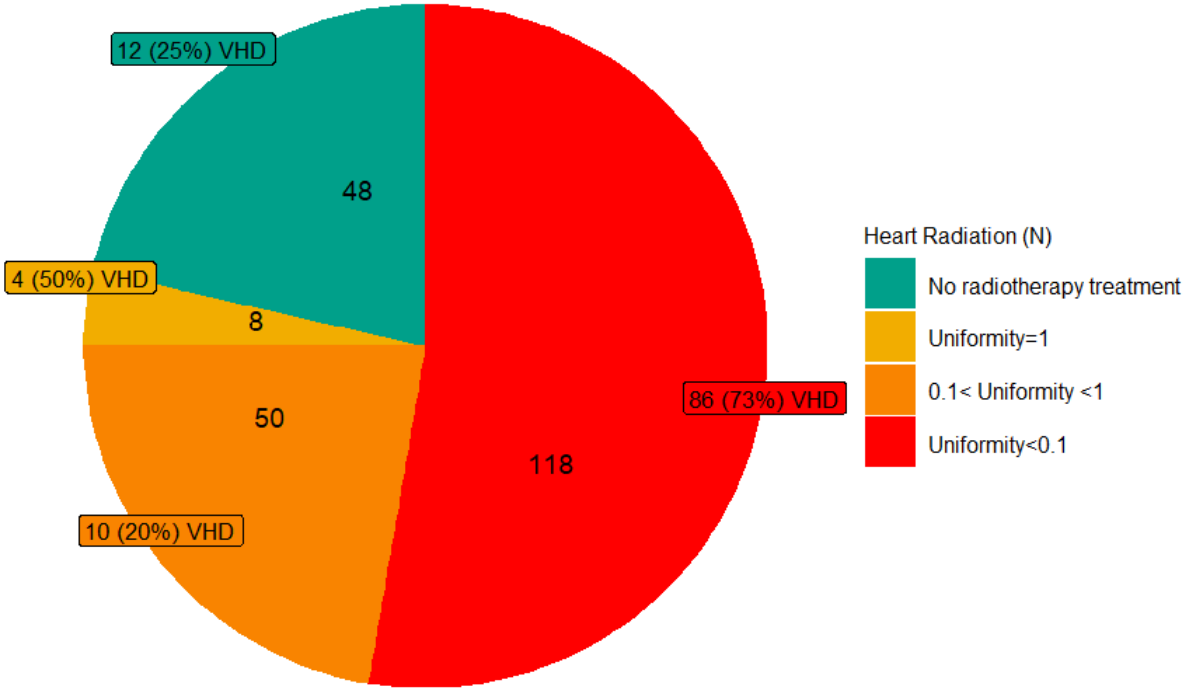

Figure 6.5: Uniformity distribution in the PanCare study.

The Uniformity variable

Partitioning the population according to the Heart Dose Uniformity was not an option with this study, except by ignoring the pairing. This action would lead to biased estimates, as survivors have already been pooled from a larger population. However, examining the repartition of Uniformity in this population is interesting. We can briefly observe that 73 % of those with Heart Dose Uniformity are cases, which makes 86/112 $\approx$ 77% cases in this slice of the pie, which is an indication that the reasoning behind considering the heterogeneity of the heart dose could be accurate.

Precautions with the Matched Random Forest method

The Matched Random Forest seemed like the appropriate choice for the study design of this case-control population. However, there are two significant drawbacks: first, according to the authors (Shomal Zadeh et al., 2020), it was developed for variable selection, and second, it is not widely used in the literature. Therefore, we could not evaluate its efficacy in relation to other studies. This is why we were reluctant with its interpretation, and we chose to run a classic Random Forest without accounting for pairing.

Interpretations of the dosiomics features

The fact that dosiomics features are relatively recent and not yet popularly used for the analyses of dosimetric data contributes to the originality of our study but it also complicates the interpretation of the results. Radiomics features were defined for the description and interpretation of gray level in medical imaging, and therefore, adaptations are necessary when they are extracted from radiation dose matrices and interpreted as *dosiomics*.

For example, Large Dependence High Gray-Level Emphasis (GLDM) measures the joint distribution of large dependence with lower gray-level values. Gray-level values in the case of dosimetric data are dose intensities. A Gray Level Dependence Matrix (GLDM) quantifies gray level dependencies in an image, defined as the number of connected voxels within distance δ that are dependent on the center voxel.

Moreover, GLCM is a textural matrix used to extract data from neighboring pixels/voxels and is closely related to GLDM (Zwanenburg et al., 2020). It describes the

second-order joint probability function of an ROI. Features of the GLCM class measure dose uniformity since the GLCM matrix quantifies neighboring relationships between pairs of voxels but are not necessarily related to the feature Uniformity in a linear way. The fact that the Sum average from the class of GLCM features stands out is also interesting.

Perspectives and Conclusion

Dosiomics features can summarize complicated structures and relationships of radiation dose levels. The use of dosiomics features in prediction models seems to provide insight into the association of heart radiation with the occurrence of valvular heart disease. They could be a useful asset in the treatment planning system.

7 - General Discussion and Conclusion

7.1 . Synthesis of the contributions, their strength, and limitations

The principal objective of this work was to explore the distribution of the radiation dose to the heart with the help of voxel-scaled dose matrices and propose alternative approaches in modeling the radiation-induced risk of late valvular heart disease (VHD) after treatment for childhood cancer. Firstly, we confirmed previous literature results that there is a risk increase in experiencing a late VHD among survivors of the FCCSS that have been treated with radiotherapy. Moreover, analyses of the dosimetry data allowed us to observe that the mean heart dose (MHD) is positively associated with the risk of experiencing a VHD. We were also able to express radiation-induced risk in terms of irradiated heart volume instead of dose level absorbed by the heart (*bounded dose-volume indicators*) and found that moderate-to-low doses to a large heart volume are also risk factors. Furthermore, multivariable approaches were explored on the basis of the assumption that there could be an association of heart-dose heterogeneity with the occurrence of a late VHD. On that basis, dosiomics features were extracted and evaluated through machine learning algorithms. Our results indicate that our hypothesis on the association of heart-dose heterogeneity with the occurrence of a late VHD after treatment for childhood cancer might hold: classification models based on multiple descriptive features outperformed the baseline model (based on the mean heart dose) in predictive power. We proposed, therefore, a *dosiomics signature* for the FCCSS and completed the study by testing this signature on an independent European cohort.

The risk of VHD, contributions of dose-volume indicators

Specifically, from the analysis of bounded dose-volume indicators ($V_{d_1}|_{V_{d_2}=0\%}$), the following results were derived: high doses (≥ 40 Gy) are statistically associated with a VHD, even when absorbed by $< 10\%$ of the heart volume; doses 20-40 Gy induce a statistically significant risk when more than 50% of the heart volume is involved; and finally doses 5-20 Gy induce a statistically significant risk of experience a VHD when

large volumes of the heart (90%) are involved in the field of irradiation. The assumption that moderate and low doses (<15 or 20 Gy) to an extended heart volume might be a risk factor had only been hypothesized before our study (Cutter et al., 2015), and to the best of our knowledge, this is the first study to provide evidence to support it. These results justify that using dose-volume indicators defined by bounded dose intervals $(d_1 - d_2)$ could be informative and should be generalized in epidemiological works. This seems a simple methodological detail (already proposed by Bates et al., 2019). However, the inclusion of bounded dose-volume indicators is not yet standardized in the literature, while it allows to study and express the effect of lower doses independently of the already established effect of higher doses.

Furthermore, like Cutter et al., 2015, we could not provide evidence on the association of anthracyclines or other agents with experiencing a VHD. A possible explanation is that while the use of anthracyclines has already been associated with cardiotoxicity (Haddy et al., 2016), and VHD, in particular, (Mulrooney et al., 2009), in this study, survivors with a cardiac event before their VHD diagnosis were not considered as having experienced the event. In future studies, competing risks for cardiac complications and mortality before the occurrence of a VHD might need to be taken into account.

Some additional results of the extensive analyses on the FCCSS were derived about the risk of experiencing a late VHD after childhood cancer. An important observation was that the excess relative risk (ERR) in the FCCSS is very low before the age of 30 years old (4%), and increases each next decade (94%, 228%, and 312% for survivors > 50 years old). We did not observe a change in risk estimates when models were adjusted on the age at childhood cancer diagnosis and no association was observed with the year at diagnosis.

In the context of risk modeling, some multivariable approaches were, finally, investigated, and results are presented in Table 4.8 of Chapter 4 and Table A.2 of the Appendix A. We compared the MHD model with alternative models where the radiation-induced risk is taken into account through dose-volume histogram (DVH) parameters of doses to the heart. This approach is based on the assumption that a combination of explanatory variables derived from heart DVHs could explain the radiation-induced risk of experiencing a VHD more efficiently than the MHD. However, metrics were similar or not better compared to the baseline model (MHD), and we decided to explore a different multivariable approach.

Machine learning models

The next important results came from the *dosiomics* analyses. A rich set of variables were considered for supervised learning models in order to take into account complicated spatial characteristics of the heart dose. Feature extraction was based on standardized image biomarkers (Zwanenburg et al., 2020), and their predictive power was compared to that of the baseline MHD-based model. To the best of our knowledge, this is the first study to explore the performance of dosiomics features in predicting a late VHD.

The idea that dose-descriptive features could be more efficient than the models based on the MHD solely in predicting a late VHD when trained on a population with non-homogeneous heart doses (dose uniformity < 1 Gy) led to some fruitful results. This approach was applied in order to explore in-depth the hypothesis that there exists a radiation-induced risk due to lower doses beyond the already established risk induced by high doses. If this assumption holds, it could mean that summary statistics like the mean or median dose to the heart underestimate the risk induced by doses absorbed by the heart, and spatial characteristics of the dose should be considered. Random Forests allows us to consider relationships beyond linear and include some detailed spatial features, often correlated. Our results provide evidence that predictions are more accurate when based on multiple dosiomics features in comparison to a classic approach based on the Mean Heart Dose.

Improvements brought by the dosiomics features compared to the MHD may not yet be completely convincing, probably due, for a significant part, to the imbalanced nature of the data ($\approx 1\%$ in the FCCSS and $\approx 3\%$ among survivors with non-homogeneous heart doses). Further investigation is surely required. However, some optimistic results were derived from the confrontation with the case-control study of the PanCareSurFup-ProCardio cohort. The dosiomics signature proposed by the analyses in the FCCSS was included in classification algorithms aiming to predict the cases in the PanCare study. This allowed us to compare feature importances between the two cohorts, and observe features like the Large Dependence High Gray Level Emphasis (GLDM), the Root Mean Squared (First Order Statistics), the Sum Average (GLCM), as well as the Mean Heart Dose, that sort among the most important features in both cohorts.

The Mean or Median Heart Dose being among the features that stand out, is also

a meaningful result. The fact that the Mean or the Median Dose to the Heart could be a sufficient explanatory feature for risk prediction is a very valuable and reassuring conclusion for practitioners, especially for cohorts where voxelized dosimetry data is not available. However, it is more challenging to ascertain a 'negative' conclusion like this since it requires ensuring that the models themselves cannot be improved. This work was the first step in that large research question.

Clustering techniques for dimension reduction

During this thesis, we supervised the internship of Mamadou BALDE, a Master 2 student at the University of Rouen. We chose to place his work in Appendix B. However, since it opens some interesting perspectives, we would like to add a few comments here. In this work, the main idea was to use clustering techniques to reduce the dimension of the raw dosimetry data. Although the results were not completely conclusive, with no better accuracy in terms of prediction than the other presented approaches, this work raised some interesting points. In particular, several questions had to be investigated and could be of interest to future work in that research direction.

Firstly we needed to decide the optimal number of clusters. Using the elbow method, Mamadou showed that the optimal number of clusters ranged from five to seven, with six being the optimal number of clusters for 84 % of the population. Therefore, we decided to fix it approximatively to six for all survivors. Next, he had to compare different clustering (or partitioning) algorithms: the k-means, hierarchical, agglomeration, and density-based clustering, and evaluate them based on metrics like the Calinski and the Silhouette score. K-means was the most performant clustering method, both according to the scores as well as in terms of computational cost. This result is in line with several literature conclusions, as well as of Van Craenendonck and Blockeel, 2015, who also recommended the k-means algorithm.

Moreover, we had to discuss the choice of variables for the clustering task. Clustering based on the dose level alone was a rejected option because we decided on the integration of spatial characteristics of the dose as well to obtain clusters that would be consistent with the underlying body structure of survivors. Finally, interpretation was a complicated part of clustering. To understand and evaluate the clustering of the heart doses and their association with a late VHD, we decided to calculate some

descriptive features and train classification algorithms with them.

Some interesting and promising results were derived from these analyses. Particularly, during some preliminary analyses, classification was comparable to the dosiomics approach without, however, outperforming it. However, the danger of overfitting is always possible when separating the data, especially in the case of an imbalanced dataset, and therefore, further analyses are required for the generalization of these results.

7.2 . Perspectives

Follow-up recommendations.

One first application of this work is the direct inclusion of some results into follow-up recommendations, as well as treatment planning. For example, there exists an open question on upper and lower dose thresholds. Cutter et al., 2015 hypothesized that under a certain level, doses might not induce significant risk to the heart structures. Our results provide evidence that doses over 5 Gy delivered to more than 90% of the heart volume increase the risk of experiencing a VHD. This is a quantitative result with numerical thresholds that can already be tested in independent cohorts, and it provides indications in the research of a lower threshold of affected cardiac volume affected by given dose levels.

Towards survival analysis using neural networks

This thesis was a data-driven work based on 3D dose matrices (voxelized). The first step of the analysis was to aggregate the voxel-scaled information into summary statistics and study the risk of a radiation-induced VHD. The natural next step would be to study the raw doses. To explain the occurrence of a VHD directly from the raw doses, we would need to use methods adapted to the high dimensional data, such as neural networks. Such neural networks have already been developed in the context of survival analysis (e.g., Cox-nnet developed by Ching et al., 2018), they constantly evolve for the optimization of the algorithms (Benkirane et al., 2023; Pradat et al., 2023; Roblin, 2019), and currently provide state-of-the-art performance in a variety of fields, including medical applications. Modeling the raw data should allow us to consider the doses' heterogeneity and other spatial characteristics.

In the context of the *RadioPrediTools* project (INSERM project launched one year after the beginning of this Ph.D.), I appreciated working in a collaborative framework and contributing to scientific discussions not limited solely to my specific Ph.D. subject. In particular, I had strong interactions with Mahmoud Bentriou (Ph.D.), who investigated in his post-doctorate work whether to consider the heart substructures or the heart as a whole for the radiation-induced risk assessment of cardiac disease (article in progress). For the case of VHD, some preliminary results using the survival model based on First Order Statistics of the heart sub-structures were not promising compared to the model based on the MHD (C-index=0.65 versus 0.74). Further investigation is, however, required.

During this collaboration, we also had the chance to brainstorm about the differences in the applications of survival and classification models, their benefits, and their inconveniences. For example, survival analysis was very effective in studying the occurrence of a VHD in a population over time. However, classification models are required to develop robust predictive models of a binary outcome that have the potential of being applied directly after treatment without accounting for the time of survival. The benefit of such large cohorts, where the population is followed over a long course of time, is that the information precedes the model training. Thus, we were able to take a step back from the observations and simplify the approach into classification to provide ready-to-use models for predicting the occurrence of a VHD before observing the follow-up duration.

Towards multi-organ and multi-class classification problems.

In our work on the dosiomics approach, the objective was to answer first the more straightforward question: for a given organ, can we predict the occurrence of a given complication? The next step would be to consider, for a given organ, several potential iatrogenic complications and thus move to a multi-class problem instead of a binary (yes/no) answer. Then, benefiting from the results obtained at an independent organ scale, it will be possible to undertake the solution of a more complex problem considering whole-body voxel data and predicting as output a list of complications, including the organ where it occurs. Besides, while exploring the database, there was significant work to be done in order to recognize outliers and clean the matrices. Recognizing

and incorporating the contouring of an organ can be a challenging job. For example, in order to build prediction algorithms for the occurrence of late breast cancer, data for the breast region need to be incorporated, which is not yet fully developed during childhood. Similarly, to consider treatment for second cancer, we need to consider developmental changes, which makes the dose matrices (voxelized spatial data) very different from one another.

Data availability and their uncertainty.

Databases in this thesis included survivors whose dose distribution had been reconstructed posteriorly to the moment of treatment (Alabdoaburas, 2017; Diallo et al., 1996; Veres et al., 2014; Vũ Bezin, 2015). Dose reconstruction comes with unavoidable uncertainties: a residual level of 2 to 5% of inaccuracy is generally observed for the dose at the organ of interest. The primary sources of uncertainty associated with dose estimation are (i) imaging of patient anatomy, (ii) reconstruction of the RT treatment plan, (iii) characterization of the irradiation source, and (iv) measurements or calculation of the dose distributions. To date, such quantification of uncertainty level on dose estimations is rarely performed and has not been systematically explored at a whole-body scale. A perspective would be to assess better the contributions of the different sources of uncertainty in our databases. These uncertainties might affect our results: e.g., the valves' location is not yet entirely reliable. An interesting research topic would be investigating uncertainty propagation throughout the developed models. Prediction uncertainty would therefore be assessed, and if considered excessive regarding the clinical applications, its sources could be identified, and ways to control it could be proposed.

Another axis of progress would be considering these uncertainties in the model development process, particularly for variable selection. Indeed, we have shown that among the few approaches explored in our thesis (using explanatory variables corresponding respectively to mean dose to the heart, bounded dose-volume intervals, dosiomics, and clustering-based indicators), none strongly outperform the others. Therefore, an option to explore would be to choose the approach that would be the most robust to the presence of uncertainties. For instance, results based on statistics calculated on the whole heart can likely be more robust than those found on the valves.

Similarly, one can wonder if the performance of models based on the Mean Heart Dose could be due to the better robustness of this indicator compared to more sophisticated ones like dose-volume histograms or dosiomics. To explore this effect, a possible strategy could be to create virtual data within which different sources and uncertainties would be integrated to test and compare the different models.

However, such uncertainties should naturally decrease with time. For recently treated patients, data are automatically generated and can be archived (NEMA, 2023), and there is no reason for this trend to stop in the future. Even if they do not concern whole-body dosimetry, doses absorbed by organs of interest can be extracted, as well as DVHs. Healthcare databases are becoming popular, although data quality and standardization might still be a problem, given the complex transmission chain of information between health institutes: several researchers that have retrospectively analyzed 'big' data in health have reported that data quality and completeness is always a challenge (Adibuzzaman et al., 2018). Along with the effort concerning data acquisition, new tools are also developing to extract information in a helpful form. The significant advantage of this work is that the risk and prediction models we propose could be generalized and used routinely within a short time, thanks to increasing DICOM-RT data availability.

In our case, a tool is currently being developed for voxelized dose-contour extraction and volume calculation from DICOM-RT data (in progress by Duyen Thi DO, project *RadioPrediTools*). Although our results are still preliminary, our prediction algorithms can already be trained, automated, and incorporated as an extension of this tool for late effects risk assessment (likewise to tools already in use LEATT, 2023). An additional interesting extension of this work for future investigation would be to incorporate in the TPS an application to calculate and extract dosiomics features. This is a practical advantage of the dosiomics over the dose clustering approach, which should be more complicated to incorporate into the TPS.

Decision support for personalized follow-up protocols.

Even though the production of automated applications is not yet a reality, risk models are already in use to design personalized follow-up for each survivor. Although still in its preliminary stage, our work paves the way toward an integrated optimization tool

for recommending personalized follow-up protocols adapted to each patient's health history. Defining the follow-up protocol is a delicate problem, with potentially dramatic consequences in case of misadjustment. The solution involving all sorts of screening exams at a high frequency would not be sustainable both economically speaking and in terms of patients' comfort and even safety. A perspective is, therefore, to turn to cost-effectiveness analysis. It aims to estimate alternative interventions' relative costs and health gains, compare them, and identify the best cost-efficient strategies. Cost-effectiveness studies compare different strategies and evaluate their costs, not only purely from the economic point of view but also taking into account the life quality of patients and the probability of occurrence of each health event. The gains are typically measured in disability-adjusted life years (DALYs), representing a weighted combination of mortality and morbidity effects of an intervention. Other possible denominators could include cost per life saved or cost per life year held (WHO, 2004). Such cost-effectiveness analysis, usually performed at the population level, could be adapted to our framework specificities to help design a quantitative criterion to optimize for defining a personalized protocol for each patient based on the projections of his probabilities for different complications. Since these probabilities vary with time, this will lead to an optimal control problem to be solved.

The scientific question can indeed be formulated as an optimization problem given budget constraints (Bejarano-Quisoboni et al., 2022; Dumas et al., 2016), availability of medical professionals, and the psychological distress of survivors induced by medical exams. Given a survivor's demographic and treatment profile, what would be the optimal frequency and focus of follow-up? Optimization of personalized follow-up raises several operational and societal questions. The acceptability of such approaches by patients and doctors is still under question. In this sensitive context, more accurate risk models are necessary to inspire trust (Gebauer et al., 2020; Hudson et al., 2021; Institute of Medicine (US) and National Research Council (US) National Cancer Policy Board, 2003; Michel et al., 2019; van Kalsbeek, van der Pal, et al., 2021). It is also necessary to involve medical experts in the test procedure of the algorithms developed. Besides the standard statistical evaluations, we have already performed on our cohorts, a possible procedure would be to rely on selected patients sent to an expert panel (of onco-pediatricians), who would effortlessly establish risk scores of iatrogenic events. We can also compare their recommendations with or without providing them with our

computed scores to assess the potential clinical impact of the tool.

7.3 . Conclusion

The methodological contributions of this thesis aim to bridge a gap between epidemiology and machine/deep learning applications. Meanwhile, some results can already be considered reliable for long-term follow-up recommendations and contribute to improving childhood cancer survivors' quality of life. Our findings are only a small addition, but hopefully valuable, to the ongoing effort of optimized identification of survivors high at risk of experiencing late valvular heart disease.

A - Appendix A

Si valvulopathie		
valvulop	Frequency	Cumulative Frequency
Insuffisance mitrale	37	37
Rétrécissement mitral	3	40
Insuffisance aortique	19	59
Rétrécissement aortique	17	76
Insuffisance tricuspide	5	81
Rétrécissement tricuspide	1	82
Rétrécissement pulmonaire	1	83
autre	1	84
Frequency Missing = 27		

Figure A.1: Frequencies of the type of Valvular Heart Disease in the FCSS.

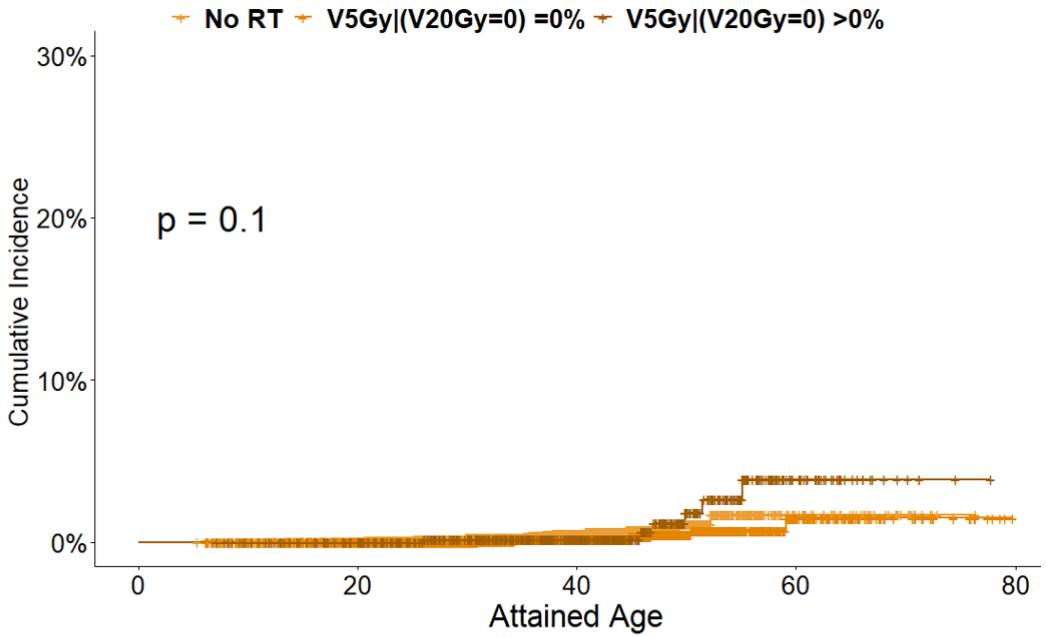

	Attained Age:	20 years old	40 years old	65 years old
No RT	Events	3	14	18
	Survivors at risk	3468	1207	28
$V_{5Gy} \mid_{V20\ Gy=0} = 0\%$	Events	0	3	7
	Survivors at risk	1882	1028	46
$V_{5Gy} \mid_{V20\ Gy=0} > 0\%$	Events	0	1	6
	Survivors at risk	525	327	13

Figure A.2: Cumulative incidence of VHD in the FCCSS cohort (7492 survivors with complete data, 81 of whom developed a VHD) by attained age, stratified on V5|V20=0. The p-value is given for the log-rank test. Abbreviations: RT: Radiotherapy

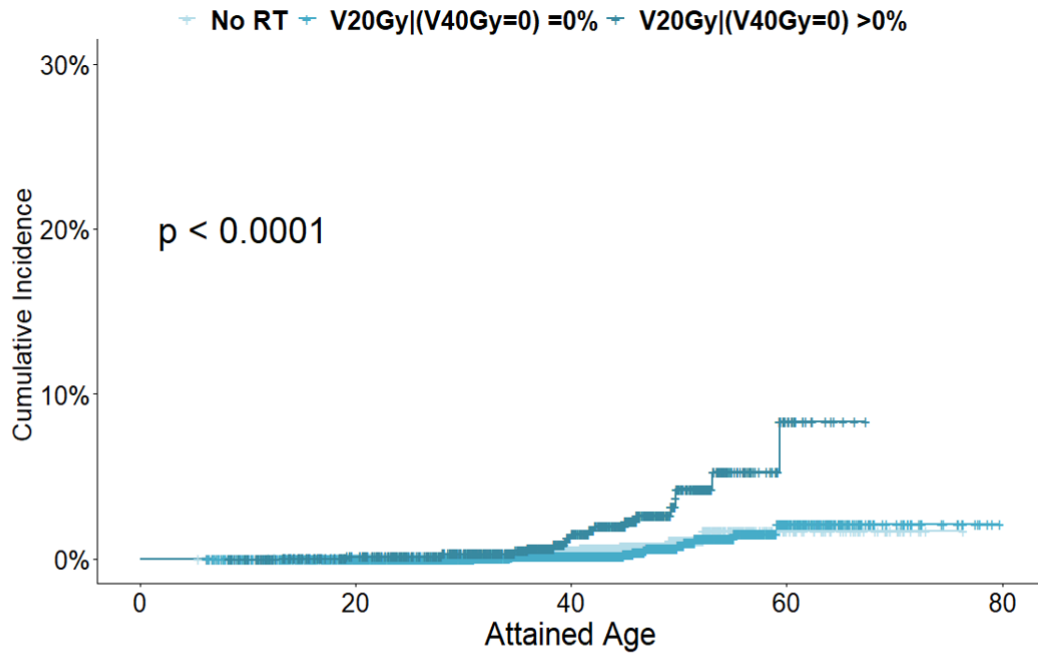

	Attained Age:	20 years old	40 years old	65 years old
No RT	Events	3	14	18
	Survivors at risk	3468	1207	28
$V_{20Gy} \mid_{V40\ Gy=0} = 0\%$	Events	0	4	13
	Survivors at risk	2407	1355	59
$V_{20Gy} \mid_{V40\ Gy=0} > 0\%$	Events	2	9	18
	Survivors at risk	845	453	3

Figure A.3: Cumulative incidence of VHD in the FCCSS cohort (7492 survivors with complete data, 81 of whom developed a VHD) by attained age, stratified on V20|V40=0. The p-value is given for the log-rank test. Abbreviations: RT: Radiotherapy

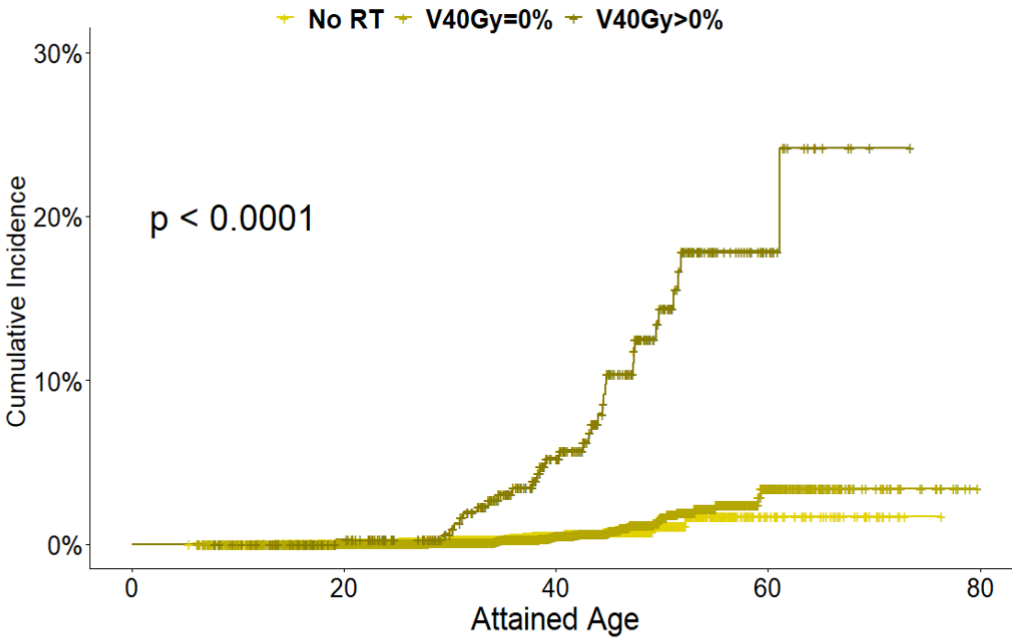

	Attained Age:	20 years old	40 years old	65 years old
No RT	Events	3	14	18
	Survivors at risk	3468	1207	28
$V_{40Gy} = 0\%$	Events	2	13	31
	Survivors at risk	3252	1808	62
$V_{40Gy} > 0\%$	Events	1	14	32
	Survivors at risk	341	201	5

Figure A.4: Cumulative incidence of VHD in the FCCSS cohort (7492 survivors with complete data, 81 of whom developed a VHD) by attained age, stratified on V40. The p-value is given for the log-rank test. Abbreviations: RT: Radiotherapy

Table A.1: Incidence of a first VHD in the FCCSS following heart radiation dose according to MHD as well as classic and bounded heart DVH parameters.

Factors	Incidence at Age 40 [95% CI]	Incidence at Age 65 [95% CI]
RT	0.01 [0.006-0.014]	0.057 [0.035-0.077]
No RT	0.006 [0.003-0.009]	0.017 [0.003-0.031]
MHD – in Gy (categorized)		
[0, 5]	0.002 [0-0.004]	0.013 [0.001-0.026]
(5, 15]	0.005 [0-0.013]	0.046 [0.001-0.088]
>15 Gy	0.040 [0.023-0.056]	0.258 [0.084-0.399]
Classic heart DVH parameters:		
V0.01Gy		
0%	0 [0-0]	0.011 [0-0.031]
>0%	0.011 [0.007-0.015]	0.053 [0.035-0.071]
V5Gy		
0%	0.002 [0-0.005]	0.015 [0-0.031]
>0%	0.019 [0.011-0.026]	0.086 [0.056-0.116]
V20Gy		
0%	0.002 [0-0.004]	0.021 [0.006-0.036]
>0%	0.026 [0.015-0.037]	0.111 [0.067-0.153]
Bounded heart DVH parameters:		
V0.01Gy|V5Gy =0		
0%	0 [0-0]	0.011 [0-0.031]
>0%	0.011 [0.007-0.015]	0.061 [0.037-0.084]
V5Gy|V20Gy =0		
0%	0.002 [0-0.005]	0.015 [0-0.031]
>0%	0.002 [0-0.006]	0.039 [0.004-0.072]
V20Gy|V40Gy=0		
0%	0.002 [0-0.004]	0.021 [0.006-0.036]
>0%	0.015 [0.005-0.025]	0.083 [0.015-0.147]
V40Gy		
0%	0.006 [0.002-0.009]	0.034 [0.017-0.051]
>0%	0.052 [0.025-0.079]	0.242 [0.097-0.364]

Abbreviations: French Childhood Cancer Survivors Study (FCCSS); Valvular Heart Disease (VHD); reference (ref.); Mean Heart Dose (MHD); Hazard Ratio (HR); 95% confidence intervals (95% CI); Proportional Hazard's assumption was verified for all models

Table A.2: Models comparison based on different types of variables that take into account radiation exposure.

Factors	HR [95%CI]	AIC	C-index
MHD	1.09 [1.08-1.11]	**1140.02**	0.741
Heart DVH parameters			
$V_{0.1Gy}$	2.69 [1.53-4.41]	1251.87	0.64
V_{5Gy}	12.14 [7.23-20.38]	1171.19	0.741
V_{20Gy}	21.81 [12.99-36.64]	1152.64	**0.755**
V_{40Gy}	65.41 [29.61-144.46]	1210.8	0.712

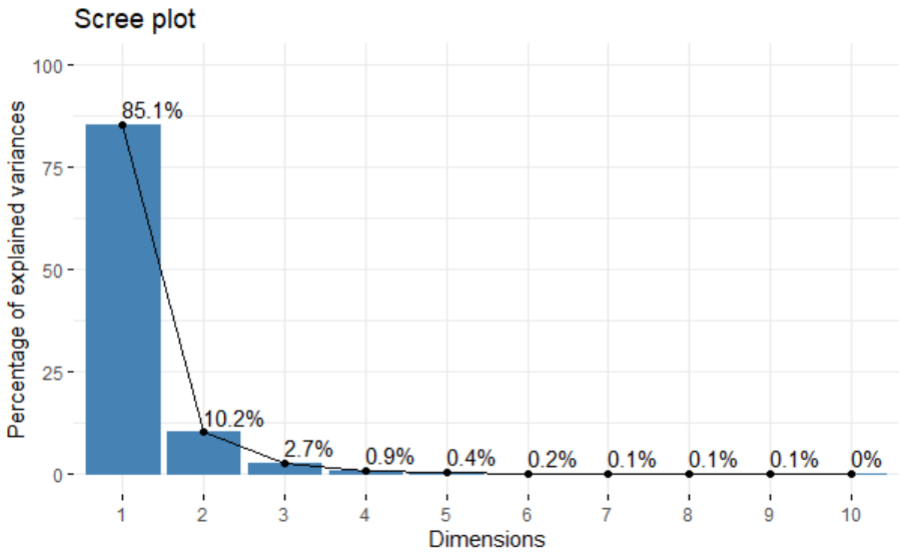

Figure A.5: Example of the scree plot calculated for the PCA on dose-indicators. We chose to calculate the two first components, that explained 85.1 + 10.2 = 95.3 % of the total variance.

DVH parameters	PCA on **Dose** indicators (2 PCs retained)		PCA on **Volume** indicators (2 PCs retained)		PCA on the **complete model** (3 PCs retained)		
Dose indicators							
$D_{01\%}$	0.42	0.426			0.42	0.426	0.352
$D_{05\%}$	0.397	0.332			0.396	0.332	0.177
$D_{10\%}$	0.378	0.232			0.378	0.232	0.016
$D_{20\%}$	0.345	0.059			0.345	0.059	-0.226
$D_{30\%}$	0.318	-0.07			0.317	-0.07	-0.338
$D_{40\%}$	0.291	-0.172			0.291	-0.172	-0.35
$D_{50\%}$ (Median dose to the heart)	0.265	-0.252			0.265	-0.252	-0.286
$D_{60\%}$	0.233	-0.324			0.233	-0.324	-0.122
$D_{70\%}$	0.197	-0.365			0.197	-0.365	0.092
$D_{80\%}$	0.159	-0.355			0.159	-0.355	0.269
$D_{90\%}$	0.12	-0.295			0.12	-0.295	0.362
$D_{95\%}$	0.099	-0.25			0.099	-0.25	0.37
$D_{99\%}$	0.078	-0.2			0.078	-0.2	0.334
Volume indicators							
$V_{\geq 0.1Gy}$			0.442	0.669	0.009	0.009	0.014
$V_{\geq 0.5Gy}$			0.46	0.244	0.011	0.01	0.015
$V_{\geq 1Gy}$			0.436	0.007	0.011	0.008	0.014
$V_{\geq 2Gy}$			0.383	-0.203	0.011	0.004	0.009
$V_{\geq 5Gy}$			0.312	-0.328	0.01	-0.002	0.001
$V_{\geq 10Gy}$			0.26	-0.333	0.009	-0.006	0
$V_{\geq 15Gy}$			0.223	-0.321	0.008	-0.007	-0.001
$V_{\geq 20Gy}$			0.158	-0.262	0.006	-0.005	-0.003
$V_{\geq 25Gy}$			0.102	-0.189	0.004	-0.004	-0.003
$V_{\geq 30Gy}$			0.075	-0.152	0.003	-0.004	-0.002
$V_{\geq 40Gy}$			0.024	-0.05	0.001	-0.001	-0.001

Figure A.6: Coefficients derived from PCA, used for the linear combinations.

Model	Factors	Penalized coefficient	Hazard Ratio [95% confidence interval] (Cox adjustment)	P-value (Cox adjustment)
LASSO (alpha= 1)				
Dose indicators (lambda= 0.0117)	$D_{60\%}$	1.02	1.02 [0.93-1.11]	0.722
	$D_{70\%}$	1.05	1.05 [0.95-1.15]	0.367
Volume indicators (lambda= 0.0112)	$V_{\geq 25}$	3.14	3.14 [0.15-64.39]	0.457
	$V_{\geq 30}$	4.32	4.32 [0.17-107.83]	0.373
Complete Model (lambda<0.0001)	$D_{60\%}$	1.01	1.01 [0.92-1.1]	0.907
	$D_{70\%}$	1.03	1.03 [0.94-1.13]	0.524
	$V_{\geq 25}$	1.01	1.11 [0.04-33.08]	0.953
	$V_{\geq 30}$	3.23	3.23 [0.12-83.8]	0.481
Ridge (alpha= 0)				
Dose indicators (lambda= 0.2822)	$D_{01\%}$	1	1 [0.91-1.11]	0.968
	$D_{05\%}$	1	1 [0.82-1.23]	0.981
	$D_{10\%}$	1	1 [0.81-1.24]	0.979
	$D_{20\%}$	1	1 [0.79-1.27]	0.977
	$D_{30\%}$	1	1 [0.77-1.32]	0.976
	$D_{40\%}$	1	1 [0.79-1.27]	0.969
	$D_{50\%}$	1.01	1.01 [0.81-1.24]	0.961
	$D_{60\%}$	1.01	1.01 [0.84-1.2]	0.947
	$D_{70\%}$	1.01	1.01 [0.85-1.2]	0.937
	$D_{80\%}$	1.01	1.01 [0.86-1.18]	0.932
	$D_{90\%}$	1.01	1.01 [0.86-1.18]	0.937
	$D_{95\%}$	1.01	1.01 [0.84-1.2]	0.952
	$D_{99\%}$	1.01	1.01 [0.89-1.14]	0.92
	Chemotherapy	1.03	1.03 [0.62-1.71]	0.918
Volume indicators (lambda= 0.2055)	$V_{\geq 0.1Gy}$	1.02	1.02 [0.41-2.52]	0.971
	$V_{\geq 0.5Gy}$	1.04	1.04 [0.14-7.78]	0.967
	$V_{\geq 1Gy}$	1.06	1.06 [0.06-18.57]	0.968
	$V_{\geq 2Gy}$	1.08	1.09 [0.05-21.87]	0.954
	$V_{\geq 5Gy}$	1.13	1.15 [0.04-34.38]	0.937
	$V_{\geq 10Gy}$	1.16	1.18 [0.02-62.5]	0.934
	$V_{\geq 15Gy}$	1.19	1.2 [0.05-29.89]	0.909
	$V_{\geq 20Gy}$	1.29	1.33 [0.1-18.14]	0.832
	$V_{\geq 25Gy}$	1.48	1.54 [0.03-84.45]	0.833
	$V_{\geq 30Gy}$	1.62	1.7 [0.06-52.21]	0.762
	$V_{\geq 40Gy}$	2.04	2.17 [0.31-15.12]	0.434
	Chemotherapy	1.03	1.04 [0.63-1.72]	0.885
Complete Model (lambda= 0.4327)	$D_{01\%}$	1	1 [0.91-1.11]	0.981
	$D_{05\%}$	1	1 [0.82-1.23]	0.988
	$D_{10\%}$	1	1 [0.81-1.24]	0.987
	$D_{20\%}$	1	1 [0.79-1.27]	0.986
	$D_{30\%}$	1	1 [0.77-1.31]	0.985
	$D_{40\%}$	1	1 [0.8-1.26]	0.98
	$D_{50\%}$	1	1 [0.82-1.23]	0.975
	$D_{60\%}$	1	1 [0.84-1.2]	0.966
	$D_{70\%}$	1	1 [0.85-1.19]	0.959
	$D_{80\%}$	1	1 [0.86-1.17]	0.957
	$D_{90\%}$	1	1 [0.86-1.18]	0.96
	$D_{95\%}$	1	1 [0.84-1.2]	0.969
	$D_{99\%}$	1	1 [0.89-1.13]	0.949
	$V_{\geq 0.1Gy}$	1.01	1.01 [0.4-2.55]	0.989
	$V_{\geq 0.5Gy}$	1.02	1.02 [0.13-8.03]	0.987
	$V_{\geq 1Gy}$	1.02	1.02 [0.05-19.48]	0.987
	$V_{\geq 2Gy}$	1.04	1.04 [0.04-24.66]	0.982
	$V_{\geq 5Gy}$	1.06	1.06 [0.03-41.58]	0.975
	$V_{\geq 10Gy}$	1.07	1.07 [0.02-62.18]	0.973
	$V_{\geq 15Gy}$	1.08	1.08 [0.04-29.18]	0.963
	$V_{\geq 20Gy}$	1.12	1.13 [0.08-15.13]	0.927
	$V_{\geq 25Gy}$	1.2	1.21 [0.02-63.54]	0.925
	$V_{\geq 30Gy}$	1.25	1.26 [0.03-59.62]	0.905
	$V_{\geq 40Gy}$	1.4	1.42 [0.08-26.83]	0.815
	Chemotherapy	1.02	1.02 [0.61-1.7]	0.946
Elastic Net (alpha= 0.5)				
Dose indicators (lambda= 0.0233)	D40	1.01	1.01 [0.87-1.17]	0.968
	med	1.01	1.01 [0.8-1.27]	0.981
	D60	1.02	1.02 [0.84-1.22]	0.979
	D70	1.02	1.02 [0.92-1.13]	0.977
Volume indicators (lambda=0.0205)	$V_{\geq 20Gy}$	1.32	1.32 [0.15-11.59]	0.803
	$V_{\geq 25Gy}$	2.66	2.66 [0.03-230.58]	0.667
	$V_{\geq 30Gy}$	3.51	3.51 [0.11-112.21]	0.477
	$V_{\geq 40Gy}$	1.02	1.02 [0.17-6.17]	0.985
Complete Model (lambda=0.0225)	$D_{40\%}$	1	1 [0.87-1.16]	0.988
	$D_{50\%}$	1	1 [0.8-1.25]	0.972
	$D_{60\%}$	1.01	1.01 [0.85-1.21]	0.908
	$D_{70\%}$	1.01	1.01 [0.92-1.12]	0.773
	$V_{\geq 25Gy}$	1.64	1.67 [0.06-48.91]	0.767
	$V_{\geq 30Gy}$	2.19	2.16 [0.09-49.71]	0.631

Figure A.7: Coefficients derived from the penalized regressions.

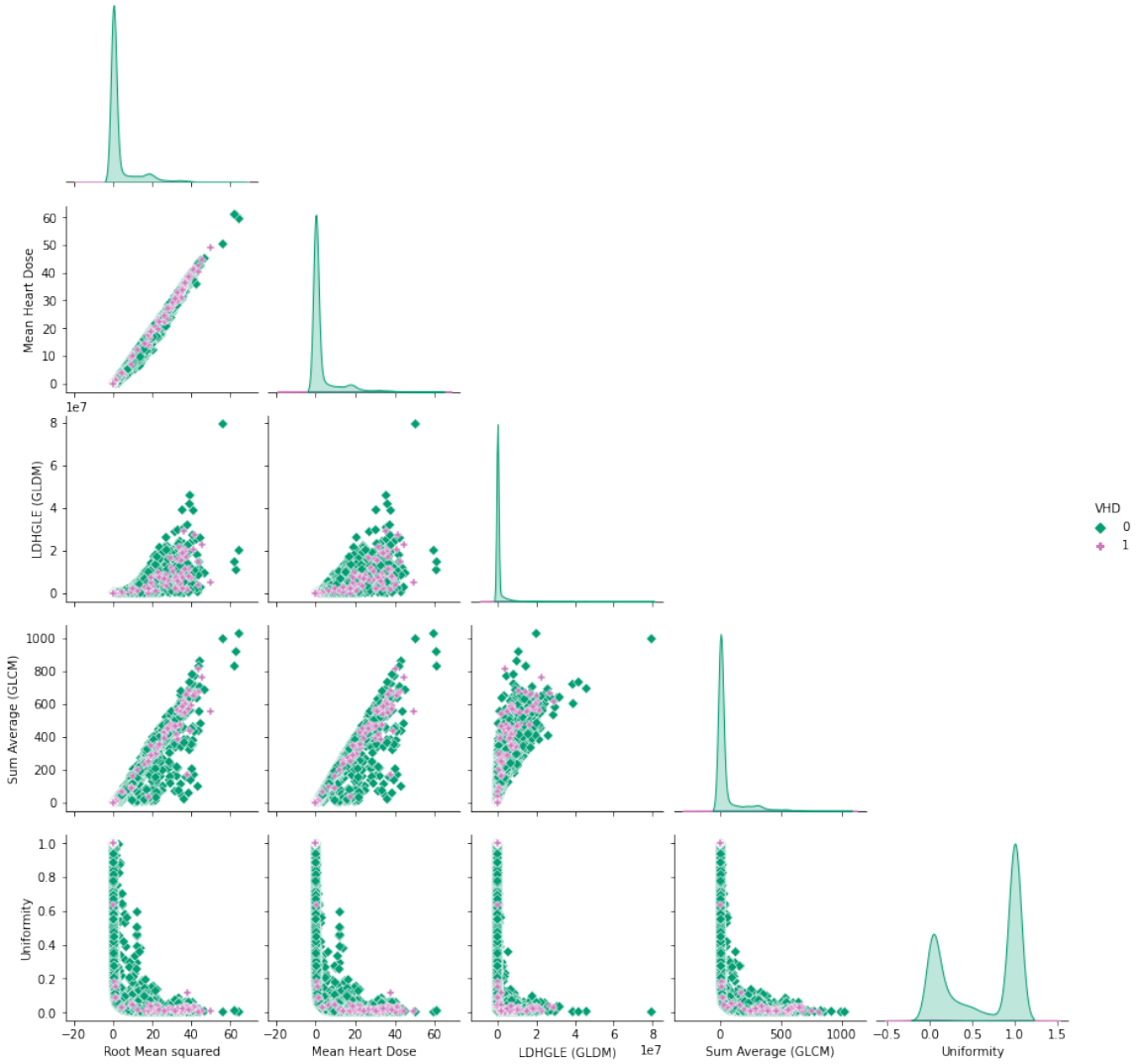

Figure A.8: Pairplots illustrating the repartition bt VHD status of some features the stand out both in the FCCSS and in PanCare.

B - Appendix B

Elbow Method	
k = nombre optimal de clusters	nombre de patients (%)
$k = 5$	393 (10%)
$k = 6$	3202 (84%)
$k = 7$	198 (6%)

Table 3: Elbow Method : K-means

Score de calinski

N_clust	$k = 2$	$k = 3$	$k = 4$	$k = 6$
score	$[min - mean - max]$	$[min - mean - max]$	$[min - mean - max]$	$[min - mean - max]$
kmeans	$[2793 - 21477 - 88103]$	$[2614 - 20770 - 87680]$	$[2456 - 19660 - 78380]$	$[2360 - 17839 - 70307]$
agglo	$[2270 - 16663 - 74079]$	$[1979 - 15841 - 66057]$	$[1935 - 15113 - 61350]$	$[1785 - 13630 - 53523]$
p-value	$< 2.2 \times 10^{-16}$	$< 2.2 \times 10^{-16}$	$< 2.2 \times 10^{-16}$	$< 2.2 \times 10^{-16}$
Le % en faveur d'un algorithme aprés comparaison des score de chaque patient sur les 2000				
kmeans	100%	100%	100%	100%
agglo	0%	0%	0%	0%

Table 1: Score de Calinski Kmeans vs Agglomerative

Score de Silhouette

nb_clust	$k = 2$	$k = 3$	$k = 4$	$k = 6$
score	$[min - mean - max]$	$[min - mean - max]$	$[min - mean - max]$	$[min - mean - max]$
kmeans	$[0.245 - 0.308 - 0.431]$	$[0.237 - 0.294 - 0.472]$	$[0.235 - 0.277 - 0.379]$	$[0.225 - 0.268 - 0.328]$
agglo	$[0.189 - 0.265 - 0.429]$	$[0.159 - 0.233 - 0.472]$	$[0.149 - 0.213 - 0.361]$	$[0.142 - 0.192 - 0.289]$
p-value	$< 2.2 \times 10^{-16}$	$< 2.2 \times 10^{-16}$	$< 2.2 \times 10^{-16}$	$< 2.2 \times 10^{-16}$
Le % en faveur d'un algorithme aprés comparaison des score de chaque patient sur les 2000				
kmeans	98.3%	100%	99.85%	100%
agglo	1.7%	0%	0.15%	0%

Table 2: Score de silhouette K-means vs Agglomerative

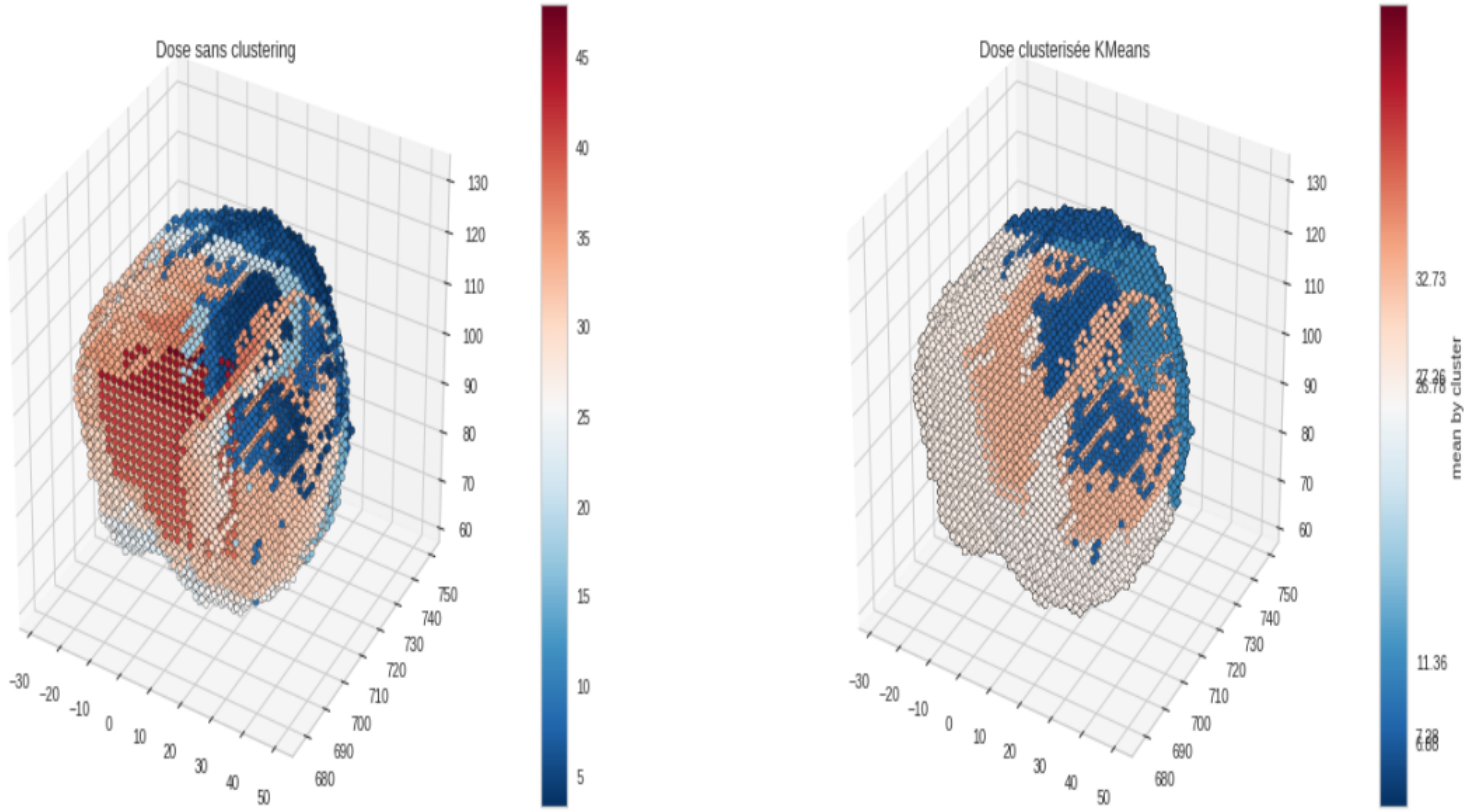

Figure 5: Représentation de la dose au cœur du patient, complète et clusterisée (échelle en Gy)

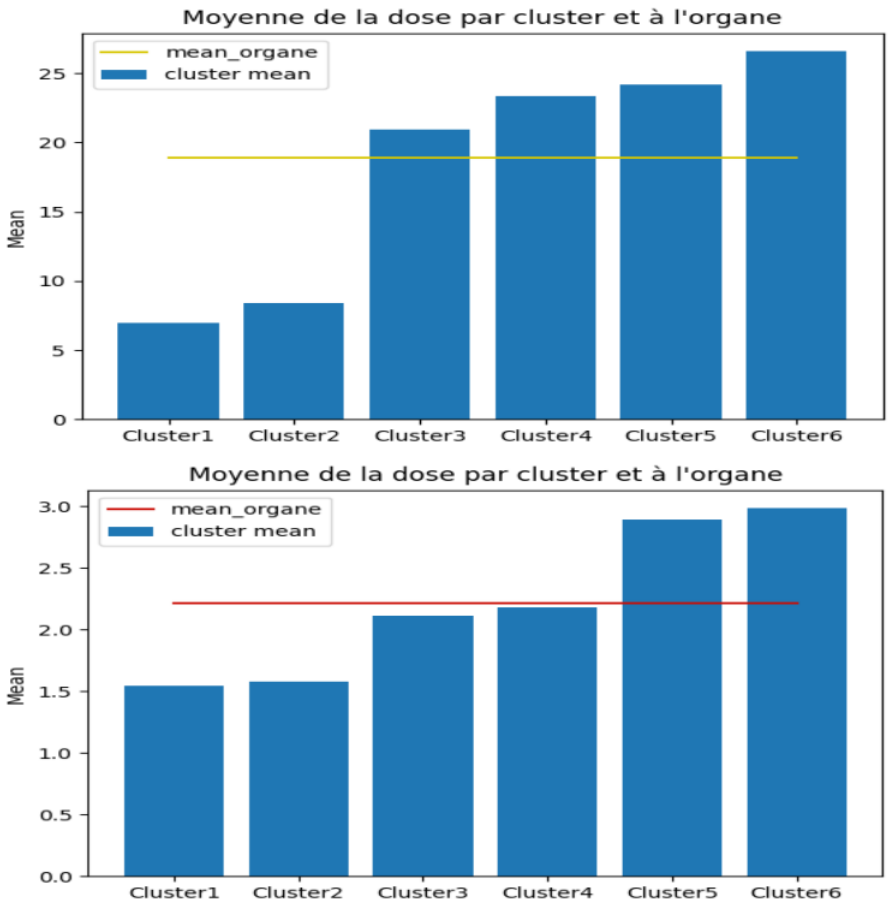

Figure B.1: Juxtaposition of the mean heart dose versus the mean dose to each cluster; example for two survivors of the FCCSS.

	min-mean		
	dose minimum		dose moyenne
	$[min - max]$	médian	
cluster 1	$[0.0 - 38.24]$	0.35	3.95
cluster 2	$[0.0 - 38.25]$	0.39	5.02
cluster 3	$[0.0 - 48.31]$	0.46	6.19
cluster 4	$[0.0 - 64.91]$	0.58	7.24
cluster 5	$[0.0 - 65.91]$	0.77	8.63
cluster 6	$[0.0 - 71.31]$	0.99	10.05

Table 4: Doses minimum et la dose moyenne de tous les patients par cluster

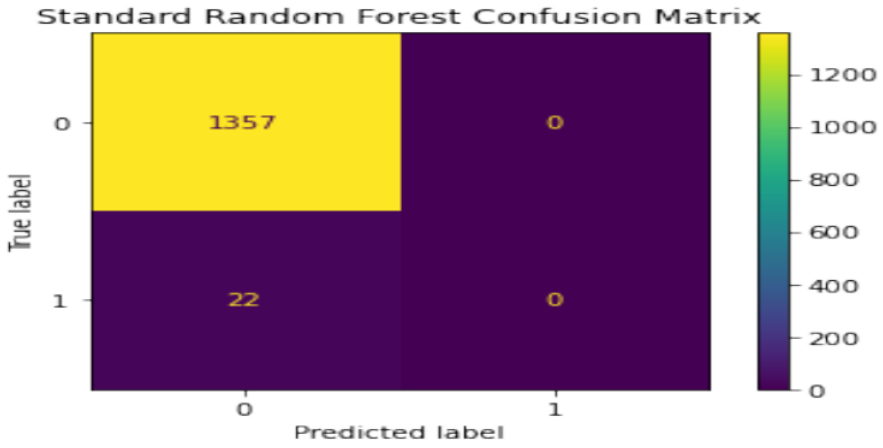

Figure 13: Matrice de confusion du RandomForest standard

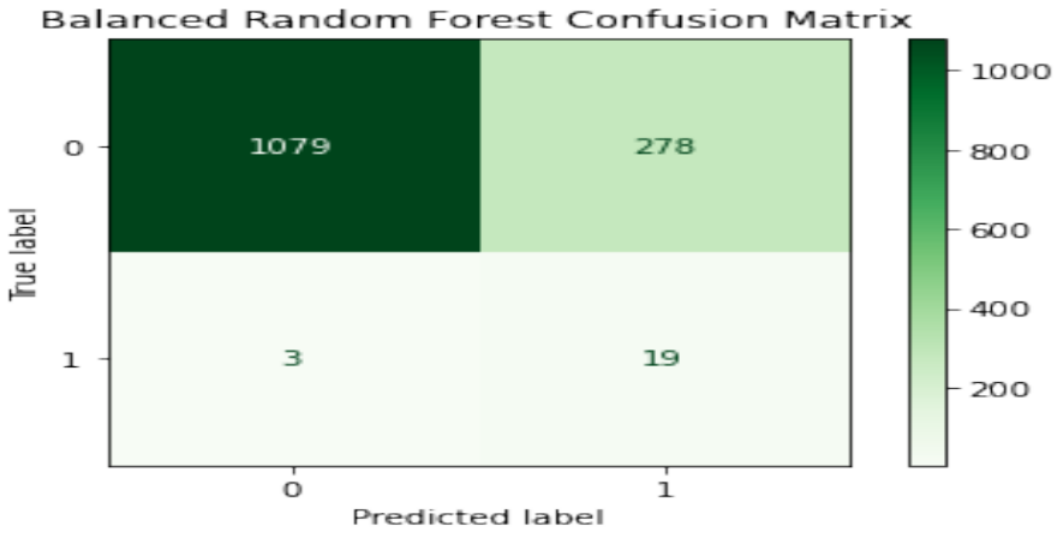

Figure 14: Matrice de confusion du BalancedRandomForest

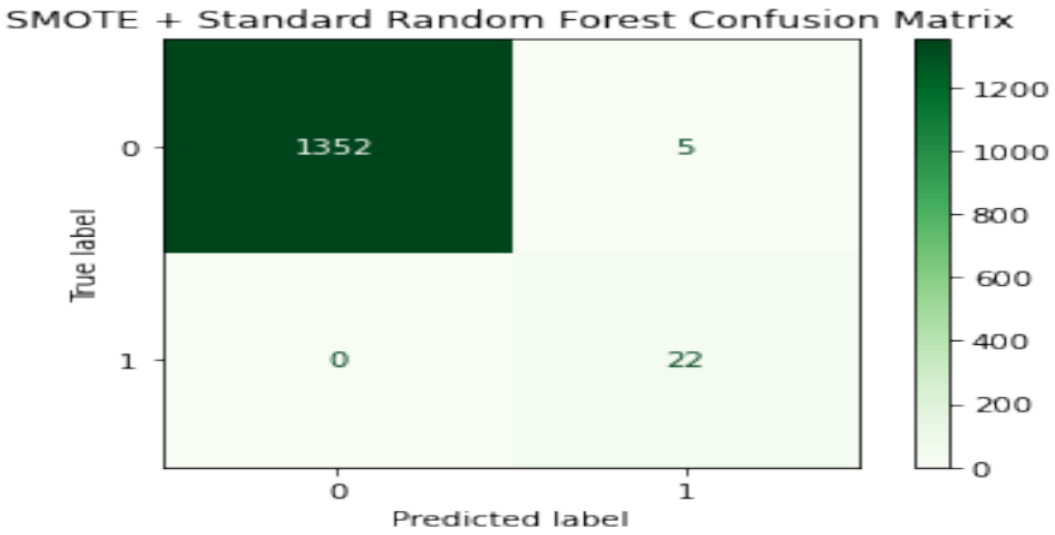

Figure 15: Matrice de confusion de RandomForest+SMOTE

C - Appendix C (publications)

Two papers are attached:

- **Published Paper - The Green Journal | Radiotherapy and Oncology**

  Chounta S, Lemler S, Haddy N, Fresneau B, Mansouri I, Bentriou M, Demoor-Goldschmidt C, Diallo I, Souchard V, Do TD, Veres C, Surun A, Doz F, Llanas D, Vu-Bezin G, Rubino C, de Vathaire F, Letort V, Allodji RS.

  The risk of valvular heart disease in the French Childhood Cancer Survivors' Study: contribution of dose-volume histogram parameters

  DOI: 10.1016/j.radonc.2023.109479

  PMID: 36657724

- **Published Paper - Cancers (Basel)**

  Chounta S, Allodji RS, Vakalopoulou M, Bentriou M, Thi Do D, De Vathaire F, Diallo I, Fresneau B, Charrier T, Zossou V, Christodoulidis S, Lemler S, Letort Le Chevalier V.

  Dosiomics-based prediction algorithms of radiation-induced valvulopathy (application on data from childhood cancer survivors in France)

  DOI: 10.3390/cancers15123107

  PMID: 37370717

Radiotherapy and Oncology 180 (2023) 109479

Contents lists available at ScienceDirect

Radiotherapy and Oncology

journal homepage: www.thegreenjournal.com

Original Article

The risk of valvular heart disease in the French Childhood Cancer Survivors' Study: Contribution of dose-volume histogram parameters

Stefania Chounta [a,b,c,d], Sarah Lemler [d], Nadia Haddy [a,b,c], Brice Fresneau [e], Imene Mansouri [a,b,c,f,g], Mahmoud Bentriou [d], Charlotte Demoor-Goldschmidt [a,b,c,h], Ibrahima Diallo [i,j], Vincent Souchard [a,b,c], Thi-Duyen Do [a,b,c], Cristina Veres [i,j], Aurore Surun [k], François Doz [k,l], Damien Llanas [a,b,c], Giao Vu-Bezin [a,b,c], Carole Rubino [a,b,c], Florent de Vathaire [a,b,c], Véronique Letort [d], Rodrigue Setcheou Allodji [a,b,c,m,*]

[a] Université Paris-Saclay, Univ. Paris-Sud, UVSQ; [b] INSERM, CESP, Cancer and Radiation Team; [c] Gustave Roussy, Department of Clinical Research, Cancer and Radiation Team, F-94805 Villejuif; [d] Université Paris-Saclay, CentraleSupélec, Mathématiques et Informatique pour la Complexité et les Systèmes, 91190, Gif-sur-Yvette; [e] Gustave Roussy, Université Paris-Saclay, Department of Pediatric oncology, Villejuif, F-94805; [f] EPI-PHARE Scientific Interest Group; [g] French National Agency for the Safety of Medicines and Health Products (ANSM), Saint-Denis; [h] Chu de Nantes, Pediatric Oncology, 38 Bd Jean Monnet, Nantes 44093; [i] Department of Radiation Oncology, Gustave Roussy; [j] Gustave Roussy, Inserm, Radiothérapie Moléculaire et Innovation Thérapeutique, Paris-Saclay University, Villejuif, Île-de-France; [k] SIREDO Oncology Center (Care, Innovation, Research for Children, Adolescents and Young Adults with Cancer), Institut Curie; [l] Université Paris Cité, Paris, France; [m] Polytechnic School of Abomey-Calavi (EPAC), University of Abomey-Calavi, 01 P.O. Box 2009, Cotonou, Benin

ARTICLE INFO

Article history:
Received 25 May 2022
Received in revised form 17 November 2022
Accepted 9 January 2023
Available online 16 January 2023

Keywords:
Valvular heart disease
Valvulopathy
Radiotherapy
Dosimetry
Dose-volume histogram parameters
Childhood cancer

ABSTRACT

Background and purpose: Valvular Heart Disease (VHD) is a known complication of childhood cancer after radiotherapy treatment. However, the dose-volume-effect relationships have not been fully explored.
Materials and methods: We obtained individual heart Dose Volume Histograms (DVH) for survivors of the French Childhood Cancer Survivors Study (FCCSS) who had received radiotherapy. We calculated the Mean Dose to the Heart (MHD) in Gy, as well as the heart DVH parameters ($V_{d\ Gy}$, which represents the percentage of heart volume receiving at least d Gy), fixing the thresholds to 0.1 Gy, 5 Gy, 20 Gy, and 40 Gy. We analyzed them furtherly in the subpopulation of the cohort that was treated with a dose lower than 5 Gy ($V_{0.1Gy}|_{V5Gy=0\%}$), 20 Gy ($V_{5Gy}|_{V20Gy=0\%}$), and 40 Gy ($V_{20Gy}|_{V40Gy=0\%}$), respectively. We investigated their role in the occurrence of a VHD in this population-based observational cohort study using the Cox proportional hazard model, adjusting for age at cancer diagnosis and chemotherapy exposure.
Results: Median follow-up was 30.6 years. Eighty-one patients out of the 7462 (1 %) with complete data experienced a severe VHD (grade $\geq$ 3). The risk of VHD increased along with the MHD, and it was associated with high doses to the heart (V_{40Gy} < 50 %, hazard ratio (HR) = 7.96, 95 % CI: 4.26–14.88 and $V_{20Gy}|_{V40Gy=0\%}$ >50 %, HR = 5.03, 95 % CI: [2.35–10.76]). Doses 5–20 Gy to more than 50 % ($V_{5Gy}|_{V20Gy=0\%}$ >50 %) of the heart induced a marginally non-significant estimated risk. We also observed a remarkable risk increase with attained age.
Conclusions: Our results provide new insight into the VHD risk that may impact current treatments and long-term follow-up of childhood cancer survivors.
© 2023 Elsevier B.V. All rights reserved. Radiotherapy and Oncology 180 (2023) 1–9

Survival rates after childhood cancer have increased over the last several decades in high-income countries [1], thanks to pediatric oncology advances. However, according to a report from the Childhood Cancer Survivor Study (CCSS) cohort, two out of three survivors treated during the end of the last century developed at least one treatment-associated life-threatening disease in adulthood [2–4]. Cancer treatments are an established risk factor for cardiac diseases [5–7]. Heart Failure, Coronary Artery Disease, as well as Valvular Heart Disease (VHD) are frequent cardiac disorders among childhood cancer survivors [8–9] and in the French Childhood Cancer Survivors' Study (FCCSS) in particular [10]. However, to our knowledge, unlike the Heart Failure and Coronary Artery Disease [11–13], the long-term risk of developing a VHD after treatment for childhood cancer has not been comprehensively investigated yet.

While treatment with irradiation has proven to be highly efficient and life-saving, it nevertheless has a significant drawback. Despite recent technological advancements [14], irradiating sur-

Abbreviations: (VHD), Valvular Heart Disease; (DVH), Dose Volume Histograms; (FCCSS), French Childhood Cancer Survivor Study; (MHD), Mean Heart Dose.

* Corresponding author at: Radiation Epidemiology Group / CESP - Unit 1018 INSERM, Gustave Roussy, B2M, 114, rue Édouard Vaillant, 94805 Villejuif Cedex, France.
E-mail address: rodrigue.allodji@gustaveroussy.fr (R.S. Allodji).

https://doi.org/10.1016/j.radonc.2023.109479
0167-8140/© 2023 Elsevier B.V. All rights reserved.

Téléchargé pour Anonymous User (n/a) à Gustave Roussy à partir de ClinicalKey.fr par Elsevier sur février 23, 2023. Pour un usage personnel seulement. Aucune autre utilisation n'est autorisée. Copyright ©2023. Elsevier Inc. Tous droits réservés.

rounding healthy tissues is still difficult to avoid and often leads to late iatrogenic effects. Nowadays, a high Mean Dose to the Heart (MHD) is becoming increasingly exceptional during treatment for childhood cancer, except for a primary mediastinal tumor where these children get a boost up to 30 Gy. However, many patients that did not benefit from modern protocols are still being followed. A previous study has reported evidence of radiotherapy's role in the occurrence of VHD among childhood cancer survivors [15].

The most commonly used independent variable to model the risk of radiation-induced VHD is the MHD [15–16]. However, MHD does not provide insight into the role of spatial heterogeneity of received doses; this issue remains understudied in the literature, mainly due to the lack of adequate voxel-scale data for the whole heart or its substructures. The introduction of realistic virtual human phantoms [17–18], the increasing computational capacities, and the availability of high-resolution computed tomography have contributed to improvements in the individual voxel-scaled retrospective estimation of radiation doses to organs of interest. Dosimetry data for large populations are becoming available for investigation, and cumulative dose-volume histogram (DVH) parameters derived from such data have the potential to shed light on the role of the radiation dose distribution for late side effects.

Therefore, the main objectives of this study were to quantify the risk of a radiation-induced VHD in the FCCSS, evaluate the impact of low-to-moderate doses, and explore the potential existence of lower dose-volume threshold levels.

Methods

Study population and identification and ascertainment of VHD incidents

The FCCSS cohort consists of 7670 5-year survivors treated between 1946 and 2000 for the most common childhood solid cancers, including lymphomas, in five different cancer centers in France before the age of 21. The FCCSS was approved by a regional committee on ethics and the French national agency regulating data protection (Commission Nationale Informatique et Liberté, agreements no. 902,287 and no. 12038829). Informed consent was obtained for patients who could be contacted by postal mail or during long-term clinical follow-up (n = 3312). Finally, we obtained a specific act in law from the French "Conseil d'Etat," the highest court in France (Order 2014–96 of 2014 February 3), that approved the cession of the SNIIRAM data for all patients included in the FCCSS with or without informed consent. All methods were performed following the relevant guidelines and regulations. The present analysis included 7492 5-year survivors (97.7 % of the FCCSS cohort) with complete treatment data (Figure S1).

Information on demographic and clinical characteristics received for the initial childhood cancer occurrence (defined according to the third edition of the International Classification of Childhood Cancer-ICCC-3 [19] is reported in Table 1. Indications for radiotherapy, chemotherapy, or surgery were known from the medical records of all cohort survivors. We obtained the vital status for all patients and causes of death for deceased patients from cépiDC [20] (Center of epidemiology on medical causes of death) coded according to the 9th and 10th versions of the International Classification of Diseases and confirmed by the French Registry of Death [20]. Clinical and epidemiological follow-up was performed to identify the occurrence of iatrogenic effects from self-administered questionnaires and cohort linkage with the French Hospital Database and health insurance information system (SNIIRAM [21]and clinic long-term follow-up for the patients treated in Gustave Roussy.

VHD events were identified, validated, and graded according to the Common Terminology Criteria for Adverse Events (CTCAE version 4.03 [22]. For most survivors that experienced the event (61/81), the identification of a VHD was obtained or validated by the SNIIRAM, where we looked for hospitalizations for episodes of valvular dysfunctions and valve replacements, as well as prescribed treatments for valvular dysfunctions. Additionally, for one part of the cohort, long-term clinical follow-up allowed us to consider examinations that have been registered (e.g., heart echography). The identification was also obtained through long-term epidemiological follow-up via self-administered questionnaires confirmed by medical files.

In this study, we took into account only severe VHD cases (grade ≥ 3), a decision based on the fact that non-severe cardiovascular disease is often self-declared and could cause a reporting bias in the data [23]. Moreover, we censored the incidents that we were unable to confirm. Finally, for patients with VHD among their causes of death, VHD was directly considered grade 5.

Radiation dosimetry and heart dose-volume histogram

Whole-body radiation dose reconstruction data is available for 3906 patients who had received radiotherapy following a methodology that has already been published [24–25]. Of the patients with missing data, only one developed a severe VHD. Dose-volume metrics can be calculated for any organ or anatomical region of interest selected within the three-dimensional voxel phantom. For this study, we considered the doses to the heart and calculated the cumulative DVH to the heart for each patient (Fig. 1). In addition to the MHD, we extracted for each patient the DVH parameters indicating the heart volume that received at least d Gy ($V_{d\ Gy}$), with thresholds set to 0.1 Gy, 5 Gy, 20 Gy, and 40 Gy. To thoroughly evaluate the association of low to moderate radiation doses to the heart with a subsequent VHD, we also analyzed heart DVH parameters with an upper bound of 5 Gy ($V_{0.1Gy}|_{V5Gy=0\%}$), 20 Gy ($V_{5Gy}|_{V20Gy=0\%}$), and 40 Gy ($V_{20Gy}|_{V40Gy=0\%}$), respectively. These are hereafter called *bounded* DVH parameters [12–13].

Chemotherapy

Chemotherapy data is available for most patients. Drug names and administration dates are available for any initial and subsequent therapy for childhood cancer, as well as the total dose per unit of body surface area as milligrams per square meter (mg or g/m^2) of every antineoplastic drug. Antineoplastic drugs are categorized into pharmacological groups according to their known mechanisms of action in the cell: anthracycline, alkylating agents, vinca alkaloids, antimetabolites, other antibiotics/antineoplastic agents, and other cytotoxic drugs (abstracted in Table S1).

Statistical analysis

Both descriptive and association analyses were carried out on the 7492 survivors with complete data (Figure S1). For each patient, we only considered the first incidence of VHD and not if a cardiac event had taken place before the VHD occurrence [15]. We calculated the cumulative incidence in the FCCSS while stratifying on radiotherapy (categorized MHD, $V_{5Gy}|_{V20Gy=0\%}$, $V_{20Gy}|_{V40Gy=0\%}$, V_{40Gy}). The deemed time scale throughout the analyses was the attained age [26], which was calculated as the time between birth and the event for patients that presented a VHD, death for people that passed without presenting a known VHD, and the date of last medical news for the rest of the cohort.

Hazard ratios (HR) and 95 % confidence intervals (95 % CI) [27–28] were estimated according to the Cox proportional hazards model. Ties were calculated with the Breslow method, and we verified the proportional hazards assumption in every model [29]. We

Téléchargé pour Anonymous User (n/a) à Gustave Roussy à partir de ClinicalKey.fr par Elsevier sur février 23, 2023. Pour un usage personnel seulement. Aucune autre utilisation n'est autorisée. Copyright ©2023. Elsevier Inc. Tous droits réservés.

Table 1
Demographic and treatment features of five-year survivors of the FCCSS and of survivors who developed a subsequent VHD after treatment for a childhood cancer with complete data.

Factors	7492 five-year survivors of the FCCSS No. (%) or median [Range]	81 VHD patients of the FCCSS No. (%) or median [Range]
Biological sex		
Male	3386 (45.2)	37 (45.7)
Female	4106 (54.8)	44 (54.3)
Age at childhood cancer diagnosis		
Median (in years)	*5.3 [0–20.6]*	*7.5 [0.2–18.8]*
≤ 5 years	3615 (48.3)	26 (32.1)
5–10 years	1646 (22)	26 (32.1)
10–15 years	1606 (21.4)	19 (23.5)
> 15 years	625 (8.3)	10 (12.3)
Year of childhood cancer diagnosis		
Median (in years)	*1986 [1946–2000]*	*1976 [1961–2000]*
≤ 1980	2422 (32.3)	55 (67.9)
1981–1989	2422 (32.3)	18 (22.2)
≥ 1990	2648 (35.3)	8 (9.9)
Type of childhood cancer		
Hodgkin Lymphoma	471 (**6.3**)	33 (**40.7**)
Other lymphomas and reticuloendothelial neoplasms	788 (10.5)	9 (11.1)
CNS and miscellaneous intracranial and intraspinal neoplasms	1124 (15)	4 (4.9)
Neuroblastoma and other peripheral nervous cell tumors	1029 (13.7)	8 (9.9)
Soft tissue and other extraosseous sarcomas	846 (11.3)	7 (8.6)
Retinoblastoma	519 (6.9)	1 (1.2)
Renal tumors	1137 (15.2)	7 (8.6)
Hepatic tumors	79 (1.1)	1 (1.2)
Malignant bone tumors	680 (9.1)	5 (6.2)
Germ cell tumors, trophoblastic tumors, and neoplasms of gonads	469 (6.3)	6 (7.4)
Others	350 (4.7)	0
Chemotherapy		
Yes	5664 (75.6)	70 (**86.4**)
No	1828 (24.4)	11 (13.6)
Radiotherapy (RT)		
Yes	3906 (**52.1**)	63 (**77.8**)
No	3586 (**47.9**)	18 (22.2)
Mean Dose to the Heart (MHD)		
Median (in Gy), on those treated with radiotherapy	***1.37** [0–61.2]*	***28.26** [0.004–49.1]*
MHD (categorized) – in Gy		
No RT	3586 (47.9)	18 (22.2)
[0, 1]	1799 (24)	5 (6.2)
(1, 5]	747 (10)	4 (4.9)
(5, 15]	584 (7.8)	6 (7.4)
> 15 Gy	776 (10.4)	48 (59.3)
Combination of treatments		
RT (alone)	871 (11.6)	9 (11.1)
Chemotherapy (alone)	2629 (35.1)	16 (19.8)
Both	3035 (40.5)	54 (**66.7**)
Neither/missing	957 (12.8)	2 (2.5)
Attained age		
Median (in years)	*37.9 [5.4–79.8]*	*39.9 [5.7–61.1]*
≤ 20 years	431 (5.8)	6 (7.4)
20–30 years	1574 (21)	9 (11.1)
30–40 years	2272 (30.3)	26 (32.1)
40–50 years	2121 (28.3)	29 (35.8)
> 50 years	1094 (14.6)	11 (13.6)
Follow up $^{\neq}$		
Median (in years)	*30.6 [3–73.9]*	*31.8 [3–49.5]*
≤ 10 years	365 (4.9)	4 (4.9)
10–20 years	578 (7.7)	8 (9.9)
20–30 years	2664 (35.6)	25 (30.9)
30–40 years	2268 (30.3)	25 (30.9)
> 40 years	1617 (21.6)	19 (23.5)
Deceased	1459 (19.5)	40 (49.4)

Abbreviations: French Childhood Cancer Survivors Study (FCCSS); Valvular Heart Disease (VHD); Mean Heart Dose (MHD);
$^{\neq}$: Follow-up was defined as the difference between the date of the first childhood cancer diagnosis and VHD diagnosis for VHD patients, death or date of last medical news for the rest of the cohort.

initially conducted univariate analyses with demographic or treatment covariates. We studied the radiation-induced risk first in relation to radiotherapy exposure, then the MHD as well as its categorized version (using the MHD distribution quantiles of the cohort as cut-offs: 1 Gy, 5 Gy, and 15 Gy), and lastly, the classic or bounded heart DVH parameters ($V_{0.1Gy}$, V_{5Gy}, V_{20Gy}, and V_{40Gy} or $V_{0.1Gy}|_{V5Gy=0\%}$, $V_{5Gy}|_{V20Gy=0\%}$, and $V_{20Gy}|_{V40Gy=0\%}$). We categorized each of the $V_{d\ Gy}$ parameters mentioned above into the following classes: patients who were not treated with radiotherapy, patients that received less than d Gy to the heart, patients that received d Gy to ≤ 50 % of the heart and patients that received d Gy to > 50 % of the heart. The reference category contained the patients not treated with radiotherapy. In the study of the chemotherapy effect on the occurrence of a VHD, we tested some

Téléchargé pour Anonymous User (n/a) à Gustave Roussy à partir de ClinicalKey.fr par Elsevier sur février 23, 2023. Pour un usage personnel seulement. Aucune autre utilisation n'est autorisée. Copyright ©2023. Elsevier Inc. Tous droits réservés.

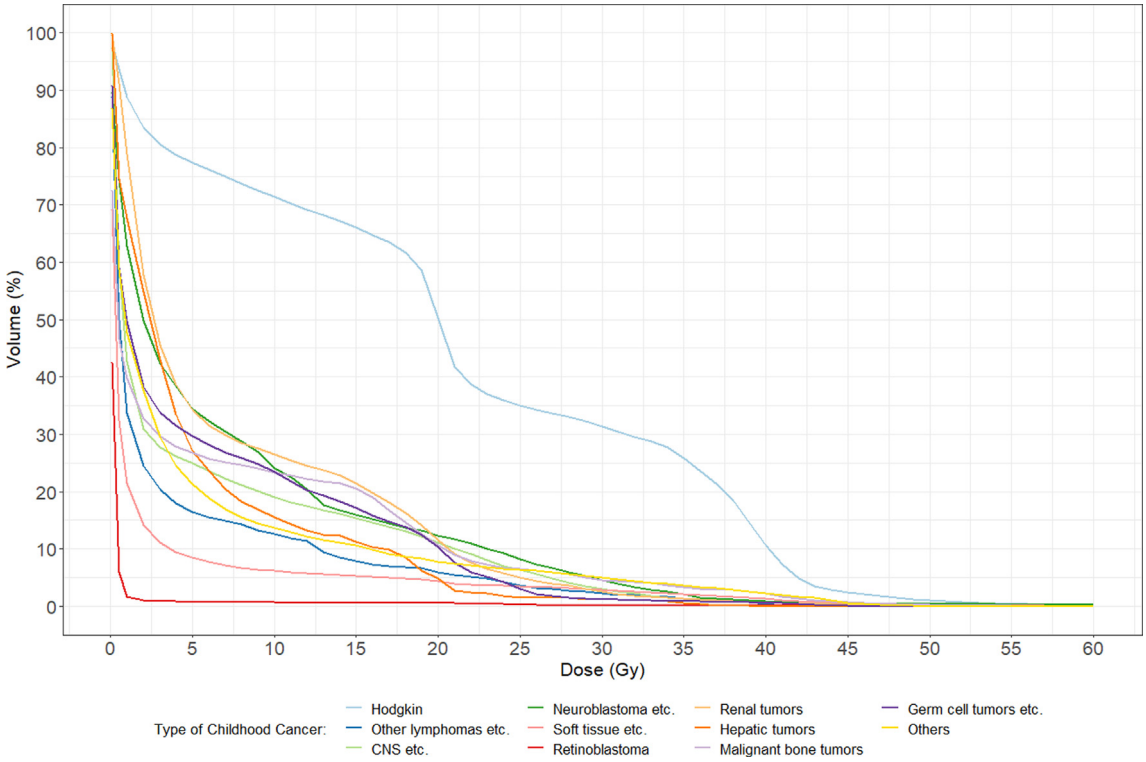

Fig. 1. Cumulative dose-volume histograms (DVH) according to the type of childhood cancer; the average DVH was calculated per group (type of childhood cancer).

alternatives (chemotherapy exposure, and exposure to agents belonging to particular pharmacological groups) but the final multivariable models were adjusted on chemotherapy exposure.

We modeled the dose–effect relationship of the MHD with Poisson regression to investigate the linearity of the dose–response relationship by estimating the Excess of Relative Risk (ERR) [30] per Gy (linear term) and Gy^2 (quadratic term). We compared the linear model to the linear-quadratic and quadratic models to assess a possibly nonlinear behavior of the dose–effect relationship.

We conducted all of the analyses using *R version 4.0.3 (2020–10-10) -- "Bunny-Wunnies Freak Out" Copyright (C) 2020 -- The R Foundation for Statistical Computing.* The Poisson regression was conducted in EPICURE [31]. All P-values were two-sided, and we fixed the significance threshold at 0.05 throughout the analyses.

Results

Among the 7492 5-year childhood cancer survivors of the FCCSS cohort with complete data with a median follow-up of 30.6 years, 81 individuals (1 %) developed a severe VHD after treatment for childhood cancer. Table 1 gathers demographic and treatment information for the entire cohort and the subpopulation that developed a subsequent VHD. We observed an over-representation of Hodgkin survivors among the sub-population of the cohort that developed a VHD (40.7 %), while the same is not true throughout the cohort (6.3 %). Moreover, 86.4 % of the patients who developed a VHD were treated with chemotherapy and 77.8 % with radiotherapy. Most people who experienced a VHD had been treated with both chemotherapy and radiotherapy (66.7 %).

Additionally, the median of the MHD among irradiated people who developed a VHD is 28.26 Gy compared to that of the cohort, which is 1.37 Gy (Wilcoxon's test P-value [32] < 0.0001). Additional comparisons with respect to the type of childhood cancer are abstracted in Table S2. Finally, an elevated median MHD is observed when the irradiation field was the Thorax or the Abdomen, a descriptive abstracted in Table S3 with further information about the distribution of the MHD according to the technique and field of irradiation.

Cumulative incidence at 40 years old was 0.6 % in the non-irradiated sub-population and 4 % among those who received radiotherapy with MHD higher than 15 Gy (Fig. 2, Table S4).. For patients who received 5–20, 20–40, and $\geq$ 40 Gy to the heart, cumulative incidences increase as the dose increases (0.2 %, 1.5 %, and 5.2 % at 40 years old). Cumulative incidence at 65 years old was 1.7 % in the non-irradiated subpopulation and 25.8 % in the irradiated population when MHD > 15 Gy. The cumulative incidences were 3.9 %, 8.3 %, and 24.2 %, respectively, in the subpopulations that received 5–20 Gy (in the absence of any part receiving 20 Gy), 20–40 Gy, and $\geq$ 40 Gy to the heart, (Table S4).

Patients treated with radiotherapy were twice more likely to develop a subsequent VHD (HR = 2, 95 % CI: 1.18–3.41, Table 2). VHD risk was significantly associated with chemotherapy (HR = 2.83, 95 % CI: 1.49–5.39, Table S5) but not with any antineoplastic agents group (hazard ratios after adjustment for MHD and age at diagnosis in Table S6), nor with age at initial childhood cancer diagnosis. The radiation-induced risk estimates hardly changed when we adjusted for chemotherapy or/and age at childhood cancer diagnosis (Table 2).

Patients that received heart-radiation following Hodgkin lymphoma have a high risk of VHD, that increases when adjusted on chemotherapy and age at diagnosis (Table S7). The risk of a subsequent VHD increased by 10 % as the MHD increased by 1 Gy (HR/Gy = 1.10, 95 % CI: 1.08–1.11) and was much higher when MHD was over 15 Gy (HR = 7.63, 95 % CI: 4.39–13.29, adjusted on chemotherapy exposure and age at childhood cancer diagnosis). Interactions between chemotherapy and radiotherapy and the age at childhood cancer diagnosis were tested, and none was observed.

Additional results can be found in Table S8, where hazard ratios are calculated by technique and field of irradiation, adjusted on chemotherapy and the MHD. While the risk of VHD is significant for patients treated with Cobalt or Photon LINAC (HR: 4.58,

Téléchargé pour Anonymous User (n/a) à Gustave Roussy à partir de ClinicalKey.fr par Elsevier sur février 23, 2023. Pour un usage personnel seulement. Aucune autre utilisation n'est autorisée. Copyright ©2023. Elsevier Inc. Tous droits réservés.

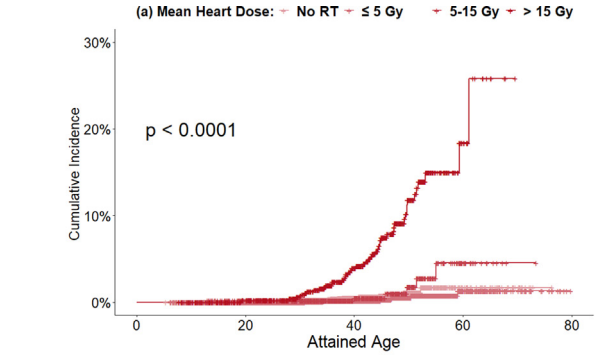

	Attained Age:	20 years old	40 years old	65 years old
No RT	Events	3	14	18
	Survivors at risk	3468	1207	28
MHD ≤ 5Gy	Events	0	4	9
	Survivors at risk	2355	1318	57
5Gy < MHD ≤ 15Gy	Events	1	2	6
	Survivors at risk	532	293	5
MHD > 15 Gy	Events	2	21	48
	Survivors at risk	706	398	5

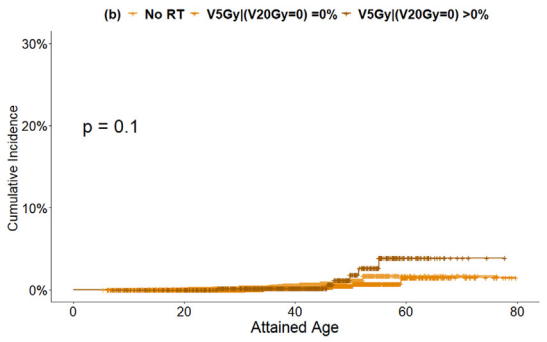

	Attained Age:	20 years old	40 years old	65 years old
No RT	Events	3	14	18
	Survivors at risk	3468	1207	28
V_{5Gy} | $_{V20\,Gy=0}$ = 0%	Events	0	3	7
	Survivors at risk	1882	1028	46
V_{5Gy} | $_{V20\,Gy=0}$ > 0%	Events	0	1	6
	Survivors at risk	525	327	13

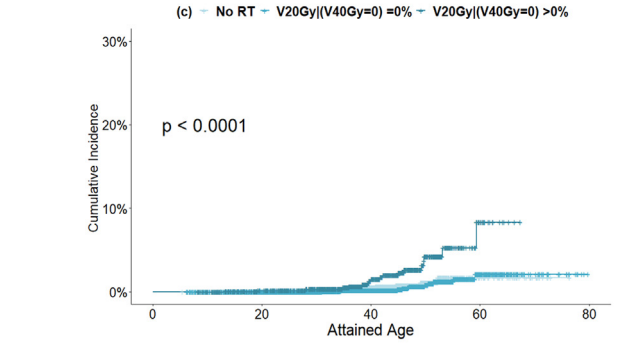

	Attained Age:	20 years old	40 years old	65 years old
No RT	Events	3	14	18
	Survivors at risk	3468	1207	28
V_{20Gy} | $_{V40\,Gy=0}$ = 0%	Events	0	4	13
	Survivors at risk	2407	1355	59
V_{20Gy} | $_{V40\,Gy=0}$ > 0%	Events	2	9	18
	Survivors at risk	845	453	3

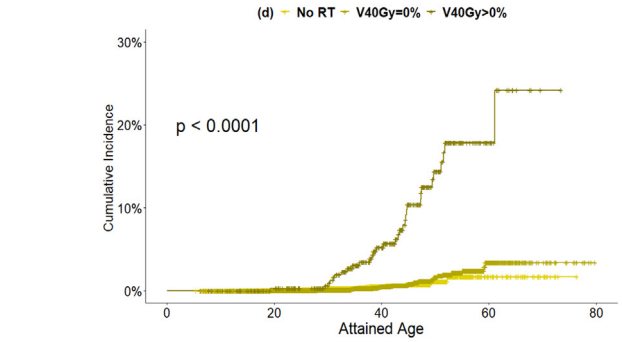

	Attained Age:	20 years old	40 years old	65 years old
No RT	Events	3	14	18
	Survivors at risk	3468	1207	28
V_{40Gy} = 0%	Events	2	13	31
	Survivors at risk	3252	1808	62
V_{40Gy} > 0%	Events	1	14	32
	Survivors at risk	341	201	5

Fig. 2. (a, b, c, d): Cumulative incidence of VHD in the FCCSS cohort (7492 survivors with complete data, 81 of whom developed a VHD) by attained age, stratified on the MHD (a), V5|V20 = 0 (b), V20|V40 = 0 (c) and V40 (d). P-values are given for the log-rank test. Abbreviations: RT: Radiotherapy.

CI95%: [1.39–15.1] and HR: 4.01, CI95%: [1.13–14.2] respectively), the risk is no longer significant when the MHD is included in the model. The same applies to patients treated with thoracic radiotherapy. Finally, as illustrated in Fig. 3, the ERR/GY increased remarkably with attained age: it was 0.04 (95 % CI: 0–0.17) up to 30 years old, 0.94 (95 % CI: 0.47–1.83) up to 40 year old, 2.28 (95 % CI: 1.23–4.23) up to 50 years old and finally 3.12 (95 % CI: 1.31–6.71) after the age of 50 years old. In addition, the ERR increase is described more appropriately by the quadratic model than the linear as summarized in the abstracted Figure S2 and Table S9.

Concerning the heart DVH parameters, we found a 2.19 times higher risk of experiencing the event when the patients have received a dose $\geq$ 0.1 Gy to the heart ($V_{0.1Gy}$ > 50 %) in comparison to patients who had not been treated with radiotherapy (95 % CI: 1.29–3.73, Table 3). However, this risk was no longer present once we eliminated the patients that received > 5 Gy to the heart from the estimates ($V_{0.1Gy}|_{V5Gy=0\%}$). We also observed a risk increase with V_{5Gy} (HR = 5.4, 95 % CI: 3.14–9.29, Table 3) that became non-significant once we eliminated patients that received > 20 Gy to the heart ($V_{5Gy}|_{V20Gy=0\%}$-HR: 2.75, CI95%: [0.92–8.24], Table 3), from the estimates. However, the estimated risk was significant for a different heart-volume threshold (90 % receiving doses between 5 and 20 Gy) (HR = 3.94, CI95%: 1.15–13.49, Fig. 4). Doses over 20 Gy (V_{20Gy} and $V_{20Gy}|_{V40Gy=0\%}$) were associated with an increased VHD risk (HR = 9.74, 95 % CI: 5.57–17.04, and HR = 5.03, 95 % CI: 2.35–10.76, Table 3) when > 50 % of the heart-volume had been irradiated. High doses (V_{40Gy}) to small heart volumes (<50 %) were also associated with an increased VHD risk (HR = 7.96, 95 % CI: 4.26–14.88, Table 3).

Discussion

For many decades, radiotherapy has been one of the principal assets in cancer treatment. As irradiation of healthy tissues cannot be avoided entirely, the occurrence of radiation-induced VHD must be studied in relation to the dose delivered to the heart.

Radiation-induced heart disease ranges widely from early manifestations, such as acute pericarditis, to late effects, like valvular heart disease (VHD). The precise pathophysiological mechanisms of radiation-induced valvulopathy are not altogether understood [33–35]. However, irradiation is thought by radiation biologists to directly affect the calcification of the valvular apparatus in

Téléchargé pour Anonymous User (n/a) à Gustave Roussy à partir de ClinicalKey.fr par Elsevier sur février 23, 2023. Pour un usage personnel seulement. Aucune autre utilisation n´est autorisée. Copyright ©2023. Elsevier Inc. Tous droits réservés.

Table 2
Risk of radiation-induced VHD in the FCCSS adjusted on chemotherapy exposure and age at childhood cancer diagnosis.

Factors	**HR [95 %CI]** univariate	**HR [95 %CI]** Adjusted on chemotherapy	**HR [95 %CI]** Adjusted on chemotherapy and age at childhood cancer diagnosis
Radiotherapy (RT)			
No	(ref.)	(ref.)	(ref.)
Yes	**2.00 [1.18–3.41]**	**1.96 [1.15–3.3]**	**1.97 [1.16–3.36]**
MHD	**1.10 [1.08–1.11]**	**1.09 [1.08–1.11]**	**1.10 [1.08–1.11]**
MHD – in Gy (categorized)			
No RT	(ref.)	(ref.)	(ref.)
[0, 1]	0.35 [0.13–0.95]	0.36 [0.14–0.99]	0.36 [0.13–0.99]
(1, 5]	0.57 [0.19–1.7]	0.54 [0.18–1.61]	0.50 [0.17–1.50]
(5, 15]	1.28 [0.51–3.24]	1.22 [0.48–3.09]	1.14 [0.45–2.90]
> 15 Gy	**7.94 [4.59–13.72]**	**7.36 [4.25–12.76]**	**7.63 [4.39–13.29]**

Abbreviations: French Childhood Cancer Survivors Study (FCCSS); Valvular Heart Disease (VHD); reference (ref.); Mean Heart Dose (MHD); Hazard Ratio (HR); 95% confidence intervals (95% CI);
Proportional Hazard's assumption was verified for all models.

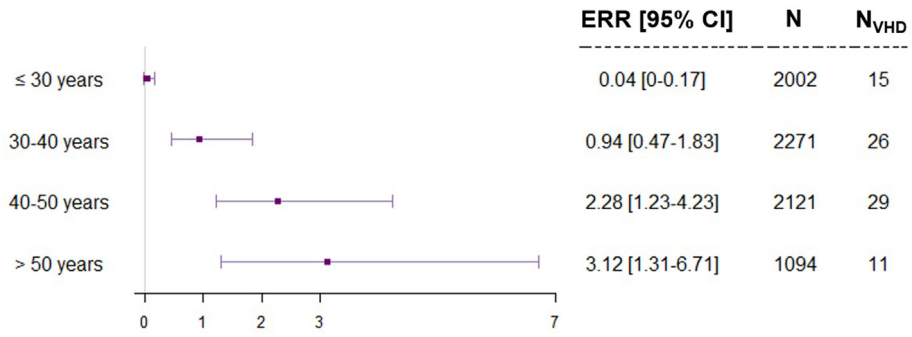

Fig. 3. Excess relative risk of Valvular Heart Disease per Gray (ERR/Gy) in the FCCSS cohort (7492 survivors with complete data, 81 of whom developed a VHD) of radiation to the heart and chemotherapy exposure according to attained age.

patients with breast cancer. In addition, pathologic fibrosis has been observed in lymphoma patients who have been treated with radiotherapy. This difference is likely due to the young age of radiation exposure in lymphoma patients [36]. In the case of a primary mediastinal tumor, when it is impossible to spare parts of the heart or to reduce the dose without modern irradiation techniques like breath gating or deep inspiration breath hold techniques, establishing care with a cardio-oncologist for close cardiac monitoring will help facilitate early detection and allow for timely preventative and therapeutic interventions. A recent study has demonstrated that large volumes irradiated with low doses could increase the rate of any cardiac disease, coronary artery disease and heart failure [12], but not the rate of VHD. Investigating this problem remains crucial; while recent advancements make high MHD increasingly rare nowadays, novel radiotherapy delivery techniques such as IMRT or VMAT may increase the volume that receives low-to-intermediate radiation doses. Our results strongly call for continued efforts to minimize both the heart radiation dose and exposed heart volume to avoid late VHD.

Main findings

We conducted this study on a large, well-defined population of childhood cancer survivors over a long period of treatment time (1946–2000), with longitudinal follow-up and data collected from self-reported questionnaires, hospital-based databases/registries, as well as some clinically assessed data for survivors evaluated in the long-term follow-up clinic at Gustave Roussy. We confirm prior study results that the risk of experiencing late VHD increases with the MHD [15–16] as well as with high doses to the heart [12,37]. Finally, we found that the ERR increases with attained age [38–39].

In addition, our data allow us to calculate DVH parameters and specify the VHD risk induced by low (<5Gy) and low-to-moderate (5–20 Gy) radiation doses. The latter was possible using bounded heart DVH parameters that restrained the heart volume affected by high doses to the heart. We report novel findings with valuable clinical implications to help identify survivors at higher risk for VHD after radiation therapy. Our results suggest that doses < 5 Gy might introduce no risk for VHD; however, we found a substantially elevated risk of VHD associated with either low-to-moderate radiation dose (V5Gy|V20Gy = 0 %) to a large volume of the heart (>90 %). This fruitful conclusion is in line with Bates et al. [12], who also observed an increased relative risk for any cardiac event when half of the heart volume or more received 5–20 Gy (Fig. 4). However, it would remain to be confirmed with larger cohorts. Eventually, the composite nature of the heart could also be considered to deepen the analyses by investigating if the dose effect would be modified depending on which specific substructures are irradiated.

One previous study [15] has examined the relationship between VHD and radiation therapy for Hodgkin lymphoma in a case-control study with 66 severe cases of VHD and 200 control survivors. This study showed a nonlinear relationship, with little or no increase following doses below 30 Gy. For doses over 30 Gy, the hazard ratio estimates increase progressively as the dose to the valves increases. In our study, we observe an elevated risk for an MHD > 15 Gy (Table 2) and an ERR that increases with the MHD. From the metrics in Table S9, the linear-quadratic model seems to outperform the other models slightly. A visual inspection of Figure S2 would favor the quadratic model. Our findings are consistent with those in the study of Cutter et.al [15]. Additionally, no association was observed between the year of diagnosis and the occurrence of a VHD (Univariate analysis, Table S5) which agrees

Téléchargé pour Anonymous User (n/a) à Gustave Roussy à partir de ClinicalKey.fr par Elsevier sur février 23, 2023. Pour un usage personnel seulement. Aucune autre utilisation n'est autorisée. Copyright ©2023. Elsevier Inc. Tous droits réservés.

Table 3
Risk of radiation-induced VHD in the FCCSS calculated by percentage of irradiated heart volume (in four classes), adjusted on chemotherapy; first according to a minimum dose, then by dose interval and by truncating the population affected by a maximum dose.

Heart dose-volume indicators (%)	Whole FCCSS cohort (7492)		Bounded heart dose-volume Indicators (%)	Truncated Population	
	N_{VHD}	HR (95 % CI)		N_{VHD}	HR (95 % CI)
$V_{0.1Gy}$			**$V_{0.1Gy}\|_{V5Gy=0}$**		
No RT	18		No RT	18	(ref.)
< 0.1 Gy	1	0.42 [0.06–3.18]	<0.1 Gy	1	0.45 [0.06–3.38]
]0, 50] *% of ≥ 0.1 Gy*	0	-	]0, 50] *% of ≥ 0.1 to 5 Gy*	0	0 [0-Inf]
> 50 *% of ≥ 0.1 Gy*	62	**2.19 [1.29–3.73]**	> 50 *% of ≥ 0.1 to 5 Gy*	6	0.53 [0.21–1.36]
V_{5Gy}			**$V_{5Gy}\|_{V20Gy=0}$**		
No RT	18	(ref.)	No RT	18	(ref.)
< 5 Gy	7	0.44 [0.18–1.06]	< 5 Gy	7	0.44 [0.18–1.08]
]0, 50] *% of ≥ 5 Gy*	3	0.45 [0.13–1.55]	]0, 50] *% of ≥ 5 to 20 Gy*	2	0.48 [0.11–2.12]
> 50 *% of ≥ 5 Gy*	53	**5.40 [3.14–9.29]**	> 50 *% of ≥ 5 to 20 Gy*	4	**2.75 [0.92–8.24]***
V_{20Gy}			**$V_{20Gy}\|_{V40Gy=0}$**		
No RT	18	(ref.)	No RT	18	(ref.)
< 20 Gy	13	0.61 [0.29–1.24]	< 20 Gy	13	0.6 [0.29–1.24]
]0, 50] *% of ≥ 20 Gy*	7	1.09 [0.45–2.62]	]0, 50] *% of ≥ 20 to 40 Gy*	7	1.28 [0.53–3.08]
> 50 *% of ≥ 20 Gy*	43	**9.74 [5.57–17.04]**	> 50 *% of ≥ 20 to 40 Gy*	11	**5.03 [2.35–10.76]**
V_{40Gy}					
No RT	18	(ref.)			
< 40 Gy	31	1.08 [0.6–1.95]			
]0, 50] *% of ≥ 40 Gy*	23	**7.96 [4.26–14.88]**			
> 50 *% of ≥ 40 Gy*	9	**19.92 [8.91–44.53]**			

Abbreviations: Valvular Heart Disease (VHD); French Childhood Cancer Survivors Study (FCCSS); Hazard Ratio (HR); 95% confidence intervals (95% CI); Radiotherapy (RT); N_{VHD} is the number of events in the class.
Proportional Hazard's assumption was verified for all models; Hazards that were not calculated due to lack of events in the respective class, are noted with a dash.
*becomes significant when the percentage of irradiated heart volume exceeds 90 % (HR = 3.94, CI95%: 1.15–13.49).

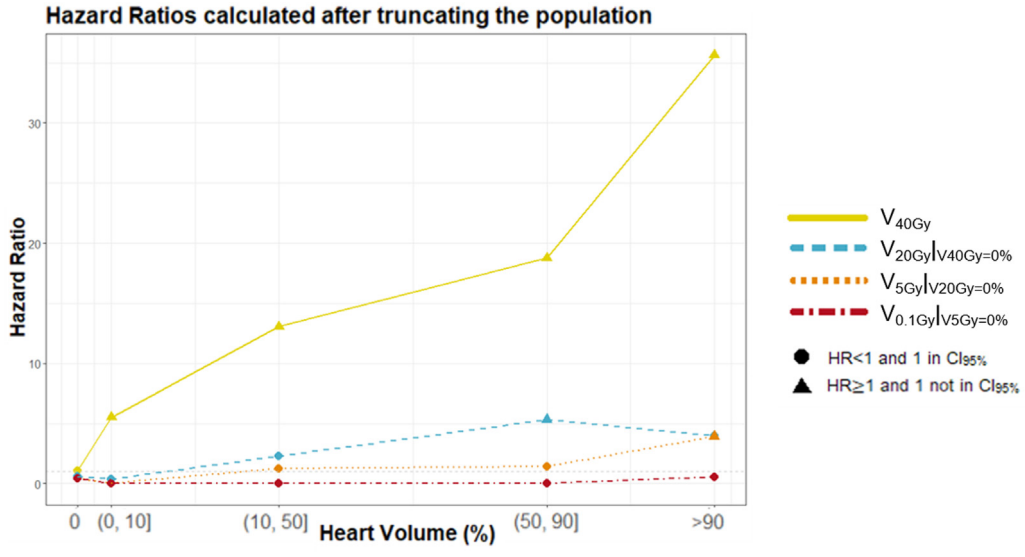

Survivors that experienced a VHD by each sub-category:

V_{40Gy}	49	11	12	8	1
$V_{20Gy}\|_{V40Gy=0}$	31	1	6	11	0
$V_{5Gy}\|_{V20Gy=0}$	25	0	2	1	3
$V_{0.1Gy}\|_{V5Gy=0}$	19	0	0	0	6

Fig. 4. Hazard Ratio evolution along five subparts of irradiated heart volume (with reference group the patients that were not treated with radiotherapy), for four dose-intensity intervals, adjusted on chemotherapy; calculated by truncating the part of the population that received a dose to the heart superior to the respected upper bound.

with Henson et al. (2016) [38], who did not find a significant variation of AER within a decade of diagnosis. In the present analysis, VHD risk was independently associated with chemotherapy but not with anthracyclines or any other particular agent (Table S6). These results are consistent with those of Cutter et al. [15]. In contrast, Mulrooney et al. [40] reported an increased risk of developing VHD following treatment with anthracyclines after childhood cancer. A possible explanation for this apparent inconsistency could be

Téléchargé pour Anonymous User (n/a) à Gustave Roussy à partir de ClinicalKey.fr par Elsevier sur février 23, 2023. Pour un usage personnel seulement. Aucune autre utilisation n'est autorisée. Copyright ©2023. Elsevier Inc. Tous droits réservés.

attributed to a lack of power due to a small number of patients that experienced a late VHD receiving anthracyclines, as we only considered severe cases of VHD. Furthermore, to our knowledge, this association's underlying pathophysiologic mechanism remains poorly understood. Future studies are needed to clarify the sound effect of anthracyclines in valvular dysfunction.

Finally, alternative models are detailed in Table S8, where the risk of a subsequent VHD is estimated according to the technique and field of irradiation. When adjusted on the MHD, the risks are no longer significant. We propose this alternative model (adjusted on chemotherapy) in the case where the MHD is not available but information on the type and field of irradiation is.

Limitations

Some limitations of our study merit discussion, even though they do not call our main conclusions into question.

Due to the long period considered (1946–2000), most patients did not have a CT for planning to allow for individual anatomy-based DVH. Still, instead, a phantom-based reconstruction algorithm was used. This is an established approach but has its known limitation regarding inter-individual anatomic variability. However, this limitation is shared by all retrospective dosimetric studies with a follow-up long enough to address cardiac diseases after RT.

Moreover, the labeling of our data would allow for calculations of metrics to the following sub-structures: myocardium, left and right ventricle, left and right atrium, and the four valves. However, the potential role of the different sub-structures of the heart will be further investigated in our study cohort and the cardiac toxicity studies of the European Pancare consortium [41]. Because of the potential anatomic uncertainties associated with the valves' location, we considered the whole heart in this study.

In addition, whole-body radiation dose reconstruction is not available for 175 out of the 4081 survivors of the FCCSS cohort treated with external irradiation. However, this missing data has little impact because the risk associated with radiation therapy (yes/no) remains unchanged with or without including these survivors. In addition, we were unable to specify the affected valve of each subsequent VHD [15] and study each type of VHD separately due to the fact that data were collected from multiple sources. For the same reason, we were unable to include lifestyle and medical adjustment factors like smoking, obesity, and other cardiovascular factors like hypertension and diabetes, which have been associated with VHD risk after treatment for cancer in previous studies [42–43] conducted on survivors of adult cancer.

Finally, 1 % of our cohort experienced a severe VHD, i.e., of grade ≥ 3. A previous study identified a lower prevalence of grade 3–5 valvular disease (0.1 %) among siblings (that was considered the healthy/control population) compared to survivors (0.5 %) in the Childhood Cancer Survivor Study [44]. Severe VHD increased from 54 to 70 [45] in this cohort, resulting in a VHD frequency close to this of our study.

Conclusions

This study provides new insight concerning the association of low and moderate doses to an extended part of the heart with VHD. The results can potentially impact treatment planning and highlight the need for cardiologic follow-up [46–47] several decades after childhood cancer treatment for survivors with elevated risk for a VHD. Further research is needed to determine the costs and benefits of early cardiovascular screening for these survivors.

Ethics approval and consent to participate

We performed this cohort study after approval from the French Data Protection Authority (CNIL) and the National Institute of Medical Research and Health ethics committee.

Declaration of Competing Interest

The authors declare that they have no known competing financial interests or personal relationships that could have appeared to influence the work reported in this paper.

Acknowledgements

Paul-Henry Cournède, Neige Journy, Isao Kobayashi, Amel Belhout, Françoise Terrier, Amel Boumaraf, Mathilde Sautreuil.

Funding

This work was supported and funded by the Gustave Roussy Foundation (Pediatric Program "Guérir le Cancer de l'Enfant"), the ITMO (Instituts thématiques multiorganismes) Cancer d'Aviesan Program (RadioPrediTool project N° 20CM112-00), the INCa/ARC (Institut national du cancer) foundation (CHART project), the Foundation ARC for Cancer Research (grant no. Pop-HaRC 201401208), the "START" PAIR Research Program (grant no. INCa-Fondation ARC-LNCC 11902), and the "Ligue Nationale Contre le Cancer" association. These funding agencies had no role in the design and conduct of the study, in the collection, management, analysis, and interpretation of the data, or in the preparation, review, and approval of the manuscript.

Appendix A. Supplementary material

Supplementary data to this article can be found online at https://doi.org/10.1016/j.radonc.2023.109479.

References

[1] Cancer Statistics Review, 1975-2015 - Previous Version - SEER Cancer Statistics Review. SEER. Accessed December 16, 2020. https://seer.cancer.gov/archive/csr/1975_2015/index.html.
[2] Landier W, Skinner R, Wallace WH, et al. Surveillance for late effects in childhood cancer survivors. J Clin Oncol 2018;36:2216–22. https://doi.org/10.1200/JCO.2017.77.0180.
[3] Armanious MA, Mohammadi H, Khodor S, Oliver DE, Johnstone PA, Fradley MG. Cardiovascular effects of radiation therapy. Curr Probl Cancer 2018;42:433–42. https://doi.org/10.1016/j.currproblcancer.2018.05.008.
[4] Erdmann F, Frederiksen LE, Bonaventure A, et al. Childhood cancer: Survival, treatment modalities, late effects and improvements over time. Cancer Epidemiol 2021;71:101733. https://doi.org/10.1016/j.canep.2020.101733.
[5] Olsen M, Schmidt M, Lash TL, Sorensen K, Pedersen L, Sorensen HT. Cardiovascular disease risk in childhood cancer survivors. Am J Epidemiol 2014;180:120–3. https://doi.org/10.1093/aje/kwu144.
[6] Hau EM, Caccia JN, Kasteler R, et al. Cardiovascular disease after childhood acute lymphoblastic leukaemia: a cohort study. *Swiss Med Wkly*. Published online March 10, 2019. doi:10.4414/smw.2019.20012.
[7] Leerink JM, de Baat EC, Feijen EAM, et al. Cardiac disease in childhood cancer survivors. JACC CardioOncol 2020;2:363–78. https://doi.org/10.1016/j.jaccao.2020.08.006.
[8] Mulrooney DA, Hyun G, Ness KK, et al. Major cardiac events for adult survivors of childhood cancer diagnosed between 1970 and 1999: report from the Childhood Cancer Survivor Study cohort. *BMJ*. Published online January 15, 2020:l6794. doi:10.1136/bmj.l6794.
[9] Nathan PC, Amir E, Abdel-Qadir H. Cardiac outcomes in survivors of pediatric and adult cancers. Can J Cardiol 2016;32:871–80. https://doi.org/10.1016/j.cjca.2016.02.065.
[10] Haddy N, Diallo S, El-Fayech C, et al. Cardiac diseases following childhood cancer treatment: cohort study. Circulation 2016;133:31–8. https://doi.org/10.1161/CIRCULATIONAHA.115.016686.
[11] Mansouri I, Allodji RS, Hill C, et al. The role of irradiated heart and left ventricular volumes in heart failure occurrence after childhood cancer. Eur J Heart Fail 2019;21:509–18. https://doi.org/10.1002/ejhf.1376.

Téléchargé pour Anonymous User (n/a) à Gustave Roussy à partir de ClinicalKey.fr par Elsevier sur février 23, 2023. Pour un usage personnel seulement. Aucune autre utilisation n'est autorisée. Copyright ©2023. Elsevier Inc. Tous droits réservés.

[12] Bates JE, Howell RM, Liu Q, et al. Therapy-related cardiac risk in childhood cancer survivors: an analysis of the childhood cancer survivor study. J Clin Oncol 2019;37:1090–101. https://doi.org/10.1200/JCO.18.01764.
[13] Shrestha S, Bates JE, Liu Q, et al. Radiation therapy related cardiac disease risk in childhood cancer survivors: updated dosimetry analysis from the childhood cancer survivor study. Radiother Oncol 2021;163:199–208. https://doi.org/10.1016/j.radonc.2021.08.012.
[14] Hoppe BS, Flampouri S, Su Z, et al. Effective dose reduction to cardiac structures using protons compared with 3DCRT and IMRT in mediastinal hodgkin lymphoma. Int J Radiat Oncol 2012;84:449–55. https://doi.org/10.1016/j.ijrobp.2011.12.034.
[15] Cutter DJ, Schaapveld M, Darby SC, et al. Risk for valvular heart disease after treatment for hodgkin lymphoma. JNCI J Natl Cancer Inst 2015;107. https://doi.org/10.1093/jnci/djv008.
[16] Cella L, Oh JH, Deasy JO, et al. Predicting radiation-induced valvular heart damage. Acta Oncol 2015;54:1796–804. https://doi.org/10.3109/0284186X.2015.1016624.
[17] Francois P, Beurtheret C, Dutreix A, De Vathaire F. A mathematical child phantom for the calculation of dose to the organs at risk. Med Phys 1988;15:328–33. https://doi.org/10.1118/1.596226.
[18] Diallo I, Lamon A, Shamsaldin A, Grimaud E, de Vathaire F, Chavaudra J. Estimation of the radiation dose delivered to any point outside the target volume per patient treated with external beam radiotherapy. Radiother Oncol 1996;38:269–71. https://doi.org/10.1016/0167-8140(96)01713-6.
[19] ICCC, Third Edition (ICD-O-3), Main Classification Table - SEER Recodes. SEER. Accessed February 21, 2022. https://seer.cancer.gov/iccc/iccc3.html.
[20] Accueil | CépiDc. Accessed May 16, 2022. https://www.cepidc.inserm.fr/.
[21] Système national d'information inter-régimes de l'Assurance maladie. In: ; 2022. Accessed May 16, 2022. https://www.snds.gouv.fr/SNDS/Open-Data.
[22] Common Terminology Criteria for Adverse Events (CTCAE).
[23] Taylor N, Absolom K, Michel G, et al. Comparison of self-reported late effects with medical records among survivors of childhood cancer. Eur J Cancer 2010;46:1069–78. https://doi.org/10.1016/j.ejca.2010.01.022.
[24] Veres C, Allodji RS, Llanas D, et al. Retrospective reconstructions of active bone marrow dose-volume histograms. Int J Radiat Oncol 2014;90:1216–24. https://doi.org/10.1016/j.ijrobp.2014.08.335.
[25] Vũ Bezin J, Allodji RS, Mège JP, et al. A review of uncertainties in radiotherapy dose reconstruction and their impacts on dose-response relationships. J Radiol Prot Off J Soc Radiol Prot 2017;37:R1–R18. https://doi.org/10.1088/1361-6498/aa575d.
[26] Chalise P, McGee D. Time Scales in Cox Model : Effect of Variability Among Entry Ages on Coefficient Estimates. Published 2010. Accessed January 12, 2021. /paper/Time-Scales-in-Cox-Model-%3A-Effect-of-Variability-on-Chalise-McGee/30d84566351da867f44dbb76c39be65344189770.
[27] Therneau TM, until 2009) TL (original S >R port and R maintainer, Elizabeth A, Cynthia C. survival: Survival Analysis. Published online April 26, 2021. Accessed July 26, 2021. https://CRAN.R-project.org/package=survival.
[28] Borgan Ø. Modeling Survival Data: Extending the Cox Model. Terry M. Therneau and Patricia M. Grambsch, Springer-Verlag, New York, 2000. No. of pages: xiii + 350. Price: $69.95. ISBN 0-387-98784-3. *Stat Med*. 2001;20 (13):2053-2054. doi:10.1002/sim.956.
[29] Pm G, Tm T. Proportional hazards tests and diagnostics based on weighted residuals. Biometrika 1994;81:515–26. https://doi.org/10.1093/biomet/81.3.515.
[30] Suissa S. Relative excess risk: an alternative measure of comparative risk. Am J Epidemiol 1999;150:279–82. https://doi.org/10.1093/oxfordjournals.aje.a009999.
[31] The EPICURE Regression Programs. Accessed July 29, 2021. http://epicurehelp.risksciences.com/index.html#!Documents/theepicureregressionprograms.htm.
[32] Bauer DF. Constructing Confidence Sets Using Rank Statistics. Journal of the American Statistical Association 1972;67(339):687–90. https://doi.org/10.2307/2284469.
[33] Veinot JP, Edwards WD. Pathology of radiation-induced heart disease: a surgical and autopsy study of 27 cases. Hum Pathol 1996;27:766–73. https://doi.org/10.1016/S0046-8177(96)90447-5.
[34] Nadlonek NA, Weyant MJ, Yu JA, et al. Radiation induces osteogenesis in human aortic valve interstitial cells. J Thorac Cardiovasc Surg 2012;144:1466–70. https://doi.org/10.1016/j.jtcvs.2012.08.041.
[35] Yarnold J, Brotons MCV. Pathogenetic mechanisms in radiation fibrosis. Radiother Oncol J Eur Soc Ther Radiol Oncol 2010;97:149–61. https://doi.org/10.1016/j.radonc.2010.09.002.
[36] Patil S, Pingle SR, Shalaby K, Kim AS. Mediastinal irradiation and valvular heart disease. Cardio-Oncol 2022;8:7. https://doi.org/10.1186/s40959-022-00133-2.
[37] Schellong G, Riepenhausen M, Bruch C, et al. Late valvular and other cardiac diseases after different doses of mediastinal radiotherapy for hodgkin disease in children and adolescents: report from the longitudinal GPOH follow-up project of the German-Austrian DAL-HD studies. Pediatr Blood Cancer 2010;55:1145–52. https://doi.org/10.1002/pbc.22664.
[38] Henson K. Cardiac mortality among 200 000 five-year survivors of cancer diagnosed at 15 to 39 years of age | circulation. Circulation 2016;134.
[39] Monte IP, Cameli M, Losi V, Privitera F, Citro R. Valvular Damage. *J Cardiovasc Echography*. 2020;30:S26-S32. doi:10.4103/jcecho.jcecho_5_19.
[40] Mulrooney DA, Armstrong GT, Huang S, et al. Cardiac outcomes in adult survivors of childhood cancer exposed to cardiotoxic therapy. Ann Intern Med 2016;164:93–101. https://doi.org/10.7326/M15-0424.
[41] de Baat EC, Feijen EAM, Reulen RC, et al. Risk Factors for Heart Failure Among Pan-European Childhood Cancer Survivors: A PanCareSurFup and ProCardio Cohort and Nested Case-Control Study. *J Clin Oncol Off J Am Soc Clin Oncol*. Published online September 8, 2022:JCO2102944. doi:10.1200/JCO.21.02944.
[42] van Nimwegen FA, Schaapveld M, Janus CPM, et al. Cardiovascular disease after hodgkin lymphoma treatment: 40-year disease risk. JAMA Intern Med 2015;175:1007. https://doi.org/10.1001/jamainternmed.2015.1180.
[43] Bijl JM, Roos MM, van Leeuwen-Segarceanu EM, et al. Assessment of Valvular Disorders in Survivors of Hodgkin's Lymphoma Treated by Mediastinal Radiotherapy ± Chemotherapy. Am J Cardiol 2016;117(4):691–6. https://doi.org/10.1016/j.amjcard.2015.11.027.
[44] Armstrong GT, Oeffinger KC, Chen Y, et al. Modifiable risk factors and major cardiac events among adult survivors of childhood cancer. J Clin Oncol 2013;31:3673–80. https://doi.org/10.1200/JCO.2013.49.3205.
[45] Bates JE, Shrestha S, Liu Q, et al. Low-dose radiation to cardiac substructures and late-onset cardiac disease: A report from the Childhood Cancer Survivor Study (CCSS). *J Clin Oncol*. 2021;39:10027-10027. doi:10.1200/JCO.2021.39.15_suppl.10027.
[46] van Kalsbeek RJ, van der Pal HJH, Kremer LCM, et al. European PanCareFollowUp recommendations for surveillance of late effects of childhood, adolescent, and young adult cancer. Eur J Cancer 2021;154:316–28. https://doi.org/10.1016/j.ejca.2021.06.004.
[47] Emami B, Lyman J, Brown A, et al. Tolerance of normal tissue to therapeutic irradiation. Int J Radiat Oncol 1991;21:109–22. https://doi.org/10.1016/0360-3016(91)90171-Y.

Téléchargé pour Anonymous User (n/a) à Gustave Roussy à partir de ClinicalKey.fr par Elsevier sur février 23, 2023. Pour un usage personnel seulement. Aucune autre utilisation n'est autorisée. Copyright ©2023. Elsevier Inc. Tous droits réservés.

cancers

MDPI

Article

Dosiomics-Based Prediction of Radiation-Induced Valvulopathy after Childhood Cancer

Stefania Chounta [1,2,3,4,*], Rodrigue Allodji [1,2,3,5,*], Maria Vakalopoulou [4], Mahmoud Bentriou [4], Duyen Thi Do [1,2,3], Florent De Vathaire [1,2,3], Ibrahima Diallo [6,7], Brice Fresneau [8], Thibaud Charrier [1,2,3,9], Vincent Zossou [1,2,3,5,10], Stergios Christodoulidis [4], Sarah Lemler [4] and Veronique Letort Le Chevalier [4]

1 Université Paris-Saclay, Univ. Paris-Sud, UVSQ, CESP, Cancer and Radiation Team, F-94805 Villejuif, France
2 INSERM, CESP, Cancer and Radiation Team, F-94805 Villejuif, France
3 Gustave Roussy, Department of Clinical Research, Cancer and Radiation Team, F-94805 Villejuif, France
4 Université Paris-Saclay, CentraleSupélec, Mathématiques et Informatique pour la Complexité et les Systèmes, F-91190 Gif-sur-Yvette, France
5 Polytechnic School of Abomey-Calavi (EPAC), University of Abomey-Calavi, 01, Cotonou P.O. Box 2009, Benin
6 Department of Radiation Oncology, Gustave Roussy, F-94800 Villejuif, France
7 Gustave Roussy, Inserm, Radiothérapie Moléculaire et Innovation Thérapeutique, Paris-Saclay University, F-94800 Villejuif, France
8 Gustave Roussy, Université Paris-Saclay, Department of Pediatric Oncology, F-94805 Villejuif, France
9 Institut Curie, PSL Research University, INSERM, U900, F-92210 Saint Cloud, France
10 Institut de Formation et de Recherche en Informatique, (IFRI-UAC), Cotonou P.O. Box 2009, Benin
* Correspondence: stefania.chounta@gustaveroussy.fr (S.C.); rodrigue.allodji@gustaveroussy.fr (R.A.)

Simple Summary: Childhood cancer survivors are often prone to experiencing late effects due to treatment complications. Valvular Heart Disease is a known iatrogenic effect of radiation leakage to the heart during radiotherapy and is often linked with the occurrence of other cardiac diseases like heart failure. Early identification and treatment of survivors prone to develop valvular heart disease is an important public health issue that remains challenging. In the FCCSS, a voxel-scaled reconstruction of radiation dose to the heart is available for patients that had been treated with radiotherapy. This type of uncommon data allows us to take into consideration information on the dose level that was absorbed by the cardiac tissues, as well as on the spatial characteristics of radiation dose distribution to the heart. With the help of machine learning algorithms, we attempted to train models capable of accurately predicting survivors high at risk of experiencing a late valvular heart disease after radiotherapy for childhood cancer. We suggest that there is an underlying association of the radiation dose with the occurrence of a valvular heart disease that goes beyond the mean dose to the heart and can be explained by the combination of spatial and descriptive features of the dose.

Abstract: Valvular Heart Disease (VHD) is a known late complication of radiotherapy for childhood cancer (CC), and identifying high-risk survivors correctly remains a challenge. This paper focuses on the distribution of the radiation dose absorbed by heart tissues. We propose that a dosiomics signature could provide insight into the spatial characteristics of the heart dose associated with a VHD, beyond the already-established risk induced by high doses. We analyzed data from the 7670 survivors of the French Childhood Cancer Survivors' Study (FCCSS), 3902 of whom were treated with radiotherapy. In all, 63 (1.6%) survivors that had been treated with radiotherapy experienced a VHD, and 57 of them had heterogeneous heart doses. From the heart–dose distribution of each survivor, we extracted 93 first-order and spatial dosiomics features. We trained random forest algorithms adapted for imbalanced classification and evaluated their predictive performance compared to the performance of standard mean heart dose (MHD)-based models. Sensitivity analyses were also conducted for sub-populations of survivors with spatially heterogeneous heart doses. Our results suggest that MHD and dosiomics-based models performed equally well globally in our cohort and that, when considering the sub-population having received a spatially heterogeneous dose distribution, the predictive capability of the models is significantly improved by the use of the dosiomics features. If these findings are further validated, the dosiomics signature may be incorporated into machine

check for updates

Citation: Chounta, S.; Allodji, R.; Vakalopoulou, M.; Bentriou, M.; Do, D.T.; De Vathaire, F.; Diallo, I.; Fresneau, B.; Charrier, T.; Zossou, V.; et al. Dosiomics-Based Prediction of Radiation-Induced Valvulopathy after Childhood Cancer. *Cancers* **2023**, *15*, 3107. https://doi.org/10.3390/cancers15123107

Academic Editor: Dietmar Georg

Received: 1 March 2023
Revised: 16 May 2023
Accepted: 5 June 2023
Published: 8 June 2023

Copyright: © 2023 by the authors. Licensee MDPI, Basel, Switzerland. This article is an open access article distributed under the terms and conditions of the Creative Commons Attribution (CC BY) license (https://creativecommons.org/licenses/by/4.0/).

learning algorithms for radiation-induced VHD risk assessment and, in turn, into the personalized refinement of follow-up guidelines.

Keywords: dosiomics; late effects; childhood cancer; dosimetry; radiotherapy; valvulopathy; random forest; imbalanced classification

1. Introduction

Childhood cancer (CC) survival rates have risen over the past decades in high-income countries, owing to advances in oncology treatment [1–3]. Radiotherapy, in particular, radically improves cancer survival in many cases [4], and modern optimizations [5–8] have had a substantial impact in reducing toxicity and side risks. Meanwhile, during treatment with radiotherapy, healthy tissues cannot be avoided entirely; this can potentially lead childhood cancer survivors to suffer chronic damage; especially at risk are those who did not benefit from modern protocols.

Identifying high-risk individuals and providing them with early diagnosis and treatment is an ever-present public health concern, especially with such vulnerable populations as CC survivors. While data-driven clinical predictions are an ancient medical practice, modern machine learning algorithms can significantly improve accuracy and become a helpful asset in predicting the late cardiac effects of CC treatments [9,10].

According to the American Childhood Cancer Survivors Study, two out of three survivors experience at least one late iatrogenic effect [11]. Heart disease is among the known complications of CC treatment [12–15]. In this study, we are interested in identifying CC survivors with an increased risk of experiencing severe Valvular Heart Disease (VHD) several decades after treatment for CC.

It has been established that the risk of experiencing VHD increases with the level of radiation absorbed by heart tissues during radiotherapy [16–18]. In addition, an association of high (>25 Gy) radiation doses to the heart with the occurrence of VHD has already been reported, both for adult [19,20] and pediatric [16,21,22] cancer treatment. There is, however, an open question concerning the potential risk induced by extensive low and moderate radiation doses to the cardiac region. In [23], the relative risk of cardiac events was expressed with respect to the percentage of the heart volume which absorbed a dose between 5 and 20 Gy, and was found to be significant when more than 50% of the heart volume was affected. Meanwhile, in [16], it was suggested that a cut-off might exist below which there is no risk of subsequent Valvular Heart Disease. In [18], evidence was provided that such a threshold could be around 5 Gy, and that doses between 5 and 20 Gy absorbed by more than 90% of the heart volume are statistically associated with the occurrence of VHD. Consequently, we hypothesize that some distribution patterns could also be associated with the occurrence of VHD.

The most common explanatory variables to model the radiation-induced risk of VHD are the mean or the median dose to the heart [17,19,24]. However, mean and median dose to the heart do not provide insight into the role of spatial heterogeneity of received doses; more specifically, they do not allow an exhaustive representation of the characteristics of the dose distribution when it is heterogeneous. This issue remains understudied in the literature, mainly due to a lack of adequate whole-body voxel-scale data. In some studies with access to such data, the role of dose–volume histogram parameters in experiencing a cardiac disease has been investigated with fruitful results [18,19,23,25]. These first results encourage further investigation of the potential role of heart dose heterogeneity in experiencing VHD, using more systematic approaches.

In this study, we adopted the dosiomics approach, which involves extracting first-order statistics and 3D spatial features from radiation dose distribution, to go one step further. Studies have been exploring the role of dosiomics in risk modeling to predict radiation-induced temporal lobe injury [26], radiation pneumonitis [27], locoregional recurrences after

treatment for head and neck carcinoma [28], and radiation-induced hypothyroidism [29], to name a few applications. Dosiomics features have proven promising and, in some cases, more effective than the conventionally used dose–volume histogram parameters [29,30]. To our knowledge, this is the first study where dosiomics are extracted from the heart dose to estimate the risk of subsequent VHD. We chose to tackle the subject as a classification problem of VHD prediction several decades after treatment with radiotherapy for CC. We grew Random Forests based on the mean heart dose (MHD) (baseline model) and dosiomics features of survivors that experienced VHD, to deduce a signature in high-risk survivors. The main objectives of this study were to identify critical variables in risk estimation (*dosiomics signature*) and to grow efficient Random Forests that can accurately screen high-risk CC survivors prone to experiencing VHD.

2. Materials and Methods

2.1. Population and Identification of VHD Events

In the FCCSS cohort, information on demographic and clinical characteristics were gathered for 7670 5-year CC survivors treated between 1945 and 2001 for the most common childhood solid cancers (defined according to the third edition of the International Classification of Childhood Cancer-ICCC-319 [31]) in 5 different cancer centers in France before the age of 21, as previously reported [12,18,32–34]. Of these, 7488 had complete data and were included in the analyses. The FCCSS was approved by a regional committee on ethics and the French national agency regulating data protection (Commission Nationale Informatique et Liberté, agreements no. 902287 and no. 12038829). All patients, parents, or guardians have signed a written informed consent form under national research ethics requirements. The present analysis included 7488 5-year survivors (97.7% of the FCCSS cohort) with complete treatment data.

Vital status was obtained for all patients and causes of death from cépiDC (Center of epidemiology on medical causes of death) [35], coded according to the 9th and 10th versions of the International Classification of Diseases and confirmed by the French Registry of Death [31]. Clinical and epidemiological follow-up is being performed to identify the occurrence of iatrogenic effects from self-administered questionnaires, cohort linkage with the French Hospital Database and health insurance information system [36], and clinical follow-up for the patients of Gustave Roussy.

VHD events were identified, validated, and graded according to the Common Terminology Criteria for Adverse Events (CTCAE version 4.0322 [37]). We considered only severe VHD cases (grade $\geq$ 3), since there are concerns that non-severe cardiovascular disease is often self-declared and could cause a reporting bias in the data [38]. We identified 81 ($\approx$1%) survivors who had either experienced severe VHD before any other cardiac disease or for whom VHD was among their three first causes of death. Severe VHD is hereafter called VHD.

2.2. Voxelised Dosimetric Data: Dosimetry Factors and Dosiomics Features

Whole-body voxel-scale radiation dosimetry was available for 3902 patients who had received radiotherapy, following a methodology of absorbed dose reconstruction that has already been published [39,40]. For this study, we only included the heart dose reconstruction. An example is demonstrated in Figure 1.

The dosiomics definition is derived from the now well-established radiomics, a technique developed for image analysis [41,42], where voxel intensity plays the role of dose level. This allows high throughput extraction of numeric data (image 'biomarkers') from 3D images, in order to represent various aspects of the image characteristics (spatial patterns, texture, distribution statistics, etc.).

We extracted 93 dosiomics features from the dose to the heart using the pyradiomics package (3.0.1) [42]. The features can be categorized into six classes:

- Eighteen first-order statistics of the heart dose;
- Twenty-four Gray Level Co-occurrence Matrix (GLCM) features;

- Sixteen Gray Level Run Length Matrix (GLRLM) features;
- Sixteen Gray Level Size Zone Matrix (GLSZM) features;
- Fourteen Gray Level Dependence Matrix (GLDM) features;
- Five Neighboring Gray Tone Difference Matrix (NGLDM) features.

The complete list of features is provided in Appendix A (Table A1).

The extracted features provide information on the dose intensities and have already been described [42]. Shape features (2D and 3D) were not calculated, as they concern the size and shape of the region of interest. In the context of this study, the region of interest is the heart. As the shape and size of the organs have been approximated by phantoms for many survivors and there is often uncertainty in relation to organ contouring, it would not be informative to include size features in the models. The binwidth of dose histograms was set to 0.1 Gy where applicable (set according to the Freedman–Diaconis rule [43]).

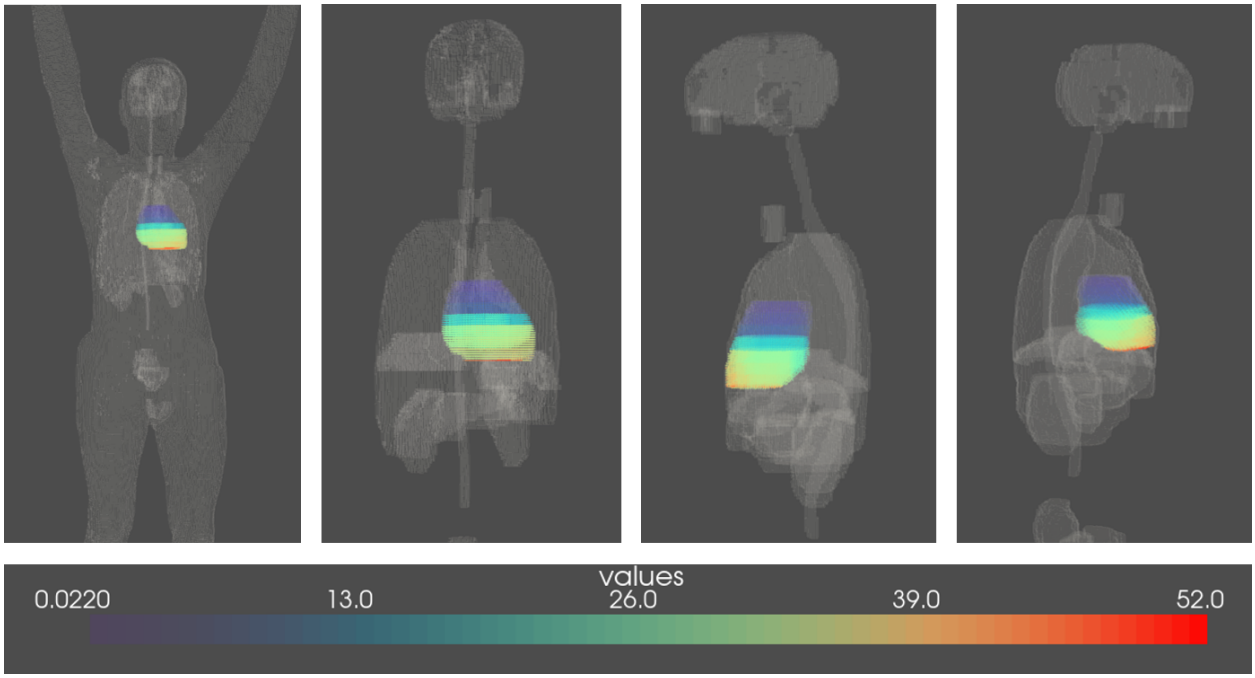

Figure 1. Representation of the voxelized heart–dose reconstruction; four views (front, back, left, and right) of one childhood cancer survivor; voxels are of size 2 mm^3, and the color shades represent the level of the radiation dose (in Gy). This survivor was treated at 3.5 years old in 1961 for Hodgkin lymphoma and received a mean heart dose of 19.6 Gy.

2.3. Imbalanced Classification and Feature Selection

Our analyses concerned a retrospective cohort, and survivors experienced VHD up to 50 years after treatment for childhood cancer. We attempted to identify high-risk survivors with a supervised classification problem. However, only 1% of the survivors were diagnosed with severe VHD. Therefore, we were dealing with an imbalanced classification problem of identifying survivors diagnosed with severe VHD, where the prediction that no survivor was at risk would result in a 99% accuracy (Number of correct predictions/Total number of predictions).

Chen et al. [44] proposed two possible adaptations of the classic Random Forest algorithm to tackle the problem of imbalanced data: Weighted Random Forest (wtRF) and Balanced Random Forest (BRF). The wtRF is based on the idea of cost-sensitive learning to penalize misclassification of the minority class. A weight is assigned to each class and incorporated into two steps of the random forest algorithm: (i) in the tree induction procedure, class weights are used to weight the Gini criterion for finding splits, and (ii) in the terminal nodes of each tree, where class weights are again taken into consideration

to determine the prediction according to a weighted majority vote. The BRF incorporates the idea of down-sampling the majority class during each bootstrap step by selecting a bootstrap sample from the minority class and then randomly drawing the same number of cases from the majority class.

To evaluate the models based on the extracted dosiomics features, we compared them to forests grown from the MHD. An adjusted version is also presented based on the following adjustment variables: biological sex, age (in years) and year of the first childhood cancer diagnosis, and chemotherapy exposure (binary: 1 if chemotherapy was administered during childhood cancer, 0 otherwise).

2.4. Modeling Workflow

Given the largely unbalanced nature of the dataset, particular attention was paid to avoiding biased estimates and overfitting. To increase the robustness of our results, we repeated our entire analysis pipeline over 30 random instances of train–test split. It should be noted that another strategy could have been cross-validation, but this has been shown to not provide better accuracy [45]. The 30 random and overlapping divisions of the training and test sets were chosen so as to respect the balance in relation to the proportion of VHD incidents.

For the dosiomics-based models, as illustrated in Figure 2, we started the pipeline with variable selection through an Elastic Net, which is appropriate when the variables form groups that contain highly correlated variables, as is the case with diosiomics [46]. The regularization hyper-parameters were tuned through a grid search with cross-validation. Then, we performed 5-fold cross-validation on the train set to calibrate the Random Forest parameters (number of trees to grow and maximum leaf nodes). We then calculated variable importances for each instance (computed as the mean and standard deviation of accumulation of the impurity decrease within each tree) and confusion matrices. From the confusion matrices, we calculated the following metrics, aggregated across the 30 instances: Sensitivity (Recall), Specificity, Balanced Accuracy (BA), and AUC ROC (defined below). Metrics results are presented in the corresponding section as average ± standard deviation. All p-values computed for the performance comparisons were obtained from t-tests under the assumption of variance homogeneity. For the MHD-based models, the pipeline was similar, except for the feature selection step.

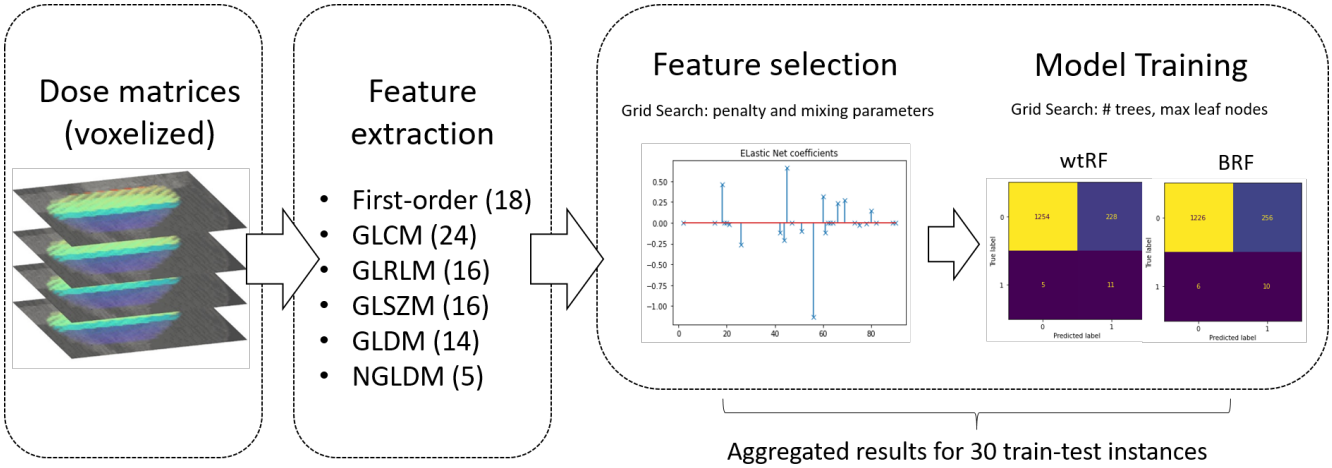

Figure 2. Workflow of the dosiomics-based models, as described in Section 2.4. We extracted 93 dosiomics features from the radiation dose to build the heart matrices, split the cohort into train–test groups 30 times, used the Elastic Net to do a variable selection, and after 5-fold cross validation for hyperparameters calibration (number (#) of trees and maximum leaf nodes) we, then, trained the weighted (wtRF) and balanced random forests (BRF). Then we calculated the metrics of performance for each of the two types of Random Forest by aggregating the results of the 30 splits.

2.5. Dosiomics Signature

Each presented feature was selected from at least 25 of the 30 iterations of the Elastic Net. Feature importance was evaluated by the Random Forest algorithm and was impurity-based (the sum over the number of splits—across all trees—that included the feature, proportionally to the number of samples split). A feature was selected for inclusion in the dosiomics signature if it was, on average, among the 30 most important features according to the Random Forest while having been selected by the Elastic Net. Features were ordered by feature class and then alphabetically.

2.6. Model Evaluation

The two possible types of wrong predictions have different implications: False Positives (or Type I error, i.e., falsely predicting that a survivor is at high risk of experiencing the event) would cost the CC survivors and the health system resources and time, while a False Negative (or Type II error, i.e., falsely predicting that a survivor is not at risk) could put CC survivors' lives at risk. The statistical challenge is to accurately identify as many as possible high-risk individuals (True Positives) with the lowest possible 'cost' of wrong predictions: the so-called 'avalanche problem' [47]. Notably, Recall (sensitivity) is the metric that evaluates the algorithm's ability to detect True Positives and not misclass them falsely as Negatives. On the other hand, Specificity is the probability of correctly identifying a survivor that will not experience the event; therefore, it evaluates the 'cost' of the algorithm in terms of False Positives. Thus, in this specific medical application, a low Recall means that the algorithm is inappropriate, while a low specificity is much more tolerable and secondary in terms of priorities for improvement. Finally, Balanced Accuracy is the average of sensitivity (Recall) and specificity (weighted Recall), and AUC is the area under the ROC curve (the integral of the curve of sensitivity against 1-specificity at various threshold settings). Therefore, both metrics simultaneously combine multiple quadrants of the confusion matrix (True Positives, False Positives, True Negatives, and False Negatives), providing an in-depth evaluation of models.

2.7. Cohort Partition Based on Heart Dose Heterogeneity

To explore and work out the imbalanced classification problem, we proposed a partition of the data based on the assumption that heart–dose heterogeneity might be an important factor for the occurrence of VHD. Two potential features measure heterogeneity: entropy and uniformity, negatively correlated. We chose uniformity, a normalized measure (taking values between 0 and 1). Uniformity is calculated as the sum of squares of each intensity value:

$$Uniformity = \sum_{i=1}^{N_g} p(i)^2 \quad (1)$$

where, in Equation (1), N_g is the number of non-zero bins of intensity level, equally spaced from 0 with a width defined in the binwidth parameter, $p(i) = \frac{P(i)}{N_p}$ is the normalized first-order histogram $P(i)$, and N_p is the total number of voxels. This measures the homogeneity of the radiation dose distribution. In this study, it was only computed for the doses absorbed from the heart. A high uniformity (close to 1) is interpreted either as homogeneity in the dose distribution or a smaller range of discrete intensity values [42].

We trained the wtRF and the BRF on three cohorts: (i) the entire cohort (7488 survivors, 81 of whom experienced a VHD) using dummy feature values for the patients that had not been treated with radiotherapy by setting to 0 the dose level absorbed by the heart voxels, (ii) the sub-population that had been exposed to non-homogeneous heart radiation (3556 survivors with Uniformity$<$ 1, 61 of whom experienced a VHD), and finally (iii) the sub-population with very heterogeneous heart doses (1963 survivors with uniformity$<$ 0.1, 57 of whom experienced a VHD).

Analyses were performed with Python 3.8.13. Data analysis was carried out with the libraries pandas [48], numPy [49], seaborn [50], and matplotlib [51]; dosiomics were extracted with the pyradiomics library [42]; and the pipelines for the modeling were built with Scikit-learn [52] and imbalanced-learn [53]. The threshold of significance was set to 0.05.

3. Results

3.1. Descriptive Analysis

In Tables 1 and 2, we gathered information on the FCCSS and the sub-cohorts, defined according to the value of heart dose uniformity: no treatment with radiotherapy, uniformity $= 1$, uniformity inside the range $[0.1, 1)$, and uniformity < 0.1.

From the 7488 5-year survivors of the FCCSS with complete data, 81 experienced a VHD (≈1%). A total of 63 of the survivors that experienced the event had been treated with radiotherapy, among whom, 2 had a heart–dose uniformity $= 1$, 4 had a uniformity between 0.1 and 1, and 57 had a uniformity <0.1. The prevalence of VHD among survivors with uniformity <0.1 is, thus, 2.9%. In the sub-population with uniformity $= 1$, the average mean, median, and maximum dose to the heart were all very low (0.2, 0.2, and 0.4 Gy, respectively), as well as each of their maximum values (0.25, 0.25, and 0.26 Gy respectively). On the contrary, among survivors with uniformity <0.1, the average mean, median, and maximum dose to the heart increased by three orders of magnitude. In Table 2, we gathered information on the repartition of CC types in each cohort part. It is noteworthy that 84% of the survivors of Hodgkin lymphoma (394) had heart dose uniformity <0.1. In addition, among survivors treated for renal tumors, 47% (531) had heart dose uniformity below 0.1, 9% between 1 and 0.1, and the rest (44%) were not treated with radiotherapy. Finally, 35% of survivors treated for the central nervous system and miscellaneous intracranial and intraspinal neoplasms (395) were among the 1963 survivors with heart dose uniformity <0.1.

Table 1. Descriptive table of the cohort (FCCSS) in the first column; then by radiotherapy status: survivors that had not been treated with radiotherapy (No RT), and survivors that had been treated with radiotherapy and had a heart dose uniformity $= 1$, between 0.1 and 1, and finally <0.1.

	FCCSS [1]	**No RT** [2]	**Uniformity = 1**	**Uniformity in [0.1, 1)**	**Uniformity < 0.1**
Total	7488	3586	346	1593	1963
VHD [3]	81 (1.08%)	18 (0.5%)	2 (0.58%)	4 (0.25%)	57 (2.9%)
Age at CC [4] diagnosis	6.62 [0–20.61]	6.18 [0–20.41]	6.01 [0–18.41]	7.08 [0–20.28]	7.17 [020.61]
Year at CC diagnosis	1984 [1946–2000]	1988 [1949–2000]	1983 [1951–2000]	1982 [1946–2000]	1980 [1948–2000]
Attained age	37.76 [5.39–79.83]	35.79 [5.392–76.37]	39.37 [7.27–79.83]	38.94 [6.16–78.65]	40.12 [6.66–77.82]
Biological Sex					
Male	3384 (45.19%)	1622 (45.23%)	146 (42.2%)	701 (44.01%)	915 (46.61%)
Female	4104 (54.81%)	1964 (54.77%)	200 (57.8%)	892 (55.99%)	1048 (53.39%)
Chemotherapy					
No	1828 (24.41%)	957 (26.69%)	109 (31.5%)	480 (30.13%)	282 (14.37%)
Yes	5660 (75.59%)	2629 (73.31%)	237 (68.5%)	1113 (69.87%)	1681 (85.63%)
Mean dose to the heart	6.82 [0–61.20]	0 [0–0]	0.02 [0–0.25]	0.98 [0–37.65]	12.76 [0–61.20]
Median dose to the heart	6.75 [0–67.54]	0 [0–0]	0.02 [0–0.25]	0.88 [0–37.66]	12.69 [0–67.54]
Maximum dose to the heart	13.68 [0–109.43]	0 [0–0]	0.04 [0–0.26]	2.18 [0.1–60.28]	25.424 [1.326–109.43]
Heart dose uniformity	0.27 [0.003–1]	1 [1–1]	1 [1–1]	0.4 [0.1–1)	0.036 [0.003–0.1]

For continuous variables, the average is given as well as minimum and maximum (average [min–max]). For categorical variables, percentages are calculated over the total of the relevant sub-population. [1] French Childhood Survivors Study; [2] No Radiotherapy; [3] Valvular Heart Disease ; [4] Childhood Cancer.

Table 2. The distribution of the type of first cancer in the cohort (FCCSS) in the first column; then by radiotherapy status: survivors that had been treated without radiotherapy (No RT), uniformity of radiation dose to the heart = 1, between 0.1 and 1, and <0.1.

	FCCSS [1]	No RT [2]	Uniformity = 1	Uniformity in [0.1, 1)	Uniformity < 0.1
Total	7488	3586 (48%)	346 (5%)	1593 (21%)	1963 (26%)
VHD [3]	81	18 (22%)	2 (2%)	4 (5%)	57 (70%)
Type of CC [4]:					
Hodgkin lymphoma	471	27 (6%)	5 (1%)	45 (10%)	394 (84%)
Other lymphomas and reticuloendothelial neoplasms	788	540 (69%)	16 (2%)	158 (20%)	74 (9%)
CNS and miscellaneous intracranial and intraspinal neoplasms	1124	160 (14%)	17 (2%)	552 (49%)	395 (35%)
Neuroblastoma and other peripheral nervous cell tumors	1028	646 (63%)	12 (1%)	144 (14%)	226 (22%)
Retinoblastoma	519	310 (60%)	114 (22%)	91 (18%)	4 (1%)
Renal tumors	1136	503 (44%)	0 (0%)	102 (9%)	531 (47%)
Hepatic tumors	79	62 (78%)	0 (0%)	5 (6%)	12 (15%)
Malignant bone tumors	679	392 (58%)	64 (9%)	124 (18%)	99 (15%)
Soft tissue and other extraosseous sarcomas	846	387 (46%)	99 (12%)	261 (31%)	99 (12%)
Germ cell tumors, trophoblastic tumors, and neoplasms of gonads	469	332 (71%)	6 (1%)	65 (14%)	66 (14%)
Other	349	227 (65%)	13 (4%)	46 (13%)	63 (18%)

Percentages are calculated over the cohort totals (column *FCCSS*). [1] French Childhood Survivors Study; [2] No Radiotherapy; [3] Valvular Heart Disease ; [4] Childhood Cancer.

3.2. Dosiomics versus Mean Heart Dose

We first trained the models on the entire FCCSS (Table 3, rows 1–4). According to the BA and the AUC, models based on either the MHD or the dosiomics features performed similarly when trained with the wtRF algorithm (within the margin of error for the BA and the AUC). Most of the metrics' comparisons were not statistically significant, neither with the wtRF nor with the BRF, when the models were trained on the entire population (both treated and not treated with radiotherapy). According to the BA, the AUC, and the Sensitivity, the MHD-based and the dosiomics-based models performed equally well in our cohort. Specificity was higher with the MHD-based wtRF (0.90 > 0.88, p-value = 0.001) and also with the dosiomics-based BRF (0.86 > 0.84, p-value = 0.044). In the case of both types of algorithms—wtRF and BRF—the MHD and the dosiomics-based algorithms seemed to perform similarly.

We then trained the same forests on the sub-population with non-homogeneous doses to the heart (3556 out of the 3902 survivors that had been treated with radiotherapy, based on the heart–dose uniformity being < 1—Table 3, rows 5–8). All models seemed to improve (overall, metrics are higher for both types of Random Forests, wtRF or BRF, and both heart radiation measures, MHD or dosiomics features). With the wtRF, comparisons were not statistically significant. With the BRF, the dosiomics-based approach significantly outperformed the MHD (Table 3 row 8), based on three out of four metrics (BA: 0.79 > 0.74, p-value 0.004; AUC: 0.86 > 0.83, p-value = 0.046; and Specificity: 0.79 > 0.76, p-value = 0.001).

Finally, we attempted a stricter cut-off for the cohort partition and trained the models on the sub-population with heart–dose uniformity < 0.1 (Table 3, rows 9–12). The dosiomics-based model outperforms the MHD with both algorithms according to the Specificity (0.82 > 0.79, p-value = 0.001 with the wtRF and 0.77 > 0.73, p-value = 0.002 with the BRF).

Models trained on the sub-population of the FCCSS with heart–dose uniformity <1 performed better than models trained on the sub-population with heart–dose uniformity <0.1.

Table 3. Performance metrics, derived from training forests on the FCCSS and two sub-populations of the FCCSS (the part of the cohort with heart dose uniformity <1 and the part of the cohort with heart dose uniformity <0.1), according to two types of classification algorithms (weighted Random Forest—wtRF, and Balanced Random Forest—BRF), where the radiation-induced risk is explained by either the mean heart dose (MHD) or a selection of dosiomics features. Results are aggregated over the 30 instances of train–test spitting, and here we present the mean ± standard deviation of each metric.

		Heart Radiation Measure	Balanced Accuracy	AUC ROC	Sensitivity (Recall)	Specificity	
FCCSS	wtRF	**Mean heart dose**	0.74 ± 0.04	0.77 ± 0.051	0.57 ± 0.083	**0.90 ± 0.019**	
		Dosiomics features	0.74 ± 0.038	0.77 ± 0.047	0.59 ± 0.075	0.88 ± 0.015	
	p-values		*0.792*	*0.883*	*0.319*	*0.001*	
	BRF	**Mean heart dose**	0.73 ± 0.04	0.76 ± 0.046	0.61 ± 0.088	0.84 ± 0.034	
		Dosiomics features	0.74 ± 0.039	0.77 ± 0.051	0.62 ± 0.074	**0.86 ± 0.018**	4
	p-values		*0.234*	*0.358*	*0.627*	*0.044*	
Uniformity < 1	wtRF	**Mean heart dose**	0.78 ± 0.057	0.85 ± 0.059	0.72 ± 0.127	0.84 ± 0.029	
		Dosiomics features	0.78 ± 0.057	0.86 ± 0.059	0.73 ± 0.126	0.83 ± 0.031	
	p-values		*0.981*	*0.483*	*0.617*	*0.057*	
	BRF	**Mean heart dose**	0.74 ± 0.054	0.83 ± 0.057	0.73 ± 0.113	0.76 ± 0.043	
		Dosiomics features	**0.79 ± 0.056**	**0.86 ± 0.057**	0.78 ± 0.113	**0.79 ± 0.021**	8
	p-values		*0.004*	*0.046*	*0.08*	*<0.001*	
Uniformity < 0.1	wtRF	**Mean heart dose**	0.76 ± 0.068	0.81 ± 0.069	0.71 ± 0.146	0.79 ± 0.031	
		Dosiomics features	0.76 ± 0.062	0.82 ± 0.073	0.69 ± 0.13	**0.82 ± 0.026**	
	p-values		*0.909*	*0.773*	*0.4*	*0.001*	
	BRF	**Mean heart dose**	0.72 ± 0.076	0.79 ± 0.064	0.72 ± 0.151	0.73 ± 0.052	
		Dosiomics features	0.75 ± 0.056	0.8 ± 0.071	0.74 ± 0.126	**0.77 ± 0.028**	12
	p-values		*0.162*	*0.437*	*0.701*	*0.002*	

The last column corresponds to the enumeration of the table lines. *p*-values correspond to two-sided *t*-tests. The bolded metrics' values are the ones that, compared to the model of the same type of forest but with a different heart radiation measure, are significantly higher.

3.3. Models Adjusted on Clinical Variables

We also attempted to train the models adjusted on clinical variables. MHD and dosiomics-based models performed similarly well. Aggregated performance metrics for models trained on the entire FCCSS (Table A2—lines 1–4) and the sub-populations with heart–dose uniformity <1 (Table A2—lines 5–8) and 0.1 (Table A2—lines 9–12) are included in Appendix A.

3.4. Sensitivity Analysis According to the Type of First Childhood Cancer

Table A3, in Appendix A , presents the results of a sensitivity analysis. We trained the models on survivors that had been treated for Hodgkin lymphoma, central nervous system malignancies, and renal tumors. Aggregated metrics and *p*-values are presented for non-adjusted and adjusted models. Comparison were not statistically significant and we cannot conclude that one model would outperform the others.

3.5. Dosiomics Signature

In Table 4, we provide information on the most important features by population (FCCSS, uniformity < 1, and uniformity < 0.1) and on whether they were selected as one of the most important features by each type of random forest (weighted and balanced). We present descriptives of the following 22 features that we propose as a dosiomics signature of a late VHD in the FCCSS:

- First order statistics: Tenth percentile, ninetieth percentile, energy, kurtosis, mean heart dose, median heart dose, minimum heart dose, root mean squared, total energy;
- GLCM: Autocorrelation, IDMN, IDN, joint average, sum average;
- GLDM: High gray level emphasis, large dependence high gray level emphasis, small dependence high gray level emphasis;
- GLRLM: High gray level run emphasis, long run high gray level emphasis, short run high gray level emphasis;
- GLSZM: Gigh gray level zone emphasis, small area high gray level emphasis.

Additionally, boxplots describing variable importance in the BRF trained in the subpopulation with uniformity <1 are provided in Figure 3. We can observe that the median and the mean heart dose sort among the 5 most important features, along with the 10th dose percentile, the minimum, and the Root Mean Squared.

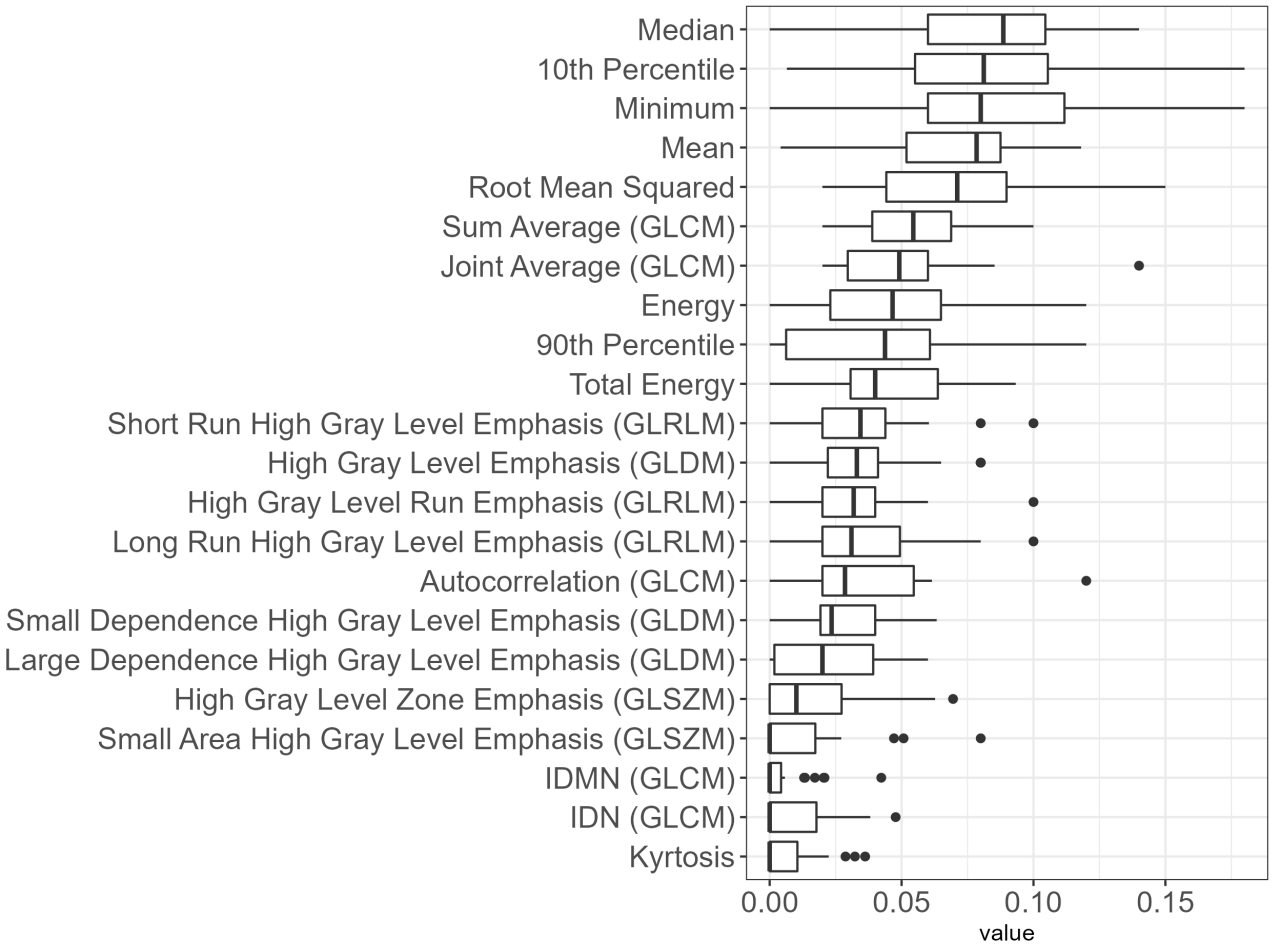

Figure 3. Boxplots of feature importance (aggregated over 30 train–test iterations) for the BRF trained on the population with uniformity <1.

Table 4. Dosiomics signature according to the sub-population (FCCSS, uniformity < 1 and uniformity < 0.1), and type of random forest (weighted or balanced).

	FCCSS			Uniformity < 1			Uniformity < 0.1		
Features	**wtRF**	**BRF**	**Average [min–max]**	**wtRF**	**BRF**	**Average [min–max]**	**wtRF**	**BRF**	**Average [min–max]**
First Order Statistics:									
10th percentile	✓	✓	1.78 [0–49.23]	✓	✓	3.75 [0–49.23]	✓	✓	6.18 [0–49.23]
90th percentile	✓	✓	5.37 [0–89.78]			11.31 [0–89.78]			19.36 [1.01–89.78]
energy	✓	✓	3.7×10^6 [0–2.1×10^8]	✓	✓	7.9×10^6[2.49–2.1×10^8]	✓	✓	14×10^6 [8.4×10^3–2.1×10^8]
kyrtosis		✓	3.49 [0–1753.9]			7.14 [1.1–1753.9]			6.03 [1.1–115.99]
mean heart dose	✓	✓	3.55 [0–61.09]	✓	✓	7.48 [0–61.09]	✓	✓	12.75 [0.64–61.09]
median heart dose	✓	✓	3.51 [0–67.91]	✓	✓	7.4 [0–67.91]	✓	✓	12.68 [0.44–67.91]
minimum heart dose	✓	✓	0.88 [0–38.24]	✓	✓	1.85 [0–38.24]			2.88 [0–38.24]
root mean squared	✓	✓	3.98 [0–64.33]	✓	✓	8.37 [0.01–64.33]	✓	✓	14.27 [0.7–64.33]
total energy	✓	✓	3×10^7 [0–1.7×10^9]	✓	✓	6.3×10^7[19.89–1.7×10^9]	✓	✓	11×10^7 [6.710^4–1.7×10^9]
GLCM:									
autocorrelation	✓	✓	0.58×10^4 [1–3.1×10^5]	✓	✓	1.2×10^4 [1–3.1×10^5]	✓	✓	2.1×10^4 [41–3.1×10^5]
IDMN		✓	1 [0.86–1]		✓	0.99 [0.86–1]			0.99 [0.86–1]
IDN		✓	0.99 [0.83–1]		✓	0.98 [0.83–1]	✓	✓	0.98 [0.83–1]
joint average	✓	✓	27.72 [1–512.79]	✓	✓	57.27 [1–512.79]	✓	✓	99.75 [5.38–512.79]
sum average	✓	✓	54.97 [1–10^4]	✓	✓	114.54 [2–10^4]	✓	✓	199.49 [10.76–10^4]
GLDM:									
high gray level emphasis	✓	✓	0.59×10^4 [1–3.1×10^5]	✓	✓	1.2×10^4 [1–3.1×10^5]	✓	✓	2.2×10^4 [42–3.1×10^5]
large dependence high gray level emphasis	✓	✓	0.89×10^6 [1–7.9×10^7]			1.8×10^6 [593–7.9×10^7]			3.3×10^6 [4.2×10^3–7.9×10^7]
small dependence high gray level emphasis	✓	✓	325.95 [0–39,643.4]	✓	✓	685.36 [0–39,643.4]	✓	✓	1239.17 [0.18–39,643.4]
GLRLM:									
high gray level run emphasis	✓	✓	6120.11 [1–321,807.62]	✓	✓	12,886.24 [1–321,807.62]	✓	✓	23,021.99 [45.97–321,807.62]
long run high gray level emphasis	✓	✓	55,488.09 [1–9,755,180.03]	✓	✓	116,805.48 [77.31–9,755,180.03]	✓	✓	205,185.69 [514.48–9755180.03]
short run high gray level emphasis	✓	✓	4118.5 [0.05–247,740.25]	✓	✓	8671.47 [0.07–247,740.25]	✓	✓	15,560.49 [14.08–247,740.25]
GLSZM:									
high gray level zone emphasis	✓	✓	6717.88 [1–347,651.5]			14,144.98 [1.2–347,651.5]			24,962.32 [50.85–347,651.5]
small area high gray level emphasis	✓	✓	1206.64 [0–99,793.65]			2539.85 [0–99,793.65]			4533 [0.09–99,793.65]

A check mark indicates that the feature was among the 30 most important of the model (averaged on 30 iterations). All of the features were selected via Elastic Net at least 25 out of 30 times.

4. Discussion

The main finding of this study is that a random forest performs better in predicting CC survivors at risk of a radiation-induced VHD under a selection of dosiomics features describing the heart dose in comparison to the mean heart dose, and comparisons are statistically significant when applied to a population with some heterogeneity. We found a dosiomics signature of cardiac doses for the prediction of a late VHD in the FCCSS. To the best of our knowledge, this is the first study that explores the role of dosiomics features in the occurrence of a late VHD after treatment for a CC.

The particularity of the FCCSS is that it is the only study with a whole-body voxelized dosimetry reconstruction available for almost every participant that was treated with radiotherapy. This allows an in-depth investigation of the distribution of radiation dose and, in combination with the information on other treatments and interventions in the context of childhood cancer treatment, the long follow-up duration with available medical records, the access to the French Health Insurance Information System, as well as the adapted self-questionnaires may lead to reliable analyses that can be incorporated into international guidelines for rigorous and effective personalized follow-up with childhood cancer survivors.

Concerning the risk of VHD in particular, there is an established risk of VHD when strong doses are absorbed by heart tissues during treatment for adult [20,54] or childhood cancer [13,22,23], and there exist hypotheses on the role of low and moderate doses [16,18,23]. Meanwhile, studies claim that no level of radiation dose to the heart can be safe [55]. The aim of this study was to explore the effect of radiation doses absorbed by the heart by taking into account the heterogeneity of the dose. For that matter, we chose to extract dosiomics features from the dose matrices, a method that is becoming popular [56] and provides insight into the spatial and statistical characteristics of radiation dose.

4.1. The Role of Heterogeneity of the Heart Dose in Late Valvular Heart Disease

We proposed a sensitivity analysis, based on the heart dose uniformity. We observed that predictions improved when models were trained on the sub-population of the FCCSS with heart dose uniformity <1, in comparison to models trained on the sub-population of the FCCSS with heart dose uniformity <0.1. We hypothesize that the heart–dose heterogeneity is in fact a meaningful factor, in the sense that some of the features probably influence the predictions of survivors with heterogeneous doses. Therefore, the model was unable to distinguish survivors most at-risk to experience VHD when trained among survivors with a small uniformity range. This is one of the most fruitful results of this study.

We also included models trained on the entire FCCSS cohort, that contained survivors treated and not treated with radiotherapy. The model underperforms in comparison with the models trained on the sub-population of the FCCSS with heart dose uniformity <1. Based on the assumption that cardiac radiation dose is not the only risk-factor responsible for a VHD, a dosiomics-based model is inappropriate for prediction for the non-irradiaded part of the cohort: the non-irradiated survivors that experience a VHD will always be incorrectly sorted in a model based on the radiation-induced risk.

Our main objective was to explore whether we can go beyond the use of the mean heart dose as an explanatory variable in the risk model. The idea was, thus, to see if descriptive statistics of the dose distribution, other than the mean dose, could carry additional information to improve predictions. When the dose distribution is uniform or nearly uniform, the mean dose is a sufficient descriptor of the distribution: other indicators might bring useful additional information only in the case of heterogeneous distributions. This part of the study aimed at investigating the effect of dose heterogeneity, not in itself, but as a criterion to discriminate cases where mean dose is likely to be a sufficient descriptor.

4.2. Model Choice and Performance

In [44], weighted and balanced random forests both improved prediction of the minority class in comparison to other algorithms. In our study, comparisons held between models with different predictors; comparing different types of algorithms was not one of the objectives in this study. Among performance metrics, Sensitivity (or Recall or True Positive Rate) is the most important for this application. It illustrates the existence of false negatives, whether all survivors who experienced the event were correctly sorted as high-risk. We also observed some models outperforming others based on Specificity. However, improving Specificity is a secondary objective of prediction models, as it evaluates the false positives. Therefore, between two models with contradictory results, we would choose the one with the highest True Positive Rate.

The two models with the highest Sensitivity are the MHD-based and the dosiomics-based BRF adjusted on clinical variables and trained on the sub-population with heart–dose uniformity <1 (0.8 and 0.82 respectively—Table A2). However, the comparison between them is not statistically significant, and we cannot conclude if one of them outperforms the other. Next-highest is the dosiomics-based BRF, trained on the same population without adjustment on clinical variables (0.78—Table 3). In this scenario, the difference from the sensitivity of the MHD model (0.73) is close to being statistically significant. Taking into account that the other three metrics are significantly higher in comparison to the MHD-based model, we can derive that the dosiomics-based BRF trained on the sub-population with heart dose uniformity <1 is the best-performing model in this study. Based on these observations, we conclude that the distribution of the radiation dose to the heart plays a complicated role in the occurrence of a VHD, which cannot be entirely captured by the MHD.

4.3. The Dosiomics Signature

The dosiomics signature can reflect the spatial complexity of the radiation dose and its association with the occurrence of a late VHD. It is noteworthy that, apart from very few exceptions, the two types of random forest evaluate the same variables as important on each sub-cohort. We observe that, in any case, MHD is among the most important features.

All of the features selected when models are trained among survivors with uniformity <0.1 are also selected in at least one more model, trained on a larger population that includes survivors with higher heart dose uniformity (uniformity <1 and the entire FCCSS). All models select energy and total energy, which depend on the magnitude of the voxel values, in the region of interest and, according to the authors [42], are volume-confounded. The mean and median heart dose as well as the root mean square, among the most important features of the model that seems to stand out (BRF on the sub-population with Uniformity <1), are selected by all models.

GLCM features indicate how often pairs of voxels with specific values and in a specified spatial relationship occur. According to the authors, the sum average measures the relationship between pairs of voxels with lower intensity values and pairs of voxels with higher intensity values. We could, therefore, hypothesize that the sum average provides information on the effect of low doses in the occurrence of a late VHD. On the contrary, the high gray level emphasis and the small dependence high gray level emphasis from the GLDM class of features, as well as the GLRLM and GLSZM classes, cover different aspects of the effect of high dose levels in the prediction of a late VHD.

4.4. Limitations

One inconvenience of the method of this paper is that the interpretability of the dosiomics features is not always obvious, since most of the features are not widely used for statistical analyses. Also, dosiomics features are not directly extracted from the treatment-planning syste; it is, therefore, not always simple for the medical staff to incorporate them into prediction models.

Concerning the content of the data, a limitation also derives from the lack of information on comorbidities. Data related to comorbidities could improve prediction algorithms' performance and the reliability of the results. Also, dose reconstruction comes with unavoidable uncertainties: a residual level of 2 to 5% in inaccuracy is generally observed for the dose at the organ of interest. The primary sources of uncertainty associated with dose estimation are (i) imaging of patient anatomy, (ii) reconstruction of the RT treatment plan, (iii) characterization of the irradiation source, and (iv) measurements or calculation of the dose distributions [39,40,57,58]. We assume that the voxelized dataset we are treating is sufficiently reliable. However, the advantage of this study is that the pipeline will still be applicable when uncertainties will have been removed from the dosimetric reconstruction.

The most important limitation is the lack of a validation set, a common problem in this type of study [59]. The number of events in the cohort is too low. Therefore, further partitioning the population to put aside a validation set would lead to loss of critical information necessary for the training. We decided the best strategy to eliminate some uncertainty from the results was to use the whole cohort in train–test partitioning and aggregate the results of 30 random stratified splits. External validation is, therefore, necessary. In this study, we aimed to propose a signal on the cardiac dosiomics signature for a late VHD, as well as a suggestion to incorporate information on the dose heterogeneity into the design of prediction algorithms and TPS guidelines.

4.5. Perspectives

For recently treated patients, data are automatically generated and can be archived [60], and for contoured organs of interest, the voxelized dose distribution can be extracted without significant cost. Therefore, these data can be used to derive dose–volume histograms, but also can be used as inputs for dosiomics analyses for radiation therapy side effects risk assessment.

Radiotherapists do their best to protect vital organs from strong radiation exposure [61]. However, it is still unclear if and how harmful exposure to low and moderate doses to the heart [62] could be. Meanwhile, while recent advancements make high MHD increasingly rare nowadays, novel radiotherapy delivery techniques such as IMRT or VMAT may increase the heart-volume receiving low-to-moderate radiation doses (<15 Gy). Dosiomics features could provide useful insight on the effect of spatially heterogeneous doses on the occurrence of late effects including VHD. Extracting dosiomics features directly from the treatment-planning system could be an interesting and useful perspective in this case.

For survivors who have received these treatments above a certain dose, several international guidelines recommend the completion of lifelong regular echocardiograms to allow earlier detection of asymptomatic cardiomyopathy, and thus reduce or delay sequelae by treating it. The recommended frequency of echocardiography ranges from every year to every five years, depending on the guidelines [63]. Even though the production of automated dosiomics applications is not yet a reality, risk models are already in use to design personalized follow-ups for each survivor.

Although still in its preliminary stage, our work paves the way toward an integrated optimization tool for recommending personalized follow-up protocols adapted to each patients' health history [64]. In addition, the creation of a new branch of cardiology, "cardio-oncology", with the aims of preventing cardiovascular complications related to antineoplastic treatment, achieving early diagnosis and treatment of any complications, and allowing completion of the expected antineoplastic treatment [65], should increase the offer of care for cancer survivors and encourage research in cardio-oncology. Defining the follow-up protocol is a delicate problem, with potentially dramatic consequences in case of maladjustment. The solution involving all sorts of screening exams at a high frequency would not be sustainable, both economically speaking and in terms of patients' comfort and even safety. A perspective is, therefore, to turn to cost-effectiveness analysis.

5. Conclusions

Dosiomics are proving to be a promising strategy for exploring the radiation dose distribution and exposing information on the underlying pathophysiology of radiation-induced pathologies. The dosiomics-based BRF is the only model in this predictive attempt that, when compared to the relevant MHD-based model, stands out, and this comparison is statistically significant. This result could prove beneficial in identifying high-risk individuals even in a context where detailed clinical data are not available, but dosimetry data are available. If these findings hold, the dosiomics signature may be incorporated into machine learning classification algorithms for radiation-induced VHD risk assessment.

Author Contributions: Conceptualization, S.C. (Stefania Chounta), R.A., M.V., M.B., D.T.D., F.D.V., S.C. (Stergios Christodoulidis), S.L. and V.L.L.C.; Data curation, S.C. (Stefania Chounta), M.B., D.T.D. and I.D.; Formal analysis, S.C. (Stefania Chounta); Funding acquisition, R.A., F.D.V., S.L. and V.L.L.C.; Methodology, S.C. (Stefania Chounta), R.A., M.V., M.B., D.T.D., F.D.V., S.C. (Stergios Christodoulidis), S.L. and V.L.L.C.; Project administration, R.A., M.V., S.C. (Stergios Christodoulidis), S.L. and V.L.L.C.; Software, S.C. (Stefania Chounta) and M.B.; Supervision, R.A., M.V., S.C. (Stergios Christodoulidis), S.L. and V.L.L.C.; Validation, S.C. (Stefania Chounta); Visualization, S.C. (Stefania Chounta) and D.T.D.; Writing—original draft, S.C. (Stefania Chounta); Writing—review and editing, R.A., M.V., M.B., D.T.D., F.D.V., I.D., B.F., T.C., V.Z., S.C. (Stergios Christodoulidis), S.L. and V.L.L.C. All authors have read and agreed to the published version of the manuscript.

Funding: This work was supported and funded by the Gustave Roussy Foundation (Pediatric Program "Guérir le Cancer de l'Enfant"), the ITMO (Instituts thématiques multiorganismes) Cancer d'Aviesan Program (RadioPrediTool project N° 20CM112-00), the INCa/ARC (Institut national du cancer) foundation (CHART project), the Foundation ARC for Cancer Research (grant no. Pop-HaRC 201401208), the "START" PAIR Research Program (grant no. INCa-Fondation ARC-LNCC 11902), and the "Ligue Nationale Contre le Cancer" association. These funding agencies had no role in the design and conduct of the study; in the collection, management, analysis, and interpretation of the data; nor in the preparation, review, and approval of the manuscript.

Institutional Review Board Statement: Not applicable.

Informed Consent Statement: We performed this cohort study after approval from the French Data Protection Authority (CNIL) and the National Institute of Medical Research and Health ethics committee.

Data Availability Statement: The datasets used and/or analyzed during the current study are available from the corresponding author upon reasonable request.

Acknowledgments: Françoise Terrier; Paul-Henry Cournède; Neige Journy; Sofia Kiassou.

Conflicts of Interest: The authors declare no conflict of interest.

Abbreviations

The following abbreviations are used in this manuscript:

VHD	Valvular Heart Disease
CC	Childhood Cancer
FCCSS	French Childhood Cancer Survivors Study
wtRF	weighted Random Forest
BRF	Balanced Random Forest
MHD	Mean Heart Dose

Appendix A

Table A1. The full list of calculated features.

Feature Class	First-Order Statistics	Gray Level Co-Occurrence Matrix (GLCM)	Gray Level Run Length Matrix (GLRLM)	Gray Level Size Zone Matrix (GLSZM)	Gray Level Dependence Matrix (GLDM)	Neighbouring Gray Tone Difference Matrix (NGLDM)
Number of features	18	24	16	16	14	5
	mean heart dose (MHD)	autocorrelation	gray level non-uniformity	gray level non-uniformity	dependence entropy	busyness
	median	cluster prominence	non-uniformity normalized	gray level non-uniformity normalized	dependence non-uniformity	coarseness
	minimum	cluster shade	gray level variance	gray level variance	dependence non-uniformity normalized	complexity
	maximum	cluster tendency	high gray level run emphasis	high gray level zone emphasis	dependence variance	contrast
	variance	contrast	long run emphasis	large area emphasis	gray level non-uniformity	strength
	skewness	correlation	long run high gray level emphasis	large area high gray level emphasis	gray level variance	
	kurtosis	difference average	long run low gray level emphasis	large area low gray level emphasis	high gray level emphasis	
	entropy	difference entropy	low gray level run emphasis	low gray level zone emphasis	large dependence emphasis	
	uniformity	difference variance	run entropy	size zone non-uniformity	large dependence high gray level emphasis	
	10th percentile	Inverse Difference (ID)	run length non-uniformity	size zone non-uniformity normalized	large dependence low gray level emphasis	
	90th percentile	Inverse Difference Moment (IDM)	run length non-uniformity normalized	small area emphasis	low gray level emphasis	
	energy	Inverse Difference Moment Normalized (IDMN)	run percentage	small area high gray level emphasis	small dependence emphasis	
	total energy	Inverse Difference Normalized (IDN)	run variance	small area low gray level emphasis	small dependence high gray level emphasis	
	range	Informational Measure of Correlation 1 (IMC1)	short run emphasis	zone entropy	small dependence low gray level emphasis	
	interquartile range	Informational Measure of Correlation 2 (IMC2)	short run high gray level emphasis	zone 6 percentage		
	mean absolute deviation	inverse variance	short run low gray level emphasis	zone variance		
	robust mean absolute deviation	joint average				
	root mean squared	joint energy				
		joint entropy				
		Maximal Correlation Coefficient (MCC)				
		maximum probability				
		sum average				
		sum entropy				
		sum squares				

Table A2. Models trained and metrics calculated on the entire FCCSS (7488) cohort, and then on the sub-populations with heart–dose uniformity <1 and <0.1, according to two types of classification algorithms (weighted Random Forest—wtRF, and Balanced Random Forest—BRF), where the radiation-induced risk is introduced by either the mean heart does—MHD, or a selection of dosiomics features. Results are aggregated over the 30 instances of train–test splitting, and here we present the mean ± standard deviation of each metric. Models in this table are adjusted on clinical variables: year and age of CC diagnosis, biological sex, and chemotherapy (y/n).

		Heart Radiation Measure	Balanced Accuracy	AUC ROC	Sensitivity (Recall)	Specificity	
FCCSS	wtRF	**Mean heart dose**	0.75 ± 0.041	**0.8** ± 0.044	0.62 ± 0.091	0.89 ± 0.027	
		Dosiomics features	0.74 ± 0.039	0.77 ± 0.051	0.6 ± 0.077	0.88 ± 0.012	
	p-values		*0.208*	*0.028*	*0.403*	*0.141*	
	BRF	**Mean heart dose**	0.76 ± 0.045	0.8 ± 0.054	0.68 ± 0.097	0.84 ± 0.029	
		Dosiomics features	0.74 ± 0.04	0.78 ± 0.054	0.65 ± 0.073	0.82 ± 0.023	4
	p-values		*0.057*	*0.126*	*0.169*	*0.092*	
Uniformity < 1	wtRF	**Mean heart dose**	0.81 ± 0.054	0.87 ± 0.048	0.74 ± 0.108	**0.87 ± 0.028**	
		Dosiomics features	0.78 ± 0.063	0.86 ± 0.057	0.73 ± 0.134	0.83 ± 0.028	
	p-value		*0.117*	*0.594*	*0.666*	*<0.001*	
	BRF	**Mean heart dose**	0.82 ± 0.053	0.88 ± 0.046	0.82 ± 0.106	**0.82 ± 0.023**	
		Dosiomics features	0.8 ± 0.062	0.86 ± 0.057	0.8 ± 0.123	0.8 ± 0.019	8
	p-values		*0.171*	*0.219*	*0.526*	*<0.001*	
Uniformity < 0.1	wtRF	**Mean heart dose**	0.76 ± 0.077	0.85 ± 0.052	0.69 ± 0.155	0.83 ± 0.025	
		Dosiomics features	0.77 ± 0.061	0.85 ± 0.057	0.71 ± 0.145	0.83 ± 0.031	
	p-values		*0.718*	*0.086*	*0.811*	*0.482*	
	BRF	**Mean heart dose**	0.77 ± 0.059	0.84 ± 0.057	0.76 ± 0.123	0.78 ± 0.026	
		Dosiomics features	0.78 ± 0.049	0.86 ± 0.05	0.76 ± 0.113	0.8 ± 0.032	12
	p-values		*0.779*	*0.183*	*0.673*	*0.482*	

The last column corresponds to the enumeration of the table lines. *p*-values correspond to two-sided *t*-tests. The bolded metrics' values are the ones that, when compared to the model of the same type of forest but with a different heart radiation measure, are significantly higher.

Table A3. Comparison of the metrics of 4 models: MHD, dosiomics features and their adjusted versions in Hodgkin lymphoma, central nervous system malignancies, and renal tumor survivors.

		Heart Radiation Measure	Balanced Accuracy	AUC ROC	Sensitivity (Recall)	Specificity	
Non Adjusted models	wtRF	**Mean heart dose**	0.78 ± 0.09	0.82 ± 0.071	0.7 ± 0.199	0.86 ± 0.033	
		Dosiomics features	0.75 ± 0.08	0.83 ± 0.053	0.66 ± 0.182	0.85 ± 0.028	
	p-values		*0.527*	*0.751*	*0.628*	*0.588*	
	BRF	**Mean heart dose**	0.78 ± 0.086	0.83 ± 0.062	0.73 ± 0.2	0.82 ± 0.035	
		Dosiomics features	0.76 ± 0.072	0.83 ± 0.065	0.71 ± 0.166	0.81 ± 0.029	4
	p-values		*0.712*	*0.870*	*0.801*	*0.705*	
Adjusted models	wtRF	**Mean heart dose**	0.79 ± 0.086	0.87 ± 0.059	0.71 ± 0.187	0.87 ± 0.033	
		Dosiomics features	0.76 ± 0.088	0.83 ± 0.059	0.67 ± 0.192	0.84 ± 0.028	
	p-values		*0.406*	*0.155*	*0.627*	*0.088*	
	BRF	**Mean heart dose**	0.8 ± 0.056	0.87 ± 0.059	0.76 ± 0.12	**0.84 ± 0.016**	
		Dosiomics features	0.78 ± 0.062	0.85 ± 0.064	0.73 ± 0.142	0.82 ± 0.027	8
	p-values		*0.394*	*0.544*	*0.723*	*0.022*	

The last column corresponds to the enumeration of the table lines. *p*-values correspond to two-sided *t*-tests. The bolded metrics' values are the ones that, compared to the model of the same type of forest but with a different heart radiation measure, are significantly higher.

References

1. INSERM. *5-Year Overall Survival Rates of Childhood Cancer in Mainland France over 2000–2014. by Diagnostic and Age Groups-RNCE*; INSERM: Pairs, France, 2022.
2. Society, A.C. *Key Statistics for Childhood Cancers*; American Cancer Society: Atlanta, GA, USA, 2023.
3. SIOP Europe. Mission and Vision. 2022. Available online: https://siope.eu/about-siope/mission-and-vision/ (accessed on 28 February 2023).
4. Shen, C.J.; Terezakis, S.A. The Evolving Role of Radiotherapy for Pediatric Cancers with Advancements in Molecular Tumor Characterization and Targeted Therapies. *Front. Oncol.* **2021**, *11*, 679701. [CrossRef] [PubMed]
5. Jairam, V.; Roberts, K.B.; Yu, J.B. Historical Trends in the use of radiation for pediatric cancers: 1973–2008. *Int. J. Radiat. Oncol. Biol. Phys.* **2013**, *85*, e151–e155. [CrossRef] [PubMed]
6. Lautenschlaeger, S.; Iancu, G.; Flatten, V.; Baumann, K.; Thiemer, M.; Dumke, C.; Zink, K.; Hauswald, H.; Vordermark, D.; Mauz-Körholz, C.; et al. Advantage of proton-radiotherapy for pediatric patients and adolescents with Hodgkin's disease. *Radiat. Oncol.* **2019**, *14*, 157. [CrossRef] [PubMed]
7. Baues, C.; Marnitz, S.; Engert, A.; Baus, W.; Jablonska, K.; Fogliata, A.; Vásquez-Torres, A.; Scorsetti, M.; Cozzi, L. Proton versus photon deep inspiration breath hold technique in patients with hodgkin lymphoma and mediastinal radiation. *Radiat. Oncol.* **2018**, *13*, 122. [CrossRef]
8. Butler, E.; Ludwig, K.; Pacenta, H.L.; Klesse, L.J.; Watt, T.C.; Laetsch, T.W. Recent progress in the treatment of cancer in children. *CA Cancer J. Clin.* **2021**, *71*, 315–332. [CrossRef]
9. Güntürkün, F.; Akbilgic, O.; Davis, R.L.; Armstrong, G.T.; Howell, R.M.; Jefferies, J.L.; Ness, K.K.; Karabayir, I.; Lucas, J.T., Jr.; Srivastava, D.K.; et al. Artificial intelligence-assisted prediction of late-onset cardiomyopathy among childhood cancer survivors. *JCO Clin. Cancer Inform.* **2021**, *5*, 459–468. [CrossRef]
10. Isaksson, L.J.; Pepa, M.; Zaffaroni, M.; Marvaso, G.; Alterio, D.; Volpe, S.; Corrao, G.; Augugliaro, M.; Starzyńska, A.; Leonardi, M.C.; et al. Machine learning-based models for prediction of toxicity outcomes in radiotherapy. *Front. Oncol.* **2020**, *10*, 790. [CrossRef]
11. Landier, W.; Skinner, R.; Wallace, W.H.; Hjorth, L.; Mulder, R.L.; Wong, F.L.; Yasui, Y.; Bhakta, N.; Constine, L.S.; Bhatia, S.; et al. Surveillance for Late Effects in Childhood Cancer Survivors. *J. Clin. Oncol.* **2018**, *36*, 2216–2222. [CrossRef]
12. Haddy, N.; Diallo, S.; El-Fayech, C.; Schwartz, B.; Pein, F.; Hawkins, M.; Veres, C.; Oberlin, O.; Guibout, C.; Pacquement, H.; et al. Cardiac Diseases Following Childhood Cancer Treatment: Cohort Study. *Circulation* **2016**, *133*, 31–38. [CrossRef]
13. Mulrooney, D.A.; Hyun, G.; Ness, K.K.; Ehrhardt, M.J.; Yasui, Y.; Duprez, D.; Howell, R.M.; Leisenring, W.M.; Constine, L.S.; Tonorezos, E.; et al. Major cardiac events for adult survivors of childhood cancer diagnosed between 1970 and 1999: Report from the Childhood Cancer Survivor Study cohort. *BMJ* **2020**, *368*, l6794. [CrossRef]

14. Leerink, J.M.; de Baat, E.C.; Feijen, E.A.; Bellersen, L.; van Dalen, E.C.; Grotenhuis, H.B.; Kapusta, L.; Kok, W.E.; Loonen, J.; van der Pal, H.J.; et al. Cardiac Disease in Childhood Cancer Survivors. *JACC Cardio Oncol.* **2020**, *2*, 363–378. [CrossRef] [PubMed]
15. Hau, E.M.; Caccia, J.N.; Kasteler, R.; Spycher, B.; Suter, T.; Ammann, R.A.; von der Weid, N.X.; Kuehni, C.E. Cardiovascular disease after childhood acute lymphoblastic leukaemia: A cohort study. *Swiss Med. Wkly.* **2019**, *149*, w20012. [CrossRef] [PubMed]
16. Cutter, D.J.; Schaapveld, M.; Darby, S.C.; Hauptmann, M.; van Nimwegen, F.A.; Krol, A.D.G.; Janus, C.P.M.; van Leeuwen, F.E.; Aleman, B.M.P. Risk for Valvular Heart Disease after Treatment for Hodgkin Lymphoma. *JNCI J. Natl. Cancer Inst.* **2015**, *107*, djv008. [CrossRef] [PubMed]
17. Cella, L.; Oh, J.H.; Deasy, J.O.; Palma, G.; Liuzzi, R.; D'avino, V.; Conson, M.; Picardi, M.; Salvatore, M.; Pacelli, R. Predicting radiation-induced valvular heart damage. *Acta Oncol.* **2015**, *54*, 1796–1804. [CrossRef]
18. Chounta, S.; Lemler, S.; Haddy, N.; Fresneau, B.; Mansouri, I.; Bentriou, M.; Demoor-Goldschmidt, C.; Diallo, I.; Souchard Msc, V.; Do Thi, D.; et al. The risk of valvular heart disease in the french childhood cancer survivors' study: Contribution of dose-volume histogram parameters. *Radiother. Oncol.* **2023**, *180*, 109479. [CrossRef]
19. Cella, L.; Liuzzi, R.; Conson, M.; Torre, G.; Caterino, M.; De Rosa, N.; Picardi, M.; Camera, L.; Solla, R.; Farella, A.; et al. Dosimetric predictors of asymptomatic heart valvular dysfunction following mediastinal irradiation for Hodgkin's lymphoma. *Radiother. Oncol.* **2011**, *101*, 316–321. [CrossRef]
20. Gujral, D.M.; Lloyd, G.; Bhattacharyya, S. Radiation-induced valvular heart disease. *Heart* **2016**, *102*, 269–276. [CrossRef]
21. Schellong, G.; Riepenhausen, M.; Bruch, C.; Kotthoff, S.; Vogt, J.; Bölling, T.; Dieckmann, K.; Pötter, R.; Heinecke, A.; Brämswig, J.; et al. Late valvular and other cardiac diseases after different doses of mediastinal radiotherapy for hodgkin disease in children and adolescents: Report from the longitudinal GPOH follow-up project of the German-Austrian DAL-HD studies. *Pediatr. Blood Cancer* **2010**, *55*, 1145–1152. [CrossRef]
22. van der Pal, H.J.; van Dijk, I.W.; Geskus, R.B.; Kok, W.E.; Koolen, M.; Sieswerda, E.; Oldenburger, F.; Koning, C.C.; van Leeuwen, F.E.; Caron, H.N.; et al. Valvular abnormalities detected by echocardiography in 5-year survivors of childhood cancer: A long-term follow-up study. *Int. J. Radiat. Oncol. Biol. Phys.* **2015**, *91*, 213–222. [CrossRef]
23. Bates, J.E.; Howell, R.M.; Liu, Q.; Yasui, Y.; Mulrooney, D.A.; Dhakal, S.; Smith, S.A.; Leisenring, W.M.; Indelicato, D.J.; Gibson, T.M.; et al. Therapy-Related Cardiac Risk in Childhood Cancer Survivors: An Analysis of the Childhood Cancer Survivor Study. *J. Clin. Oncol.* **2019**, *37*, 1090–1101. [CrossRef]
24. Galper, S.L.; Yu, J.B.; Mauch, P.M.; Strasser, J.F.; Silver, B.; LaCasce, A.; Marcus, K.J.; Stevenson, M.A.; Chen, M.H.; Ng, A.K. Clinically significant cardiac disease in patients with Hodgkin lymphoma treated with mediastinal irradiation. *Blood* **2011**, *117*, 412–418. [CrossRef] [PubMed]
25. Shrestha, S.; Bates, J.E.; Liu, Q.; Smith, S.A.; Oeffinger, K.C.; Chow, E.J.; Gupta, A.C.; Owens, C.A.; Constine, L.S.; Hoppe, B.S.; et al. Radiation therapy related cardiac disease risk in childhood cancer survivors: Updated dosimetry analysis from the Childhood Cancer Survivor Study. *Radiother. Oncol.* **2021**, *163*, 199–208. [CrossRef] [PubMed]
26. Yang, S.S.; OuYang, P.Y.; Guo, J.G.; Cai, J.J.; Zhang, J.; Peng, Q.H.; He, Y.; Zhang, B.Y.; Liu, Z.Q.; Hu, X.F.; et al. Dosiomics Risk Model for Predicting Radiation Induced Temporal Lobe Injury and Guiding Individual Intensity Modulated Radiation Therapy. *Int. J. Radiat. Oncol. Biol. Phys.* **2022**, *115*, S0360301622036057. [CrossRef] [PubMed]
27. Liang, B.; Yan, H.; Tian, Y.; Chen, X.; Yan, L.; Zhang, T.; Zhou, Z.; Wang, L.; Dai, J. Dosiomics: Extracting 3D Spatial Features from Dose Distribution to Predict Incidence of Radiation Pneumonitis. *Front. Oncol.* **2019**, *9*, 269. [CrossRef] [PubMed]
28. Wu, A.; Li, Y.; Qi, M.; Lu, X.; Jia, Q.; Guo, F.; Dai, Z.; Liu, Y.; Chen, C.; Zhou, L.; et al. Dosiomics improves prediction of locoregional recurrence for intensity modulated radiotherapy treated head and neck cancer cases. *Oral Oncol.* **2020**, *104*, 104625. [CrossRef]
29. Ren, W.; Liang, B.; Sun, C.; Wu, R.; Men, K.; Xu, Y.; Han, F.; Yi, J.; Qu, Y.; Dai, J. Dosiomics-based prediction of radiation-induced hypothyroidism in nasopharyngeal carcinoma patients. *Phys. Medica* **2021**, *89*, 219–225. [CrossRef]
30. Murakami, Y.; Soyano, T.; Kozuka, T.; Ushijima, M.; Koizumi, Y.; Miyauchi, H.; Kaneko, M.; Nakano, M.; Kamima, T.; Hashimoto, T.; et al. Dose-Based Radiomic Analysis (Dosiomics) for Intensity Modulated Radiation Therapy in Patients with Prostate Cancer: Correlation Between Planned Dose Distribution and Biochemical Failure. *Int. J. Radiat. Oncol.* **2022**, *112*, 247–259. [CrossRef]
31. ICCC. Third Edition (ICD-O-3), Main Classification Table-SEER Recodes. 2022. Available online: https://seer.cancer.gov/iccc/iccc3.html (accessed on 28 February 2023).
32. Mansouri, I.; Allodji, R.S.; Hill, C.; El-Fayech, C.; Pein, F.; Diallo, S.; Schwartz, B.; Vu-Bezin, G.; Veres, C.; Souchard, V.; et al. The role of irradiated heart and left ventricular volumes in heart failure occurrence after childhood cancer. *Eur. J. Heart Fail.* **2019**, *21*, 509–518. [CrossRef]
33. Allodji, R.S.; Haddy, N.; Vu-Bezin, G.; Dumas, A.; Fresneau, B.; Mansouri, I.; Demoor-Goldschmidt, C.; El-Fayech, C.; Pacquement, H.; Munzer, M.; et al. Risk of subsequent colorectal cancers after a solid tumor in childhood: Effects of radiation therapy and chemotherapy. *Pediatr. Blood Cancer* **2019**, *66*, e27495. [CrossRef]
34. Journy, N.M.Y.; Zrafi, W.S.; Bolle, S.; Fresneau, B.; Alapetite, C.; Allodji, R.S.; Berchery, D.; Haddy, N.; Kobayashi, I.; Labbé, M.; et al. Risk Factors of Subsequent Central Nervous System Tumors after Childhood and Adolescent Cancers: Findings from the French Childhood Cancer Survivor Study. *Cancer Epidemiol. Biomark. Prev.* **2021**, *30*, 133–141. [CrossRef]
35. Accueil CépiDc. 2022. Available online: https://www.cepidc.inserm.fr/ (accessed on 28 February 2023).
36. *Système National D'information Inter-Régimes de l'Assurance Maladie;* Caisse Nationale De L'assurance Maladie Des Travailleurs Salaries: Paris, France, 2022. Available online: https://www.snds.gouv.fr/SNDS/Open-Data (accessed on 28 February 2023).

37. *Common Terminology Criteria for Adverse Events (CTCAE)*; U.S. Department of Health and Human Services: Washington, DC, USA; National Institutes of Health, National Cancer Institute: Bethesda, Maryland, 2009; p. 196.
38. Taylor, N.; Absolom, K.; Michel, G.; Urquhart, T.; Gerrard, M.; Jenkins, A.; Lee, V.; Vora, A.; Eiser, C. Comparison of self-reported late effects with medical records among survivors of childhood cancer. *Eur. J. Cancer* **2010**, *46*, 1069–1078. [CrossRef] [PubMed]
39. Veres, C.; Allodji, R.S.; Llanas, D.; Vu Bezin, J.; Chavaudra, J.; Mège, J.P.; Lefkopoulos, D.; Quiniou, E.; Deutsh, E.; de Vathaire, F.; et al. Retrospective Reconstructions of Active Bone Marrow Dose-Volume Histograms. *Int. J. Radiat. Oncol.* **2014**, *90*, 1216–1224. [CrossRef] [PubMed]
40. Diallo, I.; Lamon, A.; Shamsaldin, A.; Grimaud, E.; de Vathaire, F.; Chavaudra, J. Estimation of the radiation dose delivered to any point outside the target volume per patient treated with external beam radiotherapy. *Radiother. Oncol.* **1996**, *38*, 269–271. [CrossRef] [PubMed]
41. Zwanenburg, A.; Vallières, M.; Abdalah, M.A.; Aerts, H.J.W.L.; Andrearczyk, V.; Apte, A.; Ashrafinia, S.; Bakas, S.; Beukinga, R.J.; Boellaard, R.; et al. The image biomarker standardization initiative: Standardized quantitative radiomics for high-throughput image-based phenotyping. *Radiology* **2020**, *295*, 328–338. [CrossRef]
42. van Griethuysen, J.J.; Fedorov, A.; Parmar, C.; Hosny, A.; Aucoin, N.; Narayan, V.; Beets-Tan, R.G.; Fillion-Robin, J.C.; Pieper, S.; Aerts, H.J. Computational Radiomics System to Decode the Radiographic Phenotype. *Cancer Res.* **2017**, *77*, e104–e107. [CrossRef]
43. Freedman, D.; Diaconis, P. On the histogram as a density estimator: L2 theory. *Z. Für Wahrscheinlichkeitstheorie Verwandte Geb.* **1981**, *57*, 453–476. [CrossRef]
44. Chen, C.; Liaw, A.; Breiman, L. *Using Random Forest to Learn Imbalanced Data;* Technical Report 666; Department of Statistics: Berkley, CA, USA, 2004.
45. Shan, G. Monte Carlo cross-validation for a study with binary outcome and limited sample size. *BMC Med. Inform. Decis. Mak.* **2022**, *22*, 270. [CrossRef]
46. Zou, H.; Hastie, T. Regularization and variable selection via the elastic net. *J. R. Stat. Soc. Ser. B Stat. Methodol.* **2005**, *67*, 301–320. [CrossRef]
47. Dkengne Sielenou, P.; Viallon-Galinier, L.; Hagenmuller, P.; Naveau, P.; Morin, S.; Dumont, M.; Verfaillie, D.; Eckert, N. Combining random forests and class-balancing to discriminate between three classes of avalanche activity in the French Alps. *Cold Reg. Sci. Technol.* **2021**, *187*, 103276. [CrossRef]
48. McKinney, W. Data Structures for Statistical Computing in Python. In Proceedings of the 9th Python in Science Conference 2010 (SciPy 2010), Austin, TX, USA, 28 June–3 July 2010. Available online: https://conference.scipy.org/proceedings/scipy2010/mckinney.html (accessed on 28 February 2023).
49. Harris, C.R.; Millman, K.J.; van der Walt, S.J.; Gommers, R.; Virtanen, P.; Cournapeau, D.; Wieser, E.; Taylor, J.; Berg, S.; Smith, N.J.; et al. Array programming with NumPy. *Nature* **2020**, *585*, 357–362. [CrossRef]
50. Waskom, M.L. seaborn: Statistical data visualization. *J. Open Source Softw.* **2021**, *6*, 3021. [CrossRef]
51. Hunter, J.D. Matplotlib: A 2D graphics environment. *Comput. Sci. Eng.* **2007**, *9*, 90–95. [CrossRef]
52. Pedregosa, F.; Varoquaux, G.; Gramfort, A.; Michel, V.; Thirion, B.; Grisel, O.; Blondel, M.; Prettenhofer, P.; Weiss, R.; Dubourg, V.; et al. Scikit-learn: Machine Learning in Python. *J. Mach. Learn. Res.* **2011**, *12*, 2825–2830.
53. Lemaître, G.; Nogueira, F.; Aridas, C.K. Imbalanced-learn: A Python Toolbox to Tackle the Curse of Imbalanced Datasets in Machine Learning. *J. Mach. Learn. Res.* **2017**, *18*, 1–5.
54. Patil, S.; Pingle, S.R.; Shalaby, K.; Kim, A.S. Mediastinal irradiation and valvular heart disease. *Cardio-Oncol.* **2022**, *8*, 7. [CrossRef]
55. Menezes, K.M.; Wang, H.; Hada, M.; Saganti, P.B. Radiation matters of the heart: A mini review. *Front. Cardiovasc. Med.* **2018**, *5*, 83. [CrossRef]
56. Placidi, L.; Gioscio, E.; Garibaldi, C.; Rancati, T.; Fanizzi, A.; Maestri, D.; Massafra, R.; Menghi, E.; Mirandola, A.; Reggiori, G.; et al. A multicentre evaluation of dosiomics features reproducibility, stability and sensitivity. *Cancers* **2021**, *13*, 3835. [CrossRef]
57. Vũ Bezin, J.; Allodji, R.S.; Mège, J.P.; Beldjoudi, G.; Saunier, F.; Chavaudra, J.; Deutsch, E.; de Vathaire, F.; Bernier, V.; Carrie, C.; et al. A review of uncertainties in radiotherapy dose reconstruction and their impacts on dose-response relationships. *J. Radiol. Prot.* **2017**, *37*, R1–R18. [CrossRef]
58. Alabdoaburas, M. Etude DosiméTrique et ModéLisation des Composantes de la Dose à Distance Pour les Faisceaux D'éLectrons en RadiothéRapie Externe. Ph.D. Thesis, Université Paris-Saclay (ComUE), Paris, France, 2017.
59. Appelt, A.L.; Elhaminia, B.; Gooya, A.; Gilbert, A.; Nix, M. Deep learning for radiotherapy outcome prediction using dose data—A review. *Clin. Oncol. R Coll. Radiol.* **2022**, *34*, e87–e96. [CrossRef]
60. DICOM-NEMA. DICOM in Radiotherapy—dicom.nema.org. 2023. Available online: https://dicom.nema.org/dicom/geninfo/brochure/rtaapm.htm (accessed on 24 April 2023).
61. Dumane, V.A.; Saksornchai, K.; Zhou, Y.; Hong, L.; Powell, S.; Ho, A.Y. Reduction in low-dose to normal tissue with the addition of deep inspiration breath hold (DIBH) to volumetric modulated arc therapy (VMAT) in breast cancer patients with implant reconstruction receiving regional nodal irradiation. *Radiat. Oncol.* **2018**, *13*, 187. [CrossRef]
62. Gomarteli, K.; Fleckenstein, J.; Meyer, M.; Henzler, T.; Kirschner, S.; Kraenzlin, B.; Brockmann, M.A.; Welzel, G.; Glatting, G.; Wenz, F.; et al. Focus on the low-dose bath: No increased cancer risk after mediastinal VMAT versus AP/PA irradiation in a tumor-prone rat model. *Int. J. Radiat. Oncol. Biol. Phys.* **2017**, *99*, S76–S77. [CrossRef]
63. COG Homepage—childrensoncologygroup.org. Available online: https://childrensoncologygroup.org/ (accessed on 16 May 2023).

64. Lyon, A.R.; López-Fernández, T.; Couch, L.S.; Asteggiano, R.; Aznar, M.C.; Bergler-Klein, J.; Boriani, G.; Cardinale, D.; Cordoba, R.; Cosyns, B.; et al. 2022 ESC guidelines on cardio-oncology developed in collaboration with the European hematology association (EHA), the European society for therapeutic radiology and oncology (ESTRO) and the international cardio-oncology society (IC-OS). *Eur. Heart J. Cardiovasc. Imaging* **2022**, *23*, e333–e465. [CrossRef] [PubMed]
65. Novo, G.; Santoro, C.; Manno, G.; Di Lisi, D.; Esposito, R.; Mandoli, G.E.; Evola, V.; Pastore, M.C.; Sperlongano, S.; D'Andrea, A.; et al. Usefulness of stress echocardiography in the management of patients treated with anticancer drugs. *J. Am. Soc. Echocardiogr.* **2021**, *34*, 107–116. [CrossRef] [PubMed]

Disclaimer/Publisher's Note: The statements, opinions and data contained in all publications are solely those of the individual author(s) and contributor(s) and not of MDPI and/or the editor(s). MDPI and/or the editor(s) disclaim responsibility for any injury to people or property resulting from any ideas, methods, instructions or products referred to in the content.

Bibliography

Adibuzzaman, M., DeLaurentis, P., Hill, J., & Benneyworth, B. (2018). Big data in healthcare - the promises, challenges and opportunities from a research perspective: a case study with a model database. *AMIA Annu Symp Proc.*, *2017*(PMCID: PMC5977694.), 384–392.

Alabdoaburas, M. (2017). *Etude dosimétrique et modélisation des composantes de la dose à distance pour les faisceaux d'électrons en radiothérapie externe* (These de doctorat). Université Paris-Saclay (ComUE).

Alziar, I., Bonniaud, G., Couanet, D., Ruaud, J. B., Vicente, C., Giordana, G., Ben-Harrath, O., Diaz, J. C., Grandjean, P., Kafrouni, H., Chavaudra, J., Lefkopoulos, D., de Vathaire, F., & Diallo, I. (2009). Individual radiation therapy patient whole-body phantoms for peripheral dose evaluations: method and specific software. *Phys. Med. Biol.*, *54*(17), N375–83.

Appelt, A. L., Elhaminia, B., Gooya, A., Gilbert, A., & Nix, M. (2022). Deep learning for radiotherapy outcome prediction using dose data - a review. *Clin. Oncol. (R Coll. Radiol.)*, *34*(2), e87–e96.

Armanious, M. A., Mohammadi, H., Khodor, S., Oliver, D. E., Johnstone, P. A., & Fradley, M. G. (2018). Cardiovascular effects of radiation therapy. *Current Problems in Cancer*, *42*(4), 433–442. https://doi.org/10.1016/j.currproblcancer.2018.05.008

Armstrong, G. T., Oeffinger, K. C., Chen, Y., Kawashima, T., Yasui, Y., Leisenring, W., Stovall, M., Chow, E. J., Sklar, C. A., Mulrooney, D. A., Mertens, A. C., Border, W., Durand, J.-B., Robison, L. L., & Meacham, L. R. (2013). Modifiable Risk Factors and Major Cardiac Events Among Adult Survivors of Childhood Cancer. *Journal of Clinical Oncology*, *31*(29), 3673–3680. https://doi.org/10.1200/JCO.2013.49.3205

Bates, J., Howell, R. M., Liu, Q., Yasui, Y., Mulrooney, D. A., Dhakal, S., Smith, S. A., Leisenring, W. M., Indelicato, D. J., Gibson, T. M., Armstrong, G. T., Oeffinger, K. C., & Constine, L. S. (2019). Therapy-Related Cardiac Risk in Childhood Cancer Survivors: An Analysis of the Childhood Cancer Sur-

vivor Study. *Journal of Clinical Oncology*, *37*(13), 1090–1101. https://doi.org/10.1200/JCO.18.01764

Bates, J., Shrestha, S., Liu, Q., Mulrooney, D. A., Smith, S. A., Leisenring, W. M., Gibson, T. M., Chow, E. J., Oeffinger, K. C., Robison, L. L., Armstrong, G. T., Constine, L. S., Hoppe, B., Lee, C., Yasui, Y., & Howell, R. M. (2021). Low-dose radiation to cardiac substructures and late-onset cardiac disease: a report from the childhood cancer survivor study (CCSS). *Journal of Clinical Oncology*, *39*(15_suppl), 10027–10027. https://doi.org/10.1200/jco.2021.39.15_suppl.10027

Bejarano-Quisoboni, D., Pelletier-Fleury, N., Allodji, R. S., Lacour, B., GrosClaude, P., FRANCIM Group, Pacquement, H., Doz, F., Berchery, D., Pluchart, C., Bondiau, P.-Y., Nys, J., Jackson, A., Demoor-Goldschmidt, C., Dumas, A., Thomas-Teinturier, C., Vu-Bezin, G., Valteau-Couanet, D., Haddy, N., … de Vathaire, F. (2022). Health care expenditures among long-term survivors of pediatric solid tumors: results from the french childhood cancer survivor study (FCCSS) and the french network of cancer registries (FRANCIM). *PLoS One*, *17*(5), e0267317.

Benkirane, H., Pradat, Y., Michiels, S., & Cournède, P.-H. (2023). CustOmics: a versatile deep-learning based strategy for multi-omics integration (W. S. Noble, Ed.). *PLOS Computational Biology*, *19*(3), e1010921. https://doi.org/10.1371/journal.pcbi.1010921

Bijl, J. M., Roos, M. M., van Leeuwen-Segarceanu, E. M., Vos, J. M., Bos, W.-J. W., Biesma, D. H., & Post, M. C. (2016). Assessment of Valvular Disorders in Survivors of Hodgkin's Lymphoma Treated by Mediastinal Radiotherapy ± Chemotherapy. *The American Journal of Cardiology*, *117*(4), 691–696. https://doi.org/10.1016/j.amjcard.2015.11.027

Borgan, Ø. (2001). Modeling Survival Data: Extending the Cox Model. Terry M. Therneau and Patricia M. Grambsch, Springer-Verlag, New York, 2000. No. of pages: xiii + 350. Price: $69.95. ISBN 0-387-98784-3 [_eprint: https://onlinelibrary.wiley.c *Statistics in Medicine*, *20*(13), 2053–2054. https://doi.org/10.1002/sim.956

Botta, L., Gatta, G., Capocaccia, R., Stiller, C., Cañete, A., Dal Maso, L., Innos, K., Mihor, A., Erdmann, F., Spix, C., Lacour, B., Marcos-Gragera, R., Murray, D., Rossi, S., & EUROCARE-6 Working Group. (2022). Long-term survival and

cure fraction estimates for childhood cancer in europe (EUROCARE-6): results from a population-based study. *Lancet Oncol.*, *23*(12), 1525–1536.

Breiman, L. (2001). Random forests. *Machine Learning*, *45*(1), 5–32. https://doi.org/10.1023/a:1010933404324

Cancer atlas [[Accessed 21-Mar-2023]]. (2023).

Cancer.gov [[Accessed 21-Mar-2023]]. (2023).

CDC. (2023). Cdc. Retrieved April 21, 2023, from https://www.cdc.gov/nchs/nhis/

Cella, Liuzzi, R., Conson, M., Torre, G., Caterino, M., De Rosa, N., Picardi, M., Camera, L., Solla, R., Farella, A., Salvatore, M., & Pacelli, R. (2011). Dosimetric predictors of asymptomatic heart valvular dysfunction following mediastinal irradiation for Hodgkin's lymphoma. *Radiotherapy and Oncology*, *101*(2), 316–321. https://doi.org/10.1016/j.radonc.2011.08.040

Cella, Oh, Deasy, J. O., Palma, G., Liuzzi, R., D'avino, V., Conson, M., Picardi, M., Salvatore, M., & Pacelli, R. (2015). Predicting radiation-induced valvular heart damage. *Acta Oncologica*, *54*(10), 1796–1804. https://doi.org/10.3109/0284186X.2015.1016624

CépiDC. (n.d.). Retrieved April 16, 2023, from https://www.cepidc.inserm.fr/

Chalise, P., Chicken, E., & McGee, D. (2016). Time Scales in Epidemiological Analysis: An Empirical Comparison. *International Journal of Statistics and Probability*, *5*(3), 91. https://doi.org/10.5539/ijsp.v5n3p91

Chen, C., Liaw, A., & Breiman, L. (2004). *Using random forest to learn imbalanced data* (Technical Report No. 666). Department of Statistics, UC Berkley.

Ching, T., Zhu, X., & Garmire, L. X. (2018). Cox-nnet: an artificial neural network method for prognosis prediction of high-throughput omics data. *PLOS Computational Biology*, *14*(4), 1–18. https://doi.org/10.1371/journal.pcbi.1006076

Chounta, S., Lemler, S., Haddy, N., Fresneau, B., Mansouri, I., Bentriou, M., Demoor-Goldschmidt, C., Diallo, I., Souchard Msc, V., DO Thi, D., Veres, C., Surun, A., Doz, F., LLanas, D., Vu-Bezin, G., Rubino, C., de Vathaire, F., Letort, V., & Allodji, R. S. (2023). The risk of valvular heart disease in the french childhood cancer survivors' study: contribution of dose-volume histogram parameters. *Radiotherapy and Oncology*. https://doi.org/10.1016/j.radonc.2023.109479

Chow, E. J., Chen, Y., Kremer, L. C., Breslow, N. E., Hudson, M. M., Armstrong, G. T., Border, W. L., Feijen, E. A. M., Green, D. M., Meacham, L. R., Meeske, K. A., Mulrooney, D. A., Ness, K. K., Oeffinger, K. C., Sklar, C. A., Stovall, M., van der Pal, H. J., Weathers, R. E., Robison, L. L., & Yasui, Y. (2015). Individual prediction of heart failure among childhood cancer survivors. *J. Clin. Oncol.*, *33*(5), 394–402.

Common Terminology Criteria for Adverse Events (CTCAE) [Version 4.0, Published: May 28, 2009, (v4.03: June 14, 2010)]. (n.d.).

Cox, D. R. (1972). Regression models and life-tables. *J. R. Stat. Soc.*, *34*(2), 187–202.

Cutter, D. J., Schaapveld, M., Darby, S. C., Hauptmann, M., van Nimwegen, F. A., Krol, A. D. G., Janus, C. P. M., van Leeuwen, F. E., & Aleman, B. M. P. (2015). Risk for Valvular Heart Disease After Treatment for Hodgkin Lymphoma. *JNCI: Journal of the National Cancer Institute*, *107*(4). https://doi.org/10.1093/jnci/djv008

Desai, M. Y., Windecker, S., Lancellotti, P., Bax, J. J., Griffin, B. P., Cahlon, O., & Johnston, D. R. (2019). Prevention, diagnosis, and management of radiation-associated cardiac disease: JACC scientific expert panel. *J. Am. Coll. Cardiol.*, *74*(7), 905–927.

Diallo, I., Lamon, A., Shamsaldin, A., Grimaud, E., de Vathaire, F., & Chavaudra, J. (1996). Estimation of the radiation dose delivered to any point outside the target volume per patient treated with external beam radiotherapy. *Radiotherapy and Oncology*, *38*(3), 269–271. https://doi.org/10.1016/0167-8140(96)01713-6

Dkengne Sielenou, P., Viallon-Galinier, L., Hagenmuller, P., Naveau, P., Morin, S., Dumont, M., Verfaillie, D., & Eckert, N. (2021). Combining random forests and class-balancing to discriminate between three classes of avalanche activity in the French Alps. *Cold Regions Science and Technology*, *187*, 103276. https://doi.org/10.1016/j.coldregions.2021.103276

Dumane, V. A., Saksornchai, K., Zhou, Y., Hong, L., Powell, S., & Ho, A. Y. (2018). Reduction in low-dose to normal tissue with the addition of deep inspiration breath hold (DIBH) to volumetric modulated arc therapy (VMAT) in breast cancer patients with implant reconstruction receiving regional nodal irradiation. *Radiat. Oncol.*, *13*(1), 187.

Dumas, A., Berger, C., Auquier, P., Michel, G., Fresneau, B., Allodji, R. S., Haddy, N., Rubino, C., Vassal, G., Valteau-Couanet, D., Thouvenin-Doulet, S., Casagranda, L., Pacquement, H., El-Fayech, C., Oberlin, O., Guibout, C., & de Vathaire, F. (2016). Educational and occupational outcomes of childhood cancer survivors 30 years after diagnosis: a french cohort study. *Br. J. Cancer*, *114*(9), 1060–1068.

The elements of statistical learning: data mining, inference, and prediction, second edition (2nd ed.). (2009). Springer.

The EPICURE Regression Programs. (n.d.). Retrieved July 29, 2021, from http://epicurehelp.risksciences.com/index.html#!Documents/theepicureregressionprograms.htm

Erdmann, F., Frederiksen, L. E., Bonaventure, A., Mader, L., Hasle, H., Robison, L. L., & Winther, J. F. (2021). Childhood cancer: Survival, treatment modalities, late effects and improvements over time. *Cancer Epidemiology*, *71*, 101733. https://doi.org/10.1016/j.canep.2020.101733

Francois, P., Beurtheret, C., Dutreix, A., & De Vathaire, F. (1988). A mathematical child phantom for the calculation of dose to the organs at risk. *Medical Physics*, *15*(3), 328–333. https://doi.org/10.1118/1.596226

Freedman, D., & Diaconis, P. (1981). On the histogram as a density estimator:L2 theory. *Zeitschrift für Wahrscheinlichkeitstheorie und Verwandte Gebiete*, *57*(4), 453–476. https://doi.org/10.1007/BF01025868

Friedman, J., Tibshirani, R., & Hastie, T. (2010). Regularization paths for generalized linear models via coordinate descent. *Journal of Statistical Software*, *33*(1), 1–22. https://doi.org/10.18637/jss.v033.i01

Galper, S. L., Yu, J. B., Mauch, P. M., Strasser, J. F., Silver, B., LaCasce, A., Marcus, K. J., Stevenson, M. A., Chen, M. H., & Ng, A. K. (2011). Clinically significant cardiac disease in patients with Hodgkin lymphoma treated with mediastinal irradiation. *Blood*, *117*(2), 412–418. https://doi.org/10.1182/blood-2010-06-291328

Gebauer, J., Baust, K., Bardi, E., Grabow, D., Stein, A., van der Pal, H. J., Calaminus, G., & Langer, T. (2020). Guidelines for long-term follow-up after childhood cancer: practical implications for the daily work. *Oncol. Res. Treat.*, *43*(3), 61–69.

Gerds, T. A. (2023). *Pec: prediction error curves for risk prediction models in survival analysis* [R package version 2023.04.12]. https://CRAN.R-project.org/package=pec

Gomarteli, K., Fleckenstein, J., Meyer, M., Henzler, T., Kirschner, S., Kraenzlin, B., Brockmann, M. A., Welzel, G., Glatting, G., Wenz, F., Herskind, C., & Giordano, F. A. (2017). Focus on the low-dose bath: no increased cancer risk after mediastinal VMAT versus AP/PA irradiation in a tumor-prone rat model. *Int. J. Radiat. Oncol. Biol. Phys.*, *99*(2), S76–S77.

Grabow, D., Kaiser, M., Hjorth, L., Byrne, J., Alessi, D., Allodji, R. S., Bagnasco, F., Bárdi, E., Bautz, A., Bright, C. J., de Vathaire, F., Feijen, E. A. M., Garwicz, S., Hagberg, O., Haupt, R., Hawkins, M. M., Jakab, Z., Kremer, L. C. M., Kuehni, C. E., … PanCareSurFup Consortium. (2018). The PanCareSurFup cohort of 83,333 five-year survivors of childhood cancer: a cohort from 12 european countries. *Eur. J. Epidemiol.*, *33*(3), 335–349.

Grambsch, P. M., & Therneau, T. M. (1994). Proportional hazards tests and diagnostics based on weighted residuals. *Biometrika*, *81*(3), 515–526. https://doi.org/10.1093/biomet/81.3.515

Gujral, D. M., Lloyd, G., & Bhattacharyya, S. (2016). Radiation-induced valvular heart disease. *Heart*, *102*(4), 269–276. https://doi.org/10.1136/heartjnl-2015-308765

Haddy, N., Diallo, S., El-Fayech, C., Schwartz, B., Pein, F., Hawkins, M., Veres, C., Oberlin, O., Guibout, C., Pacquement, H., Munzer, M., N'Guyen, T. D., Bondiau, P.-Y., Berchery, D., Laprie, A., Scarabin, P.-Y., Jouven, X., Bridier, A., Koscielny, S., … de Vathaire, F. (2016). Cardiac Diseases Following Childhood Cancer Treatment: Cohort Study. *Circulation*, *133*(1), 31–38. https://doi.org/10.1161/CIRCULATIONAHA.115.016686

Harrell, F. E., Jr, Califf, R. M., Pryor, D. B., Lee, K. L., & Rosati, R. A. (1982). Evaluating the yield of medical tests. *JAMA*, *247*(18), 2543–2546.

Harris, C. R., Millman, K. J., van der Walt, S. J., Gommers, R., Virtanen, P., Cournapeau, D., Wieser, E., Taylor, J., Berg, S., Smith, N. J., Kern, R., Picus, M., Hoyer, S., van Kerkwijk, M. H., Brett, M., Haldane, A., del Rio, J. F., Wiebe, M., Peterson, P., … Oliphant, T. E. (2020). Array programming with NumPy. *Nature*, *585*(7825), 357–362. https://doi.org/10.1038/s41586-020-2649-2

Hau, E. M., Caccia, J. N., Kasteler, R., Spycher, B., Suter, T., Ammann, R. A., von der Weid, N. X., & Kuehni, C. E. (2019). Cardiovascular disease after childhood acute lymphoblastic leukaemia: a cohort study. *Swiss Medical Weekly*. https://doi.org/10.4414/smw.2019.20012

Health Risks from Exposure to Low Levels of Ionizing Radiation: BEIR VII Phase 2 [Pages: 11340]. (2006). National Academies Press. https://doi.org/10.17226/11340

Henson, K. (2016). Cardiac Mortality Among 200000 Five-Year Survivors of Cancer Diagnosed at 15 to 39 Years of Age | Circulation. *Circulation*, *134*(20).

Hjorth, L., Haupt, R., Skinner, R., Grabow, D., Byrne, J., Karner, S., Levitt, G., Michel, G., van der Pal, H., Bárdi, E., Beck, J. D., de Vathaire, F., Essig, S., Frey, E., Garwicz, S., Hawkins, M., Jakab, Z., Jankovic, M., Kazanowska, B., … PanCare Network. (2015). Survivorship after childhood cancer: PanCare: a european network to promote optimal long-term care. *Eur. J. Cancer*, *51*(10), 1203–1211.

Hoppe, B. S., Flampouri, S., Su, Z., Latif, N., Dang, N. H., Lynch, J., Joyce, M., Sandler, E., Li, Z., & Mendenhall, N. P. (2012). Effective Dose Reduction to Cardiac Structures Using Protons Compared With 3DCRT and IMRT in Mediastinal Hodgkin Lymphoma. *International Journal of Radiation Oncology*Biology*Physics*, *84*(2), 449–455. https://doi.org/10.1016/j.ijrobp.2011.12.034

Hudson, M. M., Bhatia, S., Casillas, J., Landier, W., & SECTION ON HEMATOLOGY/ONCOLOGY, CHILDREN'S ONCOLOGY GROUP, AMERICAN SOCIETY OF PEDIATRIC HEMATOLOGY/ONCOLOGY. (2021). Long-term follow-up care for childhood, adolescent, and young adult cancer survivors. *Pediatrics*, *148*(3), e–2021053127.

Hunter, J. D. (2007). Matplotlib: a 2d graphics environment. *Computing in Science & Engineering*, *9*(3), 90–95. https://doi.org/10.1109/MCSE.2007.55

ICCC, Third Edition (ICD-O-3), Main Classification Table - SEER Recodes. (n.d.). Retrieved February 21, 2022, from https://seer.cancer.gov/iccc/iccc3.html

ICRPaedia [[Accessed 21-Mar-2023]]. (2023).

Institut curie [[Accessed 21-Mar-2023]]. (2023).

Institut national du cancer [[Accessed 21-Mar-2023]]. (2023).

Institute of Medicine (US) and National Research Council (US) National Cancer Policy Board. (2003). *Childhood Cancer Survivorship: Improving Care and Quality of Life* (M. Hewitt, S. L. Weiner, & J. V. Simone, Eds.). National Academies Press (US).

Jolliffe, I. T. (2013). *Principal component analysis* (1986th ed.). Springer.

Kaplan, E. L., & Meier, P. (1958). Nonparametric Estimation from Incomplete Observations [Publisher: [American Statistical Association, Taylor & Francis, Ltd.]]. *Journal of the American Statistical Association*, *53*(282), 457–481. https://doi.org/10.2307/2281868

Kovalchik, S. A., Ronckers, C. M., Veiga, L. H. S., Sigurdson, A. J., Inskip, P. D., de Vathaire, F., Sklar, C. A., Donaldson, S. S., Anderson, H., Bhatti, P., Hammond, S., Leisenring, W. M., Mertens, A. C., Smith, S. A., Stovall, M., Tucker, M. A., Weathers, R. E., Robison, L. L., & Pfeiffer, R. M. (2013). Absolute risk prediction of second primary thyroid cancer among 5-year survivors of childhood cancer. *J. Clin. Oncol.*, *31*(1), 119–127.

Landier, W., Skinner, R., Wallace, W. H., Hjorth, L., Mulder, R. L., Wong, F. L., Yasui, Y., Bhakta, N., Constine, L. S., Bhatia, S., Kremer, L. C., & Hudson, M. M. (2018). Surveillance for Late Effects in Childhood Cancer Survivors. *Journal of Clinical Oncology*, *36*(21), 2216–2222. https://doi.org/10.1200/JCO.2017.77.0180

Le, S., Josse, J., & Husson, F. (2008). Factominer: anrpackage for multivariate analysis. *J. Stat. Softw.*, *25*(1).

Lê, S., Josse, J., & Husson, F. (2008). FactoMineR: a package for multivariate analysis. *Journal of Statistical Software*, *25*(1), 1–18. https://doi.org/10.18637/jss.v025.i01

LEATT. (2023). Late Effects Assessment — leatt.thenccs.org [[Accessed 24-Apr-2023]].

Leerink, J. M., de Baat, E. C., Feijen, E. A., Bellersen, L., van Dalen, E. C., Grotenhuis, H. B., Kapusta, L., Kok, W. E., Loonen, J., van der Pal, H. J., Pluijm, S. M., Teske, A. J., Mavinkurve-Groothuis, A. M., Merkx, R., & Kremer, L. C. (2020). Cardiac Disease in Childhood Cancer Survivors. *JACC: CardioOncology*, *2*(3), 363–378. https://doi.org/10.1016/j.jaccao.2020.08.006

Lemaître, G., Nogueira, F., & Aridas, C. K. (2017). Imbalanced-learn: a python toolbox to tackle the curse of imbalanced datasets in machine learning. *Journal of Machine Learning Research*, *18*(17), 1–5.

Liang, B., Yan, H., Tian, Y., Chen, X., Yan, L., Zhang, T., Zhou, Z., Wang, L., & Dai, J. (2019). Dosiomics: Extracting 3D Spatial Features From Dose Distribution to Predict Incidence of Radiation Pneumonitis. *Frontiers in Oncology*, *9*, 269. https://doi.org/10.3389/fonc.2019.00269

Liaw, A., & Wiener, M. (2002). Classification and regression by randomforest. *R News*, *2*(3), 18–22. https://CRAN.R-project.org/doc/Rnews/

Mansouri, I., Allodji, R. S., Hill, C., El-Fayech, C., Pein, F., Diallo, S., Schwartz, B., Vu-Bezin, G., Veres, C., Souchard, V., Dumas, A., Bolle, S., Thomas-Teinturier, C., Pacquement, H., Munzer, M., Bondiau, P.-Y., Berchery, D., Fresneau, B., Oberlin, O., … Haddy, N. (2019). The role of irradiated heart and left ventricular volumes in heart failure occurrence after childhood cancer. *European Journal of Heart Failure*, *21*(4), 509–518. https://doi.org/10.1002/ejhf.1376

Matta, A., & Moussallem, N. (2019). Coronary artery disease is associated with valvular heart disease, but could it be a predictive factor? *Indian Heart J.*, *71*(3), 284–287.

McCullagh, P., & Nelder, J. A. (1983). *Generalized linear models* (1983rd ed.). Chapman; Hall.

Menezes, K. M., Wang, H., Hada, M., & Saganti, P. B. (2018). Radiation matters of the heart: a mini review. *Front. Cardiovasc. Med.*, *5*, 83.

Michel, G., Mulder, R. L., van der Pal, H. J. H., Skinner, R., Bárdi, E., Brown, M. C., Vetsch, J., Frey, E., Windsor, R., Kremer, L. C. M., & Levitt, G. (2019). Evidence-based recommendations for the organization of long-term follow-up care for childhood and adolescent cancer survivors: a report from the PanCareSurFup guidelines working group. *J. Cancer Surviv.*, *13*(5), 759–772.

Mogensen, U. B., Ishwaran, H., & Gerds, T. A. (2012). Evaluating random forests for survival analysis using prediction error curves. *Journal of Statistical Software*, *50*(11), 1–23. https://doi.org/10.18637/jss.v050.i11

Monte, I. P., Cameli, M., Losi, V., Privitera, F., & Citro, R. (2020). Valvular Damage. *Journal of Cardiovascular Echography*, *30*(Suppl 1), S26–S32. https://doi.org/10.4103/jcecho.jcecho_5_19

Mulrooney, D. A., Yeazel, M. W., Kawashima, T., Mertens, A. C., Mitby, P., Stovall, M., Donaldson, S. S., Green, D. M., Sklar, C. A., Robison, L. L., & Leisenring, W. M. (2009). Cardiac outcomes in a cohort of adult survivors of childhood and adolescent cancer: retrospective analysis of the Childhood Cancer Survivor Study cohort. *BMJ*, *339*(dec08 1), b4606–b4606. https://doi.org/10.1136/bmj.b4606

Mulrooney, D. A., Hyun, G., Ness, K. K., Ehrhardt, M. J., Yasui, Y., Duprez, D., Howell, R. M., Leisenring, W. M., Constine, L. S., Tonorezos, E., Gibson, T. M., Robison, L. L., Oeffinger, K. C., Hudson, M. M., & Armstrong, G. T. (2020). Major cardiac events for adult survivors of childhood cancer diagnosed between 1970 and 1999: report from the Childhood Cancer Survivor Study cohort. *BMJ*, l6794. https://doi.org/10.1136/bmj.l6794

Murakami, Y., Soyano, T., Kozuka, T., Ushijima, M., Koizumi, Y., Miyauchi, H., Kaneko, M., Nakano, M., Kamima, T., Hashimoto, T., Yoshioka, Y., & Oguchi, M. (2022). Dose-Based Radiomic Analysis (Dosiomics) for Intensity Modulated Radiation Therapy in Patients With Prostate Cancer: Correlation Between Planned Dose Distribution and Biochemical Failure. *International Journal of Radiation Oncology*Biology*Physics*, *112*(1), 247–259. https://doi.org/10.1016/j.ijrobp.2021.07.1714

Nadlonek, N. A., Weyant, M. J., Yu, J. A., Cleveland, J. C., Reece, T. B., Meng, X., & Fullerton, D. A. (2012). Radiation induces osteogenesis in human aortic valve interstitial cells. *The Journal of Thoracic and Cardiovascular Surgery*, *144*(6), 1466–1470. https://doi.org/10.1016/j.jtcvs.2012.08.041

Nathan, P. C., Amir, E., & Abdel-Qadir, H. (2016). Cardiac Outcomes in Survivors of Pediatric and Adult Cancers. *Canadian Journal of Cardiology*, *32*(7), 871–880. https://doi.org/10.1016/j.cjca.2016.02.065

NEMA, D. (2023). DICOM IN RADIOTHERAPY — dicom.nema.org [[Accessed 24-Apr-2023]].

Olsen, M., Schmidt, M., Lash, T. L., Sorensen, K., Pedersen, L., & Sorensen, H. T. (2014). Cardiovascular Disease Risk in Childhood Cancer Survivors. *Amer-*

ican Journal of Epidemiology, *180*(1), 120–123. https://doi.org/10.1093/aje/kwu144

PanCareSurFup [[Accessed 12-Apr-2023]]. (2023).

pandas development team, T. (2020). *Pandas-dev/pandas: pandas* (Version latest). Zenodo. https://doi.org/10.5281/zenodo.3509134

Patil, S., Pingle, S.-R., Shalaby, K., & Kim, A. S. (2022). Mediastinal irradiation and valvular heart disease. *Cardio-Oncology*, *8*(1), 7. https://doi.org/10.1186/s40959-022-00133-2

Pedregosa, F., Varoquaux, G., Gramfort, A., Michel, V., Thirion, B., Grisel, O., Blondel, M., Prettenhofer, P., Weiss, R., Dubourg, V., Vanderplas, J., Passos, A., Cournapeau, D., Brucher, M., Perrot, M., & Duchesnay, E. (2011). Scikit-learn: machine learning in Python. *Journal of Machine Learning Research*, *12*, 2825–2830.

Placidi, L., Gioscio, E., Garibaldi, C., Rancati, T., Fanizzi, A., Maestri, D., Massafra, R., Menghi, E., Mirandola, A., Reggiori, G., Sghedoni, R., Tamborra, P., Comi, S., Lenkowicz, J., Boldrini, L., & Avanzo, M. (2021). A multicentre evaluation of dosiomics features reproducibility, stability and sensitivity. *Cancers (Basel)*, *13*(15).

Pradat, Y., Viot, J., Yurchenko, A. A., Gunbin, K., Cerbone, L., Deloger, M., Grisay, G., Verlingue, L., Scott, V., Padioleau, I., Panunzi, L., Michiels, S., Hollebecque, A., Jules-Clément, G., Mezquita, L., Lainé, A., Loriot, Y., Besse, B., Friboulet, L., … Nikolaev, S. I. (2023). Integrative pan-cancer genomic and transcriptomic analyses of refractory metastatic cancer. *Cancer Discovery*, *13*(5), 1116–1143. https://doi.org/10.1158/2159-8290.cd-22-0966

Ren, W., Liang, B., Sun, C., Wu, R., Men, K., Xu, Y., Han, F., Yi, J., Qu, Y., & Dai, J. (2021). Dosiomics-based prediction of radiation-induced hypothyroidism in nasopharyngeal carcinoma patients. *Physica Medica*, *89*, 219–225. https://doi.org/10.1016/j.ejmp.2021.08.009

Rnce. (n.d.). Retrieved June 9, 2022, from https://rnce.inserm.fr/index.php/en/statistiques/survie/taux-de-survie-a-5-ans-sur-la-periode-2000-2014-par-groupe-diagnostique-et-sexe/2-uncategorised/35-5-year-overall-survival-rates-of-childhood-cancer-in-mainland-france-over-2000-2014-by-diagnostic-and-age-groups

Roblin, E. (2019). *Développements des réseaux de neurones pour données censurées: prédiction de survie associée à une mesure d'incertitude et recommandation de traitement* (These en préparation). université Paris-Saclay.

Schellong, G., Riepenhausen, M., Bruch, C., Kotthoff, S., Vogt, J., Bölling, T., Dieckmann, K., Pötter, R., Heinecke, A., Brämswig, J., & Dörffel, W. (2010). Late valvular and other cardiac diseases after different doses of mediastinal radiotherapy for hodgkin disease in children and adolescents: Report from the longitudinal GPOH follow-up project of the German-Austrian DAL-HD studies. *Pediatric Blood & Cancer*, *55*(6), 1145–1152. https://doi.org/10.1002/pbc.22664

SEER Cancer Statistics Review. (n.d.). Retrieved December 16, 2020, from https://seer.cancer.gov/archive/csr/1975_2015/index.html

Shomal Zadeh, N., Lin, S., & Runger, G. C. (2020). Matched forest: supervised learning for high-dimensional matched case-control studies. *Bioinformatics*, *36*(5), 1570–1576.

Shrestha, S., Bates, J. E., Liu, Q., Smith, S. A., Oeffinger, K. C., Chow, E. J., Gupta, A. C., Owens, C. A., Constine, L. S., Hoppe, B. S., Leisenring, W. M., Qiao, Y., Weathers, R. E., Court, L. E., Pinnix, C. C., Kry, S. F., Mulrooney, D. A., Armstrong, G. T., Yasui, Y., & Howell, R. M. (2021). Radiation therapy related cardiac disease risk in childhood cancer survivors: Updated dosimetry analysis from the Childhood Cancer Survivor Study [Publisher: Elsevier]. *Radiotherapy and Oncology*, *163*, 199–208. https://doi.org/10.1016/j.radonc.2021.08.012

Simon, N., Friedman, J., Tibshirani, R., & Hastie, T. (2011). Regularization paths for cox's proportional hazards model via coordinate descent. *Journal of Statistical Software*, *39*(5), 1–13. https://doi.org/10.18637/jss.v039.i05

St jude children's research hospital [[Accessed 21-Mar-2023]]. (2023).

Suissa, S. (1999). Relative Excess Risk: An Alternative Measure of Comparative Risk. *American Journal of Epidemiology*, *150*(3), 279–282. https://doi.org/10.1093/oxfordjournals.aje.a009999

Système national d'information inter-régimes de l'Assurance maladie [Page Version ID: 192159863]. (2022). Retrieved May 16, 2022, from https://www.snds.gouv.fr/SNDS/Open-Data

Tay, J. K., Narasimhan, B., & Hastie, T. (2023). Elastic net regularization paths for all generalized linear models. *Journal of Statistical Software*, *106*(1), 1–31. https://doi.org/10.18637/jss.v106.i01

Taylor, N., Absolom, K., Michel, G., Urquhart, T., Gerrard, M., Jenkins, A., Lee, V., Vora, A., & Eiser, C. (2010). Comparison of self-reported late effects with medical records among survivors of childhood cancer. *European Journal of Cancer*, *46*(6), 1069–1078. https://doi.org/10.1016/j.ejca.2010.01.022

Therneau, T. M. (2023). *A package for survival analysis in r* [R package version 3.5-5]. https://CRAN.R-project.org/package=survival

Therneau, T. M., until 2009), T. L. (S.->. p. a. R. m., Elizabeth, A., & Cynthia, C. (2021). Survival: Survival Analysis. Retrieved July 26, 2021, from https://CRAN.R-project.org/package=survival

Tibshirani, R. (1996). Regression shrinkage and selection via the lasso. *J. R. Stat. Soc.*, *58*(1), 267–288.

(UK), O. (2023). Childhood cancer survival in England - Office for National Statistics. Retrieved April 20, 2023, from https://www.ons.gov.uk/

Van Craenendonck, T., & Blockeel, H. (2015). Using internal validity measures to compare clustering algorithms.

van der Pal, H. J., van Dijk, I. W., Geskus, R. B., Kok, W. E., Koolen, M., Sieswerda, E., Oldenburger, F., Koning, C. C., van Leeuwen, F. E., Caron, H. N., Kremer, L. C., & van Dalen, E. C. (2015a). Valvular abnormalities detected by echocardiography in 5-year survivors of childhood cancer: a long-term follow-up study. *Int. J. Radiat. Oncol. Biol. Phys.*, *91*(1), 213–222.

van der Pal, H. J., van Dijk, I. W., Geskus, R. B., Kok, W. E., Koolen, M., Sieswerda, E., Oldenburger, F., Koning, C. C., van Leeuwen, F. E., Caron, H. N., Kremer, L. C., & van Dalen, E. C. (2015b). Valvular abnormalities detected by echocardiography in 5-year survivors of childhood cancer: a long-term follow-up study. *International Journal of Radiation Oncology, Biology, Physics*, *91*(1), 213–222. https://doi.org/10.1016/j.ijrobp.2014.09.010

van Griethuysen, J. J., Fedorov, A., Parmar, C., Hosny, A., Aucoin, N., Narayan, V., Beets-Tan, R. G., Fillion-Robin, J.-C., Pieper, S., & Aerts, H. J. (2017). Computational Radiomics System to Decode the Radiographic Phenotype. *Can-*

cer Research, *77*(21), e104–e107. https://doi.org/10.1158/0008-5472.CAN-17-0339

van Kalsbeek, R. J., van der Pal, H. J. H., Kremer, L. C. M., Bardi, E., Brown, M. C., Effeney, R., Winther, J. F., Follin, C., den Hartogh, J., Haupt, R., Hjorth, L., Kepak, T., Kepakova, K., Levitt, G., Loonen, J. J., Mangelschots, M., Muraca, M., Renard, M., Sabic, H., … Mulder, R. L. (2021). European PanCareFollowUp recommendations for surveillance of late effects of childhood, adolescent, and young adult cancer. *Eur. J. Cancer*, *154*, 316–328.

van Kalsbeek, R. J., van der Pal, H. J., Kremer, L. C., Bardi, E., Brown, M. C., Effeney, R., Winther, J. F., Follin, C., den Hartogh, J., Haupt, R., Hjorth, L., Kepak, T., Kepakova, K., Levitt, G., Loonen, J. J., Mangelschots, M., Muraca, M., Renard, M., Sabic, H., … Mulder, R. L. (2021). European PanCareFollowUp Recommendations for surveillance of late effects of childhood, adolescent, and young adult cancer. *European Journal of Cancer*, *154*, 316–328. https://doi.org/10.1016/j.ejca.2021.06.004

van Nimwegen, F. A., Schaapveld, M., Janus, C. P. M., Krol, A. D. G., Petersen, E. J., Raemaekers, J. M. M., Kok, W. E. M., Aleman, B. M. P., & van Leeuwen, F. E. (2015). Cardiovascular Disease After Hodgkin Lymphoma Treatment: 40-Year Disease Risk. *JAMA Internal Medicine*, *175*(6), 1007. https://doi.org/10.1001/jamainternmed.2015.1180

Veinot, J. P., & Edwards, W. D. (1996). Pathology of radiation-induced heart disease: A surgical and autopsy study of 27 cases. *Human Pathology*, *27*(8), 766–773. https://doi.org/10.1016/S0046-8177(96)90447-5

Veres, C., Allodji, R. S., Llanas, D., Vu Bezin, J., Chavaudra, J., Mège, J. P., Lefkopoulos, D., Quiniou, E., Deutsh, E., de Vathaire, F., & Diallo, I. (2014). Retrospective Reconstructions of Active Bone Marrow Dose-Volume Histograms. *International Journal of Radiation Oncology*Biology*Physics*, *90*(5), 1216–1224. https://doi.org/10.1016/j.ijrobp.2014.08.335

Vũ Bezin, J. (2015). *Optimisation et validation des méthodes de calcul de dose à distance des faisceaux d'irradiation pour leur application dans les études épidémiologiques et cliniques en radiothérapie* (These de doctorat). Université Paris-Saclay (ComUE).

Vũ Bezin, J., Allodji, R. S., Mège, J.-P., Beldjoudi, G., Saunier, F., Chavaudra, J., Deutsch, E., de Vathaire, F., Bernier, V., Carrie, C., Lefkopoulos, D., & Diallo, I. (2017). A review of uncertainties in radiotherapy dose reconstruction and their impacts on dose-response relationships. *Journal of Radiological Protection: Official Journal of the Society for Radiological Protection*, *37*(1), R1–R18. https://doi.org/10.1088/1361-6498/aa575d

Waskom, M. L. (2021). Seaborn: statistical data visualization. *Journal of Open Source Software*, *6*(60), 3021. https://doi.org/10.21105/joss.03021

WHO. (2004). *Making choices in health*. World Health Organization.

Wickham, H. (2016). *Ggplot2: elegant graphics for data analysis*. Springer-Verlag New York. https://ggplot2.tidyverse.org

Wickham, H., Averick, M., Bryan, J., Chang, W., McGowan, L. D., François, R., Grolemund, G., Hayes, A., Henry, L., Hester, J., Kuhn, M., Pedersen, T. L., Miller, E., Bache, S. M., Müller, K., Ooms, J., Robinson, D., Seidel, D. P., Spinu, V., … Yutani, H. (2019). Welcome to the tidyverse. *Journal of Open Source Software*, *4*(43), 1686. https://doi.org/10.21105/joss.01686

Wickham, H., François, R., Henry, L., Müller, K., & Vaughan, D. (2023). *Dplyr: a grammar of data manipulation* [https://dplyr.tidyverse.org, https://github.com/tidyverse/dplyr]

Wikipedia. (2023). Receiver operating characteristic - Wikipedia — en.wikipedia.org [[Accessed 08-May-2023]].

Wu, A., Li, Y., Qi, M., Lu, X., Jia, Q., Guo, F., Dai, Z., Liu, Y., Chen, C., Zhou, L., & Song, T. (2020). Dosiomics improves prediction of locoregional recurrence for intensity modulated radiotherapy treated head and neck cancer cases. *Oral Oncology*, *104*, 104625. https://doi.org/10.1016/j.oraloncology.2020.104625

Xu, X. G. e. a. (2008). A review of dosimetry studies on external-beam radiation treatment with respect to second cancer induction. *Phys. Med. Biol.*, *53*(13), R193–241.

Yang, S.-S., OuYang, P.-Y., Guo, J.-G., Cai, J.-J., Zhang, J., Peng, Q.-H., He, Y., Zhang, B.-Y., Liu, Z.-Q., Hu, X.-F., Chen, Y.-F., Chen, C.-Y., & Xie, F.-Y. (2022). Dosiomics Risk Model for Predicting Radiation Induced Temporal Lobe Injury and Guiding Individual Intensity Modulated Radiation Therapy. *Interna-*

*tional Journal of Radiation Oncology*Biology*Physics*, S0360301622036057. https://doi.org/10.1016/j.ijrobp.2022.11.036

Yarnold, J., & Brotons, M.-C. V. (2010). Pathogenetic mechanisms in radiation fibrosis. *Radiotherapy and Oncology: Journal of the European Society for Therapeutic Radiology and Oncology*, *97*(1), 149–161. https://doi.org/10.1016/j.radonc.2010.09.002

Zaidi, H. e. a. (2007). Computational anthropomorphic models of the human anatomy: the path to realistic monte carlo modeling in radiological sciences. *Annu. Rev. Biomed. Eng.*, *9*(1), 471–500.

Zou, H., & Hastie, T. (2005). Regularization and variable selection via the elastic net. *Journal of the Royal Statistical Society: Series B (Statistical Methodology)*, *67*(2), 301–320. https://doi.org/10.1111/j.1467-9868.2005.00503.x

Zwanenburg, A., Vallières, M., Abdalah, M. A., Aerts, H. J. W. L., Andrearczyk, V., Apte, A., Ashrafinia, S., Bakas, S., Beukinga, R. J., Boellaard, R., Bogowicz, M., Boldrini, L., Buvat, I., Cook, G. J. R., Davatzikos, C., Depeursinge, A., Desseroit, M.-C., Dinapoli, N., Dinh, C. V., … Löck, S. (2020). The image biomarker standardization initiative: standardized quantitative radiomics for high-throughput image-based phenotyping. *Radiology*, *295*(2), 328–338.